The Handbook of Environmental Chemistry 37
Series Editors: Damià Barceló · Andrey G. Kostianoy

Ivan Bergier
Mario Luis Assine *Editors*

Dynamics of the Pantanal Wetland in South America

Springer

The Handbook of Environmental Chemistry

Founded by Otto Hutzinger

Volume 37

More information about this series at http://www.springer.com/series/698

Dynamics of the Pantanal Wetland in South America

Volume Editors: Ivan Bergier · Mario Luis Assine

With contributions by

L.M. Alves · M.L. Assine · D. Bastviken · G. Bayma-Silva · I. Bergier · L.S. Buller · T.G.T. Catalani · G.H. Cavazzana · J.S.V. da Silva · E.F.G. de Carvalho Dores · A. de Moraes · B.T. Freitas · T. Goulart · F. Guérin · R.L. Guerreiro · A. Krusche · G. Lastoria · H.A. Macedo · J.A. Marengo · P.P. Mattos · M.M. McGlue · E.R. Merino · H. Monteiro · G.S. Oliveira · E. Ortega · C.R. Padovani · A.C. Paranhos-Filho · A. Pott · F.d.N. Pupim · F. Quaglio · C. Riccomini · K.F. Roche · S.M. Salis · H.O. Sawakuchi · A. Silva · A.P.S. Silva · M.G. Simões · J.C. Stevaux · L.V. Warren · M.R. Zanetti

Springer

Editors
Ivan Bergier
Laboratório de Conversão de Biomassa
Empresa Brasileira de Pesquisa Agropecuária (Embrapa)
Corumbá
Brazil

Mario Luis Assine
IGCE – Departamento de Geologia Aplicada
UNESP – Universidade Estadual Paulista
Rio Claro
São Paulo
Brazil

ISSN 1867-979X ISSN 1616-864X (electronic)
The Handbook of Environmental Chemistry
ISBN 978-3-319-18734-1 ISBN 978-3-319-18735-8 (eBook)
DOI 10.1007/978-3-319-18735-8

Library of Congress Control Number: 2015957803

Springer Cham Heidelberg New York Dordrecht London

Printed on acid-free paper

Springer International Publishing AG Switzerland is part of Springer Science+Business Media (www.springer.com)

The Handbook of Environmental Chemistry Also Available Electronically

The Handbook of Environmental Chemistry is included in Springer's eBook package *Earth and Environmental Science*. If a library does not opt for the whole package, the book series may be bought on a subscription basis.

For all customers who have a standing order to the print version of *The Handbook of Environmental Chemistry,* we offer free access to the electronic volumes of the Series published in the current year via SpringerLink. If you do not have access, you can still view the table of contents of each volume and the abstract of each article on SpringerLink (www.springerlink.com/content/110354/).

You will find information about the

– Editorial Board
– Aims and Scope
– Instructions for Authors
– Sample Contribution

at springer.com (www.springer.com/series/698).

All figures submitted in color are published in full color in the electronic version on SpringerLink.

Aims and Scope

Since 1980, *The Handbook of Environmental Chemistry* has provided sound and solid knowledge about environmental topics from a chemical perspective. Presenting a wide spectrum of viewpoints and approaches, the series now covers topics such as local and global changes of natural environment and climate; anthropogenic impact on the environment; water, air and soil pollution; remediation and waste characterization; environmental contaminants; biogeochemistry; geoecology; chemical reactions and processes; chemical and biological transformations as well as physical transport of chemicals in the environment; or environmental modeling. A particular focus of the series lies on methodological advances in environmental analytical chemistry.

Series Preface

With remarkable vision, Prof. Otto Hutzinger initiated *The Handbook of Environmental Chemistry* in 1980 and became the founding Editor-in-Chief. At that time, environmental chemistry was an emerging field, aiming at a complete description of the Earth's environment, encompassing the physical, chemical, biological, and geological transformations of chemical substances occurring on a local as well as a global scale. Environmental chemistry was intended to provide an account of the impact of man's activities on the natural environment by describing observed changes.

While a considerable amount of knowledge has been accumulated over the last three decades, as reflected in the more than 70 volumes of *The Handbook of Environmental Chemistry,* there are still many scientific and policy challenges ahead due to the complexity and interdisciplinary nature of the field. The series will therefore continue to provide compilations of current knowledge. Contributions are written by leading experts with practical experience in their fields. *The Handbook of Environmental Chemistry* grows with the increases in our scientific understanding, and provides a valuable source not only for scientists but also for environmental managers and decision-makers. Today, the series covers a broad range of environmental topics from a chemical perspective, including methodological advances in environmental analytical chemistry.

In recent years, there has been a growing tendency to include subject matter of societal relevance in the broad view of environmental chemistry. Topics include life cycle analysis, environmental management, sustainable development, and socio-economic, legal and even political problems, among others. While these topics are of great importance for the development and acceptance of *The Handbook of Environmental Chemistry,* the publisher and Editors-in-Chief have decided to keep the handbook essentially a source of information on "hard sciences" with a particular emphasis on chemistry, but also covering biology, geology, hydrology and engineering as applied to environmental sciences.

The volumes of the series are written at an advanced level, addressing the needs of both researchers and graduate students, as well as of people outside the field of

"pure" chemistry, including those in industry, business, government, research establishments, and public interest groups. It would be very satisfying to see these volumes used as a basis for graduate courses in environmental chemistry. With its high standards of scientific quality and clarity, *The Handbook of Environmental Chemistry* provides a solid basis from which scientists can share their knowledge on the different aspects of environmental problems, presenting a wide spectrum of viewpoints and approaches.

The Handbook of Environmental Chemistry is available both in print and online via www.springerlink.com/content/110354/. Articles are published online as soon as they have been approved for publication. Authors, Volume Editors and Editors-in-Chief are rewarded by the broad acceptance of *The Handbook of Environmental Chemistry* by the scientific community, from whom suggestions for new topics to the Editors-in-Chief are always very welcome.

Damià Barceló
Andrey G. Kostianoy
Editors-in-Chief

Volume Preface

This book presents the Pantanal wetland in a singular perspective where the reader can envisage changes in the Pantanal landscape under variable lenses of time and space, since its early formation to the actual and likely future states. The book reveals that today's Pantanal is an evolutionary sequence of geologic, ecologic, and more recently manmade events taking place at distinct space-time frequencies. Under this perspective, the notion of preserving the Pantanal wetland "as today" in the long term is somehow idealistic, as much stronger planetary forces are involved in its dynamics and configuration.

Geotectonics and Sun–Earth interaction largely dictate the rate of drastic environmental changes that eventually disrupt the ecological stability, radically rebuilding the regional landscape as already occurred in the past. Warren et al. (chapter "Underneath the Pantanal Wetland: A Deep-Time History of Gondwana Assembly, Climate Change, and the Dawn of Metazoan Life") show that Precambrian rocks that form the hills, locally known as "morrarias," register the supercontinent assembling, the origin of metazoans like *Cloudina* and *Corumbella*, and past climate changes. On the other hand, at intermediate timescales, the biota-climate system is a major driver reshaping the ecohydrology functioning in the landscape. Assine et al. (chapter "Geology and Geomorphology of the Pantanal Basin") provide evidences that the Pantanal is an active sedimentary basin with faults and associated earthquakes that delimit the most flood-prone areas and point that geomorphology is the product of climatic fluctuations and environmental changes that have been occurring since the Late Pleistocene. McGlue et al. (chapter "Paleolimnology in the Pantanal: Using Lake Sediment Archives to Track Late Quaternary Environmental Change in the World's Largest Neotropical Wetland") suggest that severe widespread drought is the response of the Pantanal to high-latitude glaciation, perhaps due to linkages among effective precipitation, ITCZ position, and North Atlantic sea surface temperatures. Assine et al. (chapter "Avulsive Rivers in the Hydrology of the Pantanal Wetland") illustrate that avulsions and bottlenecks dictate geomorphology, hydrodynamics, and the ecohydrology of the Pantanal wetland. The models and evidences presented in chapter

"Avulsive Rivers in the Hydrology of the Pantanal Wetland" is a step further in the comprehension of the Pantanal hydrodynamics.

Very recently, in the Anthropocene, short-term timescale changes in ecohydrology and biodiversity are due to both land-use and in course climate change. Chapter "Terrestrial and Aquatic Vegetation Diversity of the Pantanal Wetland" by Pott and Silva is a comprehensive review of aquatic and terrestrial vegetation diversity in the Pantanal, demonstrating how manmade land-use has been altering the vegetation landscape. Pott and Silva conclude that vegetation is very resilient and flexible and adapts to wet-and-dry seasonal and decadal cycles, including fire, and shall remain diverse as long as the hydrological balance is not disrupted by homogenization toward either an entirely dry or a fully wet system. Bergier et al. (chapter "Metabolic Scaling Applied to Native Woody Savanna Species in the Pantanal of Nhecolândia") show for the Nhecolândia subregion how forest biomass allocation, independently of the species, follows the metabolic scaling theory, though close-to-soil groundwater makes the ratio below/above biomass lower than unit probably to cope with evapotranspiration. Still in the Nhecolândia, Bergier et al. (chapter "Alkaline Lakes Dynamics in the Nhecolândia Landscape") show that alkaline lakes can be segregated into three ecological functional groups accordingly to their biogeochemistry and greenhouse gas exchanges and that these singular lakes are steadily reducing in area and number likely due to land-use changes in highlands that affect the ecohydrology of the whole Upper Paraguay River Basin. Bergier et al. (chapter "Methane and Carbon Dioxide Emissions from the Paraguay River floodplain (Pantanal) during Episodic Anoxia Events") bring lacking data on methane and carbon dioxide dynamics in the Paraguay River floodplain during the natural and very anoxic "dequada" or "decoada" event that develops in variable intensity and magnitude at every annual flood.

Regarding human interferences, Dores (chapter "Pesticides in the Pantanal") provides a discussion highlighting that agricultural activities occur mainly in the highlands and represent the main source of pesticides to the Pantanal. Nevertheless, although detected with low frequency and relatively low concentrations, pesticides may interfere in the Pantanal ecosystem, and little is known about potential effects, indicating that more research is needed. Buller et al. (chapter "Historical Land-use Changes in São Gabriel do Oeste at the Upper Taquari River Basin") illustrate that human appropriation of the net primary production in highlands has been improving human development index and economic concentration, although the agribusiness development has diminished ecosystem services and resilience. Buller et al. emphasize that new sustainable design of agroecosystems (integrated crop-livestock and forestry) in the Upper Taquari River Basin can maximize and optimize both the sharing of rural productivity and carbon/water regulations that positively reflect to the lowlands of the Pantanal. Cavazanna et al. (chapter "Natural and Environmental Vulnerability along the Touristic "Estradas Parque Pantanal" by GIS Algebraic Mapping") traced the vulnerability of tourism activities in the lowlands (*Estradas Parque Pantanal*), which is a major economic activity in the region. The Estradas Parque Pantanal is undergoing ecological pressure, which means that further changes applied to the landscape can alter its "status" to

vulnerable. Finally, Marengo et al. (chapter "Climate Change Scenarios in the Pantanal") show future scenarios of climate change indicating that by the end of the century temperatures can increase upon to 7°C and rainfall can decrease in austral summer and particularly in austral winter seasons. Marengo et al. highlight the relevance of restoring the natural interannual flood pulse dynamics and to improve the resilience of the wetland ecosystems with regard to future climate change risk.

In summary, the ability to recognize how those variable processes occurring at different temporal scales and strength dynamically affect the Pantanal wetland opens new opportunities to adaptation strategies for increasing ecosystem's resilience by means of the sustainable development in low- and highlands. The Pantanal is a place of changing rivers and public policies must consider this intrinsic dynamism.

Corumbá, Brazil Ivan Bergier and Mario Luís Assine
March 2015

Contents

Underneath the Pantanal Wetland: A Deep-Time History of Gondwana Assembly, Climate Change, and the Dawn of Metazoan Life

Lucas V. Warren, Fernanda Quaglio, Marcello G. Simões, Bernardo T. Freitas, Mario L. Assine, and Claudio Riccomini

Abstract Underneath the wetlands of the Brazilian Pantanal are hidden key ecological and geological events of the history of our planet. In this chapter we show that Precambrian rocks forming the hills and mountains surrounding the Pantanal floodplains record (a) the cyclic process of supercontinents assembling, (b) the origin of complex life forms on Earth, and (c) the past global climate changes. It further unveiled the most recent geochronological data and paleontological and tectonic discoveries for modeling the evolution of the Pantanal basement rocks. Various questions are also addressed, including the formation time of the Rodinia and Gondwana supercontinents, the triggering factor leading to animal skeleton biomineralization, and the "Snowball Earth Hypothesis."

Keywords Araras Group, Brazilian Pantanal wetland, Corumbá Group, Jacadigo Group, Precambrian

L.V. Warren (✉), F. Quaglio, and M.L. Assine
Applied Geology Department, Geosciences and Exact Sciences Institute, São Paulo State University, Av. 24A, 1515, Rio Claro 13506-900, Brazil
e-mail: warren@rc.unesp.br

M.G. Simões
Zoology Department, Biosciences Institute, São Paulo State University, Distrito de Rubião Júnior, Botucatu 18618-000, Brazil

B.T. Freitas and C. Riccomini
Geosciences Institute, University of São Paulo (USP), Rua do Lago, 562, São Paulo 05508-080, Brazil

I. Bergier and M.L. Assine (eds.), *Dynamics of the Pantanal Wetland in South America*, Hdb Env Chem (2016) 37: 1–22, DOI 10.1007/698_2014_326,

Contents

1 Introduction

The region that currently comprises the Pantanal – the world's largest tropical wetland – is a noteworthy example of an active sedimentary basin. By looking at its huge flooded area, one could not expect that a vast geological record is found underneath its very young sediments. This record is nearly half as old as the Earth itself, which means that an important part of the ancient Earth's history is covered by the wetland's waters and sediments. Questions such as "when did the supercontinent Gondwana assemble?" can be answered by studying the geological record of the Pantanal region. Several geological units form the basement of the present-day Pantanal Basin, spanning from the Proterozoic Eon to the Cambrian Period of the Phanerozoic Eon. These are key records to understand the origin and evolution of an enormous supercontinent, which went through a ~300 Ma stable phase.

Although mostly underneath the wetlands, fragments of early Earth history are scattered through the uneven relief of this region, revealed by different lithotypes and structural styles of the basement rocks. Presently, the rocks comprising the basement of the Pantanal Basin are exposed mainly in plateaus and highlands. The Bodoquena Plateau (Fig. 1a) in Mato do Grosso do Sul State and Serrana Province in Mato Grosso are two spectacular examples. In addition, the basement is embodied in the mountains and relict highlands, as exemplified by the Urucum Massif nearby Corumbá City at Mato Grosso do Sul (Fig. 1b, c). These highlands limit the floodplains and occur as hills, mountains, or sedimentary plateaus surrounded by Quaternary plain terrains, which are the Pantanal wetlands themselves (Fig. 1d). The occurrence of highlands and plateaus with such characteristics suggests recent large-scale tectonic activity, which possibly caused these terrains to uplift and surrounding areas to subside, forming the Pantanal Basin. Residual elevations shaped as "table mountains" or plateaus were developed over Ediacaran deposits of banded iron formations (BIF) of the Jacadigo Group, as well as the karst terrain that sculpted the carbonates of the Corumbá Group in Serra da Bodoquena (Fig. 1a). In the last example, the whole relief is resulted from erosion of rocks deformed by an Ediacaran–Cambrian mobile belt named Paraguay–Araguaia Belt [1, 2].

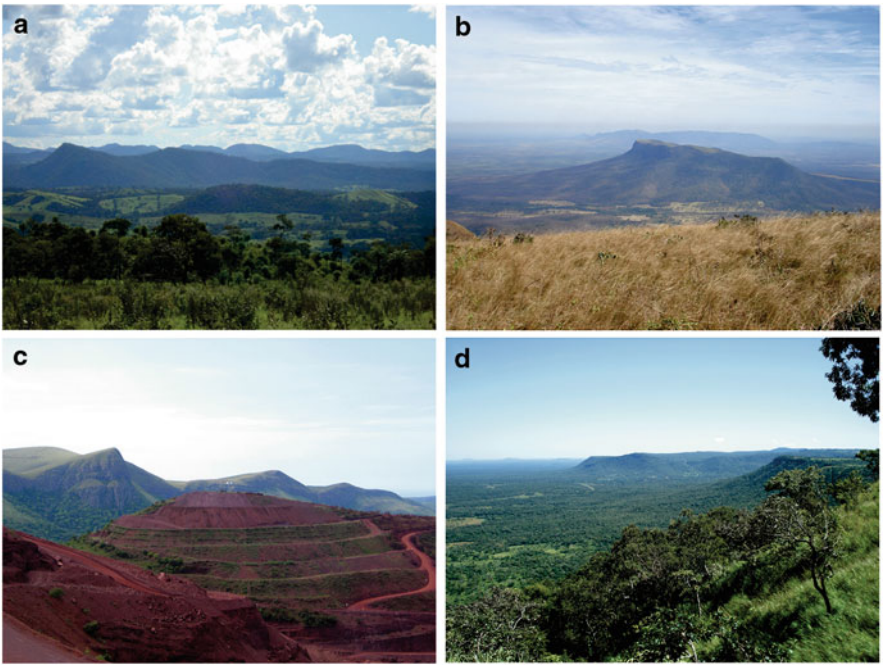

Fig. 1 The landforms developed over rocks of the Precambrian basement in the Pantanal wetland. (**a**) Mountains and aligned hills of the Bodoquena Plateau. (**b**) View of the "Tromba dos Macacos" tabular hill with the Jacadigo–Mutum Plateau as background. (**c**) Mountains of Jacadigo Massif with open-pit mine of jaspilite (iron and manganese ore). (**d**) Pantanal lower plains (*left*) bordered by the Bodoquena Plateau (Photos (**a**) and (**d**) by LV Warren; (**b**) and (**c**) by BT Freitas)

This uneven distribution of hills, plateaus, and plains is the result of a complex geotectonic history of continent assemblages and breakups. The geological units of the basement record distinct cycles of crustal reworking, granite formation, and orogenesis dated from the Paleoproterozoic to the early Paleozoic [2, 3].

During each of the different rifting cycles and continent accretion of Rodinia and Gondwana, several sedimentary basins were generated where clastic, carbonate, and other chemical rocks were deposited. Those lithologies are important records of atmospheric and geochemical changes of the Neoproterozoic Era, notably those related to the supposed global glaciation of the "Snowball Earth Theory," precipitation of thick BIF beds, and important bioevolutionary innovations. Sedimentary rocks – especially carbonate rocks – record evidence of the earliest animals in Earth history, principally those with biomineralized skeletons typical of the "Nama Assemblage," the youngest of the three evolutionary Ediacaran assemblages, with ages spanning from 549 to 542 Ma [4, 5].

The study of the basement rocks of the Pantanal wetlands is important to better understand the evolutionary history of Gondwana supercontinent, the South American continent, and the currently active Pantanal Basin as well. Scientific issues related to the evolution of the earliest metazoans, extreme climate changes, and particular geochemical processes during the Ediacaran Period can also be addressed

throughout the investigation of basement rocks of the Brazilian Pantanal. These ancient geological units are significant mining resources that are currently being exploited, including iron, manganese, and limestone, which have been key Brazilian commodities.

2 Paleo and Mesoproterozoic Basement: The Old Cratonic Terrains and the Origin of Rodinia Supercontinent

Despite the scarcity of geophysical and geochronological studies in the Pantanal sedimentary basin, limited available data suggest that the basement rocks are Proterozoic [3]. Fragments of ancient continents, several sutures, and fold belts, which resulted from different accretion and rifting cycles, have given rise to the complex Pantanal basement [6]. The Pantanal Basin overlies the Rio Apa and Amazon Cratons (Fig. 2), whose eastern limits match with the Paraguay–Araguaia Mobile Belt. This geological unit extends over South America from the Pará State in Brazil to Paraguay and delimits the crustal blocks in the east with the Paranapanema Craton and the Central Goiás Massive [8].

The south Amazon and Rio Apa Cratons are composed of orthogneisses intruded by undeformed granitic bodies belonging to the Rio Apa Complex (Fig. 2), as well as the Alumiador Suite [6]. The unit was formed during the Paleoproterozoic (approximately 1,900 Ma) and represents the oldest terrains belonging to the regional basement. The Amoguijá Group is composed of low metamorphic grade supracrustal rocks of volcano-sedimentary affinity (rhyolites, rhyodacites, metasandstones, meta-conglomerates, schists, and phyllites) discordantly overlying granitoid rocks of the Rio Apa Complex. Few Rb–Sr geochronological dating of coeval rocks named "Alto Tererê Metamorphic Association" indicated a Paleoproterozoic age of 1,780 Ma [3, 11]. Both Amoguijá Group and metamorphic rocks of Alto Tererê Association are intruded by granitic bodies known as "Baía das Garças Granites," with crystallization ages of ~1,750 Ma [3].

K–Ar ages on biotite crystals yield ages of 1,300 Ma, which suggests that the Rio Apa and Amazon Cratons underwent a cycle of heating and crustal reworking during the Mesoproterozoic Era [3]. Similar ages derived for the Amazon Craton indicate that, at least partially, the terrains from the Rio Apa and Amazon Cratons hold some correspondence to each other. This linkage is most likely due to a similar history of reworking by an orogenic event called Rondoniano-São Inácio [12]. Due to this similarity, it is possible that these cratons were part of the same segment, separated by younger rift basins, which are represented by the Chiquitos–Tucavaca Fold Belt [6]. It is import to highlight that the Rondoniano-São Inácio event affected most rocks of the Amazon and Rio Apa Cratons during the Mesoproterozoic Era. Also, the Rondoniano-São Inácio event might be considered

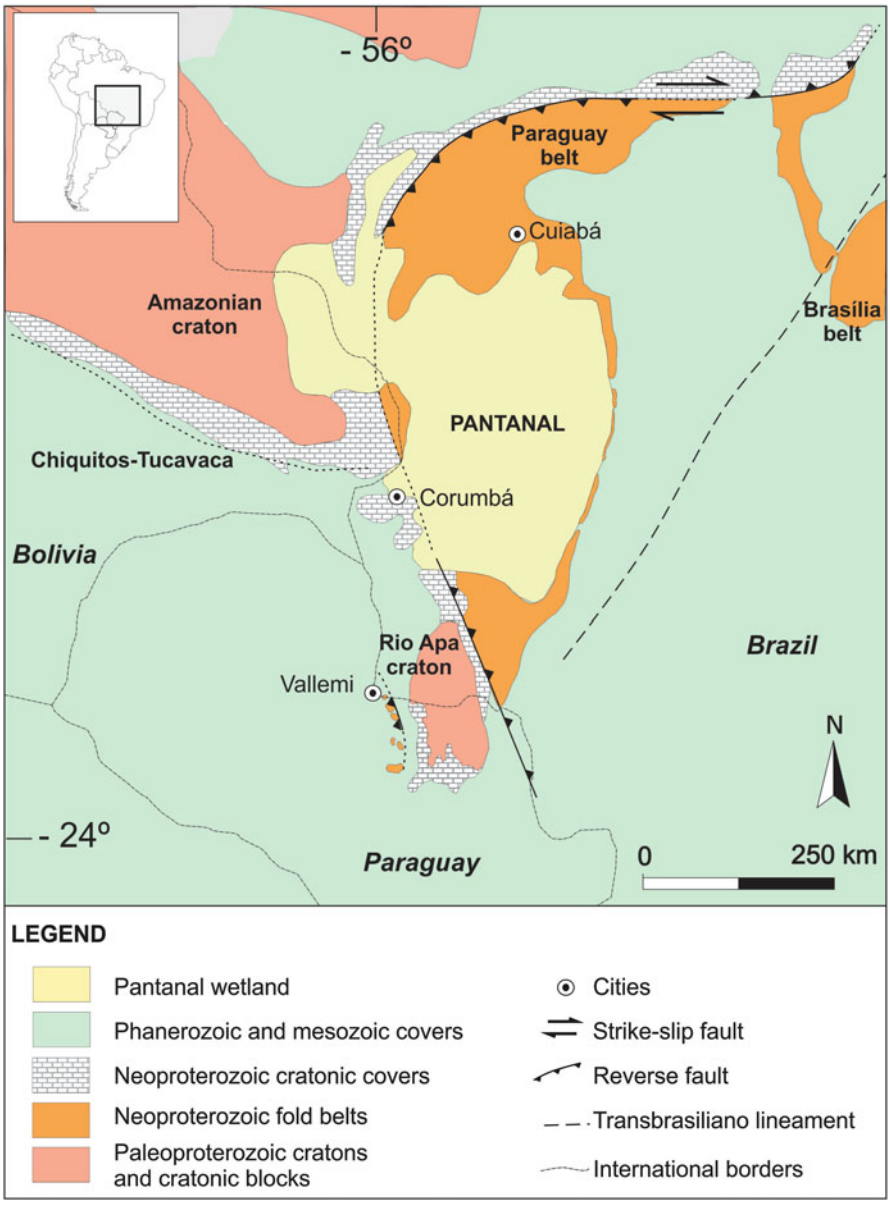

Fig. 2 Geological context of the Pantanal basement, highlighting the main geotectonic units and sedimentary covers (Based on [7–10])

to have occurred previously to the collisional processes that assembled the Amazon Craton and Laurentia continent to form the supercontinent Rodinia, around 1,000 Ma [13, 14].

3 Neoproterozoic Basins: Rodinia Breakup (the Origin of Metazoans and Extreme Climate Changes)

The last 200 million years between the transition of Proterozoic and Paleozoic include time intervals when the many important biologic, tectonic, and climatic changes in the geological record occurred (Fig. 3 [5, 21, 22]). The drastic shift in the biogeochemical carbon cycle is one of the greatest changes, as shown by positive and negative $\delta^{13}C$ incursions measured in carbonate rocks, related to glacial events that supposedly reached low latitudes [21, 23–26], the crisis of the stromatolite diversity [27], and the origin and diversification of metazoans [28, 29].

Rodinia started to break up in the early Neoproterozoic Era (Fig. 3; [23]). This comprised several continental blocks amalgamated after collisional events associated with the Grenvillian orogenesis at 1,190–950 Ma [30]. Extensions altogether with subsidence processes from 746 to 580 Ma [17, 31] caused several sedimentary rift basins to form, beginning with the accumulation of continental deposits [23, 32]. As these distentional processes evolved, followed by significant thermal subsidence, several passive margins developed, resulting in the accumulation of thick marine carbonate-terrigenous successions [31]. All successions belonging to Corumbá, Araras, and Jacadigo Groups were deposited in such context.

At least three important glaciations of global extent (Sturtian, Marinoan, and Gaskiers; Fig. 3) are believed to have occurred synchronically to the distentional events that triggered Rodinia breakup around 746 and 580 Ma [17]. These global glaciations had supposedly reached equatorial latitudes and caused oceans and emergent continental areas to freeze. This scenario of "Snowball Earth" is supported by the occurrence of glacial deposits in equatorial latitudes, variation of carbon isotope values, as well as particular stratigraphic patterns [22, 24, 33]. According to

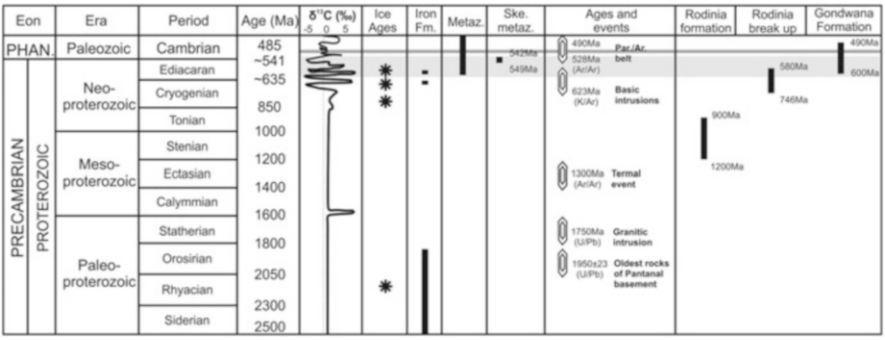

Fig. 3 The most important isotopic, climatic, bioevolutionary, and geotectonic events occurred during the Paleo-, Meso-, and Neoproterozoic Eras and Cambrian Period of the Paleozoic Era. The *light gray horizontal stripe* (~635–541 Ma) indicates the time interval of Neoproterozoic basin deposition in the Pantanal area. The *dark gray line* in the Cambrian represents the time period of metamorphism and deformation of these units and development of the Paraguay–Araguaia fold belt. *PHAN* phanerozoic, *Fm*. formation, *Metaz*. metazoans, *Ske*. *Metaz*. skeletal metazoans (Data from [2, 3, 5, 15–20])

this hypothesis, a thermal disturbance caused by enhancement in the albedo effect and weathering rates resulted in a global cooling after continental ice caps reached equatorial latitudes, resulting in the ice coverage of the whole planet's surface.

Glacial sediments were deposited under extreme cold, while several basins at the margin of Amazon and Rio Apa Cratons were opening due to the Rodinia fragmentation. Under the oceans closed by massive ice sheets, the biological productivity of most microorganisms would have stopped due to predominance of anoxic and aphotic environments. Inside such closed system, the constant rise in the atmospheric CO_2 released by the activity of submarine volcanoes would have initiated another greenhouse effect, which eventually would have contributed to the ice sheet melting [24]. Following the termination of glaciation and the initiation of ocean warming and higher primary productivity, thick beds of carbonate were deposited over the glacial sediments. This increase in photosynthetic activity helped to oxygenate ocean waters, such that the remaining reduced iron oxidized, precipitated, and formed huge volumes of BIF ([16]; Fig. 3).

The Puga Formation occurs in the northern and southern portions of the Paraguay–Araguaia Belt as anticline cores or tectonic slabs that are commonly slightly deformed and metamorphosed. This unit occurs in erosive contact overlying granites and metamorphic rocks of the Paleoproterozoic basement ([34]; Fig. 4a) and is composed of stratified sandstones, pelites, and polymictic diamictites with reworked clasts from the basement (Fig. 4b). The diamictites are interpreted as tillites deposited under glacial influence, due to the common presence of massive paraconglomerates with rare striated clasts [39]. The occurrence of rhythmic successions of pelites and tabular sandstone beds also reinforces a depositional scenario of turbidity currents in glacio-marine environments triggered by deglaciation events and tectonic instability [39].

Some zircons obtained from the Puga Formation diamictites yielded U–Pb ages younger than 706 ± 9 Ma, suggesting that the succession was deposited at the end of the Cryogenian glacial event [40]. This would support the Puga Formation as a representative of the Sturtian global glaciation (~730 Ma) and, thus, more evidence in support of the Snowball Earth Hypothesis [33]. Alternative interpretations posit that Puga diamictites were deposited by alluvial processes that developed during the initial stages of the Rodinia breakup [41].

The Cuiabá Group is a terrigenous succession and occurs in apparent association with glacial deposits of the Puga Formation [34, 39]. This unit crops out in the eastern portion of the Amazon Craton and consists of intensely deformed and metamorphosed rocks of greenschist facies [42]. The Cuiabá Group is composed mainly of sandstones, pelites, and diamictites deposited as turbidities under glacial influence [43, 44]. Its age is considered to be uncertain. Due to the facies similarity, some authors consider that the Cuiabá Group is a lateral equivalent of glacial deposits of the Puga Formation and, thus, supposedly deposited during the Sturtian glaciation [40]. Others consider that the unit is older than the Corumbá Group and constitutes part of the Proterozoic regional basement (~1,000 Ma [44]).

Fig. 4 Examples of the distinct lithotypes related to the Pantanal Precambrian basement. (**a**) Massive, very coarse-grained granite of the Paleoproterozoic Rio Apa Complex. Machete for scale, *lower left*. (**b**) Detail of slightly deformed glacial diamictite of the Puga Formation in the Bodoquena Plateau area. (**c**) Detail of jaspilite of the Banda Alta Formation, Jacadigo Group. Note the intercalation of jasper (*white*) and iron-rich thin layers (*red*). (**d**) Giant boulder in banded iron formation interpreted as a dropstone, supposedly deposited by glacial icebergs during the Marinoan global glaciation (see Figs. 3 and 6). (**e**) Basal columnar stromatolite of the Ediacaran Bocaina Formation, Corumbá Group. (**f**) Large recumbent fold in limestones of the Ediacaran Tamengo Formation, Corumbá Group. The scale is a geologist on the *bottom-right* of the picture (Photos (**a**) and (**c**) by B.T. Freitas; (**b**), (**e**), and (**f**) by L.V. Warren. Photo (**d**) by PC Boggiani)

In the Corumbá–Urucum District area, a basement high made of slightly deformed Neoproterozoic sedimentary successions splits the Pantanal and Chaco basins. The deformation of these rocks is so gentle that they preserve most of their

primary sedimentary structures, which makes them a window to the Neoproterozoic Era. The sedimentary succession forms tabular mountains, capped by iron formations, and reaches up to 1 km above the Pantanal and Chaco plains. The iron-bearing sedimentary succession is referred to as the Jacadigo Group [45, 46]. The mountains, hills, and ranges sustained by this sedimentary unit compose the Urucum District, located a few tens of kilometers southeastward from Corumbá City, Mato Grosso do Sul, in the Brazil–Bolivia border. The highest mountains embody the center of a NE-elongated dome – the Urucum Massif – surrounded by lower hills of the carbonate-dominated successions of the Corumbá Group [41]. The siliciclastic intercalations within the deepwater BIF-dominated succession have been interpreted as glacially influenced sediments deposited by gravity-driven flows due to the restricted occurrence of clasts interpreted as dropstones [47]. The ice sheet development over the deepwater environment would have favored the rise of Fe, Mn, and Si amounts in the water column, whose precipitation would be related to oxidizing melting waters [47].

The Jacadigo Group is up to 800 m thick and comprises the lower Urucum Formation, a 400 m thick siliciclastic succession of sandstone and conglomerate with minor intercalations of mudstone and carbonate rocks. Above the basal unit, the middle Córrego das Pedras Formation correspond to a mixed siliciclastic-granular iron formation (GIF) succession up to 100 m thick. The upper Banda Alta Formation is composed of approximately 300 m of classic hematite–jasper, thinly laminated banded iron formations (Fig. 4c), with subordinated siliciclastic and manganese intercalations [45]. The Neoproterozoic iron formation of the Banda Alta Formation encloses more than half of the Brazilian manganese ore and is the third Brazilian iron deposit, with nearly 15% of the Brazilian reserve [48].

The Neoproterozoic succession in the Corumbá–Urucum District area is interpreted as a sedimentary response to the evolution of a nearly E–W-elongated rift basin due to extensional tectonics in the SE-Amazon Craton [41]. The Urucum Formation siliciclastic rocks represent the earliest stages of rifting and comprise alluvial fan and fluvial and lacustrine depositional systems deposited in a basin developed during the Rodinia fragmentation (Fig. 3). This essentially subaerial to shallow water continental sedimentation transitioned into a rift-climax deep lacustrine or marine system, with deposition of mixed siliciclastic and hematite–jasper peloid and ooid grainstones in coastal areas (Córrego das Pedras Formation), and manganese and banded iron formations basin ward (Banda Alta Formation, [41]). Several jaspilite horizons are deformed by granite dropstones in the Banda Alta Formation, which led several authors to interpret these levels of the upper portion of the Jacadigo Group as deposited under glacial influence [45, 47].

The contact between the Jacadigo Group and the overlying Corumbá Group is usually observed at the Urucum Dome foothills as the Bocaina Formation dolomites overlapping the Urucum Formation siliciclastics. At the center of the Urucum Dome, the Urucum Formation unconformably overlies the basement rocks of the Rio Apa Block. The Bocaina Formation directly rests on an erosional surface

overlying the crystalline basement rocks in peripheral areas of the Urucum Dome [41].

The age of the Jacadigo Group was recently constrained between 644 ± 20 and 587 ± 7 Ma [49]. The older age is based on (U–Th)/He and (U–Th)/Ne geochronological datings from hematite, which were assumed to reflect the time of deposition of the Urucum iron formation. The younger age is based on $^{40}Ar/^{39}Ar$ from cryptomelane, which has been interpreted as the diagenetic alteration of primary Mn minerals to cryptomelane. A previous, less reliable K–Ar age of 623 ± 15 Ma was obtained from plutonic rocks associated with volcanoclastics, supposedly lying below the Jacadigo Group in Bolivia [50]. Due to its stratigraphic position, the Jacadigo Group is considered time equivalent to the Puga Formation. The granite dropstones found in the banded iron formations (Fig. 4d) are interpreted as deposited under influence by the Marinoan glacial global event. Alternatively, these clasts might be considered as lonely stones originated from surrounding granite basement and deposited by gravity-driven processes, related to subaqueous and subaerial debris flows, in a scenario detached from a global glaciation [41].

In the northern portion of the Paraguay Belt (Mato Grosso State), a significant transgressive–regressive succession overlaps the rocks of the Puga Formation and Cuiabá Group. This unit, known as Araras Group, comprises a thick succession of carbonates and siliciclastic sedimentary rocks interpreted as deposited in a passive shallow marine margin setting [51]. The limestone succession deposited directly over the Puga Formation diamictites (Mirasol D'Oeste Formation) represents a period of carbonate sedimentation immediately after the Marinoan global glacial event and, therefore, characterizes a rapid and dramatic climate change from glacial to greenhouse conditions [52]. This carbonate cap contains a significant number of stromatolites, tubelike structures, aragonite crystal fans, giant wave ripples, and other enigmatic sedimentary structures associated with postglacial cap carbonates [53, 54]. The Araras Group preserves an important microfossil content, including cyanobacterial filaments, cocoidal cells, and acritarchs typical of post-Marinoan cellular assemblages [55]. The maximum depositional age of the Araras Group is given by Pb isotope data of $\sim 633 \pm 25$ Ma, which reinforces the correlation of the base of this unit and the Marinoan Snowball event [56].

At the southern portion of the Paraguay Fold Belt (Fig. 1), the Corumbá Group rests in angular and erosional unconformable contact on the overlapping Paleoproterozoic basement, Puga Formation, as well as the Jacadigo and Cuiabá Groups. The Corumbá Group is an extensive siliciclastic-carbonate succession and includes the Cerradinho, Cadiuéus, Bocaina, Tamengo, and Guaicurus Formations. The basal Cerradinho and Cadiuéus Formations [42, 57] are made up of terrigenous rocks including conglomerates, sandstones, and pelites. Both units are interpreted to have been deposited in alluvial and fluvial systems of a rift basin that developed during the final stages of Rodinia breakup, analogously and synchronously with the initial opening of the Jacadigo rift [41, 58].

The Bocaina Formation is a dolomite-dominated, often silicified sedimentary unit composed of peloid and ooid grainstones, diverse stromatolitic boundstones (Fig. 4e), intraclastic rudstones, and minor phosphorite intercalations [59]. The carbonates of the Bocaina Formation were ascribed to the post-rift thermal subsidence, during a phase of slow generation of relative accommodation space spread over a broad area. At that time the syn-rift infilling and the adjacent crystalline basement were covered by a shallow marine rimmed-carbonate platform characterized by a large amount of microbialite facies [41, 57]. Due to its stratigraphic position (above the diamictites of Puga Formation), the Bocaina Formation is interpreted as a cap-carbonate deposited after the Marinoan global glaciation [57]. The massive presence of peritidal carbonate facies and low $\delta^{13}C$ values reinforce this hypothesis [60].

The Tamengo and Guaicurus Formations are well exposed, although highly deformed (Fig. 4f) in the Corumbá area and in the Bodoquena ridge. The Tamengo Formation is a dark to gray limestone, typically a laminated and cross-bedded peloid grainstone, with subordinated mudstone intercalations. Finer grained limestone facies preserve skeletal Ediacaran metazoan fossils such as *Cloudina lucianoi* and *Corumbella werneri* [61–63]. The Tamengo Formation is interpreted to have resulted from an important transgression over the Rio Apa Block with associated widespread carbonate deposition [64, 65] and preservation of *Cloudina* and *Corumbella* remains.

The Guaicurus Formation is a thick, monotonous succession mainly represented by dark laminated mudstones [42]. These rocks also preserve rare fossils of the vendotaenid *Eoholynia corumbensis* and a considerable variety of Ediacaran microfossils such as *Soldadophycus bossii*, *Siphonophycus robustum*, and *Leiosphaeridia* sp. [65]. The Guaicurus Formation would represent the end life of the Corumbá carbonate platform probably caused by the capture of a major drainage network and the consequent increase of fine-grained siliciclastic input to the basin.

Near the top of the Corumbá Group, an ash bed within the Tamengo Formation provided U–Pb SHRIMP zircon ages of 543 ± 3 Ma [66], associated with the Ediacaran guide-fossils *Cloudina* and *Corumbella* [61–63]. This age places the sedimentary succession exposed between the Pantanal and Chaco basins as a detailed record of the Ediacaran Period, an interval typifying the last events of the Proterozoic world, such as the extreme climate changes, the beginning of the Phanerozoic Eon, and the origin of complex life forms on Earth seas.

4 The Ediacaran Biota

Late Ediacaran rocks (549–542 Ma) of the Tamengo Formation, Corumbá Group, cropping out in Mato Grosso do Sul, contains profuse fossils of *Corumbella werneri* and *Cloudina lucianoi*, and more rarely undetermined and undescribed conulariid remains [67]. These are among the oldest known skeletonized eumetazoan animals [67, 68]. Fossils are found in limestones and shales of the Tamengo Formation from

abandoned quarry walls in the vicinities of Corumbá town, as well as in calcareous benches along the Paraguay River margin. Not surprisingly, the genus name *Corumbella* (which means "the beauty of Corumbá") derives from the name of that city in which the odd fossils were first discovered in March 1980 by Professor Detlef Walde (National University of Brasília/UnB).

Cloudina (Fig. 5a, b) is a small, tube-building, early metazoan marine organism that was abundant in certain Edicaran rocks ranging from 549 ± 1 to 542 ± 1 Ma [4, 5, 69]. Although formerly interpreted as a calcareous tubiculous annelid [70], *Cloudina* has been more recently considered a probable cnidarian polyp [71]. The shells are made of a series of nested vase-like calcareous [72] cones forming a sinuous, sometimes branched tube. Detailed three-dimensional reconstructions of well-preserved tubes have indicated that the shells had an open basal portion [71].

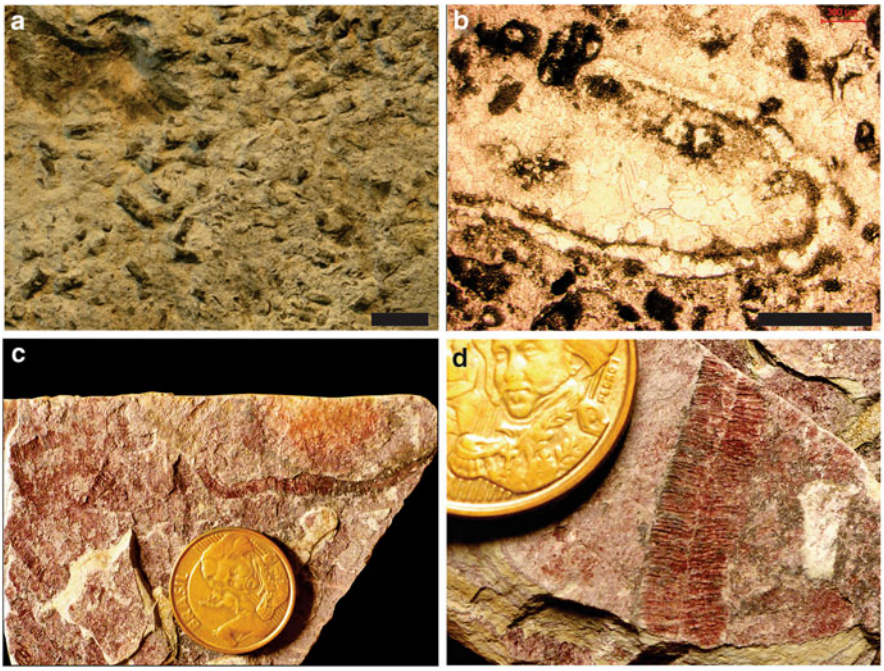

Fig. 5 Ediacaran metazoans of the Tamengo Formation, Corumbá Group. (**a**) Plan view of a *Cloudina*-rich bed, showing dispersed complete remains and fragments. (**b**) Photomicrograph of longitudinal section of *Cloudina* shell fragment filled by sparry calcite cement. (**c**) Several specimens of *Corumbella werneri* in a very thin-grained marl matrix. Observe that the largest specimen reaches ~5 cm long. (**d**) Detail of *Corumbella werneri* specimen showing the midline ridge and a series of segments/rings. The scale bar is 1 cm for (**a**) and 500 μm for (**b**). The diameter of the coin in (**c**) and (**d**) is 22 mm (Photo (**a**) by L.V. Warren; (**b**), (**c**), and (**d**) by B.T. Freitas)

Corumbella werneri (Fig. 5c and d) is a small marine invertebrate whose carapace is represented by a tetrameral flexible tube. The tube is a pronounced steep pyramid made of polygonal "rings," which are roughly square in transverse cross section [73, 74]. The "rings" articulate along their edges and alternate along the facial midline [67, 73]. Curiously, this condition is similar to that of the transverse ribs of the Paleozoic cnidarians, such as the conulariids, particularly *Climacoconus* [75]. Yet, the midline of each side or "face" of the test is sulcate, forming a low uninterrupted carina on its inner surface [67]. Ultrastructure analyses of *Corumbella* theca also indicated the presence of pores and papillae, again a condition comparable to that of conulariid tests [76]. Hence, the general morphology of *Corumbella* test is similar to that of conulariids and Coronatae cnidarians [62, 67, 77]. Indeed, recent morphology-based phylogenetic hypothesis for the Phylum Cnidaria indicates that Conulata and Corumbellata are sister groups united in a clade termed Paleoscyphozoa, which is closely related to Coronatae cnidarians [67]. *Corumbella werneri* was a colonial or solitary invertebrate, perhaps feeding upon small nektonic animals or microplankton.

Both *Corumbella* and *Cloudina* lived in very shallow waters in association with thrombolites and microbially induced sedimentary structures (MISS). In particular, *Cloudina* fossils preserved in situ in coeval Neoproterozoic rocks of Paraguay suggest that they lived preferentially in carbonate environments, "as a flexible mat-sticker rising above the seafloor by partially anchoring itself in the sediment or attaching itself to small thrombolite domes" [74]. Conulariids are the third group of Ediacaran invertebrates found in the Tamengo Formation [67]. As for *Corumbella* and *Cloudina*, conulariids are extinct cnidarians, endowed with a small phosphatic (apatite) theca shaped like a steep, four-sided pyramid [78]. The Tamengo conulariid theca is finely nodose, with adaperturally arcuate transverse ribs that terminate in the corner sulcus. The nodes commonly exhibit spinelike extensions, which project adaperturally, partway across the interspaces [67]. It is noteworthy that these anatomical features are all present in Paleozoic conulariids, such as *Paraconularia*, a basal taxon within the Conulatae clade [67]. Conulariids were marine, sessile epifaunal, suspension-feeding invertebrates, which lived in a range of shallow to deep marine, carbonatic to siliciclastic environments [78].

The three small Ediacaran metazoans of the Tamengo Formation are key elements to understand the evolutionary history of shelly invertebrates (Fig. 6). Indeed, cloudinids, corumbellas, and conulariids are among the first animals to secrete biomineralized exoskeletons on Earth, probably as a response to biological, ecological, and environmental pressures near the Ediacaran/Cambrian boundary [79]. In the ancient carbonate platforms characterized by the presence of microbialites, *Cloudina* and *Corumbella* remains were the critical source of durable biomineralized hard parts in an environment nearly free of other bioclasts. The effects on the marine substrate of these "new" organic sediments may have contributed to the decline of stromatolites and the death of extensive, widespread cyanobacteria communities [69, 80].

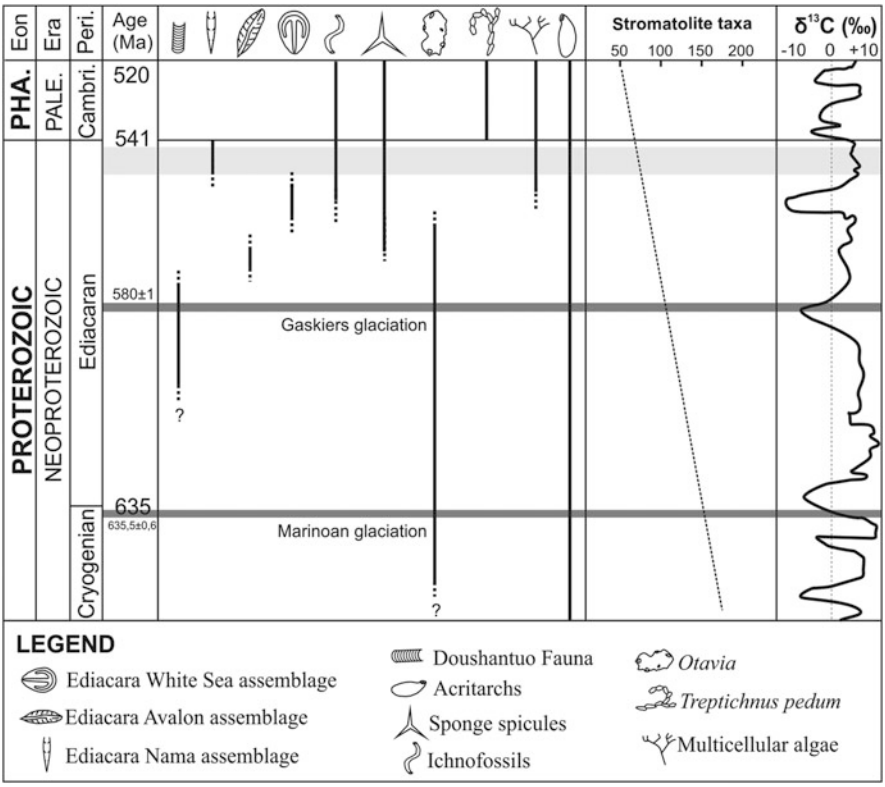

Fig. 6 Schematic representation of the most important bioevolutionary and isotope events of the end of Neoproterozoic and the beginning of the Paleozoic Era. The *light gray stripe* represents the time interval in which the Ediacaran fossil bearing rocks of Corumbá Group were deposited. *PHA* phanerozoic, *Pale*. paleozoic, *Cambri*. Cambrian, *Peri*. period (After [4, 5, 17, 27, 35–38])

5 The Paraguay–Araguaia Mobile Belt: The Rise of the Gondwana Supercontinent

The eastern portion of the Rio Apa Block is delimited by the Paraguay Belt, which was formerly defined by Almeida [1, 42] as the "Paraguay Geosyncline." This geotectonic unit conforms regionally to a collisional structure located in the central portion of the South American Plate and reaching the Brazilian territory throughout the states of Mato Grosso and Mato Grosso do Sul for around 1,200 km and continuing with the Araguaia Belt in the south of Pará State (Fig. 1). In its southern segment [81], the Paraguay Belt occurs in vicinities of the Corumbá City and presents a westward inflection toward Bolivia, which suggests that this area is a triple rift junction with the Chiquitos–Tucavaca Belt (Fig. 1; [82–84]). Toward the southeast, the structure is covered by Cenozoic sediments of the Pantanal Basin up to the northwestern portion of Miranda town. In this portion, the belt is nearly N–S

oriented and makes up a geomorphologic unit named "Serra da Bodoquena," which extends to the Apa River, in the political boundary with Paraguay. Beyond this limit, the Paraguay Belt – or its undeformed cover – extends southward for around 50 km, reaching the Paraguayan territory. In the western portion of the Rio Apa Craton, a narrow strip of folded rocks occurs in the North Paraguay, named Vallemí Belt, possibly reaching the eastern boundary of the Pampia Craton [9].

The Paraguay–Araguaia Belt comprises a deformed strip located between the Paraná Craton to the East and Rio Apa/Amazon Cratons to the West. The belt is composed of siliciclastic and carbonate successions of the Cuiabá, Corumbá, Jacadigo, and Araras Groups. Those successions bear open to isoclinal folds (sometimes with inversed flanks) associated with westward vergent thrusts. The metamorphic grade ranges from null to greenschist, and, in the same way of the deformation intensity, it tends to decrease from E to W, where the cratonic covers are almost undeformed (Fig. 1).

The timing of formation and filling of the sedimentary basins where Cuiabá, Corumbá, Araras, and Jacadigo Groups were deposited remain controversial. The deformation history following basin infill is also unconstrained by absolute geochronometers. Recent evidence indicates that those processes have occurred rapidly [19, 20]. The final evolutionary stages of those basins, as well as the subsequent Paraguay Belt formation, were formerly related to the Brazilian event (650–530 Ma), in which the convergence of the western Rio Apa Block, the eastern Amazon and São Francisco Cratons, and the southern and southeastern Paraná and Rio de La Plata Cratons would have culminated in the assembling of the western portion of the supercontinent Gondwana [85]. The age of the Paraguay Belt available to date is 545–500 Ma [86], which is younger than the uppermost limit of the Brazilian Cycle proposed to other regions of the South American Plate [32].

More recent studies based on paleomagnetic, geochronological, and paleontological data [2, 19, 20, 87] indicated that assembly of the Amazon, Rio Apa, Pambia, and West African Cratons would have initiated only at 528 Ma. The assembly of Gondwana would have caused the Cymene Ocean to close and resulted in the deformation of the Ediacaran sedimentary successions of Western Gondwana. Evidence of orogenic uplift younger than the Brazilian Cycle indicates that those assembling events would have extended up to 490 Ma [88]. Remagnetization events identified in rocks of Paraguay Belt are associated with the initial deforming stages at ~528 ± 36 Ma [2]. This age is coeval with the 525 Ma recorded to the N–S magnetization event from mafic dykes at Itabaiana City, northeastern Brazil [20]. $^{40}Ar/^{39}Ar$ geochronological dating on illites indicated a metamorphic peak at 490 Ma, which suggests that the initial deformation and the rock remagnetization in the Paraguay Belt would have initiated at 528 Ma and, hence, reached the latest Cambrian or even the very beginning of Ordovician [2]. This collisional event would have closed the Clymene Ocean and remodeled the Paraguay Belt structure, configuring the last stage of SW Gondwana supercontinent assemblage.

6 Final Remarks

The geological history recorded in the basement rocks of the Pantanal wetlands is an intricate product of sequential events deep in Earth's early history. A complex tectonic puzzle of cratons, mobile belts, and sedimentary basins lies under the extensive Cenozoic deposits of the Pantanal wetland system.

The old Paleo and Mesoproterozoic (older than 1,300 Ma) igneous and metamorphic basement are uncontested evidence of the intense tectonic processes that culminated with the formation of the Rodinia supercontinent [13, 14]. As the continuation of a cycle, the fragmentation of this vast landmass during Neoproterozoic times (746–580 Ma) was marked by the formation of several rifts and small subsidence areas [23]. Synchronously with sedimentation in these basins, global-scale glaciations supposedly covered the Earth with ice and caused important changes in the ocean and atmosphere chemistry [24, 33]. Diamictites of the Puga Formation are possibly the evidence of sedimentation influenced by extensive ice caps. With the end of these glacial periods, anomalous geochemical conditions allowed the precipitation of enormous amounts of banded iron formation, as recorded in the Jacadigo Group. The evolution of small continental rift basins to passive margins [58] caused the formation of extensive carbonate platforms of the Corumbá and Araras groups [41]. In these shallow marine settings, the environmental conditions enabled the growth of cyanobacterial communities that formed microbialites, such as stromatolites and thrombolites. Associated with this particular substrate, the first animals capable of producing their own skeleton (~550 Ma) could be established and form the first true metazoan reefs in the geological record [89]. The death and accumulation of skeletonized metazoans, such as *Cloudina* and *Corumbella*, allowed the formation of shell beds and bioclast-rich substrates for the first time in the Earth's history [69]. The simple inner organization and geometry of these deposits are typical of Cambrian-style shell beds, suggesting that the carbonate platforms on latest Ediacaran were paleoecologically and taphonomically comparable to the early Phanerozoic ones.

During Cambrian times (around 528 Ma), the siliciclastic and carbonate sequences of basins developed on the margins of Amazon and Rio Apa Cratons were intensely deformed and metamorphosed by tectonic stress associated with the final stages of the Gondwana Formation. The ultimate amalgamation of the Amazon/Rio Apa Cratons and the continental landmass comprising Australia, Antarctica, India, Kalahari, Rio de La Plata, Paraná, West Africa, and Congo–São Francisco Cratons celebrated the beginning of the Phanerozoic Eon in South America and a cycle of tectonic stability of about 360 Ma. Just after 358 Ma, the area corresponding to the current Pantanal wetlands began to suffer the tectonic stress that still today causes subsidence and the continental sedimentary deposition since then. Despite the enormous importance of the Pantanal for the study of Quaternary sedimentary basins, alluvial depositional systems, and fluvial dynamics, the analyses of its basement rocks represent an open window to an ancient Precambrian world and a unique opportunity to understand the deep-time geology responsible for the formation of the South America continent.

Acknowledgments The authors thank the CNPq (project 444070/2014-1) and PROPE/UNESP for the financial support and Dr. Michael M. McGlue (Department of Earth and Environmental Sciences, University of Kentucky) for revising the manuscript. This work has the institutional support of the São Paulo State University (UNESP).

References

1. Almeida FFM (1967) Origem e evolução da Plataforma Brasileira. Bol do DNPM Rio de Janeiro
2. Tohver E, Trindade RIF, Solum JG et al (2010) Closing the Clymene ocean and bending a Brasiliano belt: evidence for the Cambrian formation of Gondwana, southeast Amazon craton. Geology 38(3):267–270
3. Cordani UG et al (2010) The Rio Apa Craton in Mato Grosso do Sul (Brazil) and northern Paraguay: geochronological evolution, correlations and tectonic implications for Rodinia and Gondwana. Am J Sci 310:981–1023
4. Amthor JE, Grotzinger JP, Schröder S et al (2003) Extinction of *Cloudina* and *Namacalathus* at the Precambrian-Cambrian boundary in Oman. Geology 31:431–434
5. Grotzinger JP et al (1995) Biostratigraphic and geochronologic constraints on early animal evolution. Science 270:598–604
6. Cordani UG, Tassinari CCG, Rolim DR (2005) The basement of the Rio Apa Craton in Mato Grosso do Sul (Brazil) and northern Paraguay: a geochronological correlation with the tectonic provinces of the south-western Amazonian Craton. In: Abstracts of Gondwana 12, Mendoza, p 112
7. Alvarenga CJS, Trompette R (1993) Evolução Tectônica Brasiliana da Faixa Paraguai: a Estruturação da Região de Cuiabá. Rev Bras Geosci 23(1):18–30
8. Alvarenga CJS et al (2000) Paraguai and Araguaia belts. In: Cordani UG et al (eds) Tectonic evolution of South America. FINEP, Rio de Janeiro, pp 183–193
9. Campanha GAC, Warren LV, Boggiani PC et al (2010) Structural analysis of the Itapucumi Group in the Vallemi region, northern Paraguay: evidence of a new Brasiliano – Pan-African mobile belt. J S Am Earth Sci 30(1):1–11
10. Kröner A, Cordani UG (2003) African, southern Indian and South American cratons were not part of the Rodinia supercontinent: evidence from field relationships and geochronology. Tectonophysics 375:325–352
11. Araújo HJT, Santos Neto A, Trindade CAH et al (1982) Geologia. In: Projeto RADAMBRASIL, Folha SF 21, Campo Grande. Escala 1:1.00.000. Geologia, geomorfologia, pedologia, vegetação e uso potencial da terra. Rio de Janeiro, vol 28, pp 23–124
12. Tassinari CCG et al (1996) Geochronological systematics on basement rocks from the Rio Negro-Juruena Province (Amazon CRio Alegre Terrainon) and tectonic implications. Int Geol Rev 38:1161–1175
13. Cordani UG, Teixeira W (2007) Proterozoic accretionary belts in the Amazonian Craton. In: Hatcher RD Jr et al (eds) The 4D framework of continental crust, vol 200. GSA Memoir, Boulder, pp 297–320
14. Tohver E et al (2002) Paleogeography of the Amazon craton at 1,2 Ga: early Grenvillian collision with the Llano segment of Laurentia. Earth Planet Sci Lett 199:185–200
15. Cohen KM et al (2014) The ICS International Chronostratigraphic Chart. Episodes 36: 199–204
16. Cox GM, Halverson GP, Minarik WG et al (2013) Neoproterozoic iron formation: an evaluation of its temporal, environmental and tectonic significance. Chem Geol 362:232–249
17. Halverson GP et al (2005) Towards a Neoproterozoic composite carbon isotope record. Geol Soc Am Bull 117:1181–1207

18. Li ZX et al (2008) Assembly, configuration, and break-up history of Rodinia: a synthesis. Precambrian Res 160:179–210
19. Tohver E, D'Agrella-Filho MS, Trindade RIF (2006) Paleomagnetic record of Africa and South America for the 1200–500 Ma interval, and evaluation of Rodinia and Gondwana assemblies. Precambrian Res 147:193–222
20. Trindade RIF et al (2006) Paleomagnetism of early Cambrian Itabaiana mafic dikes (NE Brazil) and the final assembly of Gondwana. Earth Planet Sci Lett 244:361–377
21. Kaufman AJ, Knoll AH, Narbonne GM (1997) Isotopes, ice ages and terminal Proterozoic earth history – an exemple from the Olenek Uplift, northeastern Sibéria. Precambrian Res 73: 251–270
22. Kirschvink JL (1992) Late Proterozoic low-latitude global glaciation: the snowball Earth. In: Schopf JW, Klein C (eds) The Proterozoic biosphere – a multidisciplinary study. Cambridge University Press, Cambridge, pp 51–52
23. Hoffman PF (1999) The break-up of Rodinia, birth of Gondwana, true polar wander and the snowball Earth. J Afr Earth Sci 28:17–33
24. Hoffman PF, Schrag DP (2002) The snowball Earth hypothesis: testing the limits of global change. Terra Nova 14(3):129–155
25. Kaufman AJ, Knoll AH (1995) Neoproterozoic variations in the C-isotopic composition of seawater: stratigraphic and biogeochemical implications. Precambrian Res 73:27–49
26. Knoll AH (2000) Learning to tell Neoproterozoic time. Precambrian Res 100:3–20
27. Riding R (2006) Microbial carbonate abundance compared with fluctuations in metazoan diversity over geological time. Sediment Geol 185:229–238
28. Grey K, Walter MR, Calver CR (2003) Neoproterozoic biotic diversification: snowball Earth or aftermath of the Acraman impact? Geology 31:459–462
29. Knoll AH, Carroll SB (1999) Early animal evolution: emerging views from comparative biology and geology. Science 284:2129–2137
30. Tohver E et al (2005) Two stage tectonic history of the SW Amazon craton in the late Mesoproterozoic: identifying a cryptic suture zone. Precambrian Res 137:35–59
31. Eyles N, Januszczak N (2004) 'Zipper-rift': a tectonic model for Neoproterozoic glaciations during the breakup of Rodinia after 750 Ma. Earth Sci Rev 65:1–73
32. Trompette R (2000) Gondwana evolution: its assembly at around 600 Ma. C R Acad Sci Paris 330:305–315
33. Hoffman PF et al (1998) A Neoproterozoic snowball Earth. Science 81:1342–1346
34. Campanha GAC, Boggiani PC, Sallun WF et al (2011) A faixa de dobramento Paraguai na Serra da Bodoquena e depressão do Rio Miranda, Mato Grosso do Sul. Rev Geol USP 11(3): 79–96
35. Brain CKB, Prave AR, Hoffmann KH et al (2012) The first animals: ca. 760-million-year-old sponge-like fossils from Namibia. S Afr J Sci 108(1–2):658
36. Erwin DH (2006) Dates end rates: temporal resolution in the deep time stratigraphic record. Annu Rev Earth Planet Sci 34:569–590
37. Grotzinger JP, James NP (2000) Precambrian carbonates: evolution of understanding. In: Grotzinger JP, James NP (eds) Carbonate sedimentation and diagenesis in the evolving precambrian world, vol 67, SEPM special publication. Tulsa, SEPM, pp 3–20
38. Xiao S, Kaufman AJ (2006) Neoproterozoic geobiology and paleobiology, vol 27, Topics in geobiology series. Springer, Berlin, p 300
39. Alvarenga CJS, Trompette R (1992) Glacially influenced sedimentation in the later Proterozoic of the Paraguay Belt (Mato Grosso, Brazil). Palaeogeogr Palaeoclimatol Palaeoecol 92: 85–105
40. Babinski M, Boggiani PC, Trindade RIF et al (2013) Detrital zircon ages and geochronological constraints on the Neoproterozoic Puga diamictites and associated BIFs in the southern Paraguay Belt, Brazil. Gondwana Res 23:988–997
41. Freitas BT, Warren LV, Boggiani PC et al (2011) Tectono-sedimentary evolution of the Neoproterozoic BIF-bearing Jacadigo Group, SW-Brazil. Sediment Geol 238(1–2):48–70

42. Almeida FFM (1965) Geologia da Serra da Bodoquena (Mato Grosso), Brasil. Bol Div Geol e Mineral 219:1–96
43. Luz JS et al (1980) Projeto Coxipó. Goiania, DNPM/CPRM 1:136
44. Tokashiki CC, Saes GS (2008) Revisão estratigráfica e faciologia do Grupo Cuiabá no alinhamento Cangas-Poconé, baixada Cuiabána, Mato Grosso. Rev Bras Geosci 38(4): 661–675
45. Dorr II JVN (1945) Manganese and iron deposits of Morro do Urucum, Mato Grosso, Brazil. Bull US Geol Surv 946A:47
46. Almeida FFM (1946) Origem dos minérios de ferro e manganês de Urucum: Boletim da Divisão de Geologia e Mineralogia. DNPM 119:1–58.
47. Urban H, Stribrny B, Lippolt H (1992) Iron and manganese deposits of the Urucum district, Mato Grosso do Sul, Brazil. Econ Geol 87:1375–1392
48. DNPM (2012) Sumário Mineral 32:136
49. Piacentini T, Vasconcelos PM, Farley KA (2013) 40Ar/39Ar constraints on the age and thermal history of the Urucum Neoproterozoic banded iron-formation, Brazil. Precambrian Res 228:48–62
50. O'Connor EA, Walde DGH (1986) Recognition of an Eocambriam orogenic cycle in SW Brazil and SE Bolivia. Zbl Geol Palaeont 9/10:1441–1456
51. Alvarenga CJS, Santos RV, Dantas EL (2004) C–O–Sr isotopic stratigraphy of cap carbonates overlying Marinoan-age glacial diamictites in the Paraguay Belt, Brazil. Precambrian Res 131: 1–21
52. Nogueira ACR et al (2003) Soft- sediment deformation at the Neoproterozoic Puga cap carbonate (southwestern Amazon Craton, Brazil): conformation of rapid icehouse to greenhouse transition in snowball Earth. Geology 31:613–616
53. Allen PA, Hoffman PF (2005) Extreme winds and waves in the aftermath of a Neoproterozoic glaciation. Nature 433:123–127
54. Nogueira ACR (2003) A plataforma carbonática Araras no sudoeste do Cráton Amazônico, Mato Grosso: estratigrafia, contexto paleoambiental e correlação com os eventos glaciais do Neoproterozóico. Ph.D. thesis, University of São Paulo
55. Hidalgo RLL (2007) Vida após as glaciações globais neoproterozoicas: um estudo fossilífero de capas carbonáticas dos crátons do São Francisco e Amazônico. Ph.D. thesis, University of São Paulo
56. Babinski M (2011) Geocronologia das glaciações criogenianas do Brasil central. Habilitation thesis, University of São Paulo
57. Boggiani PC (1998) Análise Estratigráfica da Bacia Corumbá (Neoproterozoico) – Mato Grosso do Sul. Ph.D. thesis, University of São Paulo
58. Warren LW (2011) Tectônica e sedimentação do Grupo Itapucumi (Ediacarano, Paraguay Setentrional). Ph.D. thesis, University of São Paulo
59. Boggiani PC, Fairchild TR, Coimbra AM (1993) O Grupo Corumbá (Neoproterozóico-Cambriano) na região Central da Serra da Bodoquena, Mato Grosso do Sul (Faixa Paraguai). Rev Bras Geoci 23(3):301–305
60. Boggiani PC, Ferreira VP, Sial NA et al (2003) The cap carbonate of the Puga Hill (Central South America) in the context of the post-Varanger Glaciation. In: Short papers of the IV South American symposium on isotope geology, Salvador, pp 324–327
61. Beurlen K, Sommer FW (1957) Observações estratigráficas e paleontológicas sobre o Calcário Corumbá. Relatório do Departamento Nacional de Produção Mineral. DNPM 168:1–35
62. Hahn G, Hahn R, Leonardos OH et al (1982) Körporlich erhaltene Scyphozoen-Reste aus dem Jungpräkambrium Brasiliens. Geol et Paleo 16:1–18
63. Zaine MF, Fairchild TR (1985) Comparison of Aulophycus lucianoi Beurlen & Sommerfrom Ladario (MS) and the genus Cloudina Germs, Ediacaran of Namibia. Ana Acad Bras Cie 57:130

64. Boggiani PC, Gaucher C, Sial AN et al (2010) Chemostratigraphy of the Tamengo Formation (Corumbá Group, Brazil): a contribution to the calibration of the Ediacaran carbon-isotope curve. Precambrian Res 182:382–401
65. Gaucher C, Boggiani PC, Sprechmann P et al (2003) Integrated correlation of the Vendian to Cambrian Arroyo del Soldado and Corumbá Groups (Uruguay and Brazil): palaeogeographic, palaeoclimatic and palaeobiologic implications. Precambrian Res 120:241–278
66. Babinski M, Boggiani PC, Fanning CM (2008) U-PB SHRIMP geochronology and isotope chemostratigraphy (C, O, Sr) of the Tamengo Formation, Southern Paraguay Belt, Brazil. In: Book of abstracts of the VI South American symposium on isotope geology, San Carlos de Bariloche, p 160
67. Van Iten H et al (2014) Origin and early diversification of the phylum Cnidaria Verrill: major developments in the analysis of the taxon's Proterozoic-Cambrian history. Palaeontology 1–14
68. Fairchild TR et al (2012) Evolution of Precambrian life in the Brazilian geological record. Int J Astrobiol 11(4):309–323
69. Warren LV, Simões MG, Fairchild TR et al (2013) Origin and impact of the oldest metazoan bioclastic sediments. Geology 41:507–510
70. Germs GJB (1972) New shelly fossils from Nama Group, South West Africa. Am J Sci 272: 752–761
71. Vinn O, Zatón M (2012) Inconsistencies in proposed annelid affinities of early biomineralized organism *Cloudina* (Ediacaran): structural and ontogenetic evidences. Carnets de Geologie [Notebooks on Geology] - Article 2012/03(CG2012-A03):39–47
72. Grant SWF (1990) Shell structure and distribution of *Cloudina*, a potential index fossil for the terminal Proterozoic. Am J Sci 290:261–294
73. Pacheco MLAF, Leme JM, Machado AF (2011) Taphonomic analysis and geometric modeling for the reconstruction of the Ediacaran metazoan *Corumbella werneri* Hahn et al. 1982 (Tamengo Formation, Corumbá Group, Brazil). J Taphon 9:269–283
74. Warren LV, Fairchild TR, Gaucher C et al (2011) *Corumbella* and in situ *Cloudina* in association with thrombolites in the Ediacaran Itapucumi Group, Paraguay. Terra Nova 23: 382–389
75. Van Iten H (1992) Morphology and phylogenetic significance of the corners and midlines of the conulariid test. Palaeontology 35:335–358
76. Warren LV, Pacheco MLAF, Fairchild TR et al (2012) The dawn of animal skeletogenesis: ultrastructural analysis of the Ediacaran metazoan *Corumbella werneri*. Geology 40:691–694
77. Babcock LE, Grunow AM, Sadowski AR, Leslie SA (2005) *Corumbella*, an Ediacaran-grade organism from the Late Neoproterozoic of Brazil. Palaeogeogr Palaeoclimatol Palaeoecol 220: 7–18
78. Leme JM, Simões MG, Van Iten HV (2010) Phylogenetic systematics and evolution of conulariids. Lap Lambert Academic, Saarbrücken
79. Wood RA (2011) Paleoecology of the earliest skeletal metazoan communities: implications for early biomineralization. Earth Sci Rev 106:184–190
80. Pratt BR (1982) Stromatolite decline – a reconsideration. Geology 10:512–515
81. Almeida FFM (1985) Alguns problemas das relações geológicas entre o Craton Amazônico e as faixas de dobramentos marginais à leste. In: 2° Atas do Simpósio de Geologia do Centro Oeste, Goiânia, pp 3–14
82. Brito Neves BB, Campos Neto MC, Fuck AF (1999) From Rodinia to Western Gondwana: an approach to the Brasiliano-Pan African cycle and orogenic collage. Episodes 22(3):155–166
83. Jones JP (1985) The southern border of the Guaporé shield in western Brazil and Bolivia: an interpretation of its geologic evolution. Precambrian Res 28:111–135
84. O'Connor EA, Walde DGH (1986) Recognition of an Eocambriam orogenic cycle in SW Brazil and SE Bolivia. Zbl Geol Palaeontol 9/10:1441–1456
85. Alkmin FF, Marshak S, Fonseca MA (2001) Assembling West Gondwana in the Neoproterozoic: clues from the São Francisco Craton region, Brazil. Geology 29:319–322

86. Trompette R, Alvarenga CJS, Walde D (1998) Geological evolution of the Neoproterozoic Corumbá graben system (Brazil). Depositional context of the stratified Fe and Mn ores of Jacadigo Group. J S Am Earth Sci 11:587–597
87. Warren LV, Quaglio F, Riccomini C, Simões MG et al (2014) The puzzle assembled: Ediacaran guide fossil *Cloudina* reveals an old proto-Gondwana seaway. Geology 42:391–394
88. Cawood PA, Leitch EC (1998) Going down: subduction initiation in the proto-Pacific and relationship to end Neoproterozoic global events. J Afr Earth Sci 27:42
89. Penny AM, Wood R, Curtis A, Bowyer F, Tostevin R, Hoffman KH (2014) Ediacaran metazoan reefs from the Nama Group, Namibia. Science 344:1504–1506

Geology and Geomorphology of the Pantanal Basin

Mario L. Assine, Eder R. Merino, Fabiano N. Pupim, Lucas V. Warren, Renato L. Guerreiro, and Michael M. McGlue

Abstract What is an inlier sedimentary basin? What are the main mechanisms of sedimentary infilling? How do the depositional systems behave? And last, but certainly not the least, what geological events occurred in the last million years and continue to take place in the Pantanal area today? These issues are considered in this chapter, based on available geological, geomorphological, and geochronological datasets. The Pantanal is an active sedimentary basin with numerous faults and associated earthquakes. Movements along these faults cause subsidence on blocks within the basin, generating depressions that are highly susceptible to flooding, and also create accommodation space for sediment storage. One hypothesis on the origin of the Pantanal Basin relates the processes of subsidence with tectonic activity in the Andean orogen and foreland system during the Quaternary. Alternatively, the lack of geochronological data leaves open the possibility that the basin formed much earlier, perhaps during an interval of widespread tectonism in Brazil during the Eocene. The modern Pantanal depositional tract is composed of the Paraguay River trunk system, numerous fluvial megafans and interfan floodplains, and thousands of lakes, many of them integral to the Nhecolândia landscape. The Pantanal's geomorphology is most likely the product of climatic fluctuations and environmental changes that have been occurring since the Late Pleistocene.

M.L. Assine (✉), E.R. Merino, F.N. Pupim, and L.V. Warren
Universidade Estadual Paulista – Unesp, Instituto de Geociências e Ciências Exatas – IGCE, Campus de Rio Claro. Avenida 24A, 1515, Rio Claro 13506-900, Brazil
e-mail: assine@rc.unesp.br

R.L. Guerreiro
Instituto Federal do Paraná – IFPR, Campus Assis Chateaubriand, Avenida Cívica, 475, Centro Cívico, Assis, Chateaubriand 85935-000, Brazil

M.M. McGlue
Department of Earth and Environmental Sciences, University of Kentucky, Lexington, KY 40506, USA

I. Bergier and M.L. Assine (eds.), *Dynamics of the Pantanal Wetland in South America*, Hdb Env Chem (2016) 37: 23–50, DOI 10.1007/698_2015_349,

Relict morphologic features like paleochannels have been preserved on the surfaces of abandoned lobes on several large fluvial megafans. After a period dominated by arid conditions in the Late Pleistocene, the Pantanal area experienced an episode of humidification and increasing fluvial discharge in the Early Holocene. This process promoted important modifications in the extant drainage system, for example, the avulsion of the Paraguay River that caused the Nabileque paleomeander belt to be abandoned. The landscape and sedimentary deposits of Pantanal Basin are "living" geologic records of changing rivers, avulsions, floods, and climate changes that occurred in the last several thousand years. Understanding the dynamics of these transitions is critical for unveiling the geologic history of the world's largest tropical wetland.

Keywords Avulsion, Fluvial megafans, Nhecolândia, Pantanal Basin, Tectonics and sedimentation

Contents

1 Introduction

The Pantanal Basin is situated in the Upper Paraguay River depression, which is located mostly within west-central Brazil, but it also extends into frontier territories belonging to Bolivia and Paraguay (Fig. 1). With a surface area of approximately 150,000 km^2 [2] and relief ranging from 80 to 200 m, the vast network of Pantanal floodplains are connected with the Chaco floodplains (Paraguay) to the southwest.

Bedrock rivers in the fringing source areas become alluvial rivers within the Pantanal plains, and the basin has been progressively filled with sediments carried by these rivers from the surrounding plateaus and dissected marginal lowlands (Fig. 2a). Sedimentation occurs in a large alluvial depositional tract comprised of the Paraguay River plain and several fluvial megafans. Sediment infill of the modern basin has led to the formation and persistence of large flood-susceptible areas that host rich aquatic ecosystems, which has led to the development of one of the most important tropical wetlands on the planet [3, 4]. The Pantanal experiences widespread and prolonged seasonal flooding from January to June, but with

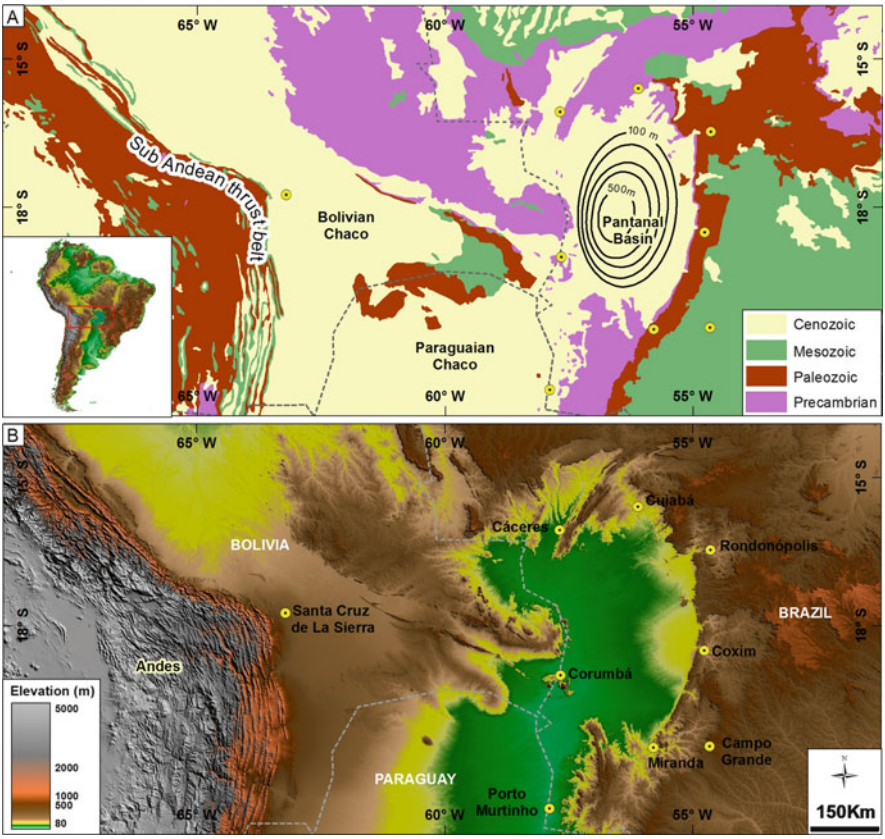

Fig. 1 Location of the Pantanal Basin. (**a**) Geological map (sediment isopach in meters from [1]). (**b**) Digital elevation model from Shuttle Radar Topographic Mission (SRTM)

diachronous flood peaks according to different geomorphologic floodplain zones [5].

What is commonly unknown about the Pantanal is the fact that the wetlands are situated in an active sedimentary basin with faults and associated earthquakes, which delimit the most flood-prone areas. Crustal movements along these faults promote differential subsidence of blocks within the basin, creating accommodation space that results in permanently flooded areas. The geological knowledge of the Pantanal Basin is still somewhat limited and studies are in their infancy, with few subsurface datasets (Fig. 2b) and scant information about the basin genesis, age and nature of the sediments, geomorphologic evolution, and modern sedimentation zones [6].

This chapter aims to present a summary of the geologic events likely responsible for the geomorphologic configuration of the Pantanal, from the uplift of the area following the fragmentation of Gondwana (lower Cretaceous) to the formation of the modern depositional tract during the Quaternary. Understanding these

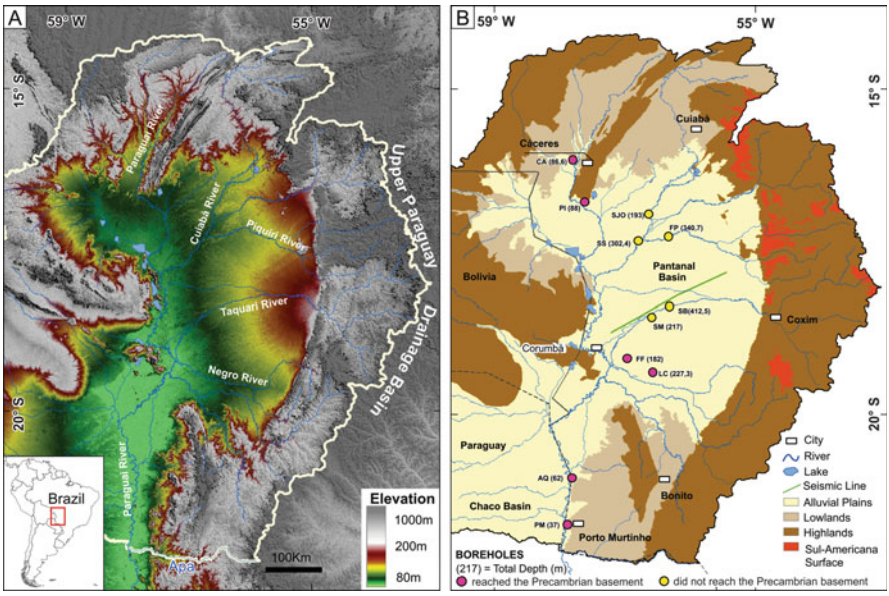

Fig. 2 Upper Paraguay drainage basin. (**a**) Digital elevation model from Shuttle Radar Topographic Mission (SRTM). (**b**) Map of geomorphological zones, showing the remnants of Sul-Americana surface on the surrounding highlands and subsurface data location within the Pantanal Basin

developments and environmental transitions is essential to revealing the extant sedimentological dynamics of the entire wetland.

2 From the Gondwana Assemblage to the Cenozoic Pantanal Sedimentary Basin

Following the assemblage of the Gondwana toward the end of Proterozoic Era (see [7]), the Pantanal region developed within the extensive domain of marginal basins that surrounded the supercontinent. This early Pantanal region was most likely a component of the Paleozoic-Mesozoic Paraná and Chaco sedimentary basins. Paleocurrent indicators, measured in sandstones of the Ivaí River Group (Ordovician and Silurian) and the Paraná Group (Devonian), suggest that there was depositional continuity between the Paraná and the Bolivian and Paraguayan Chaco basins [8, 9].

Paleozoic rocks have been almost entirely removed from the Pantanal area during the many strongly erosive dissection events during the Cenozoic. Today, few outcrops of Paleozoic rocks are present, which provide the limited evidence for the past connection between the Paraná and Chaco basins. One such example can be

found in the Silurian Coimbra Formation, which is exposed in small hills to the west of Forte Coimbra in the Nabileque area of the southern Pantanal.

The inception of the Cenozoic era was marked by a relatively quiescent tectonic period in the Pantanal, especially from the Paleocene to the lower Eocene [10]. At this time, a prolonged interval of sustained geological degradation (weathering and erosion) reduced the relief of the eastern portion of Brazil into an extensive planation surface, which has been recognized in many areas and is widely known as the Sul-Americana surface [11–13]. This regional surface has been called by several names, such as the Cristas Médias surface [14], the Japi surface [15] in the state of São Paulo, and the Purunã surface in the state of Paraná [16]. In the final stage of its development, the Sul-Americana surface was marked by deep chemical leaching, sesquioxide enrichment, and laterite (ferricrete) formation.

The laterite profiles of the Sul-Americana surface exhibit characteristics that indicate a prolonged evolution under a humid tropical climate with abundant water [17]. Despite the scarcity of geochronological data, most of the available evidences indicate that the development of the Sul-Americana surface occurred from Paleocene to Early Eocene. For example, $^{40}Ar/^{39}Ar$ dating of deep weathering profiles in the "Quadrilátero Ferrífero," Brazil, returned ages of 51–41 Ma [18]. This age range is consistent with the climate record for the Eocene obtained from ocean sediments and microfossil isotope geochemistry [19], which suggests long periods of weathering and low denudation rates under hot and wet climatic conditions of the Early Eocene Climatic Optimum.

The geomorphology of southeast and south Brazil became more clearly delineated after the genesis and subsequent disruption of the Sul-Americana surface. The main intervals of tectonic reactivation were synchronous with development of the southeast Brazilian rift system in the Eocene [20]. Tectonic reactivations caused disparate uplift and rapid dissection of topography, which were most intense in the regions near the coast [10, 21]. Remnants of the Sul-Americana surface have been recognized in the state of São Paulo at altitudes near 2,000 m in the Serra da Mantiqueira and Serra do Mar (Bocaina plateaus), decreasing in altitude toward the west [22, 23].

The flat-topped Central Plateau of Brazil (Goiás State) represents the Sul-Americana surface. Remnants of this geomorphic surface have also been recognized on the top of plateaus (e.g., *planalto*) surrounding the Pantanal at altitudes ranging from 600 to 800 m (Fig. 2). The Cachoeirinha Formation and several occurrences of thin detrital laterites dominate the sedimentary deposits atop these plateaus [24, 25]. Remnants of the surface are present on the Parecis Plateau to the north of the Pantanal, where ferruginous laterite horizons are found on the top of the plateau (700–800 m in altitude) [26]. The presence of deep laterite profiles over Neoproterozoic rocks at altitudes of approximately 1,000 m is also noteworthy on the flat top of the Urucum Massif, which is located on the western edge of the Pantanal Basin. Remains of the Sul-Americana surface in the surrounding plateaus are an uncontested piece of evidence in support of the major epeirogenic uplift before the inception of Pantanal Basin formation.

Erosive downcutting by rivers initially formed the Upper Paraguay River, which reached the Chaco Basin through a passage between the highlands of the Bodoquena plateau and the Urucum Massif. The interior paleodrainage system was subsequently reorganized, and the Paraguay watersheds, located on the Pantanal's surrounding plateaus, became the headwaters of rivers running northward to the Amazonas and eastward into the Paraná drainage basin.

Deep erosion removed almost all of the Paleozoic and Mesozoic rocks from the Upper Paraguay River depression, forming an inlier of Precambrian metamorphic terranes surrounded by plateaus sculpted on Paraná Basin sedimentary rocks. Ab'Sáber [27] used the nomenclature *boutonnière*, a French term equivalent to inlier, to name this megastructure. Following the dissection of topography and creation of new relief, the main tributaries of the Paraguay River widened their drainage basins, giving rise to broad catchments on the eastern plateaus. Today, these rivers flow toward the west, in the opposite direction of the dipping slopes of Paleozoic sedimentary layers, which serves to form a cuesta-like morphology in the catchment area.

After the period of intense downcutting, processes of planation dominated during a period of tectonic quiescence from the Oligocene to Early Miocene, giving rise to a complex inter-plateau surface. Today, the so-called Cuiabana surface occurs on the top of Cuiabá River interfluves and decreases in altitude gently from the foothills of the marginal plateaus toward the Pantanal floodplain (250–120 m above sea level). There is no consensus about whether the Cuiabana surface is a single and continuous surface throughout the Pantanal or, as some authors consider it, two different surfaces in the lowlands situated between the surrounding plateaus and the Pantanal floodplains [26, 28]. Detrital laterite deposits that document the final pediplanation phase are considered to be Pliocene-Pleistocene deposits [27], but their age has yet to be determined by absolute methods. Cosmogenic nuclide dating (^{10}Be) constrains the minimum age of detrital laterite sediments associated with the Cuiabana surface to be 500 ka [29]. Recent ^{10}Be dating found similar minimum ages (maximum exposure age of 918 ± 102 ka) and very slow erosion rates for the laterites, a key factor for the maintenance of the Cuiabana surface remains on the tops of hills [30].

The Pantanal Basin is located in the central part of the Upper Paraguay River inlier. The isopach map shown in the Fig. 1 does not reflect the real geometry of the Pantanal because it does not include the basin border nor the internal faults responsible for abrupt changes in the thickness of the sedimentary package. The basin geometry is marked by horst and graben structures, and the fault borders have dip displacements of hundreds of meters (Fig. 3). Faults are evident in the basin morphology, conditioning the occurrence of Precambrian terranes at the western edge of the basin and the modern alluvial drainage within the basin. The only available seismic section shows many small faults within the basin, displacing basement rocks of Precambrian age (see [7]). The Pantanal Basin is still tectonically active, with movements along fault planes, differential movement of blocks, and shallow earthquakes [6].

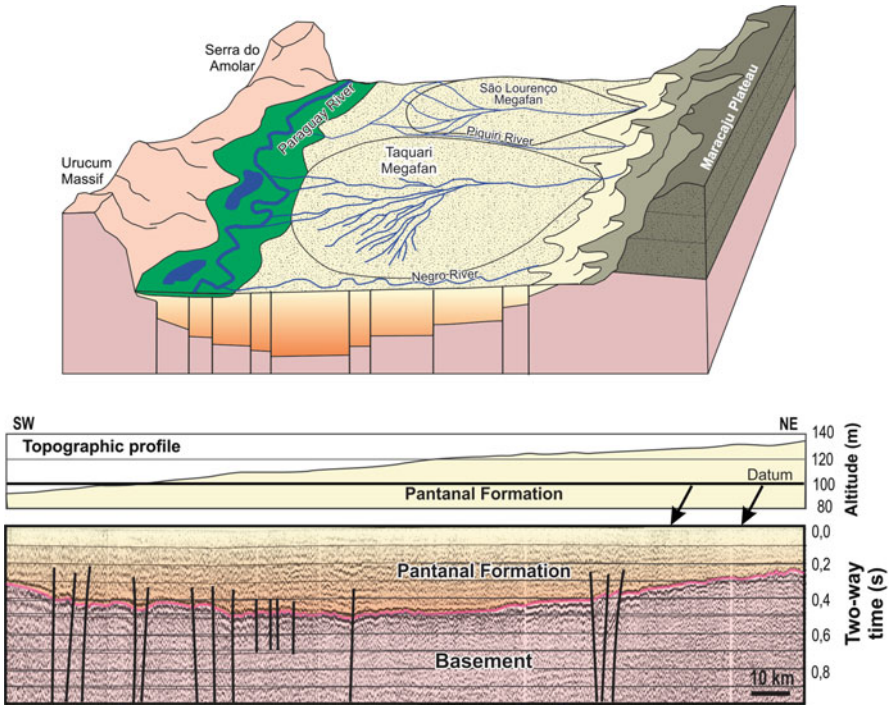

Fig. 3 Fault-structured basin. (**a**) Schematic block diagram illustrating the basin geometry. (**b**) Line drawing over the seismic section (location of the line on Fig. 2; seismic data from [31])

A crucial unanswered question regards the timing of basin formation. It is unknown when subsidence and infill of the basin with the siliciclastics of the Pantanal Formation took place. Taking into account a presumed Pliocene-Pleistocene age for the Cuiabana surface and assuming that the basin's subsidence began after that particular planation event, Ab'Sáber [27] argued for a Quaternary age for the basin origin and inception of sedimentary infill. A Quaternary age was reinforced by Ussami et al. [1], who suggested the origin of the Pantanal Basin is associated with the last compressive event in the Andean orogen ~2.5 Ma. Following this line of argument, the Cuiabana surface probably constitutes the basement of the Pantanal Basin, as represented in the schematic diagram of Fig. 4a showing the geologic evolution of the Pantanal area.

However, there is no information about the precise age of the oldest sediments of the Pantanal Basin, which reach at least 500 m in its depocenter. It is quite plausible to suppose that the basin is older, dating back to the Eocene, when an important tectonic event of uplift and basin formation took place in the southeast Brazil [10, 32], which was also coincident with an important tectonic reactivation phase in the Andes [33]. The sedimentary record of Cenozoic Taubaté Basin, one of the southeast Brazilian rift basins [20, 34, 35], consists of thick Eocene units. Based on chronological correlations with those events, an alternative hypothesis is presented

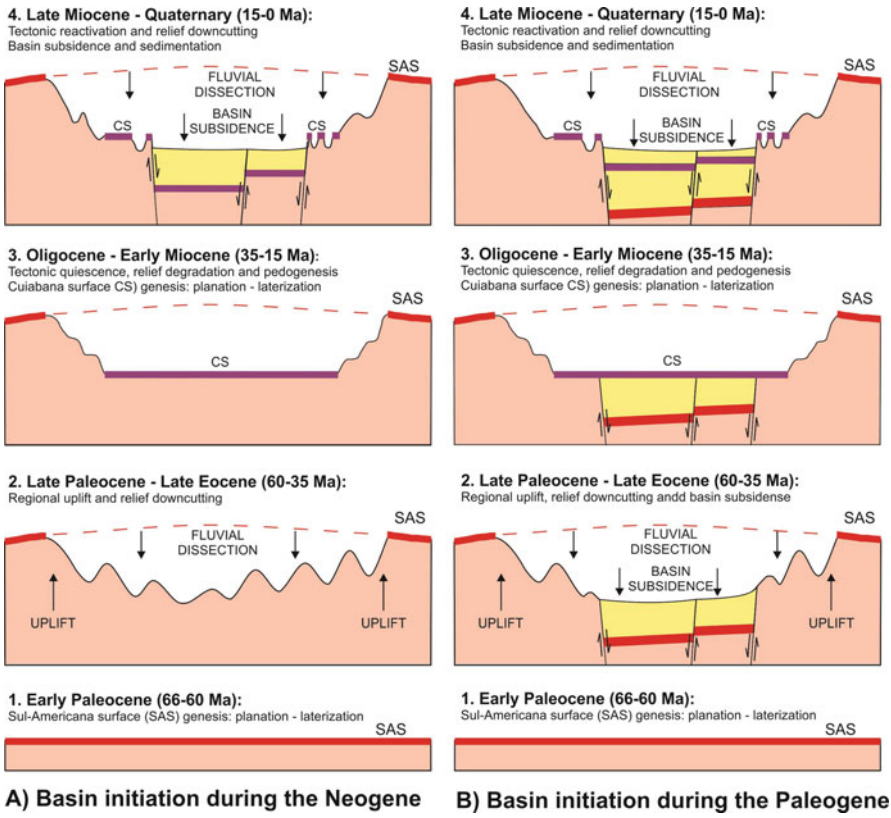

Fig. 4 Schematic diagrams of the Pantanal geologic evolution. (**a**) Basin initiation during the Neogene. (**b**) Basin initiation during the Paleogene

in the schematic diagram of Fig. 4b, which shows a model of geologic evolution in which the Pantanal Basin formed during the Paleogene by brittle tectonics. In this model, subsidence and sedimentation began in the Eocene, synchronously with epeirogenic uplift and tectonism that disrupted the Sul-Americana surface, and relicts from this surface are notionally represented on the basin floor and presently covered by the veneer of Cenozoic alluvial deposits.

The mechanism of basin formation has long been associated with Andes tectonics, an idea first presented by Almeida [36]. More recently, the basin formation was related to the Andean foreland system, more specifically to extensional stress at the forebulge [1, 37]. In contrast, Horton and DeCelles [38] presented a subsidence model in the back-bulge domain of the Andes foreland system, which includes the Chaco Basin as the foredeep area. The hypotheses that link the basin origin to the Andean tectonics are very elegant and exciting, but some of the models assume a forebulge position far away from the thrust front (700 to 1,000 km) and thick lithosphere (100 to 150 km). The question is unsolved, and new information must

be considered to understand the basin formation in detail, such as the negative velocity anomalies of seismic wave propagation at different lithosphere depths below the Pantanal region [39].

3 The Basin Infill and the Modern Depositional Tract Systems

The subsurface data are restricted to eleven boreholes drilled in the 1960s by Petrobras. Unfortunately, the destination of cuttings and cores of these boreholes are unknown and the only information available to the public derives from Petrobras internal reports [40, 41]. The SB-1 borehole drilled 412.5 m of the Pantanal Formation but did not reach the basement (Fig. 2). The lithologic data from this well reveals a monotonous stratigraphic stacking composed almost entirely by immature, fine- to coarse-grained sandstones, exhibiting a subtle tendency of fining upward. The lower section was composed dominantly of coarse-grained sandstones with occasional pebbly sands to conglomeratic intervals. Sandstones are white, yellowish, or brownish, angular to subrounded, with frequent ferruginous cementation and iron oxide concretions. Fine-grained intervals occur locally and are characterized by brown-to-yellowish sandy mudstones, which are most well expressed in the FF-1 well. Chronostratigraphic data are not available, and for this reason, there is no information about the age of the drilled sections.

Lithified debris flow deposits, as well as calcretes and ferricretes, are commonly associated with pediment surfaces in the foothills of highlands surrounding the modern depositional sites. These deposits are not well studied, but collectively they are considered to be Pliocene-Pleistocene in age. Among them, coarse sandstones and matrix-supported conglomerates related to coalesced gravity flow and alluvial fan facies form piedmont slopes on the foothills of the eastern tableland escarpments. Locally, as in the vicinities of the Corumbá urban area, there are siliciclastic and carbonate deposits (tufa) with impressions of angiosperm branches and leaves, as well as gastropod shells of undetermined ages, collectively classified as the Xaraiés Formation [42].

The modern depositional landscape is heterogeneous, which led some authors [2, 43, 44] to subdivide the Pantanal wetland in distinct areas based on diverse criteria like landscape features, flooding dynamics and hydroperiods, flowing rivers, and local names (Fig. 5). The wetland heterogeneity reflects peculiarities of different systems within a huge depositional tract dominated by alluvial sedimentation, where the Paraguay River is the trunk system that collects waters from the entire Upper Paraguay Basin (Fig. 6).

Flowing from north to south, the Paraguay River floodplain exhibits very complex geomorphological characteristics because the river crosses different geological domains and interacts with other depositional systems. Before entering the Pantanal Basin domain, the Paraguay River flows in an aggradational meander belt

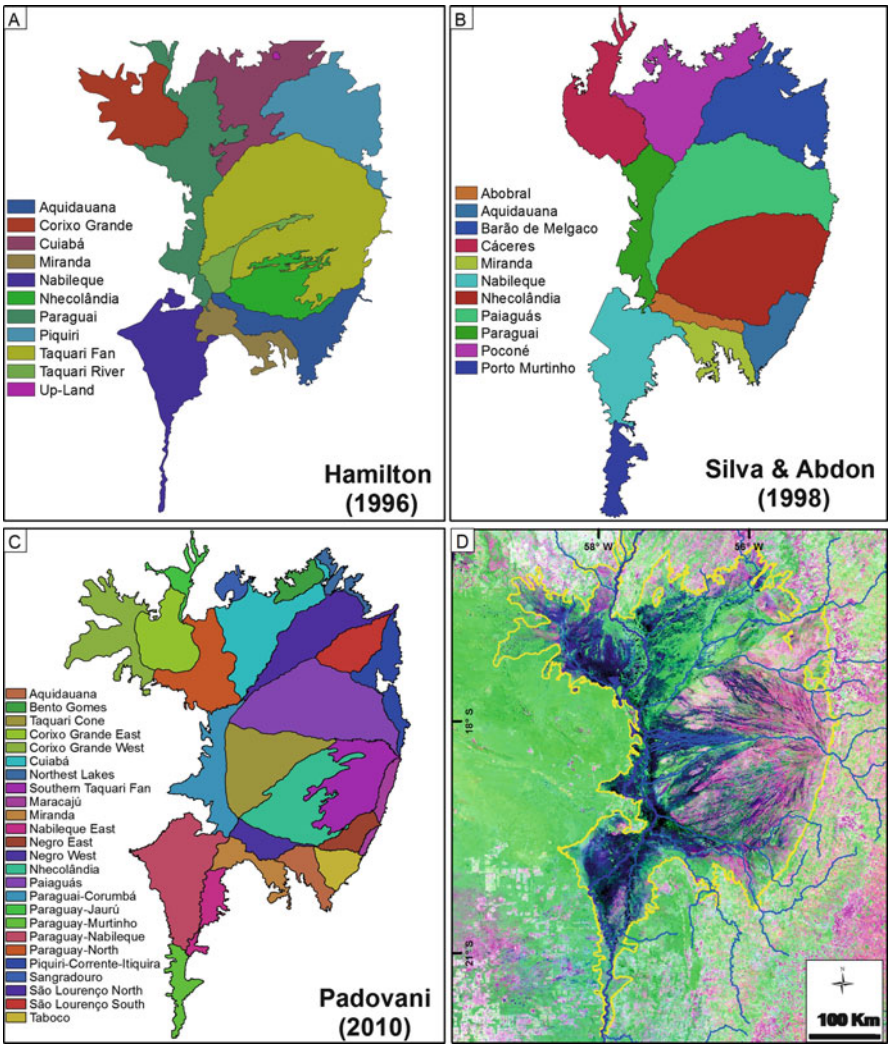

Fig. 5 Three geographic subdivisions proposed for the Pantanal and the outer limits of the wetland adopted in this chapter (Satellite image MODIS from October 2008)

approximately 4–6 km wide, built within a north–northeast-oriented incised valley on Precambrian crystalline rocks (Paraguay-Caceres river plain in Fig. 6). The river forms a fluvial megafan at its entrance into the Pantanal lowlands, because of a loss of valley confinement and decreasing topographic gradient. Paleochannels are preserved on the surface of presumably Pleistocene-aged abandoned fan lobes, forming cross-paleodrainage networks [90]. The topographic gradient abruptly diminishes at the base of the modern depositional lobe and the Paraguay fluvial plain style changes at this locality.

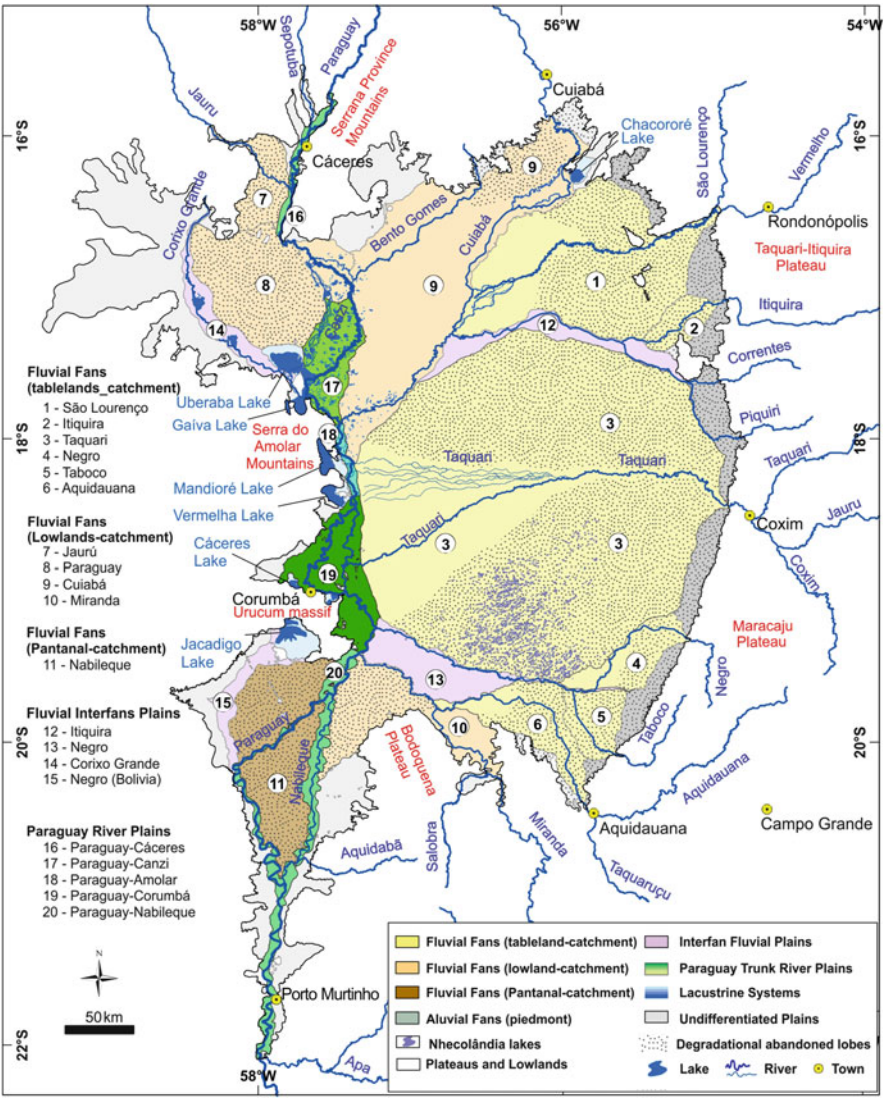

Fig. 6 Depositional tract systems of the Pantanal Basin (M.L. Assine et al. (2015) "in press" in the Brazilian Journal of Geology)

Downstream, the river meanders within a large floodplain, characterized by abandoned meander channels and punctuated by hundreds of small lakes, whose water levels fluctuate in response to annual flood cycles. This fluvial-lacustrine plain (Paraguay-Canzi river plain in Fig. 6) drains waters derived from the Cuiabá River megafan, from nearby hills and undifferentiated marginal plains, and from peripheral channels of the Corixo Grande interfan system.

The Paraguay River floodplain pattern changes in the Serra do Amolar area, where the plain becomes narrow and the river flanks mountainous Precambrian crystalline terranes on its right margin (Paraguay-Amolar river plain in Fig. 6). Aggradation in the meander belt dammed waters coming from Bolivia territory, possibly leading to the formation of the Mandioré and Vermelha lacustrine systems on the right margin of the Paraguay River [45], although the exact mechanism of lake formation is still poorly known. These lakes, surrounded by mountainous Precambrian rocks of the Amolar massif, keep important records for the reconstruction of environmental changes in the Late Quaternary in the Pantanal, a theme discussed in McGlue et al. [46].

The Paraguay River floodplain broadens downstream from the Mandioré Lake to its confluence with the Miranda River (Paraguay-Corumbá river plain in Fig. 6). The river forms a modern meander belt in this reach, superimposed on paleolandforms that formed in distinct preterit hydraulic conditions [47]. After the Miranda River confluence, the Paraguay River crosses into the Nabileque megafan and flows in a narrow, well-defined meander belt incised into Pleistocene-aged deposits. The area is a structural high between the Pantanal and the Chaco basins, where sediment thickness is less than 100 m and small hills of basement rocks crop out. Most of the Nabileque megafan is subject to erosional degradation, but abandoned lobes can be recognized by the existence of an intricate network of distributary paleochannels on its surface (Fig. 7).

The Paraguay River is the trunk system, but most of the deposystem tract is composed of fluvial megafans (Fig. 6). Many megafans are formed by rivers with catchment areas in the dissected sedimentary tablelands located to the east of the Pantanal, where deep fluvial erosion of Paleozoic and Mesozoic rocks has resulted in large sediment yields. Crossing sharp escarpments and leaving the catchment area situated on the plateau, these rivers form huge megafans by depositing their sediment loads due to much reduced topographic gradients on the plains within the Pantanal Basin. The Taquari is the most notable of the Pantanal's megafans, because of its unusual quasi-circular shape and vast area of ~50,000 km^2, making it easily recognizable on satellite images [49, 50], but also notable are the megafans formed by the rivers São Lourenço [51, 52] and Aquidauana [53]. These megafans are complex depositional systems, characterized by modern distal depositional lobes and feeder rivers entrenched in upper fan Pleistocene-aged alluvial deposits. Paleochannels are present on the surfaces of these abandoned alluvial fan lobes, providing evidence of successive avulsions during the Pleistocene, with associated deposition and merging of fluvial sand bodies, which make up the alluvial architecture of the Pantanal Formation (Fig. 8).

Besides the megafans mentioned above, the Cuiabá is another important system because of its dimensions, complexity, and presently active patterns of sediment accumulation [54]. In stark contrast to most of the other Pantanal megafans, the abandoned Cuiabá lobe is small and the modern depositional site is elongated and broad, with many crevasse splays along the main channel and abandoned channels and sandy lobes on the floodplain. Similar to the other megafans in the Pantanal wetland, the Cuiabá river belt is entrenched in the upper fan, where the river

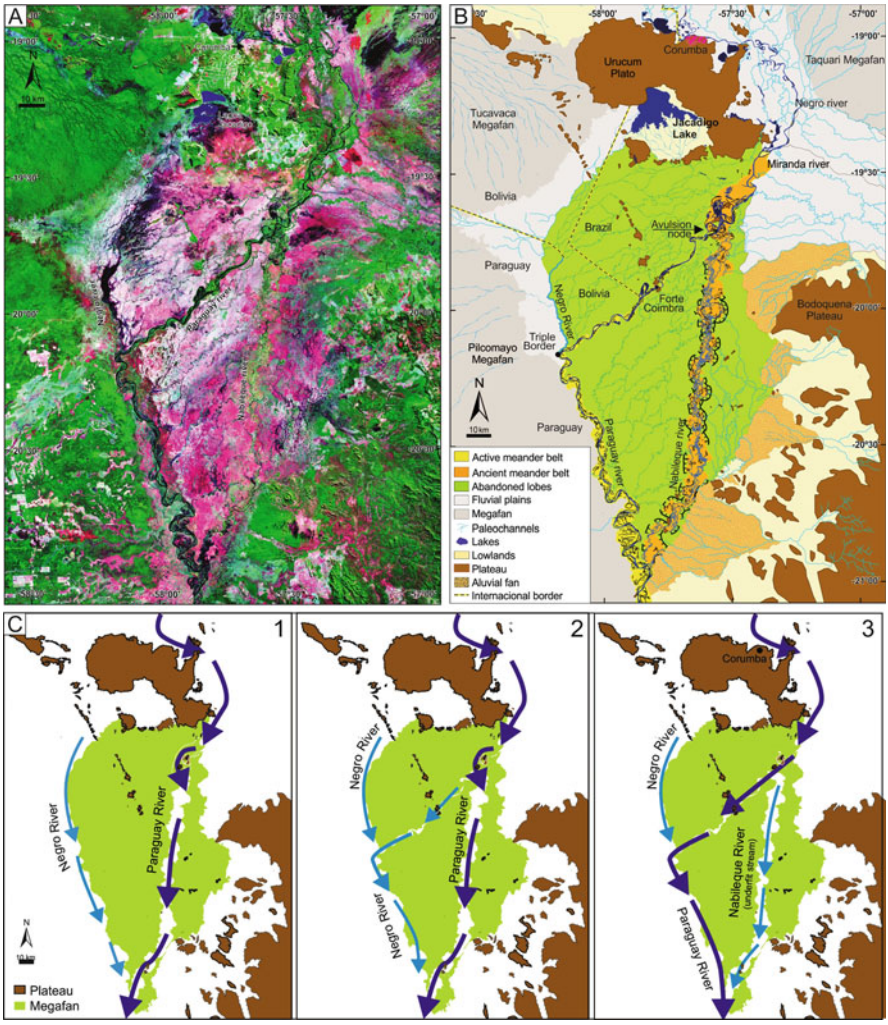

Fig. 7 Paraguay River meander belts (modern and ancient) cutting abandoned lobes of the Nabileque megafan (Modified from [48, 70]). (**a**) Satellite image Landsat Geocover Circas, RGB742, from June 2001 (dry season). (**b**) Geomorphologic zonation showing the actual and the ancient position of the Paraguay River. (**c**) Model of the Paraguay River avulsion

changes style from meandering to anabranching in some reaches. The altitudes range from approximately 160 m at the apex to 95 m at the confluence with the Paraguay River, resulting in a topographic gradient that is less than 0.20 m/km.

Interfan fluvial systems that are present in between megafans serve to collect water and sediments from these larger riverine landforms. The Piquiri River plain is a typical confined meander belt sandwiched between the Taquari and São Lourenço megafans. The Negro River interfan meander belt is another active sedimentary

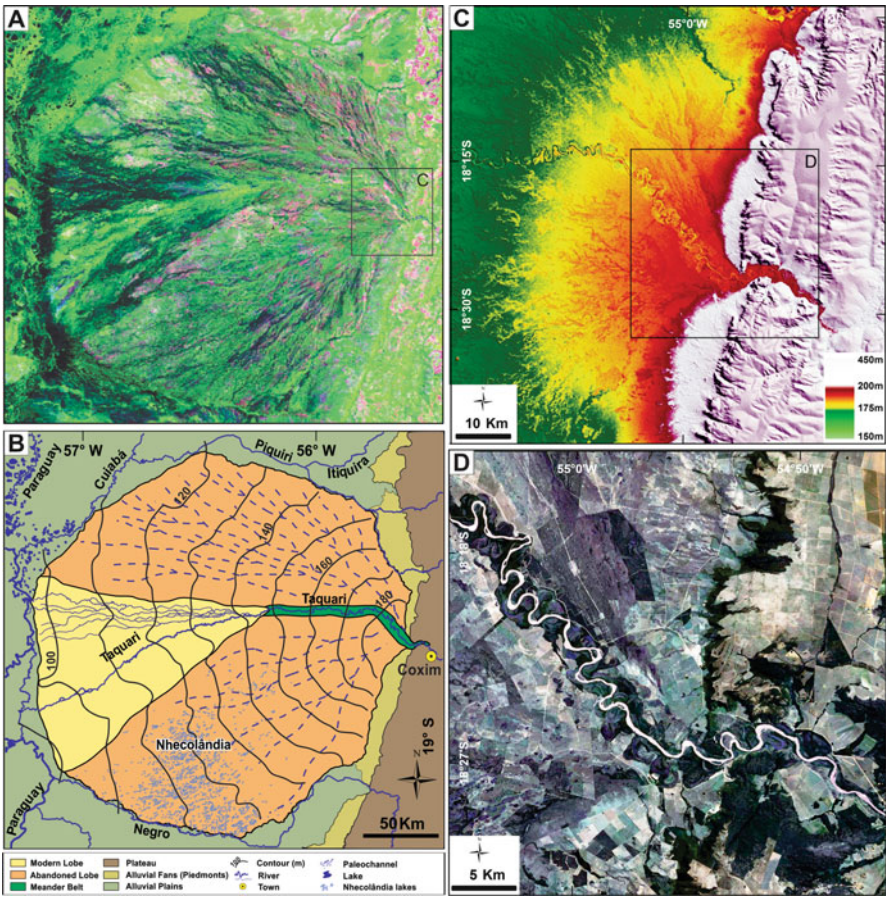

Fig. 8 Taquari fluvial megafan. (**a**) Satellite image MODIS/Terra MOD13Q1 R(MIR) G(EVI) B (Blue) from April 2011 (wet season). (**b**) Geomorphologic zonation showing abandoned and active lobes and the entrenched meander belt in the upper fan (Modified from [50, 54]). (**c**) Incision in the upper fan cutting a network of distributary paleochannels (digital elevation model from Shuttle Radar Topographic Mission (SRTM). (**d**) Actual confined meander belt (Basemap image – ArcGIS Online)

system in between the Taquari to the north and the Aquidauana and Taboco fans to the south. The Negro River floodplain has a more complex configuration than the Piquiri, as the fluvial style changes downstream from an entrenched meander belt that progressively loses confinement to the west, where the river enters in a frequently flooded area and acquires an anabranching pattern.

4 Late Quaternary Landscape Variability

The Pantanal landscape is the product of climatic fluctuations and environmental changes during the Late Quaternary [56]. Braun [49] was the first to mention that the Taquari megafan is mostly comprised of relict depositional landforms that developed under semiarid conditions of the Late Pleistocene. Similar interpretations were put forward in later publications [57, 58]. Ab'Sáber [27], based on regional paleoclimate correlations, argued that the climate was desert-like during the Last Glacial Maximum (LGM), with sparse vegetation (*caatinga*) and intermittent torrential flows along the alluvial fans. These early insights led Clapperton [59] to assume that the modern landscape had been formed during a period of aridity in the Late Pleistocene.

In the central portion of South America, environmental conditions of dry climate and highly seasonal rainfall are mainly ascribed to the Late Pleistocene; this interval is associated with intense fluvial system activity, elevated coarse sediment yield ([60, 91]), and concomitant development of megafans in the Bolivian Chaco [61]. Sediment radiocarbon dating and palynological data support the interpretation of arid conditions in the Late Pleistocene of Pantanal [62, 63]. The combination of poor vegetation cover, strong seasonal precipitation, torrential flow regimes, and high sediment supply from the fringing catchments to the Pantanal Basin led to the development of large distributary systems. Paleodrainage networks are still preserved on the surface of the Taquari megafan abandoned lobes [6, 54, 56, 64]. Well-preserved Late Pleistocene-aged distributary braided paleochannels on the surface of abandoned fan lobes in the upper portion of the São Lourenço megafan are excellent examples of this relict paleodrainage style (Fig. 9) [52].

An important environmental transition occurred near the end of the Pleistocene, where the climate was thought to be relatively dry and colder than present, to wetter and warmer conditions in the Holocene [27, 56]. With increasing fluvial discharge during the Early Holocene [65], river incision occurred at the apical portions of the megafans fed by the rivers Taquari, São Lourenço, and Aquidauana, which all have catchments on sedimentary plateaus located to the east of the Pantanal Basin. The incision moved the intersection point of these systems toward the west, and the modern depositional lobes established in the lower fan settings, with apical lobe positions immediately downstream of the entrenched valleys. Deposition on the modern lobes caused a rise of river equilibrium profiles and aggradation within the incised valleys, which at that time were characterized by the presence of confined meander belts in the upper fan of the Taquari, São Lourenço, and Aquidauana megafans.

As proxy and radiocarbon data [62, 63] are restricted to the Gaíva and Mandioré lakes, situated on the western margin of the Paraguay River and influenced by environments and sediment provenance of the Bolivian Chaco, a very relevant issue to understand the geomorphological evolution of the Pantanal landscape arises: when did the Pantanal become the environment we know today as the world's largest tropical wetland [66]?

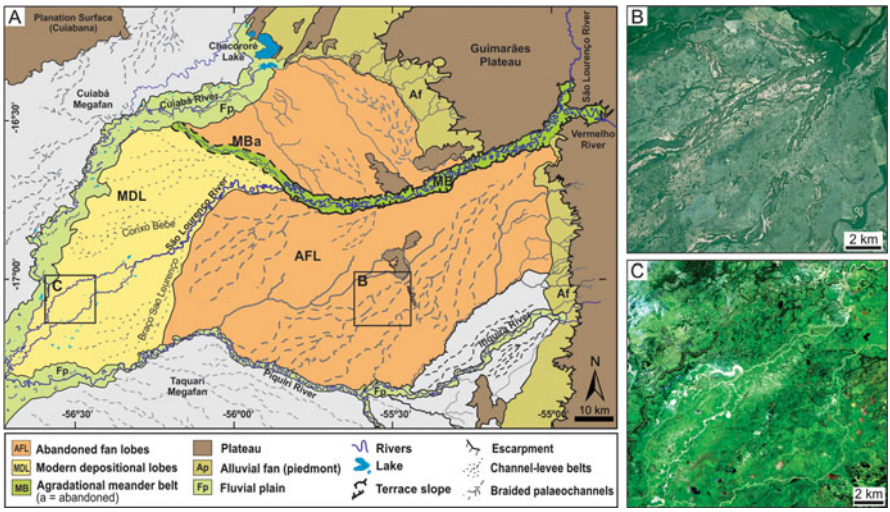

Fig. 9 São Lourenço megafan. (**a**) Geomorphologic zonation (Modified from [51, 52]). (**b**) Distributary braided paleochannels. (**c**) Distributary and anabranching channels that characterize the modern depositional lobe (Satellite image SPOT 5, 2007/2008 mosaic)

The expansion of the Pantanal flooded areas may have begun from the Paraguay River fluvial plain, once it enters into lower relief within the basin; importantly it also serves as the trunk river collecting water from the surrounding plateaus. However, the Paraguay plain has changed in a partitioned and irregular way, which points to the formation of the Negra and Castelo lakes, respectively, at 10,200 and 5,100 years before the present [67, 68]. The rising of the regional groundwater level, controlled by the Paraguay River fluvial plain, which is the base level for the majority of the megafans and fluvial plains of the Pantanal, increased the flooded areas from downstream to upstream for all of the surrounding systems. Humidification was not synchronous nor linear in time, since minor oscillations occurred in the Holocene [63], causing biogeographical changes, especially the revegetation of the area (see modern vegetation on Pott and Silva [69]).

The Paraguay River is confined in a narrow meander belt that is entrenched on Pleistocene deposits in the Nabileque megafan. The modern river course has resulted from a major avulsion that commenced during the mid-Holocene, which caused the Nabileque meander belt to be abandoned (Fig. 7; [50, 70]). The visually striking north–south-oriented paleomeander belt is now occupied by the Nabileque River, an underfit river that is much smaller than the abandoned channels found in the paleomeander belt where it flows.

A similar avulsion phenomenon was discovered for the Paraguay River system, north of Corumbá city. Recognizing three distinct depositional associations, based on cross-cutting relations, Macedo et al. [47] established a relative succession of geomorphic events: (1) an abandoned drainage network that consisted of anabranching, elevated ridges of channels and levees that formed during an initial

period of low river discharge; (2) a set of north–south paleomeander belts cutting through the channel-levee ridges that records an increase of river discharge, probably from the lower to the middle Holocene; and (3) an important avulsion event, probably from the middle to late Holocene, that shifted the river to its present-day meandering belt, forming the Paraguay Mirim underfit river.

Paleo-hydrological changes during Holocene are imprinted on many other Pantanal plains rivers, for example, in the Miranda River, where Merino et al. [71] recognized superimposed belts with different channel widths and meander-bend morphology. All of this evidence of change needs to be dated by absolute techniques and integrated with the various observations of the Paraguay River plain and its marginal lakes in order to reconstruct the way and trends of changing.

5 The Nhecolândia Landscape Enigma

An intriguing feature of the Pantanal Basin geomorphology is the exotic Nhecolândia landscape, which is easily identified through satellite image analysis (Fig. 10). Located in the southern portion of the Taquari megafan, the Nhecolândia is characterized by the presence of more than 10,000 shallow lakes bordered by sand ridges. The lakes are circular to elliptical shapes and they are usually elongated in the NE direction.

Most of the lakes are of freshwater hydrochemistry, invaded by seasonal floodwaters and colonized by a variety of aquatic macrophytes. Approximately 10% of the lakes are isolated from the surface drainage and characterized by the presence of brackish to saline water, which may present greenish color due to a proliferation of cyanobacteria. The existence of alkaline lakes was reported for the first time by Cunha [72], who highlighted the presence of bicarbonate, chlorinated, and sodic waters, with pH values ranging between 8 and 10. The saline lakes are devoid of aquatic vegetation and characterized by white-sandy beaches.

Tributary ephemeral (*vazantes*) and permanent (*corixos*) streams are superimposed on the landscape of lakes and sand ridges, connecting the freshwater lakes and draining floodwaters to the Negro River at the southern border of megafan. The interaction between seasonal flood waters, different floodplain morphologies, and fluctuations of groundwater level controls the location of distinct vegetation, including forests, savannas, wild fields, herbaceous vegetation, aquatic macrophytes, and marsh vegetation [73].

Several authors have attempted to explain the origins of this peculiar Pantanal landscape and the salinity of the isolated ponds. The first attempt to interpret the genesis of this landscape was made by Almeida [42], who suggested a reworking of fluvial sediments by eolian processes, based on the predominance of fine-to-very fine, white, well-sorted, clean, and bimodal sands. In this way, Almeida [36] attributed the origin of the Nhecolândia lakes to depressions caused by wind

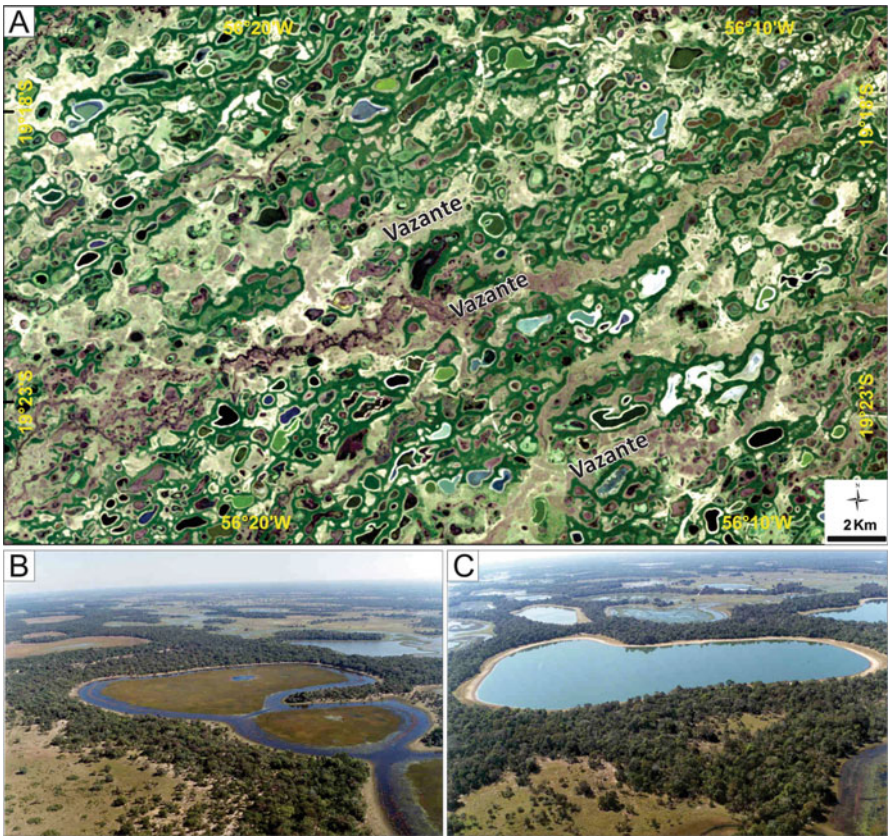

Fig. 10 Nhecolândia landscape. (**a**) Typical morphology of NE–SW-oriented lakes with superimposed modern tributary shallow streams (*vazantes*) in a Landsat TM 5 image RGB321 from July 2008. (**b**) Connected freshwater lakes with characteristic aquatic vegetation. (**c**) Saline lakes with sandy beaches

deflation processes, and Valverde [74] suggested that the ridges are vegetated dunes that formed during earlier desert conditions.

Wilhelmy [75] proposed a completely different genesis hypothesis, suggesting that the lakes formed by confinement of floodplain areas due to cross-cutting and overlapping of marginal levees. Successive lateral migration of the rivers would be responsible for the myriad lakes, an origin hypothesis that was later adopted by Ab'Sáber [27].

Braun [49] viewed the lakes as product of depressions in the alluvial plains developed over karstic terrains. However, this interpretation was considered unlikely by Por [68], arguing that, although karstic environments are common on the Bodoquena plateau surrounding the southern Pantanal, the geological substratum of Nhecolândia consists of thick layers of unconsolidated sandy sediments.

Interpretations based on eolian processes returned to favor in the 1980s. Making use of radar imagery, Klammer [58] interpreted the existence of two trends of fossil longitudinal dunes aligned, NNE–SSW and NNW–SSE, that presumably formed under a regime of constant NNE and NNW paleowinds. Based on satellite images, Tricart [57] interpreted the lakes as hollows produced by wind deflation, similar to those in the Argentine Pampas, and assumed past arid climates gave rise to the presence of saline lakes from relict *sabkhas*. Taking into account the aforementioned interpretations, the Nhecolândia lakes were considered saltpans in the review papers of Goudie [76] and Goudie and Wells [77]. A similar understanding led Clapperton [59] to consider that the Chaco-Pantanal region had an arid climate marked by the formation of dune fields, which resulted from a far south position of the South Atlantic Anticyclone in the terminal Pleistocene.

Despite the evidence and arguments for eolian processes acting in the genesis of Nhecolândia landscape, the origin of these lakes has remained a controversial topic. Some researchers argue that there is no evidence supporting the interpretation of eolian processes and products [78]. One of the greatest criticisms is based on the fact that typical wind-blown sedimentary deposits have not been found, such as dunes fields and cross-bedded sands.

In a test of the eolian hypothesis, no evidence of NNE- and NNW-oriented longitudinal dunes was found on satellite images [6, 56], as identified in the radar images of Klammer [58]. From a sedimentological perspective, it has become clear that the sands do not exhibit the microscopic and morphological characteristics of mature desert sands. Rather, a mixture of grain populations with sediment provenance from Paleozoic and Mesozoic sandstones exposed in the source area was discovered [79]. However, the absence of longitudinal dunes and compositionally mature desert sands is not a sufficient evidence to abandon the notion of a role for eolian processes. It could be the case that the Nhecolândia landscape was dominated by sand sheets with localized lunettes [56], and deflation hollows could be inundated later, for example, accompanying a regional rise of the groundwater level, thus leading to lake formation.

The origins and timing of alkalization and salinization of pond water are another controversial issue. Tricart [57] attributed the salinity to past arid climates, while Ab'Sáber [27] ascribed it to the isolation of oxbow lakes. Alkalinization by recent and presently active biogeochemical [80] and geochemical processes [81–83] has recently been suggested to explain the peculiar composition saline lakes of Nhecolândia. Geochemical studies point out that the saline lakes are the result of equilibrium between water flows and geochemical processes, in which the saline water originates from concentration of fresh vadose zone and groundwater via evaporation [81–83]. New information about ecological and biogeochemistry dynamics of the Nhecolândia alkaline lakes is presented in Bergier et al. [84].

In summary, interpretations about the origin of the Nhecolândia landscape are mainly based on interpretation of satellite data (i.e., indirect), with little sedimentologic information and no reliable dating. New data sources and new lines of interpretation must be pursued in order to reconstruct the processes and events that

have shaped the Nhecolândia landscape since the Late Pleistocene. Thus, the origin of the lakes and their morphology and hydrochemistry remains an enigma!

6 Faults Constraining Sedimentation and Frequently Flood Areas

Basin tectonics plays an important role in the development of the Pantanal landscape, particularly due to their impacts on base levels and topographic gradients. The Paraguay fluvial plain in the western margin of the Pantanal is structurally constrained by faults that separate the floodplain from the Urucum-Amolar dissected plateau. Near the Serra do Amolar, the Paraguay River runs on bedrock composed of Precambrian crystalline rocks of the Cuiabá and Corumbá groups.

To the south, the Paraguay River deflects approximately 90° in the vicinities of the city of Corumbá, and its eastward flow is controlled by WNW–ESE normal faults. Low-grade metamorphic rocks of the Neoproterozoic Corumbá and Cuiabá Groups crop out on the footwall of the fault to the south, where altitudes reach 1,000 m in the Urucum Massif (see [7]). On the right margin of the watercourse in the Corumbá urban area, the river bank locally may be higher than 20 m and consists of Precambrian metamorphic rocks and colluvium capped by carbonates of the Xaraiés Formation.

Near the Corumbá city, the Urucum Massif is characterized by hills surrounded by cliffs and escarpments that are sustained by a capping laterite crust. This juvenile relief is strongly conditioned by faults and fractures and constitutes clear evidence of neotectonic activity along the western border of the Pantanal. Most of the valleys of this geomorphologic province are developed along linear discontinuities with a dominant NE–SW trend; some of these discontinuities are situated around 450 m above the medium topographic surface of Pantanal lowlands, therefore constituting true suspended valleys. In contrast to the uplifted areas and suspended valleys, the subsidence of fault blocks creates accommodation space and low areas subject to periodic flooding.

Several trends of active faults affect modern tributary streams (*corixos* and *vazantes*), conditioning the actual drainage and the water that flows on the surface of abandoned lobes. Quite remarkable are the fractures and faults oriented in a NE–SW direction, supposedly associated with the Transbrasiliano Fault System, a regional geotectonic suture recognized in the area by Soares et al. [85]. There are regional trends of lineaments crossing the Pantanal area, and many attempts have been made to define them using remote sensing (e.g., [86]).

Based on satellite remote sensing data, a study based on the effects of neotectonics on the drainage networks in the alluvial sedimentation revealed four main sets of geologic lineaments that constrain stream direction within the Pantanal wetland (Fig. 11). The NNW–SSE lineaments are well developed on the western margin of the basin, proximal to the flow of the Paraguay River. Particularly

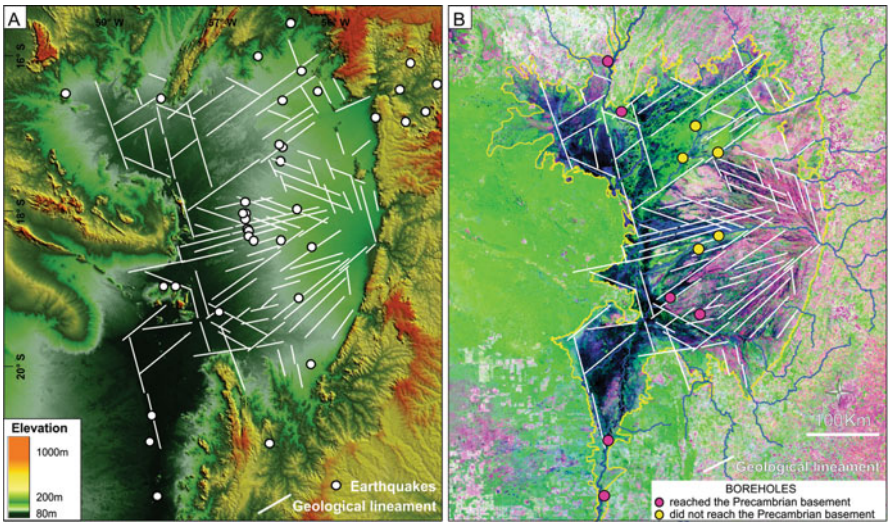

Fig. 11 Geological lineaments of the Pantanal wetland. (**a**) Digital elevation model from Shuttle Radar Topographic Mission (SRTM). (**b**) Satellite image MODIS from October 2008, MOD13Q1 R(MIR) G(EVI) B(Blue)

impressive are the ENE–WSW lineaments, which are clearly recognizable as they cross the modern depositional lobe of the Taquari megafan, where the important Caronal avulsion is in progress.

The southern boundary of the Taquari modern depositional lobe is controlled by NE–SW faults, suggesting that this limit is also associated with the Transbrasiliano Lineament. In this context, the hanging wall block is located on the NW side of the regional fault system, and it constitutes an area subject to high sedimentation rates and strong annual floods.

Subsiding fault blocks are presently creating accommodation space for sedimentation and flooding not only in the modern depositional lobe but also in the lower Negro River course. Perhaps a more striking example of this process can be found along the north portion of the Pantanal, where an important subsiding area, controlled by NE–SW and NNW–SSE faults, is receiving sediments carried from the source area by the rivers Cuiabá, São Lourenço, and Paraguay (Fig. 11). This is a long-lived subsiding area, and of the three deep (~340 m) boreholes drilled here, none reached the basement (Fig. 2). This area is an active depositional site as well and is subject to prolonged flooding events.

Downstream the mouth of the Miranda River, the basement is uplifted and controls the regional base level of the Pantanal, acting as a natural dam for the Pantanal waters. This is one of the reasons for the existence of large, frequently flooded areas in the Paraguay and Negro river floodplains. In the Nabileque megafan, the Paraguay River runs in a meander belt that cuts Pleistocene deposits of the Nabileque megafan. In this area, the sediment thickness is less than 100 m,

and the basement rocks are exposed in isolated hills surrounded by the Nabileque floodplain, as observed in Forte Coimbra and Fecho dos Morros localities.

Recent movements along fault planes have resulted in earthquakes with epicenters located in the Pantanal plains. An earthquake occurred in 1999, with an epicenter near the apex of the modern depositional lobe of the Taquari megafan, and produced a focal mechanism that indicates an E–W compressive stress [87]. Another recent earthquake occurred in 2009, also situated within the Taquari megafan, revealed an epicenter 6 km deep and focal mechanism indicative of a NE–SW compression [88]. These data are consistent with intra-plate seismicity associated with regional maximum horizontal stress directions in central Brazil, characterized by E–W to SE–NW regional compression [89]. However, probably this contemporary regime of stress is associated with tectonic process that is modifying the basin; these are most likely distinct from the tectonic movement that was responsible for basin initiation. As mentioned previously, the tectonic stresses' history of events responsible for basin formation remains unclear and awaits future in-depth studies.

7 Conclusion

Pantanal is an active sedimentary basin with faults and associated earthquakes that delimit the most flood-prone areas. Some new information about the importance of tectonics with respect to the dynamics of the Pantanal depositional system were presented in this chapter. It was emphasized that faults are evident in the basin morphology, conditioning the occurrence of Precambrian terranes at the western edge of the basin and the modern alluvial drainage within the basin. Moreover, crustal movement along these faults causes subsidence of blocks within the basin, creating accommodation space that results in permanently flooded areas. However, a lot of work must be done to comprehend the nature, geometry, and evolution of the basin, as well as the interaction between the geological substrate and the superficial geomorphologic processes. Many questions remain unanswered, awaiting the availability of appropriate tools and new techniques, which is likely to include a dense grid of high-resolution subsurface data. The structural framework of the Pantanal Basin is not yet outlined, and little is known about its neotectonics and its stress field regime.

The basin formation has been related to Quaternary processes associated with the Andean convergent orogen and foreland system, more specifically to extensional stress at the forebulge or a shallow subsidence area in the back-bulge domain, which includes the Chaco Basin as the foredeep area. Nevertheless, as there is no information about the age of the oldest sediments of the Pantanal Basin, it is plausible that the basin initiation dates back to the Eocene, when an important tectonic event of uplift and basin formation took place in the southeast Brazil. The conclusion is that the geological knowledge about the Pantanal Basin formation and evolution is still in its infancy.

Many of the existing morphological features are, in fact, relict forms overprinted on the modern landscape as evidence of distinct past conditions and environments. The Pantanal landscape is the product of climatic fluctuations and hydrological changes that occurred during the Late Quaternary. Radiocarbon dating and palynological data support the interpretation of arid conditions in the Late Pleistocene. The ancient paleodrainage style of this old and arid Pantanal is preserved on the surface of abandoned fan lobes in the upper portion of the São Lourenço and Taquari megafans.

Nevertheless, active processes are continually changing the Pleistocene landscape, either by the erosion of relict landforms or by modern sedimentation in the depositional lobes of fluvial megafans, as well as along the Paraguay River floodplain and tributary interfan river belts. The modern Pantanal wetland emerged due to climate change and increasing fluvial discharge during the Early Holocene. Since then, minor climatic fluctuations have been occurring, which are recorded in the landscape and sedimentary deposits. A good example is the extant Paraguay River course, which has resulted from a major avulsion during the mid-Holocene that caused the Nabileque paleomeander belt to be abandoned.

The Pantanal is a place of changing rivers and public policies must consider this dynamism. To achieve the sustainable development, including conservation policies, it is necessary to understand the natural systems of the Pantanal, its basin origin and evolution, neotectonics and associated subsiding fault blocks, and hydrosedimentological dynamics. In an ever-changing landscape like the Pantanal, the knowledge about the geological history of the region and about the functioning of the several active geological systems can significantly contribute to the rational occupation and preservation of the greatest world tropical wetland.

Acknowledgments The authors thank the São Paulo Research Foundation (FAPESP) (2014/06889-2) for financial support to our research in the Pantanal Basin, the National Council for Scientific and Technological Development (CNPq) for grants to MLA (308563/2013-1), and Filipe Giovanini Varejão and Michele Andriolli Custódio for their assistance in the preparation of figures.

References

1. Ussami N, Shiraiwa S, Dominguez JML (1999) Basement reactivation in a sub-Andean foreland flexural bulge: the Pantanal wetland, SW Brazil. Tectonics 18(1):25–39
2. Padovani CR (2010) Dinâmica das Inundações do Pantanal. Universidade de São Paulo/ESALQ, Piracicaba
3. Junk WJ, Brown M, Campbell IC, Finlayson M, Gopal B, Ramberg L, Warner BG (2006) The comparative biodiversity of seven globally important wetlands: a synthesis. Aquat Sci 68: 400–414
4. Junk WJ, Cunha CN, Wantzen KM, Petermann P, Strüssmann C, Marques MI, Adis J (2006) Biodiversity and its conservation in the Pantanal of Mato Grosso, Brazil. Aquat Sci 68: 279–309

5. Assine ML, Macedo HA, Stevaux JC, Bergier I, Padovani C, Silva A (2015) Avulsive rivers in the hydrology of the pantanal wetland. Hdb Environ Chem. doi:10.1007/698_2015_351
6. Assine ML (2003) Sedimentação na Bacia do Pantanal Mato-Grossense, Centro-Oeste do Brasil. Tese de Livre-Docência, Universidade Estadual Paulista – Unesp, Rio Claro
7. Warren LV, Quaglio F, Simões MG, Freitas BT, Assine ML, Ricommini C (2014) Underneath the pantanal wetland: a deep-time history of Gondwana assembly, climate change, and the dawn of metazoan life. Hdb Environ Chem. doi:10.1007/698_2014_326
8. Assine ML, Soares PC, Milani EJ (1994) Seqüências tectono-sedimentares mesopaleozóicas da Bacia do Paraná, Sul do Brasil. Revista Brasileira de Geociências 24(2):77–89
9. Assine ML, Perinotto JAJ, Alvarenga CJS, Petri S (1998) Arquitetura estratigráfica, tratos deposicionais e paleogeografia da Bacia do Paraná (Brasil) no Neo-Ordoviciano/Eo-Siluriano. Revista Brasileira de Geociências 28:61–76
10. Cogné N, Gallagher K, Cobbold PR, Riccomini C, Gautheron C (2012) Post-breakup tectonics in southeast Brazil from thermochronological data and combined inverse-forward thermal history modeling. J Geophys Res Solid Earth 117(B11), B11413
11. King LC (1956) A geomorfologia do Brasil Oriental. Revista Brasileira de Geografia 18(147–265):147–265
12. Ladeira FSB (2014) Gondwana Paleosurfaces in the State of Rio Grande do Sul, Southern Brazil. In: Rabassa J, Ollier C (eds) Gondwana landscapes in southern South America. Springer, Dordrecht, pp 135–159
13. Valadão RC (2009) Geodinâmica de superfícies de aplanamento, desnudação continental e tectônica ativa como condicionantes da megageomorfologia do Brasil oriental. Revista Brasileira Geomorfologia 10(2):77–90
14. Martonne E (1943) Problemas morfológicos do Brasil tropical atlântico. Revista Brasileira de Geografia 1(4):523–550
15. Almeida FFM (1958) O Planalto Paulistano. In: Azevedo A (ed) A cidade de São Paulo, vol v. 1 (A Região de São Paulo). Associação dos Geógrafos Brasileiros, São Paulo, pp 113–167
16. Ab'Sáber AN, Bigarella JJ (1961) Superfícies aplainadas do primeiro planalto do Paraná. Boletim Paranaense de Geografia 4(5):116–125
17. Retallack GJ (2010) Lateritization and bauxitization events. Econ Geol 105(3):655–667
18. Spier CA, Vasconcelos PM, Oliviera SM (2006) 40 Ar/39 Ar geochronological constraints on the evolution of lateritic iron deposits in the Quadrilátero Ferrífero, Minas Gerais, Brazil. Chem Geol 234(1):79–104
19. Zachos JC, Shackleton NJ, Revenaugh JS, Pälike H, Flower BP (2001) Climate response to orbital forcing across the Oligocene-Miocene boundary. Science 292(5515):274–278
20. Riccomini C, Sant'Anna LG, Ferrari AL (2004) Evolução geológica do rift continental do sudeste do Brasil. In: Mantesso-Neto V, Bartorelli A, Carneiro CDR, Brito-Neves BB (eds) Geologia do continente Sul-Americano: evolução da obra de Fernando Flávio Marques de Almeida. Beca São Paulo, pp 383–405
21. Gallagher K, Hawkesworth C, Mantovani M (1995) Denudation, fission track analysis and the long-term evolution of passive margin topography: application to the southeast Brazilian margin. J South Am Earth Sci 8(1):65–77
22. Hiruma ST, Riccomini C, Modenesi-Gauttieri MC, Hackspacher PC, Neto JCH, Franco-Magalhães AOB (2010) Denudation history of the Bocaina Plateau, Serra do Mar, southeastern Brazil: relationships to Gondwana breakup and passive margin development. Gondwana Res 18(4):674–687
23. Grohmann CH, Riccomini C (2012) Análise digital de terreno e evolução de longo-termo de relevo do centro-leste brasileiro. Geologia USP Série Científica 12(2):129–150
24. CPRM (2004) Mapa geológico e de recursos minerais do Estado de Mato Grosso. CPRM - Serviço Geológico do Brasil, Scale 1:1,000,000. Rio de Janeiro
25. CPRM (2006) Mapa geológico e de recursos minerais do Estado de Mato Grosso do Sul. CPRM – Serviço Geológico do Brasil, Scale 1:1,000,000. Rio de Janeiro

26. Ross JLS, Santos LM (1982) Geomorfologia. In: Brasil (ed) Ministério das Minas e Energia. Secretaria Geral. Projeto RADAMBRASIL. Folha SD.21 Cuiabá, vol (Levantamento de Recursos Naturais, 26). MME/SG/RADAMBRASIL, Rio de Janeiro, pp 193–256
27. Ab'Sáber AN (1988) O Pantanal Mato-Grossense e a teoria dos refúgios. Revista Brasileira de Geografia 50:9–57
28. Almeida FFM (1964) Geologia do centro-oeste mato-grossense. Boletim da Divisão de Geologia e Mineralogia 215:1–133
29. Braucher R, Bourles D, Colin F, Brown E, Boulange B (1998) Brazilian laterite dynamics using in situ-produced 10 Be. Earth Planet Sci Lett 163(1):197–205
30. Pupim FN, Bierman PR, Assine ML, Rood DH, Silva A, Merino ER (2015) Erosion rates and landscape evolution of the lowlands of the Upper Paraguay River basin (Brazil) from cosmogenic 10Be. Geomorphology 234:151–160
31. Catto AJ (1975) Análise geológica e geofísica da Bacia do Pantanal Matogrossense. Rio de Janeiro, Petrobrás, DEPEX/SEDOT report 5296, 23 pp
32. Hackspacher P, Ribeiro L, Ribeiro M, Fetter A, Neto JH, Tello C, Dantas E (2004) Consolidation and break-up of the South American platform in southeastern Brazil: tectonothermal and denudation histories. Gondwana Res 7(1):91–101
33. Ramos VA (2010) The tectonic regime along the Andes: Present day and Mesozoic regimes. Geol J 45(1):2–25
34. Melo MS, Riccomini C, Hasui Y, Almeida FFM, Coimbra AM (1985) Geologia e evolução do sistema de bacias tafrogênicas continentais do sudeste do Brasil. Revista Brasileira de Geociências 15:193–201
35. Almeida FFM, Carneiro CDR (1998) Origem e evolução da Serra do Mar. Revista Brasileira de Geociências 28(2):135–150
36. Almeida FFM (1959) Traços gerais da geomorfologia do Centro-Oeste brasileiro. In: Almeida FFM, Lima MA (eds) Planalto Centro-Ocidental e Pantanal Matogrossense, vol Guia de Excursão n° 1 do XVIII Congresso Internacional de Geografia. Conselho Nacional de Geografia, Rio de Janeiro, pp 7–65
37. Shiraiwa S (1994) Flexura da litosfera continental sob os Andes Centrais e a origem da Bacia do Pantanal. Tese de Doutoramento, Universidade de São Paulo, São Paulo
38. Horton BK, DeCelles PG (1997) The modern foreland basin system adjacent to the Central Andes. Geology 25(10):895–898
39. Feng M, van der Lee S, Assumpção M (2007) Upper mantle structure of South America from joint inversion of waveforms and fundamental mode group velocities of Rayleigh waves. J Geophys Res 112(B4), B04312
40. Weyler G (1962) Projeto Pantanal: relatório final dos poços perfurados no Pantanal Matogrossense. Petrobrás/DEBSP, Ponta Grossa
41. Weyler G (1964) Projeto Pantanal. Relatorio Final de abandono dos poços SBst-1A-MT (São Bento), FPst-1-MT (Faz. Piquiri) e LCst-1A-MT (Lagoa do Cascavel). Petrobras/DEBSP, Ponta Grossa
42. Almeida FFM (1945) Geologia do Sudoeste Mato-grossense. Boletim da Divisão de Geologia e Mineralogia 116:19–25
43. Hamilton SK, Sippel SJ, Melack JM (1996) Inundation patterns in the Pantanal wetland of South America determined from passive microwave remote sensing. Archiv für Hydrobiologie 137(1):1–23
44. Silva JSV, Abdon MM (1998) Delimitação do Pantanal brasileiro e suas sub-regiões. EMBRAPA 33 (Especial) 1703–1711
45. McGlue MM, Silva A, Corradini FA, Zani H, Trees MA, Ellis GS, Parolin M, Swarzenski PW, Cohen AS, Assine ML (2011) Limnogeology in Brazil's "forgotten wilderness": a synthesis from the large floodplain lakes of the Pantanal. J Paleolimnol 46(2):273–289
46. McGlue MM, Silva A, Assine ML, Stevaux JC, Cruz FW (2015) Paleolimnology in the pantanal: using lake sediments to track quaternary environmental change in the world's largest tropical wetland. Hdb Environ Chem. doi:10.1007/698_2015_350

47. Macedo HA, Assine ML, Pupim FN, Merino ER, Stevaux JC, Silva A (2014) Mudanças paleo-hidrológicas na planície do rio Paraguai, Quaternario do Pantanal. Revista Brasileira Geomorfologia 15:75–85
48. Kuerten S, Assine ML (2011) O rio Paraguai no megaleque do Nabileque, sudoeste do Pantanal Mato-Grossense, MS. Revista Brasileira de Geociências 41(4):642–653
49. Braun EWG (1977) Cone aluvial do Taquari, unidade geomórfica marcante da planície quaternária do Pantanal. Revista Brasileira Geografia 39(4):164–180
50. Assine ML (2005) River avulsions on the Taquari megafan, Pantanal wetland, Brazil. Geomorphology 70(3–4):357–371
51. Corradini FA, Assine ML (2012) Compartimentação geomorfológica e processos deposicionais no megaleque fluvial do rio São Lourenço, Pantanal mato-grossense. Revista Brasileira de Geociências 42:20–33
52. Assine ML, Corradini FA, Pupim FN, McGlue MM (2014) Channel arrangements and depositional styles in the São Lourenço fluvial megafan, Brazilian Pantanal wetland. Sediment Geol 301:172–184
53. Facincani EM, Assine ML (2010) Geomorfologia fluvial do rio Aquidauana, borda sudeste do Pantanal Mato-Grossense. In: Martins Junior C, Oliveira Neto AF (eds) Revelando Aquidauana. Serie Fronteiras n° 3. Editora da UFMS, Campo Grande, pp 267–284
54. Zani H, Assine ML, McGlue MM (2012) Remote sensing analysis of depositional landforms in alluvial settings: Method development and application to the Taquari megafan, Pantanal (Brazil). Geomorphology 161–162:82–92
55. Pupim FN (2014) Geomorfologia e paleo-hidrologia dos megaleques dos rios Cuiabá e São Lourenço, Quaternário da Bacia do Pantanal. Universidade Estadual Paulista – Unesp, Rio Claro
56. Assine ML, Soares PC (2004) Quaternary of the Pantanal, west-central Brazil. Quat Int 114(1): 23–34
57. Tricart J (1982) El Pantanal: un ejemplo del impacto geomorfologico sobre el ambiente. Informaciones Geograficas (Chile) 29:81–97
58. Klammer G (1982) Die Paläovüste des Pantanal von Mato Grosso und die pleistozäne Klimageschichte der brasilianischen Randtropen. Zeitschrift für Geomorphologie 26(4): 393–416
59. Clapperton C (1993) Quaternary Geology and Geomorphology of South America. Elsevier, Amsterdam
60. May JH, Zech R, Veit H (2008) Late Quaternary paleosol–sediment-sequences and landscape evolution along the Andean piedmont, Bolivian Chaco. Geomorphology 98:34–54
61. Latrubesse EM, Stevaux JC, Cremon EH, May J-H, Tatumi SH, Hurtado MA, Bezada M, Argollo JB (2012) Late Quaternary megafans, fans and fluvio-aeolian interactions in the Bolivian Chaco, Tropical South America. Palaeogeogr Palaeoclimatol Palaeoecol 356–357: 75–88
62. Whitney BS, Mayle FE, Punyasena SW, Fitzpatrick KA, Burn MJ, Guillen R, Chavez E, Mann D, Pennington RT, Metcalfe SE (2011) A 45kyr palaeoclimate record from the lowland interior of tropical South America. Palaeogeogr Palaeoclimatol Palaeoecol 307(1–4):177–192
63. McGlue MM, Silva A, Zani H, Corradini FA, Parolin M, Abel EJ, Cohen AS, Assine ML, Ellis GS, Trees MA, Kuerten S, Gradella FS, Rasbold GG (2012) Lacustrine records of Holocene flood pulse dynamics in the Upper Paraguay River watershed (Pantanal wetlands, Brazil). Quat Res 78(2):285–294
64. Zani H, Assine ML (2011) Paleocanais no megaleque do rio Taquari: mapeamento e significado geomorfológico. Revista Brasileira de Geociências 41:37–45
65. Chiessi CM, Mulitza S, Pätzold J, Wefer G (2010) How different proxies record precipitation variability over southeastern South America. Earth and Environmental Science IOP Conference Series, vol 9, 012007
66. Por FD (1995) The Pantanal of Mato Grosso (Brazil) – World's Largest Wetlands. Kluwer Academic, Dordrecht

67. Bezerra MAO (1999) O Uso de Multi-traçadores na Reconstrução do Holoceno no Pantanal Mato-grossense, Corumbá, MS. Tese de Doutorado, Universidade Federal de São Carlos, São Carlos
68. Bezerra MAO, Mozeto AA (2008) Deposição de carbono orgânico na planície de inundação do Rio Paraguai durante o Holoceno médio. Oecologia Bras 12:155–171
69. Pott A, Silva JSV (2015) Terrestrial and aquatic vegetation diversity of the pantanal wetland. Hdb Environ Chem. doi:10.1007/698_2015_352
70. Kuerten S, Parolin M, Assine ML, McGlue MM (2013) Sponge spicules indicate Holocene environmental changes on the Nabileque River floodplain, southern Pantanal, Brazil. J Paleolimnol 49(2):171–183
71. Merino ER, Assine ML, Pupim FDN (2013) Estilos fluviais e evidências de mudanças ambientais na planície do rio Miranda, Pantanal. Revista Brasileira Geomorfologia 14(2): 127–134
72. Cunha J (1943) Cobre de Jaurú e lagoas alcalinas do Pantanal (Mato Grosso). Boletim DNPM/ LPM 6:1–53
73. Evans TL, Costa M (2013) Landcover classification of the Lower Nhecolândia subregion of the Brazilian Pantanal Wetlands using ALOS/PALSAR, RADARSAT-2 and ENVISAT/ ASAR imagery. Remote Sens Environ 128:118–137
74. Valverde O (1972) Fundamentos geográficos do planejamento do Município de Corumbá. Revista Brasileira de Geografia 34:49–144
75. Wilhelmy H (1958) Umlaufseen and dammuferseen tropischer tiefland flüsse. Zeitschrift fur Geomorphologie NF 2:27–54
76. Goudie AS (1991) Pans. Prog Phys Geogr 15(3):221–237
77. Goudie AS, Wells GL (1995) The nature, distribution and formation of pans in arid zones. Earth Sci Rev 38(1):1–69
78. Colinvaux PA, Oliveira PE, Bush MB (2000) Amazonian and neotropical plant communities on glacial time-scales: the failure of the aridity and refuge hypotheses. Quat Sci Rev 19: 141–169
79. Soares AP, Soares PC, Assine ML (2003) Areiais e lagoas do Pantanal, Brasil: herança paleoclimática? Revista Brasileira de Geociências 33:211–224
80. Almeida TIR, Calijuri MC, Falco PB, Casali SP, Kupriyanova E, Paranhos Filho AC, Sigolo JB, Bertolo RA (2011) Biogeochemical processes and the diversity of Nhecolândia lakes, Brazil. Anais da Academia Brasileira de Ciências 83:391–407
81. Barbiéro L, Queiróz-Neto JP, Ciornei G, Sakamoto AY, Cappelari B, Fernandes E, Valles V (2002) Geochemistry of water and groundwater in the Nhecolândia, Pantanal of Mato Grosso, Brazil: variability and associated process. Wetlands 22(3):528–540
82. Furquim SAC, Graham RC, Barbiero L, Queiroz Neto JP, Vidal-Torrado P (2010) Soil mineral genesis and distribution in a saline lake landscape of the Pantanal Wetland, Brazil. Geoderma 154(3–4):518–528
83. Furian S, Martins ERC, Parizotto TM, Rezende-Filho AT, Victoria RL, Barbiero L (2013) Chemical diversity and spatial variability in myriad lakes in Nhecolândia in the Pantanal wetlands of Brazil. Limnol Oceanogr 58(6):2249–2261
84. Bergier I, Krusche A, Guérin F (2014) Alkaline lakes dynamics in the Nhecolândia landscape. Hdb Environ Chem. doi:10.1007/698_2014_327
85. Soares PC, Assine ML, Rabelo L The Pantanal Basin: recent tectonics, relationships to the Transbrasiliano Lineament. In: 9th Simpósio Brasileiro de Sensoriamento Remoto, Santos, 1998. INPE – São José dos Campos, pp 459–469
86. Paranhos Filho AC, Nummer AR, Albrez EA, Ribeiro AA, Machado R (2013) A study of structural lineaments in Pantanal (Brazil) using remote sensing data. Ann Braz Acad Sci 85(3):913–922
87. Ussami N, Padilha AL, Fisseha S, Porsani JL, Souza LAP, Boggiani PC, Carvalho MJ (2000) Investigações geofísicas integradas na planície do Pantanal Mato-Grossense: implicações

tectônicas e hidrogeológicas de sub-superfície. 3° Simpósio sobre Recursos Naturais e Sócio-Econômicos do Pantanal, Corumbá, Resumos, p 125
88. Dias F, Assumpção M, Facincani EM, França GS, Assine ML, Paranhos Filho AC, Gamarra RM. The 2009 earthquake, magnitude 4.8 mb, in the Pantanal Wetlands, west-central Brazil, Anais da Academia Brasileira de Ciências, submitted
89. Assumpção M, Sacek V (2013) Intra-plate seismicity and flexural stresses in central Brazil. Geophys Res Lett 40(3):487–491
90. Assine ML, Silva A (2009) Contrasting fluvial styles of the Paraguay River in the northwestern border of the Pantanal wetland, Brazil. Geomorphology 113(3–4):189–199
91. May JH, Veit H (2009) Late quaternary paleosols and their paleoenvironmental significance along the Andean piedmont, Eastern Bolivia. Geomorphology 100–116

Paleolimnology in the Pantanal: Using Lake Sediments to Track Quaternary Environmental Change in the World's Largest Tropical Wetland

Michael M. McGlue, Aguinaldo Silva, Mario L. Assine, José C. Stevaux, and Fabiano do Nascimento Pupim

Abstract In spite of its global significance to biodiversity and biogeochemical cycles (e.g., as a methane source and carbon dioxide sink), the Pantanal of western Brazil remains underexplored from the perspective of Quaternary paleoecology, paleogeography, and paleoclimatology. Long in the scientific and cultural shadow cast by the Amazon Basin, recent research using lake sediment cores from different sites across the Pantanal lowlands has provided a glimpse at the sensitivity of this savanna floodplain wetland to climate-driven perturbations in the hydrologic cycle. Understanding the controls and feedbacks associated with this sensitivity is important, as the Pantanal is a critical freshwater resource situated in the headwaters of the immense Río de la Plata Basin. Published lake sediment archives have adopted a multi-indicator analytical approach, focusing on physical sedimentology, geochemistry, palynology, and siliceous microfossils. Such studies extend in time from the late Pleistocene to the present day, with the greatest emphasis placed on reconstruction of the Holocene environmental history. Several important transitions in effective precipitation have been inferred for the Holocene, which appear to be dominantly linked to variability in insolation and the South American Summer

M.M. McGlue (✉)
Department of Earth and Environmental Sciences, University of Kentucky, Lexington, KY 40506, USA
e-mail: michael.mcglue@uky.edu

A. Silva
Department of Geography, Federal University of Mato Grosso do Sul, Corumbá, Brazil

M.L. Assine and J.C. Stevaux
Applied Geology Department, Geosciences and Exact Sciences Institute, Paulista State University, Av. 24A, 1515, Rio Claro 13506-900, Brazil

F.d.N. Pupim
Geosciences Institute, University of São Paulo (USP), Rua do Lago, 562, São Paulo 05508-080, Brazil

I. Bergier and M.L. Assine (eds.), *Dynamics of the Pantanal Wetland in South America*, Hdb Env Chem (2016) 37: 51–82, DOI 10.1007/698_2015_350,

Monsoon system. By contrast, evidence of aridity in the Pantanal during the Last Glacial Maximum suggests that the wetlands also respond in a complex manner to Northern Hemisphere ice volume and that insolation forcing alone fails to fully explain patterns of environmental change. The great diversity of lacustrine ecosystems in the Pantanal warrant additional study and hold the potential to broaden our understanding of the response of tropical wetlands to global change. Such insights will be valuable for conservation planning, resource security, and sustainable management.

Keywords Brazil, Lakes, Sediment cores, Tropical paleoclimatology, Wetlands

Contents

1 Introduction

For centuries, the vast Pantanal wetlands of central South America have fascinated explorers and scientists, to include such luminaries as Theodore Roosevelt and Cândido Rondon, who famously conducted an expedition through part of the region in the early twentieth century. Responding sensitively to the flood pulse of the Upper Paraguay River, the landlocked Pantanal remains one of South America's great wilderness waterways (Fig. 1; [1]). The annual dynamics of Upper Paraguay River flooding are a key facet controlling the form and function of these wetlands, and pursuit of a deeper temporal understanding of the Paraguay River flood pulse is quite understandably a major goal of Pantanal research. The Pantanal is best characterized as a mosaic of seasonally inundated savanna floodplains with spectacular flora and fauna [2, 3]. Numerous studies have made it clear that the Pantanal is important to global biogeochemical cycles (particularly for the atmospheric trace gases CH_4 and CO_2 [4]; see also [5, 6]) and patterns of Neotropical biodiversity [3]. At the regional scale, the wetlands are socioeconomically vital by providing a host of ecosystem services to Brazil, Bolivia, and Paraguay, including nutrient

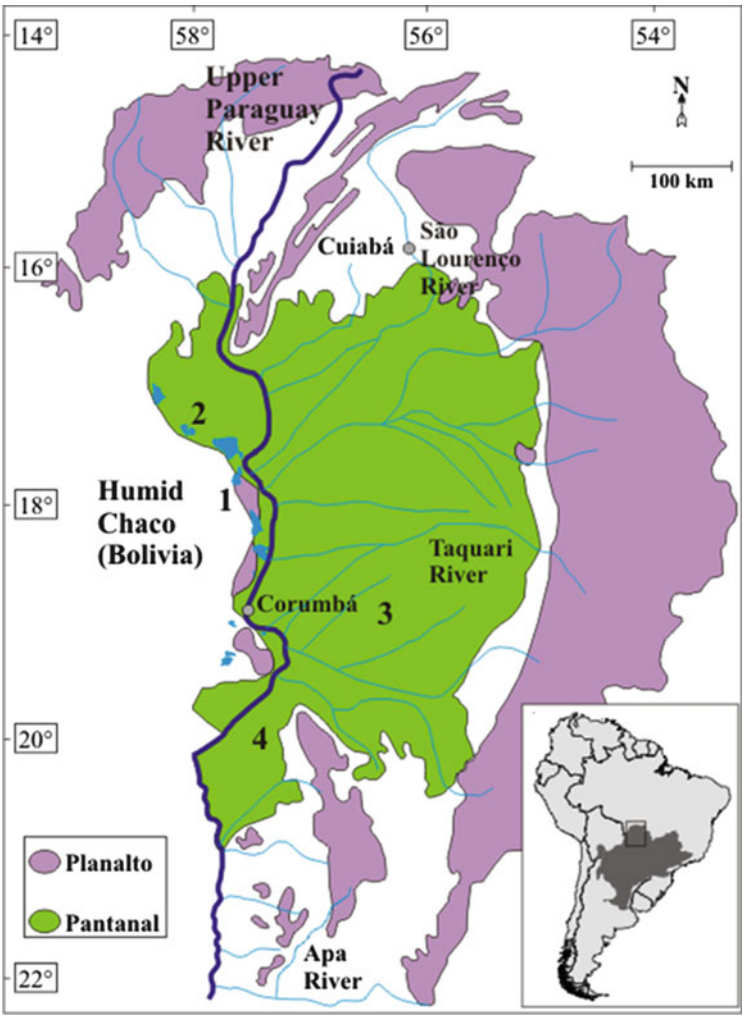

Fig. 1 Overview map of the Pantanal Basin. *Inset map* shows the location of the Pantanal in central South America (*light gray*), situated in the headwaters of the vast Río de la Plata watershed (*dark gray*). The Upper Paraguay River flows to the south along the western margin of the basin. (*1*) Location of the large floodplain lakes of the Pantanal, the subject of several recent paleolimnological studies. Some of these lakes are illustrated in detail on Fig. 5. (*2*) Location of large floodplain lakes along the distal toe of the Paraguay fluvial fan. These lakes are illustrated in detail on Fig. 6. (*3*) Nhecolândia region of the Pantanal, home to many thousands of deflation lakes; southern Nhecolândia is shown in Fig. 3. (*4*) Nabileque River megafan region. Oxbow lakes of the Nabileque River megafan are illustrated in Fig. 2

cycling, fish spawning grounds, rookery space, fertile agriculture, ranching, transportation, and recreation. Moreover, the Pantanal serves as the headwaters of the greater Paraguay-Parana River Basin, which acts as a freshwater resource for growing populations in southern South America, to include the large cities of the Mar de la Plata in Argentina and Uruguay.

Both natural and human-induced environmental changes threaten the ecologically sensitive Pantanal [1, 7], and these risks have motivated research aimed at understanding how the wetlands have responded to ancient changes in temperature and precipitation known to have affected the South American tropics [8–10]. However, efforts to study the Quaternary environmental history of the Pantanal wetlands are still in their infancy, due in large part to difficult operational conditions and the remote setting that renders acquisition of field data nearly as challenging as it was during the *Expedição Científica Rondon-Roosevelt* (1913–1914). However, this situation is improving, and a number of access points with infrastructure for logistical support now exist. Access to the heart of the Pantanal is best accomplished via the Upper Paraguay River from Corumbá, the frontier port in Mato Grosso do Sul state of western Brazil. Prospective international researchers are advised to establish collaborations with the community of Brazilian scientists working in the Pantanal to avoid potential legal complications (e.g., [11]). The Federal University of Mato Grosso do Sul State maintains a campus in Corumbá, which is growing into a center of excellence dedicated to geographic and environmental studies of the wetlands.

Most of the early hypotheses related to the influence of climate change on the Pantanal were developed using evidence gleaned from remote sensing data (e.g., [12, 13]), which is a tradition that continues today among many fluvial geomorphologists, albeit now with more highly resolved satellite imagery, the benefit of advanced computer processing, and improved access to sediment ground truth (e.g., [14–18]). Remote sensing techniques have the advantage of imaging large swaths of low-gradient floodplain, allowing scientists to discern difficult-to-access landforms, in some instances over different seasons and extents of fluvial inundation. To cite prominent early examples, Klammer [19] and Tricart [13] observed what appeared to be lunettes along the marginal fringes of shallow pans across parts of the Taquari River megafan, which they interpreted to have formed when the Pantanal experienced desertlike conditions during an interval of persistent aridity. Hamilton et al. [20] used a time series (1979–1987) of passive microwave remote sensing data to track inundation patterns across the Pantanal, which has obvious linkages to rainfall variability and wetland physiography. Assine and Silva [15] used satellite data to hypothesize about climatic influences on patterns of floodplain entrenchment and valley fill in the Paraguay River megafan, situated in the little-explored northern fringes of the Pantanal. Assine et al. [21] utilized remote sensing analysis to guide sediment coring and luminescence dating of different depositional landforms of the São Lourenço fluvial megafan (northeast Pantanal). This fully integrated approach allowed for a more comprehensive assessment of both geomorphology and Quaternary sediment accumulation history and provided a roadmap for future studies of this kind.

Whereas the aforementioned studies centered primarily on remote sensing techniques, other researchers have directly sampled geological materials. To date, archives of hydroclimatic and paleoecological information that have been assessed to probe the Pantanal's Quaternary history include lake sediments, alluvial/floodplain strata, terrestrial carbonates (speleothems, riverine tufas), and soil profiles [22–31]. A comprehensive review of all these studies is beyond the scope of this chapter, but many of the published records are either short or temporally punctuated, which is typical of many paleoclimate records from the South American lowlands [32]. Therefore, more is known about the Holocene (approximately 11.9 cal ka – present) than the Pleistocene evolution of the Pantanal wetlands.

Nonetheless, snapshots of Quaternary history can be recorded by the deposits accumulating in many of the Pantanal's lake basins. Ruddiman [33] highlighted the value of lacustrine sediments for understanding Earth's variable climate and its impact on the continents. Paleolimnology as a discipline operates from the premise that ancient lake sediments can, in certain instances, provide highly detailed and datable archives of environmental variability, albeit with the limitations imposed by so-called "hydroclimate filters," which themselves may vary over time [34]. Thus, the signal recorded by any individual geological, biological, or chemical indicator (e.g., carbonate content, particle size, diatom assemblages, pollen, among many others) recovered from a lake sediment core is potentially complex and ideally will be constrained by extensive modern limnogeological information. Because the Pantanal is very much a "land of lakes" [35], paleolimnological studies have inescapably played a role in constraining the effects of Quaternary climate change on the wetland mosaic. In fact, early maps (circa 1600) of tropical South America depicted the Pantanal as a single large lake referred to as *Laguna de los Xarayes*, after a supposed group of Indians inhabiting its margins [36]. This misconception among cartographers of the New World arose from the dramatic influence of Upper Paraguay River flooding during the austral summer, the process which exerts the single most important influence governing the hydroclimate filters of many of the Pantanal's lake systems today. Whether a large lake occupied the Pantanal Basin very early in its depositional history is not clearly known, although lithology logs developed from a few exploration wells drilled by Petrobras do not contain evidence for a widespread and persistent lacustrine system [37, 38]. Much more research is clearly needed to understand the early formation of the Pantanal – answers to questions related to basin geodynamics, linkages to Andean orogenesis and the South American Summer Monsoon, and biogeographic evolution await this future work.

In this chapter, we provide a review of paleolimnological records that have been published for the Pantanal, which in the past decade have appeared with greater frequency than in prior years. A number of important studies that use lake sediments have provided a more nuanced understanding of the Holocene hydrologic history of the wetlands and phytogeographic history of the basin, although much complexity marks these records and fertile ground exists for innovation. Only a few lakes have received detailed study, with most of these studies focusing on singular sediment cores recovered from the deepest regions of relatively shallow basins.

Core recovery techniques have emphasized either vibrocoring a desiccated landform or manual pushing or hammering of a piston coring device from a floating platform into the lake floor, either as a single drive or in overlapping segments (e.g., [22, 28, 30, 31]). The indicators or proxies used in these studies vary greatly (as do the techniques used to generate these data), from pollen and siliceous microfossils to organic matter geochemistry and siliciclastic sediments. In general, radiocarbon or optically stimulated luminescence dates have been used to develop the chronology of lake sediment cores in the Pantanal, although the sampling density and strategy usually vary a great deal. Our goal is to synthesize the information currently known, to consider the strengths and weaknesses of the data that have appeared, and to use this context to explore some fruitful future research directions for this fascinating and enigmatic wetland system.

2 The Pantanal: Overview

The reader is referred to other chapters in this volume for extensive details on the geology, hydrology, biology, and climate of the Pantanal. The overviews provided by Por [35] and Heckman [39], as well as the synthetic volume edited by Swarts [40], are other published resources that should be mined for an introduction to natural science in the Pantanal. We limit our remarks to a brief description of the Pantanal Basin and focus our attention on the environmental processes and gradients that notionally influence the interpretation of lake sediment records.

The Pantanal Basin is located in the Southern Hemisphere subtropics (~16–21°S latitude, ~55–58°W longitude; Fig. 1); the wetlands span the international borders of Brazil, Bolivia, and Paraguay, but the majority of this system lies within Brazil. The Pantanal Basin is a prominent feature in central South America due to its approximate "spoon shape" in map view [41, 42]. The center of the basin sits at low altitude (typically $<$200 m above sea level) and is comprised of Quaternary alluvium, whereas a prominent plateau ("planalto") that consists of resistant Devonian and Neoproterozoic rocks surrounds the basin on its eastern and northern margins [43]. In contrast, the western margin of the Pantanal, which borders the humid Chaco plains of eastern Bolivia, is much more diffuse. This region is largely defined by the position of the Upper Paraguay River, which flows from north to south in complex styles with meandering and anabranching patterns, making several sharp directional changes along its course (Fig. 1). Although not extensively studied, it is probable that intra-basinal faults and neotectonic deformation influence the position and geometry of the river along strike [42–44]. The geology of the western margin is notable for small remnants of a late Proterozoic fold-and-thrust mountain belt, whose strata host economically valuable iron ore deposits and are purported to contain glaciogenic features that date to the Cryogenian [45]. These remnants form the most prominent hills in the basin, but it should be emphasized that relief is otherwise limited. Because the age of the Pantanal is not rigorously constrained by absolute geochronometers, the total amount of time encompassed by

the approximately 500 m of strata in the basin remains unknown. Most estimates suggest the basin is no older than Pliocene [43], which is consistent with what is currently understood about Andean geodynamics, assuming the Pantanal is indeed a back-bulge basin as has been suggested [41, 46, 47]. This major gap in our understanding of basin evolution is one of the great challenges confronting Quaternary scientists studying the evolution of the Pantanal wetlands from a geological perspective.

Several large rivers enter the Pantanal from the north and east, forming low-gradient megafans draining toward the Upper Paraguay River, which serves as the local base level (Fig. 1; [14]). Climate in the Pantanal is strongly influenced by the seasonal migration of the Intertropical Convergence Zone (ITCZ) and the South American Summer Monsoon (SASM; [48]). Precipitation is heaviest during the austral summer (December, January, February [DJF]), when >1,000 mm of rain falls in the northern and central Pantanal in a single prolonged wet season that lasts approximately from October to April. The southern Pantanal receives slightly less rainfall, which produces a latitudinal climatic gradient in the basin. The mean annual temperature is ~25°C and evaporation exceeds precipitation during most of the year [35]. In terms of its vegetation, the Pantanal blends significant tracts of Planalto-derived *cerrado* (tropical savanna) with Amazonian semi-deciduous forest, seasonal dry forest of Chaco affinity, and aquatic plants [49]. Pinder and Rosso [50] have suggested that the spatial distribution of plants is controlled by patterns of flooding, elevation, and soil type (see also [51]).

The arrival of summer rainfall, and with it the Upper Paraguay River flood pulse, dramatically alters the hydrology of the Pantanal. The flood pulse is the defining hydrologic feature of the Pantanal because it causes the stage height of the Upper Paraguay River to rise by several meters across the basin [52]. Retention of the Upper Paraguay River flood pulse in the northern Pantanal (through floodplain storage processes; [1]) delays the onset of full inundation in the central and southern Pantanal by several months. The flood pulse is responsible for widespread inundation of megafan floodplains due to creation of a pronounced "backwater effect," as tributaries swollen with rainfall reverse flow after encountering the rising stage of the Upper Paraguay River. It is the basin's low-elevation and low-relief topography that makes the seasonal flooding of the Upper Paraguay River capable of covering an area in excess of 130,000 km^2 [52, 53]. The influence of the flood pulse on several of the large lake basins on the western margin of Upper Paraguay River (near the area of the Serra do Amolar) was discussed in the actualistic limnogeological analysis of McGlue et al. [54]. In these lakes, water levels and hydrologic closure tracked the flood pulse and were less sensitive to direct precipitation in DJF. McGlue et al. [30] demonstrated that changes in stage height of the Upper Paraguay River and arrival of flood waters strongly influenced lake levels, patterns of siliciclastic sedimentation, and sediment biogeochemistry. Thus, lakes with tie channels to the Upper Paraguay River and approximately continuous strata provide a means to evaluate ancient flood pulse dynamics sure to have influenced large tracts of the greater wetland system. Lakes or ponds lacking a well-defined physical connection to the Upper Paraguay River may still be impacted, if seasonal

flooding enacts a change in water balance, sedimentation, or hydrochemistry indirectly through floodplain inundation, overland flow, or groundwater seepage.

3 Late Quaternary Paleolimnology in the Pantanal

Comprehensive mapping of the inland lentic waters of the Pantanal has not yet been undertaken, although a few studies have attempted to count and classify the small ponds of the Nhecolândia region of the southern Taquari River megafan [55, 56]. Nonetheless, even a cursory examination of satellite imagery from the Pantanal reveals a wide array of lakes throughout the basin. These extant lakes have served as the focal point for paleolimnological analysis. Outcrops of Quaternary-aged lacustrine deposits are presumed rare in the Pantanal wetlands, although Boggiani and Coimbra [57] suggest a possible lacustrine origin for some carbonates they have studied. Ab'Saber [58] recognized four different classes of lakes in the Pantanal: (a) oxbow lakes (Fig. 2); (b) small circular-ovate ponds, particularly focused on the Taquari River megafan (Figs. 3 and 4); (c) karst lakes (Fig. 2); and (d) large floodplain lakes (Figs. 5 and 6). From the perspective of paleolimnology, the large floodplain lakes have received the most attention. Our synthesis will focus on sediment records from these lakes, as well as the recent study of oxbow lake strata by Kuerten et al. [22]. The waters and supralittoral soils of ovate ponds of the Nhecolândia, which number in the many thousands, have been studied from chemical and biological perspectives (Fig. 3 [59, 60], see also [5]). However, paleolimnological data from these basins is scarce (see [61] for an exception) and in many instances is still in the early stages of development (R. Guerreiro 2014, personal communication). Readers are directed to the synthesis of Cohen et al. [47] for an in-depth examination of the controls on lacustrine deposystems and the formation of topographic closure in the central Andean foreland, which includes the Pantanal and humid Chaco as its distal back-bulge basin.

3.1 Oxbow Lake Records

Oxbows lakes form through lateral bank erosion and migration of meandering river systems [62]. The floodplains of many rivers in the Pantanal contain oxbows, making this class of lakes very common in the wetlands today (Fig. 2). Extant oxbows are not typical targets of paleolimnological study in South America and to our knowledge have not been specifically sampled for this purpose in the Pantanal. Abandoned channel lake deposits represent a unique challenge for paleolimnological analysis, principally because meandering rivers frequently rework and scavenge their floodplains. Therefore, poor preservation and overprinting are typical of these lake deposits, and their sedimentary record is usually no more than a

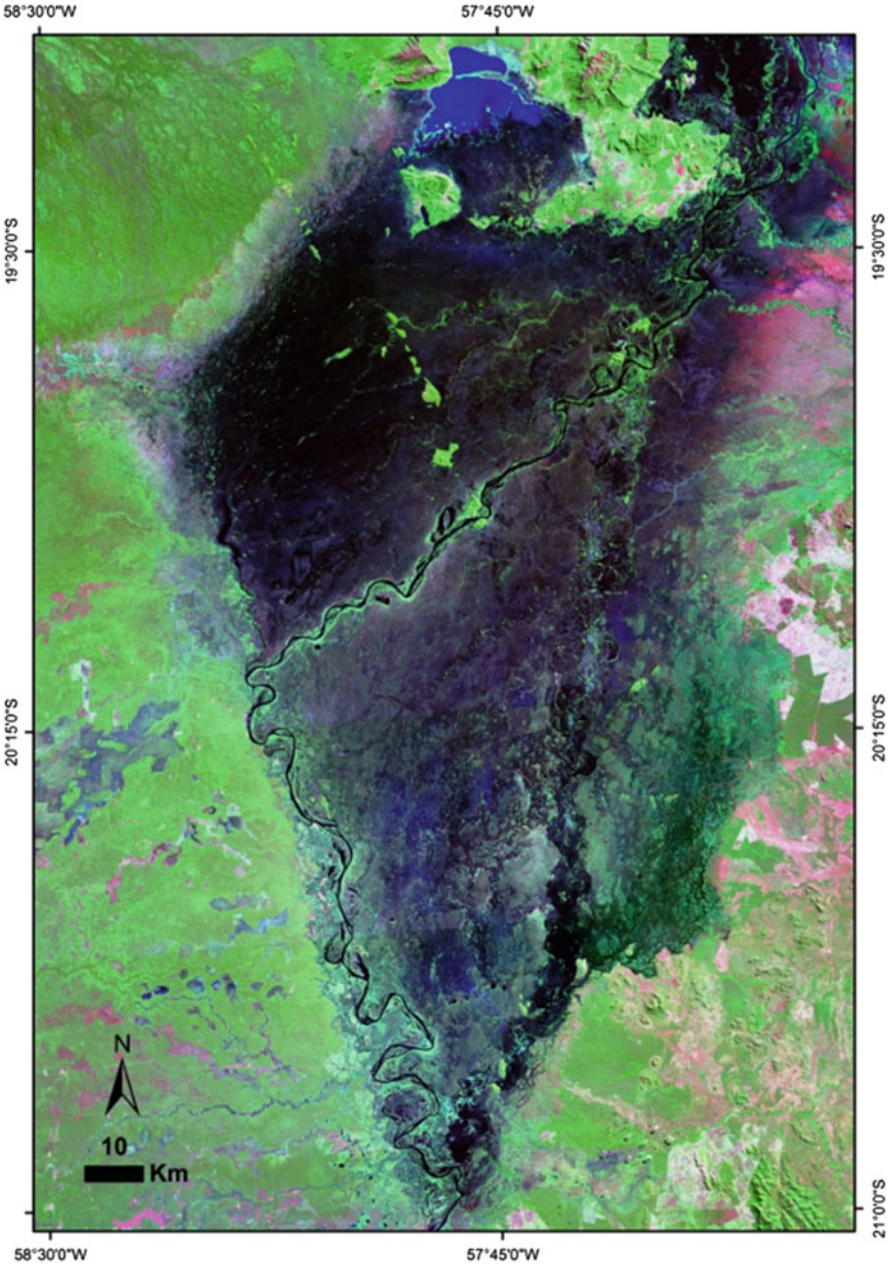

Fig. 2 NASA GeoCover Image Circa 2000 (band combination RGB: 742) of the Nabileque River megafan. Oxbow lakes are common features on the floodplains of several megafans within the Pantanal. The Nabileque River megafan contains some spectacular examples of oxbows, and oxbow lake deposits were recovered in the floodplain vibrocoring campaign and sponge spicule paleoecological analysis described in Kuerten et al. [22]. Lagoa Jacadigo, purportedly one of the Pantanal's karst lakes [35, 58], is visible at the top of the image

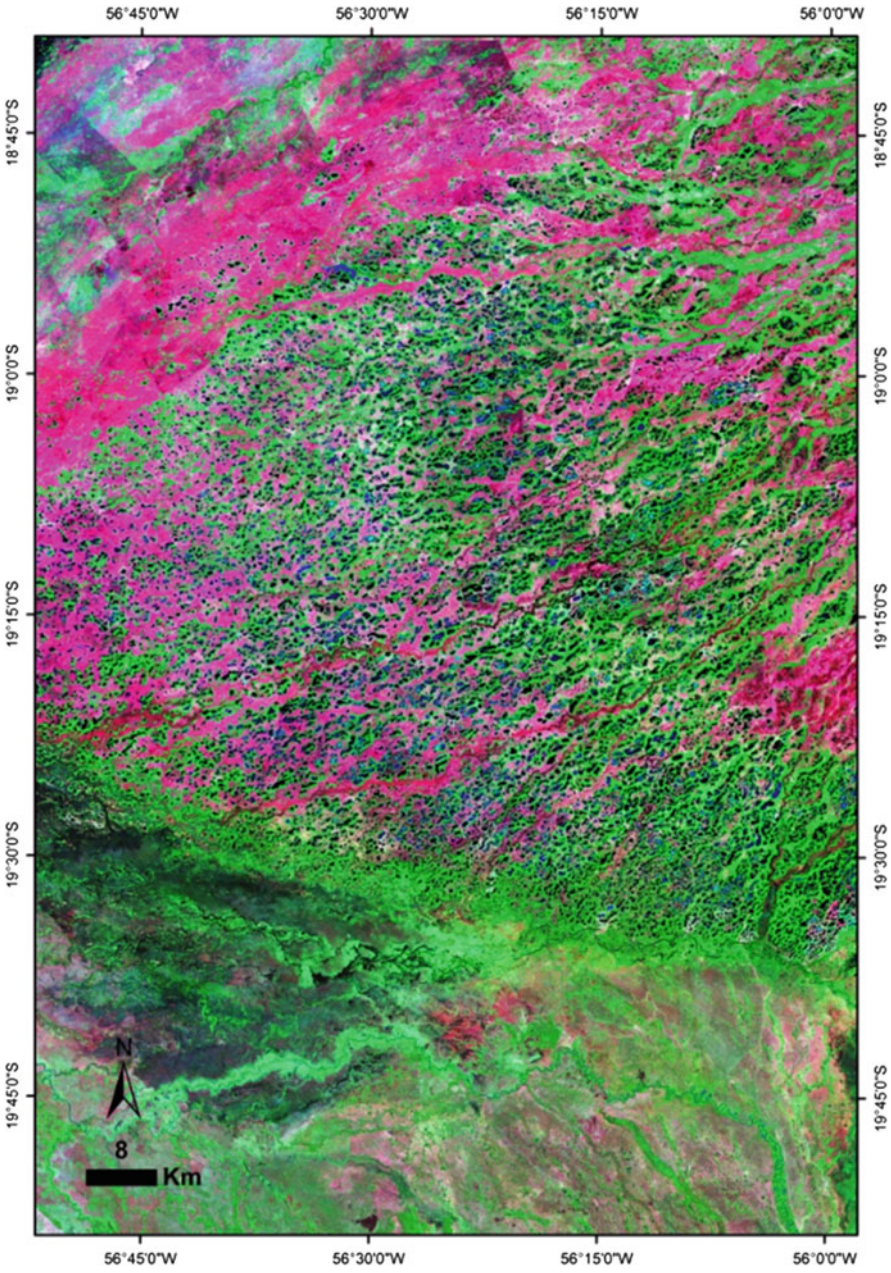

Fig. 3 NASA GeoCover Image Circa 2000 (band combination RGB: 742) of the many thousands of saline, oligo-saline, and dilute ponds juxtaposed in close proximity on the southern fringe of the Taquari River megafan, in a region known as the Nhecolândia. The ponds are believed to have formed through deflation during an interval of late Quaternary aridity. The sediments of these basins represent an underutilized paleolimnological archive for the southern Pantanal

Fig. 4 Overflight photos of the pond-rich landscape of the Nhecolândia. Saline and oligo-saline ponds are typically isolated and fringed by tree-covered sand ridges, whereas fresh ponds often become connected hydrologically during the flood season. Photo credit: Mario Assine

few thousand years in duration [34]. Oxbow lakes may also accumulate sediment in a nonlinear fashion, with a rapid early phase following levee buildup and isolation of the "U-shaped" basin, followed by episodic infill from overbank events and settling of clays from suspension. Thus, any paleolimnological records that might be obtained are likely to be marked by highly variable sedimentation rates. Finally, manually coring oxbows is often a difficult task, due to high clay content within strata and the possible presence of rooted macrophytes.

That said, short time slices of Quaternary history may be captured in oxbow lake deposits, as was demonstrated by Kuerten et al. [22]. In that study, the authors used vibracoring methods to sample the floodplain of the Nabileque River megafan in the southern Pantanal Basin (Fig. 1; approximately 20°S latitude, 57°W longitude). The Nabileque River megafan is among the most visually striking landforms in the entire Pantanal, and speculation about its Quaternary evolution has occurred for many years (Fig. 2; [58]). Casual observation of the Nabileque megafan reveals that the modern river is remarkably underfit for its channel, and Kuerten and Assine [63] used satellite images to hypothesize that the origins of the megafan were linked to a major avulsion event that led to the migration of the Upper Paraguay River to the west, near the border of the Chaco in eastern Bolivia. To test this hypothesis, Kuerten et al. [22] used a coupled geomorphological-paleolimnological assessment of the Nabileque River valley, which contains a high density of scroll bars and oxbow lakes (Fig. 2). Coring locations were determined using a surficial geological map produced by image analysis in Kuerten and Assine [63], with the main focus on a meander scroll environment, believed to be Holocene aged, situated adjacent to

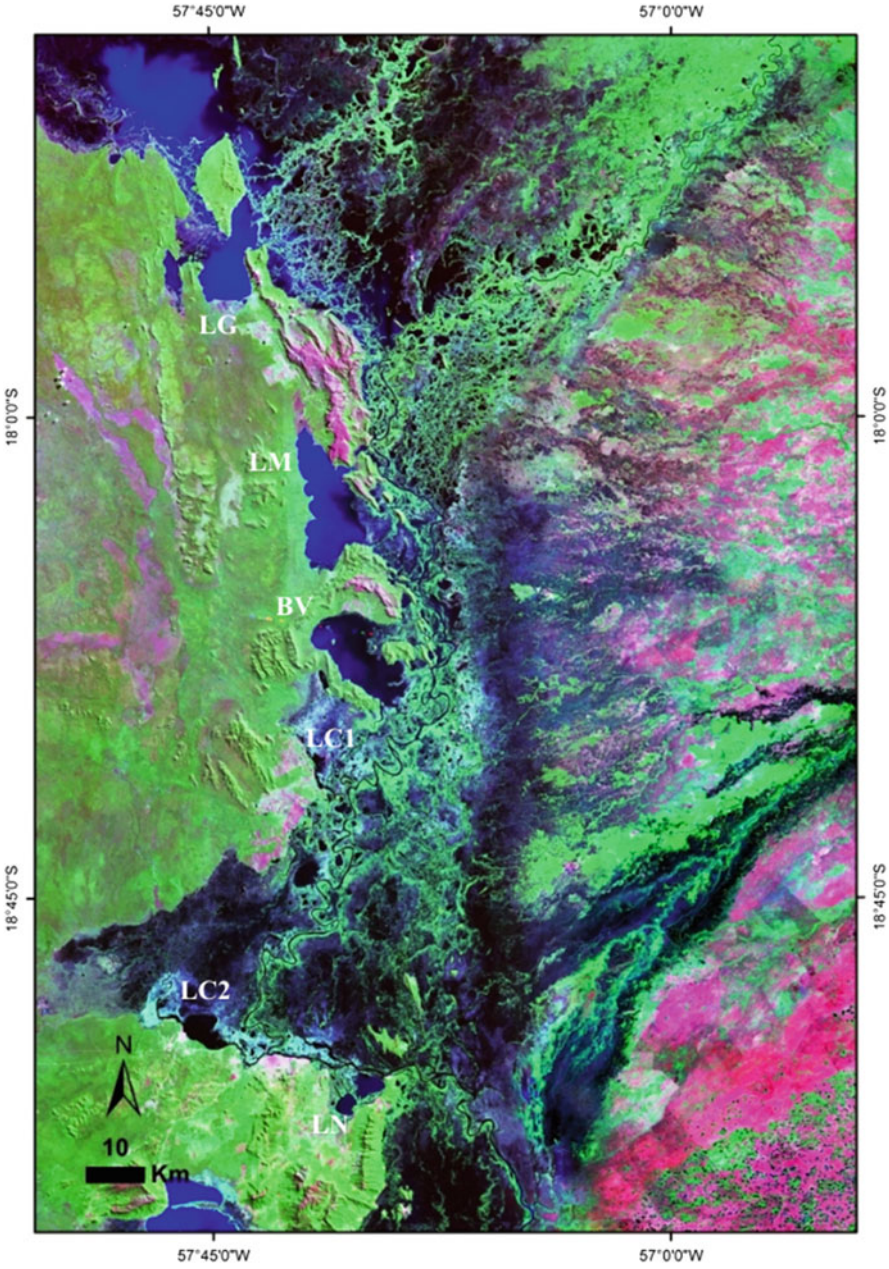

Fig. 5 NASA GeoCover Image Circa 2000 (band combination RGB: 742) of the large floodplain lakes of the central Pantanal. The lakes are interspersed among the ancient Serra do Amolar mountains. Note how these lakes are connected to the Upper Paraguay River, which flows along their eastern margins. *LG* Lagoa Gaíva, *LM* Lagoa Mandioré, *BV* Baía Vermelha, *LC1* Lagoa Castelo, *LC2* Lagoa Cáceres, *LN* Lagoa Negra

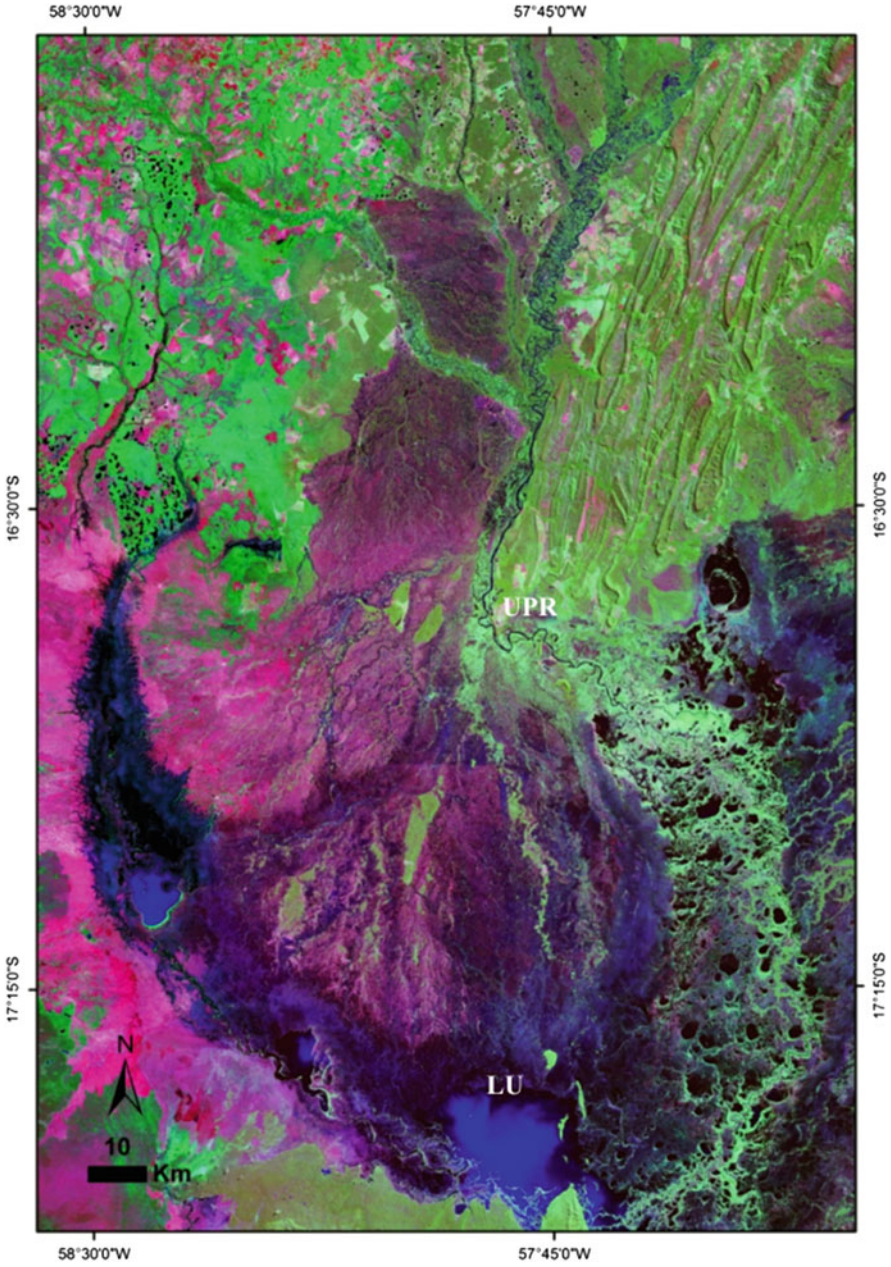

Fig. 6 NASA GeoCover Image Circa 2000 (band combination RGB: 742) of large floodplain lakes likely formed by competitive aggradation along the toe of the Paraguay fluvial fan. These lakes lack direct connections with the Upper Paraguay River (UPR) and represent new targets to obtain more continuous sedimentary records for paleolimnological analysis. *LU* Lagoa Uberaba

the extant Nabileque River. The depositional environment constrained the viable options for both geochronology and indicator materials, as the core sediments were dominated by inter-bedded sands and muds. Two dates, obtained near the top and base of the core using optically stimulated luminescence (OSL), provided a basic, albeit low-resolution, chronological framework for deposition. Those data indicated that at least 2,800 years of mid-late Holocene time was captured by the core, if sedimentation was uninterrupted in the interval between the two OSL anchor points. Kuerten et al. [22] developed a paleohydrological interpretation using sponge spicules, which are siliceous microfossils that can be identified to the species level under conditions of good preservation (Fig. 7; [64, 65]). The taxonomy of sponges is sufficiently well developed in central Brazil to allow the concept of "spongofacies" to spread through the Quaternary literature. Initially presented by Parolin et al. [66], the spongofacies concept links ancient assemblages of sponges, expressed through their spicules, with climatic and hydrologic environments through the use of modern analogs. Sponge spicules are especially valuable in the Pantanal because lotic and lentic species are relatively straightforward to unambiguously identify. For Kuerten et al. [22], lotic sponges near the base of the core suggested the presence of a large meandering river system with a significantly stronger flooding regime than the modern Nabileque River; this result was in accord with the possibility of the Upper Paraguay River flowing through the broad channel during the mid-Holocene. Delicate lentic sponge spicules (e.g., *Metania spinata*; Fig. 7) encased in muds reflected a transition to oxbow lake-type deposition around 3,700 years BP; this transition is interesting because it is one of the first paleolimnological datasets to capture apparent evidence of an avulsion event in the Upper Paraguay fluvial system. The timing of this transition is likewise important, because the extent of mid-late Holocene drought is not fully understood in the Pantanal. In his regional synthesis of soil and alluvial records, Stevaux [8] described a widespread drought in central South America from 3,500–1,500 cal year BP. Similarly, Latrubesse et al. [67] interpreted coeval alluvial and aeolian landforms in the Bolivian Chaco to reflect drought-related sedimentation. Many other areas of tropical South America likewise experienced a dramatic transition in vegetation and hydrology around this time [68]. The results of Kuerten et al. [22] suggest that aridity during this interval influenced fluvial dynamics by spurring migration of the Upper Paraguay River to its current course and abandoning the Nabileque valley.

3.2 Large Floodplain Lake Records

The origins of the large floodplain lakes of the central and northern Pantanal (e.g., Lagoas Mandioré, Gaíva, and Uberaba, Baía Chacororé) are not well studied. Wetzel [62] considered floodplain lakes as those that form either through fluvial erosion or deposition. Ponds may form within depression scours or paleo-channels after river levels recede and water drains from the floodplain, and such features may

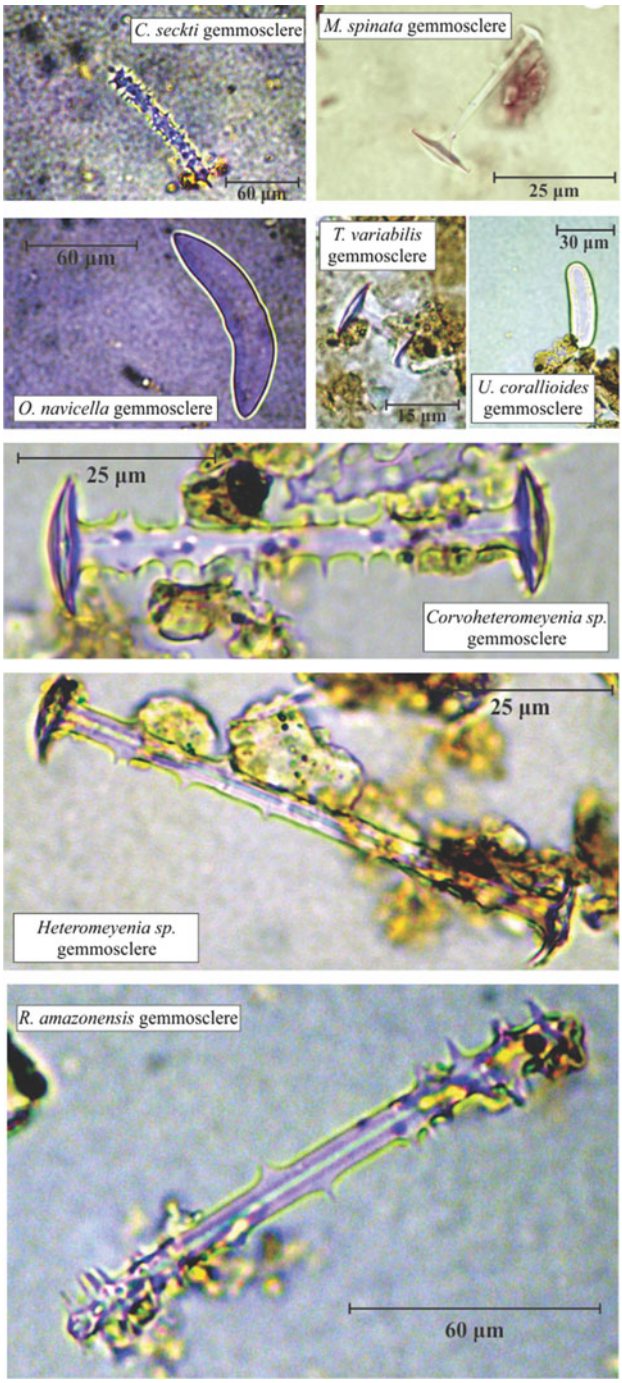

Fig. 7 Sponge spicules recovered from lake sediments in the Pantanal. Images adapted from Kuerten et al. [22] and McGlue et al. [54]. The siliceous spicules of both lotic and lentic species are frequently well preserved and can be used to infer conditions of paleohydrology

persist for thousands of years [34]. These lakes can remain connected to the river through a tie channel or be hydrologically closed and perched above the channel. Lateral lakes form through the obstruction (or damming) of tributary valleys by levee sedimentation [62] and hold the potential to contain moderately long paleolimnological records [34]. It is plausible that Lagoas Mandioré and Gaíva may represent lakes that formed in a paleo-tributary of the Upper Paraguay River (Fig. 5). Due to bathymetric patterns that deepen adjacent to shorelines with coincident topography, McGlue et al. [54] speculated on the potential for neotectonic controls influencing the limnogeology of Baía Vermelha and Lagoas Mandioré and Gaíva. More ground truth is needed to validate or refute this hypothesis. Another class of fluvial lakes is likely present in the Pantanal – lakes formed by competitive fluvial aggradation [34]. Differences in valley aggradation, subsidence patterns, and sediment accumulation rates can generate the topographic closure needed for lake formation, and a number of natural examples of these competitive processes appear along the distal fringes of the Paraguay fluvial fan (Fig. 6; [15]).

One of the earliest sediment core-based studies of the large floodplain lakes in the Pantanal was conducted by Bezerra and Mozeto [26]. These authors used gravity and vibracoring methods to recover sediments from Lagoas Negra and Castelo, which were dated using a combination of radiocarbon (expressed in ^{14}C years) and radioisotopes (Pb^{210}). Both lakes are located to the west of the Taquari River and its distal megafan, with Lagoa Castelo situated on the right margin of the Upper Paraguay River, south of Baía Vermelha by approximately 50 km [54]. Lagoa Castelo is remarkable due to its maximum depth (7.3 m), which makes it perhaps the deepest lake basin ever surveyed in the Pantanal, although it must be said that reliable bathymetric data is still not readily available for many of the wetland's lakes. Approximately 15 km south of Lagoa Cáceres, Lagoa Negra sits south of the Upper Paraguay River where it makes a sharp turn east, south of Corumbá, just before its confluence with the Taquari River. Bezerra and Mozeto [26] focus their analysis on lithostratigraphy, sediment accumulation rates, granulometry (sand content), and total organic carbon assays and attempt to discern fluvial versus lacustrine depositional patterns based on variability within these indicators. Some insights derived from pollen, C/N, and $\delta^{13}C_{OM}$ are also discussed, but these data are not presented in the paper. Although the study is constrained by a low number of radiocarbon dates and reliance on bulk elemental analysis, the authors are able to discern some interesting transitions which appear to have genetic relationships with late Quaternary climate and dynamics of the Upper Paraguay River. Core records from both lakes extend back in time to the late glacial period (>20,000 years BP) and capture the Pleistocene-Holocene transition. Deposition was assumed to be continuous over this interval, and Pb^{210} data attest to intact deposits from the past 100 years. Sedimentation rates vary in both lakes, with the terminal Pleistocene interval generally marked by faster accumulation versus a significant slowdown registered at the mid-Holocene. The lithostratigraphy of Lagoa Negra, which records a chronostratigraphically important change in sediment composition at the Pleistocene-Holocene transition, suggests that this basin is

more sensitive to environmental change than Lagoa Castelo. The authors attribute this difference to fluvial dynamics and erosion, as Lagoa Castelo is marked by a strong connection to the Upper Paraguay River throughout the late Quaternary, whereas Lagoa Negra was partially isolated from the river due to the presence of channel-margin levees. Regardless, both lakes record markedly different sedimentation characterized by high percentages of sand in the late Pleistocene. The authors suggest greater humidity as one potential driver for organic-rich, sand-poor sediment accumulation in both lakes during the Holocene, and a major hydrodynamic transition is inferred for approximately 6,500 years BP. Lake level rise, coincident with a change in climate, is discussed by Bezerra and Mozeto [26] as a likely forcing mechanism for this pattern in sedimentation, as highstand conditions would likely limit the impact of fluvial sedimentation on these basins. The authors also considered basin morphometrics, floodplain geometry, and linkages to Taquari River megafan lobe construction as other potentially related controls that may have influenced late Pleistocene lacustrine deposition. These results are largely in accord with geomorphological and paleoecological studies from the region (e.g., [58, 69]). Sediment data from the past 100 years do not show high variability in sand or organic carbon content but do contain evidence for a shift to faster sediment accumulation rates in the 1980s [26]. The relationship between this shift and the stage height of the Upper Paraguay River is briefly considered by Bezerra and Mozeto [26], and although the linkages between flooding strength and sedimentation rates in these lakes are not well expressed in the data, the authors suggest that peaks may be related to floods that follow severe droughts.

A study of the late Pleistocene and Holocene paleoclimate in the Pantanal region was produced by Whitney et al. [28], using insights derived from a radiocarbon-dated lake sediment core (expressed in calendar years). This study used overlapping Colinvaux-type hammer piston cores collected from near the center of Lagoa Gaíva (also known as Laguna La Gaiba) to generate a record of pollen and diatoms, which are classic biological indicators frequently used in paleolimnological studies to express evidence of hydroclimatic change. The authors posit that water levels in this basin are sensitive to regional precipitation. For Whitney et al., the goal of the study was to better understand the South American Summer Monsoon and moisture carried from the Amazon Basin by the South American Low Level Jet into the central lowlands of western Brazil and eastern Bolivia. A sediment record from Lagoa Gaíva, due to its position on the western margin of the Upper Paraguay River, provided a vehicle for this analysis, as evidence of change on the lake's catchment vegetation could be used to reconstruct temperature and precipitation (especially when paired with a probabilistic plant-climate computational model). This study also uses a network of lake-floor sediment samples from different water depths and sub-environments to provide a baseline of modern data in order to inform interpretation of the proxies. Deposition was assumed to be continuous throughout the approximately 45,000 cal year record, with largely invariant sedimentation rates over the Holocene (constrained by four radiocarbon dates) and more variable sedimentation over the late Pleistocene (fourteen radiocarbon dates), with a marked reduction in accumulation rates near the end of the glacial period

[28]. Intriguingly, many of the changes observed in the pollen stratigraphy are abrupt. Based on the absence of tree pollen, the presence of herb macrofossils, and abundant shallow water diatoms, the authors conclude that the late glacial period (45,000–19,500 cal year BP) in central South America was likely relatively dry and cool and Lagoa Gaíva was much smaller. Evidence of a major transition (most likely driven by warmer annual temperatures) that occurred at 19,500 cal year BP comes from the appearance of floodplain arboreal pollen in the core sediments; these data, coupled with macrofossils and diatom assemblages, suggest invasion of a favorable habitat along the southern lake margin while lake levels were low, rather than initiation of much stronger rainfall from 19,500–12,200 cal year BP. Tree pollen types, grass pollen abundance, faster sedimentation rates, and "deep water" diatom assemblages reveal a transition to higher rainfall and widespread floodplain inundation around Lagoa Gaíva after 12,200 cal year BP. Whitney et al. [28] explained that although water levels clearly rose at the Pleistocene-Holocene transition, a modest drought affected the region until approximately 3,000 cal year BP. In agreement with paleo-records from the Andes, the climate reconstruction provided by Whitney et al. [28] suggests that interglacial warming in the Southern Hemisphere tropics began several thousand years sooner than the same response in the Northern Hemisphere. Importantly, these authors confirmed early geomorphic hypotheses related to widespread aridity in the central South American lowlands during the Last Glacial Maximum, which contrasts the climate response of the high Andes at the same time (e.g., [70, 71]). This led Whitney and colleagues to interpret that glacial-interglacial cycles and associated boundary conditions in the North Atlantic are at least one important control on lowland environmental response during the late Pleistocene. Adding to the complexity, the Holocene pollen and diatom data presented by Whitney et al. [28] are consistent with a critical role for insolation varying at the beat of orbital precession on hydroclimate variability in the Pantanal over the past 12,200 cal year, which is coherent with precipitation proxy records from southeastern Brazil [10].

The study by McGlue et al. [30] was the first that explicitly set out to reconstruct late Quaternary Upper Paraguay River flood pulse dynamics using radiocarbon (expressed in calendar years)- and radioisotope (Pb^{210})-dated lake sediment cores. That study examined the strata of two large floodplain lakes in the central Pantanal: Lagoas Gaíva and Mandioré. The sites were selected based on earlier limnogeological studies by the same group of researchers who indicated that water levels in both basins were controlled by passage of the flood pulse [54]. As a consequence, the potential for stratigraphic sensitivity to climate or geomorphic change that might influence the hydrologic connection between the lakes and the river was high. Moreover, examination of two basins provided some opportunity for cross-validation of interpretations and, in concert with an assessment of other published Quaternary studies from the Pantanal, the chance to separate local versus regional paleoenvironmental signals. The sediment core from Lagoa Gaíva encompassed the Holocene, whereas the temporal record captured in the Lagoa Mandioré was much shorter but provided compelling evidence of an important depositional hiatus in the mid-late Holocene. Deposition was shown to be

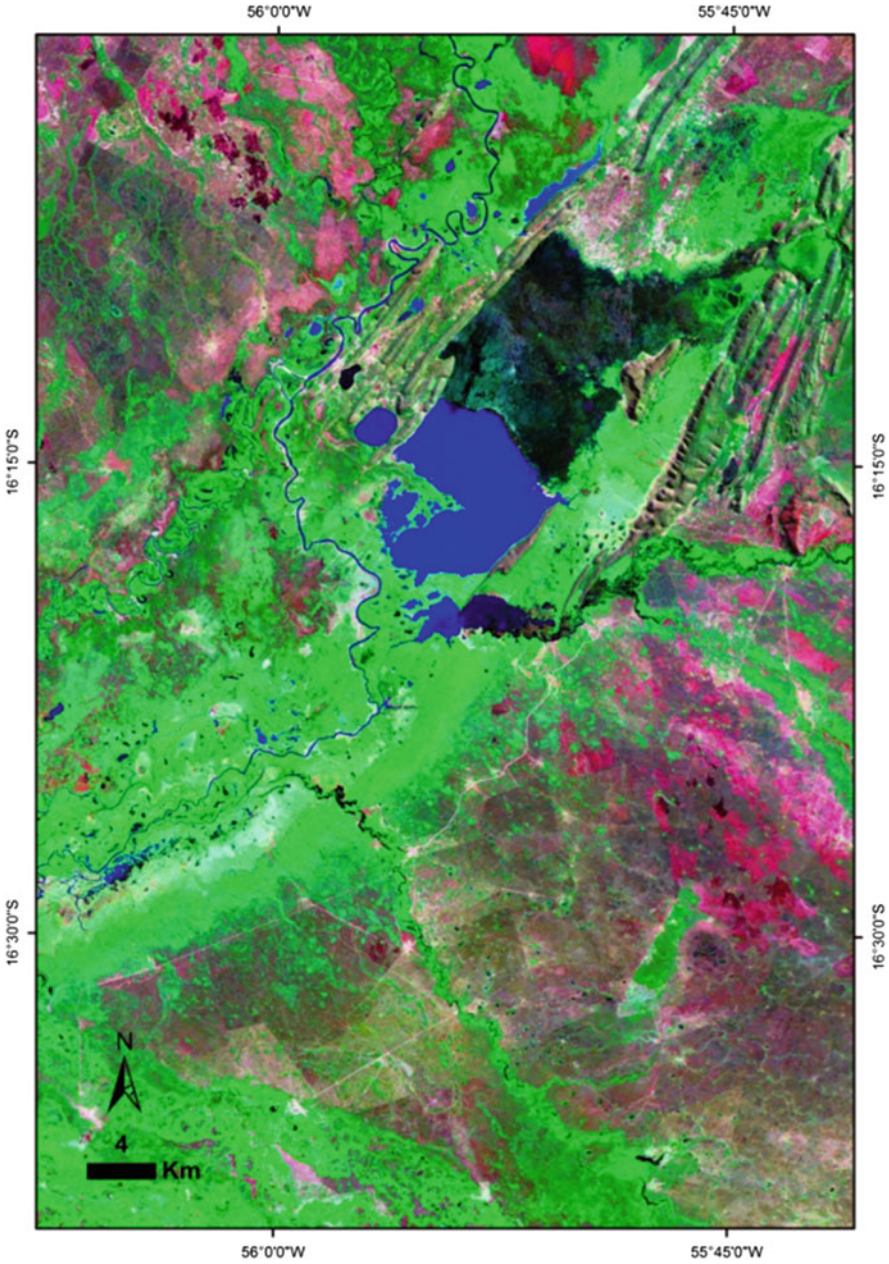

Fig. 8 NASA GeoCover Image Circa 2000 (band combination RGB: 742) of Baía do Chacororé and the Cuiabá River. Paleolimnological records from the northern Pantanal are particularly scarce, and Baía do Chacororé represents a potential target for future limnogeological analysis. As with most of the large floodplain lakes of the Pantanal, Baía do Chacororé is shallow (<3.5 m maximum depth; [87])

discontinuous over the Holocene in Lagoa Gaíva, but Pb^{210} data attest to continuous sedimentation over the past 100 years. The strata of Lagoa Gaíva were the primary focus, and the authors adopted a multi-indicator approach that centered on physical sedimentology (detrital particle size), organic geochemistry (total organic carbon [TOC], C/N, $\delta^{13}C_{OM}$), biogenic silica, and microfossils (sponge spicules and fish remains). The actualistic facies data of McGlue et al. [54] served as valuable constraints on interpretation of these indicators by providing a snapshot of lake sediment physical properties and biogeochemistry influenced by a strong seasonal flood pulse. The study results showed that inception of depositional patterns similar to modern did not occur until the late Holocene (approximately 2,600 cal year BP, with modern depositional conditions achieved around the Little Ice Age), which suggests that a fully realized Upper Paraguay River flood pulse triggered by austral summer precipitation is a transient feature in the Pantanal. Sediment composition at Lagoa Gaíva during the early Holocene, by contrast, was much more consistent with deposition in a very shallow lake with less direct influence of riverine flooding (Fig. 9). One of the most important findings of the study was the identification of a stratigraphically subtle hiatus from approximately 5,300–2,600 cal year BP. This was accomplished using a high density of radiocarbon dates, coupled with the response of multiple indicators that were consistent with inundation of a previously desiccated lake floor (e.g., a spike in productivity, signaled in biogenic silica and fish fossil abundance, perhaps associated with mixing and nutrient release [72]). The timing of this hiatus is consistent with a severe drought that impacted the Upper Parana watershed [8, 67] and correlates in time with terrestrial carbonates from Bodoquena and Aquidaban (southern Pantanal) that record reduced precipitation [24, 25]. Most importantly, the sediment core from Lagoa Mandioré clearly showed that the southern end of that basin was completely desiccated at 4,700 cal year

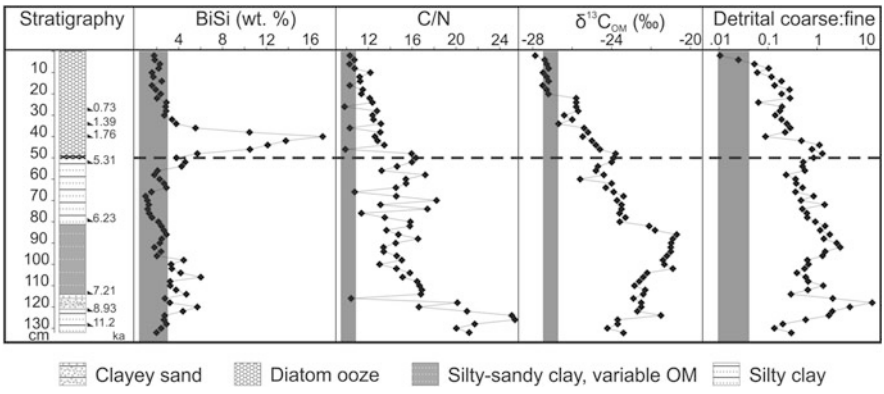

Fig. 9 Lagoa Gaíva sediment core stratigraphy, biogenic silica (BiSi), atomic carbon to nitrogen ratio (C/N), carbon isotope ($\delta^{13}C_{OM}$), and detrital grain size, expressed as a ratio of sand to silt plus clay (modified from [30]). The sample interval is 2 cm. Vertical shading represents values from modern sediment samples measured near the core site. The dashed horizontal line marks the position of a subtle hiatus

BP. The Lagoa Gaíva TOC record bears some similarity to the core data from Lagoa Castelo presented in Bezerra and Mozeto [26] around 6,500 cal year BP. As previously mentioned, Bezerra and Mozeto [26] argue for a "climatic optimum" in the middle Holocene on the basis of higher TOC values and diminished sand deposition, but the interpretations of McGlue et al. [30] suggest that changes in climate within the Pantanal are difficult to fully appreciate using paleo-indicators with limited sensitivity to the full range of environmental change that might influence a shallow floodplain lake. Nonetheless, there is evidence for more frequent floods from 6,200 to 5,300 cal year BP, which is broadly consistent with a more vigorous fluvial system inferred for the region by Assine and Soares [14] around this time.

Metcalfe et al. [31] have produced the most recent lake sediment core-derived analysis of late Pleistocene-Holocene hydroclimatic conditions for the Pantanal. This study again focused on the strata of Lagoa Gaíva and leveraged the sediment core and radiocarbon chronology initially described by Whitney et al. [28]. The authors present a wide variety of paleoenvironmental indicators (X-ray fluorescence-derived inorganic sediment chemistry, particle size, magnetic susceptibility, loss on ignition (LOI) insights on organic and inorganic carbon content, C/N, and carbon isotope data), but the main focus of the discussion is on diatom assemblages. The authors suggest that the pollen record presented by Whitney et al. [28] may be less sensitive to hydrologic change than the diatoms, in part because of the unique and unstable habitat of floodplain forest. In other words, a lake level threshold must be crossed in order to impact the shallow floodplain environment south of the lake, and as a result, the pollen data may not faithfully record the full range of possible hydroclimatic variability in the late Quaternary. Interpretation of diatom paleoecology also benefited from constraints provided by modern sediment samples (presented in [28]), whereas the other indicators presented in this study do not. Ultimately, Metcalfe et al. [31] suggest a complex response for Lagoa Gaíva to climate over the past 25,000 cal year BP, mostly in accord with the findings of Whitney et al. [28] and partially in agreement with the findings of McGlue et al. [30]. The Last Glacial Maximum through the late glacial interval (24,500–12,200 year BP) was interpreted as a relatively dry environment, marked by infrequent floods. Importantly, an abrupt transition occurs in the diatom stratigraphy from 12,200 to 11,800 year BP (encompassed within the latter part of the Younger Dryas), which suggested that Lagoa Gaíva deepened and freshened due to a higher frequency of floods, which may in turn have produced some erosion within the basin. This response is similar to some lake records on the Altiplano [70]. At approximately 10,000 cal year BP, perhaps the most distinct transition is registered in the diatom stratigraphy, with a dominance of the planktonic *Aulacoseira ambigua* and a marked decline in species of the genus *Staurosira* [31]. Based on small peaks in benthic and aerophilous taxa, in concert with indications from LOI regarding the presence of carbonate, the authors suggest that the period from 9,000 to 5,000 cal year BP was one of highly variable hydrology at Lagoa Gaíva, with a distinct and perhaps lengthy dry season. Intriguingly, Metcalfe et al. [31] found no

evidence of discontinuous sedimentation from 5,000 to 2,100 cal year BP, in contrast to the conclusions of McGlue et al. [30]. Rather, the diatoms across this interval indicated persistent "deep water" conditions. After 2,100 cal year BP, diatoms and other indicators were interpreted by Metcalfe et al. [31] to signal a stable lake system perhaps influenced by increasingly wet conditions. In terms of climate-forcing mechanisms, Metcalfe et al. [31] noted the incoherent response of Lagoa Gaíva to insolation over the late Pleistocene and Holocene and suggested the potential influence of Northern Hemisphere ice volume, considering the evidence of hydrologic variability in the later part of the Younger Dryas chronozone. Metcalfe et al. [31] suggested that climate modeling would help elucidate the major controls on the lowland environmental response, which might be tied to ITCZ position and the regional influence of convective rainfall.

Environmental variability can be natural or induced by humans, and under certain circumstances lake cores may provide archives of geomorphic processes, such as those associated with changes in land cover and development. Bonachea et al. [73] used Pb^{210}-dated sediment cores from Lagoas Jacadigo, Negra, and Castelo to probe anthropogenic and climatic influences on sedimentation rates over the past approximately 100 years. Those authors found a marked increase in sedimentation rates following the 1970s, which was attributed to higher rainfall and greater soya cultivation. The vast majority of land cover changes related to agriculture took place on the plateaus surrounding the basin, where the deforestation rate was ~59% until 2008 [74]. The marginal plateaus are highly sensitive to erosion, due the sandy soils and steep slopes that enhance anthropogenic impacts on the sediment budget and hydrologic regime. Bonachea et al. [73] suggested government policies enacted in the 1970s designed to expand agriculture and stimulate livestock production had an influence on soil erosion in the northern Pantanal through removal of natural vegetation. Human activity evidently blossomed in the Pantanal during this same period, and modifications of the land with population growth may have allowed for greater erosion with the increase in rainfall. Godoy et al. [75] also found an increase in sedimentation rates in the 1970s and 1980s in cores collected from floodplain lakes on the Taquari River megafan. Godoy et al. [75] suggested that as the Pantanal emerged from a relative dry period between 1958 and 1972, denudation of native vegetation associated with agriculture, coupled with higher annual rainfall, led to an intensification of erosion and therefore faster siltation rates on the floodplain. The flux of contaminants such as mercury (Hg) to lake basins appears to have been captured in lake sediment archives for some areas of the Pantanal [75]; higher sediment mass accumulation rates after 1970, however, may influence the expression of contaminant variability. Direct runoff of leachate associated with artisanal gold extraction (in open cast mines or small pits [76]) and atmospheric deposition are two potential pathways for mercury contamination in the Pantanal's lakes [77]. In the Poconé region (northern Pantanal), Lacerda et al. [77] discovered high relative Hg concentrations in the upper 3–7 cm of sediment cores recovered from shallow floodplain lakes and attributed this to atmospheric delivery from far afield gold mines. The results of Godoy et al. [75] suggested that Hg concentrations on the Taquari River megafan

were essentially invariant over the ^{210}Pb-dated interval, but the flux of Hg has increased due to higher sediment mass accumulation rates associated with greater erosion after 1970.

4 Knowledge Gaps and New Questions for Lakes and Lake Cores from the Pantanal

It is clear that during the Last Glacial Maximum and deglacial transition, virtually all available paleo-records from the Pantanal indicate arid conditions. The start of the Holocene witnessed the emergence of the wetlands from persistent drought into an interval of more variable rainfall that was still very unlike the modern environment, which is characterized by austral summer rainfall and pronounced Upper Paraguay River flooding. This modern-like condition appears to have initiated after 2,600 cal year BP. Interpretations of the middle Holocene environment are far more equivocal, with some records indicating drought and others indicating a wet climate.

This synthesis of environmental change inferred from lake sediment cores provokes a number of questions to be addressed by future studies. The Pantanal is an important yet underappreciated tropical wetland system, and more research is needed to expand our current level of understanding on how the wetlands will respond to global change. Lake studies will likely play a major role, but more limnogeological research is required in order to constrain the temporal resolution and "hydroclimate filter" associated with each lake. Science-based management and conservation planning will undoubtedly be critical in order to sustain the Pantanal and protect its freshwater resources and biodiversity in the future.

4.1 Was the Pantanal Impacted by Mid-Late Holocene Drought?

Sustained drought can have severe ecological consequences in the Pantanal, because so much of the wetlands' form and function rely on arrival of the annual Upper Paraguay River flood pulse. Available paleolimnological records from Lagoa Gaíva [28, 30, 31] conflict regarding the water levels in the mid-Holocene environment, which may have resulted from (1) differences in coring location (which seems unlikely, considering the basin's bathymetry), (2) coring artifacts, (3) density of radiocarbon age dates, or (4) sensitivity of indicator materials. Future research should revisit the Whitney et al. [28] coring site, which is suggested to be fully continuous. New coring methods (e.g., Uwitec percussion piston coring [78]) and seismic profiling could help to establish whether or not the lake persisted through intervals of a much diminished SASM. If water level in Lagoa Gaíva is

indeed a useful indicator of effective precipitation and flood pulse dynamics in the wetlands, this basin may hold the most valuable stratigraphic record available in the Pantanal. The total stratal thickness contained within this lake is still unknown. As a consequence, the amount of geologic time archived in the strata is likewise a mystery, although the Whitney et al. [28] dataset makes clear that dramatic changes in sedimentation rate exist in the basin. Longer records that extend to the penultimate glaciation or even the Eemian interglacial would be of tremendous value for clarifying the complex response of the basin to Northern Hemisphere ice volume and low-latitude insolation. A long sediment record from Lagoa Gaíva may warrant analysis using biomarkers, which could provide insights on amounts of precipitation, vegetation change, and methane cycling (e.g., [79, 80]).

4.2 What Types of Paleoenvironmental and Sedimentological Information Are Archived in Some of the Less Studied Lakes of the Pantanal?

It remains unclear if Lagoa Gaíva is the most complete and sensitive lacustrine stratal archive available in the Pantanal. Several other large and comparably deep lakes (e.g., Lagoa Uberaba, Baía Chacororé; Figs. 6 and 8) that lack direct connection to the Upper Paraguay River are attractive potential targets for future limnogeological analysis. How sediment delivery and the "hydroclimate filter" operate in these lakes is less certain, and these characteristics must be analyzed first in order to make the most of cores recovered from the basins. Do these lakes record flooding as discrete event beds or lamination bundles? What is the temporal resolution of the strata? Answers to these important questions are unknown. Bioturbation is seemingly high in these basins, because of shallow maximum depths and oxygenated lake floors – massive bedding in strata from the large floodplain lakes attest to this. These boundary conditions notionally limit paleolimnological records from most of Pantanal's lakes to multi-centennial resolution. Nonetheless, much can be learned from such records, especially when a multi-indicator approach is adopted. It remains to be seen if the influence of higher-frequency climate modes, like the El Niño-Southern Oscillation (ENSO) or the North Atlantic Oscillation, is recorded in any of the Pantanal's lakes (e.g., [81]). Adequately addressing the knowledge gap surrounding annual- to decadal-scale climate variability in the wetlands will likely require other proxy methods. Modeling, perhaps in tandem with tree ring-stable isotope studies, provides potentially fertile opportunities to explore the Pantanal's ecohydrological responses to ENSO.

Thousands of ovate ponds, both saline and dilute, dot the landscape of the Nhecolândia (Fig. 3). Geological evidence presented by Soares et al. [82] suggests that these lakes formed by floodplain deflation during an arid interval in the late Quaternary. The strata of these lakes are an untapped resource for expanding our understanding of environmental change in the southern Pantanal. Preliminary

results from lake sediment cores collected from Nhecolândia's ponds indicate the presence of a sharp lithostratigraphic shift from fine sand and silt to organic-rich mud (R. Guerreiro 2014, personal communication); future radiocarbon dating will help to clarify the chronological and environmental context for this transition. Floodplain trenching results presented in Furian et al. [60] reveal a similar transition, which suggests this change may be widespread across Nhecolândia. Sediment cores from Nhecolândia's ponds also afford the opportunity to test recently developed facies models, to include the potential for lacustrine carbonate accumulation on dominantly siliciclastic floodplains [83].

4.3 *Were Large Lakes Present in the Early Basin History of the Pantanal?*

Diamond wireline coring is increasingly being utilized on the continents to recover long, well-preserved sediment cores for scientific study [84]. The time is opportune to consider what value scientific drilling in the Pantanal could provide. Drilling operations in the Pantanal would surely present logistical challenges, but a number of important knowledge gaps could be addressed with an offset transect of drill cores designed to sample the approximately 500 m of sediment in the basin. Dating techniques from radiocarbon, OSL, paleomagnetics, and cosmogenic nuclides could be leveraged to date these cores, which would most likely consist of fluvial and floodplain strata, perhaps with intervals of lacustrine deposits. If large lakes were present throughout the basin's history, their strata could be continuously sampled and analyzed for fossil content, geochemistry, and sedimentology. Scientific drill cores offer the opportunity to constrain the age of the basin and thus provide much needed context for studies focused on the geodynamic evolution of the Andean foreland basin and the paleogeography of central South America. Scientific drill cores also afford the opportunity to track the history of floral biodiversity through pollen studies and the evolution of freshwater fauna via microfossil analysis. A number of basic questions related to the sedimentological and chronological development of distributary fluvial systems in tropics could also be addressed with scientific drill cores from the Pantanal.

4.4 *Lakes as Sentinels of Global Change*

Because climate change is widely regarded as a severe threat to both aquatic ecosystems and the human populations that rely upon them, the value of instrumented lakes to provide a geographically distributed signal of global change is clear [85, 86]. As regional "sinks" on the landscape, the water and sediment columns of permanent lakes register climate variability in ways that can be

recorded. Routine data logging of lake water physical, chemical, and biological properties to track "real-time" responses to climate changes currently under way would make for an evocative long-term experiment. This type of monitoring might focus on automated logger collection of water temperature, water level, transparency, and dissolved organic carbon data. These physical and chemical indicators, although complex, provide ground truth that can explain variability in solar radiation, air temperature, and precipitation patterns. Such data could be critical for sustainable management and development of the Pantanal in the coming decades. A number of sites elsewhere in Brazil are already participating in the Global Lake Ecological Observatory Network (www.gleon.org). The community of Pantanal scientists should consider exploring the possibilities for this type of field experiment applied to the large floodplain lakes.

5 Conclusions

Persistent droughts are one of the most intimate ways humankind can experience climate change. For most areas of the developing world, droughts have particularly devastating consequences, because so much of population lives off the land. This is particularly true of the lowland tropics, which are currently experiencing explosive population growth but still lack the infrastructure to adequately address the impacts of anthropogenic global change. Unfortunately, we still do not have a complete picture of how numerous lowlands tropical regions will respond to greater variability in the water cycle, which many models predict will accompany the "new normal" of an atmosphere with higher concentrations of greenhouse gases. The Pantanal is no different, but the sense of urgency for new scientific discoveries that can explain the sensitivity of the basin to climate is growing, due to valuable ecosystem services provided by the wetlands.

Lake sediment core studies have led to many insights regarding the response of the Pantanal to late Quaternary climate change, but several key questions are still unanswered. Severe widespread drought appears to be the response of the Pantanal to high-latitude glaciation, perhaps due to linkages among effective precipitation, ITCZ position, and North Atlantic sea surface temperatures. Likewise, drought appears to characterize the wetlands during low levels of Southern Hemisphere insolation. This complex response warrants further investigation using new proxies from longer and perhaps more complete lacustrine stratigraphic records. Because of the strong coupling between most lakes and the Upper Paraguay River flood pulse, paleo-records that can constrain the influence of fluvial landscape evolution on patterns of lacustrine sedimentation will likely be most successful. Other geological archives must be mined to fully assess the influence of higher-frequency climate modes, such as those originating in the Pacific Ocean (e.g., ENSO). Insights from paleo-records like these can play a vital role in shaping strategic planning, both for mitigation of environmental degradation and to inform sustainable development.

Acknowledgments We thank the many colleagues, students, family members, and friends who assisted and supported our field and laboratory research in the Pantanal from 2006 to 2014. The authors thank the Mato Grosso do Sul Research Foundation - FUNDECT (23/200.628/2012), the National Council of Technological and Scientific Development – CNPq (447402/2014-5) and Federal University of Mato Grosso do Sul for financial support to our research in the Pantanal Basin. The National Council of Technological and Scientific Development – CNPq is acknowledged for grants to AS (312386/2014-1). We thank the Laboratório de Geoprocessamento at CPAN for assistance with figures. Discussions with R. Guerreiro, E. Lo, and C. Gans improved the quality and direction of the manuscript, and reviews by the editors are gratefully acknowledged.

References

1. Hamilton SK (1999) Potential effects of a major navigation project (Paraguay-Parana Hidrovia) on inundation in the Pantanal floodplains. Regul Rivers Res Manag 15:289–299
2. Pott A, Pott VJ (2004) Features and conservation of the Brazilian Pantanal wetland. Wetl Ecol Manag 12(6):547–552
3. Junk WJ, Nunes Da Cunha K, Wantzen KM, Petermann P, Strussmann C, Marques MI, Adis J (2006) Biodiversity and its conservation in the Pantanal of Mato Grosso, Brazil. Aquat Sci 68 (3):278–309
4. Bastviken D, Santoro AL, Marotta H, Pinho LQ, Calheiros DF, Crill P, Enrich-Prast A (2010) Methane emissions from Pantanal, South America, during the low water season: toward more comprehensive sampling. Environ Sci Technol 44:5450–5455
5. Bergier I, Krusche A, Guérin F (2015) Alkaline lake dynamics in the Nhecolândia landscape. Hdb Env Chem. doi:10.1007/698_2014_327
6. Bergier I, Silva APS, Monteiro H, Guérin F, Macedo HA, Silva A, Krusche A, Sawakuchi HO, Bastviken D (2015) Methane and carbon dioxide dynamics in the paraguay river floodplain (pantanal) in episodic anoxia events. Hdb Env Chem. doi:10.1007/698_2014_353
7. Bergier I (2013) Effects of highland land-use over lowlands of the Brazilian Pantanal. Sci Total Environ 463:1060–1066
8. Stevaux JC (2000) Climatic events during the Late Pleistocene and Holocene in the Upper Paraná River: correlation with NE Argentina and South-Central Brazil. Quat Int 72:73–85
9. Cruz FW, Burns SJ, Karmann I, Sharp WD, Vuille M, Cardoso AO, Silva Dias PL, Ferrari JA, Viana O (2005) Insolation driven changes in atmospheric circulation over the past 116,000 years in subtropical Brazil. Nature 434:63–66
10. Cruz FW, Vuille M, Burns SJ, Wang X, Cheng H, Werner M, Edwards RL, Karmann I, Auler AS, Nguyen H (2009) Orbitally driven east–west antiphasing of South American precipitation. Nat Geosci 2(3):210–214
11. Arini J (2009) Nos labirintos da bioparanoia. Época 68–70
12. Braun EHG (1977) Cone aluvial do Taquari, unidade geomórfica marcante na planície quaternária do Pantanal. Rev Bras Geogr 39(4):164–180
13. Tricart J (1982) El Pantanal: Un ejemplo del impacto de la geomorfologia sobre el medio ambiente. Geografia 7(13–14):37–50
14. Assine ML, Soares PC (2004) Quaternary of the Pantanal, west-central Brazil. Quat Int 114:23–34
15. Assine ML, Silva A (2009) Contrasting fluvial styles of the Paraguay River in the northwestern border of the Pantanal wetland, Brazil. Geomorphology 113:189–199
16. Buehler HA, Weissmann GS, Scuderi LA, Hartley AJ (2011) Spatial and temporal evolution of an avulsion on the Taquari River distributive fluvial system from satellite image analysis. J Sediment Res 81(8):630–640
17. Makaske B, Maathuis BH, Padovani CR, Stolker C, Mosselman E, Jongman RH (2012) Upstream and downstream controls of recent avulsions on the Taquari megafan, Pantanal, south-western Brazil. Earth Surf Process Landf 37(12):1313–1326

18. Zani H, Assine ML, McGlue MM (2012) Revealing geoforms in Pantanal wetland (Brazil) with remote sensing: a method to enhance SRTM-DEM for megafan environments. Geomorphology 161–162:82–92
19. Klammer G (1982) Die Paleowueste des Pantanal von Mato Grosso und die pleistozaene Klimageschichte der brasilianischen Randtropen. Zeitschrift Geomorphol NF 26:393–416
20. Hamilton SK, Sippel SJ, Melack JM (2002) Comparison of inundation patterns among major South American floodplains. J Geophys Res 107(D20):8038
21. Assine ML, Corradini FA, Pupim FDN, McGlue MM (2014) Channel arrangements and depositional styles in the São Lourenço fluvial megafan, Brazilian Pantanal wetland. Sediment Geol 301:172–184
22. Kuerten S, Parolin M, Assine ML, McGlue MM (2013) Sponge spicules indicate Holocene environmental changes on the Nabileque River floodplain, southern Pantanal, Brazil. J Paleolimnol 49(2):171–183
23. Victoria RL, Fernandes F, Martinelli LA, Piccolo MC, Camargo PB, Trumbore S (1995) Past vegetation changes in the Brazilian Pantanal-Grassy Savanna ecotone by using carbon isotopes in the soil organic matter. Glob Chang Biol 1:65–71
24. Bertaux J, Sondag F, Santos R, Soubies F, Casse C, Plagnes V, Le Cornec F, Seidel F (2002) Palaeoclimatic record of speleothems in a tropical region: study of laminated sequences from a Holocene stalagmite in Central-West Brazil. Quat Int 89:3–16
25. Boggiani PC, Coimbra AM, Gesicki ALD, Sial AN, Ferreira VP, Ribeiro FB, Flexor JM (2002) Tufas Calcárias da Serra da Bodoquena, MS: cachoeiras petrificadas ao longo dos rios. In: Schobbenhaus C, Campos DA, Queiroz ET, Winge M, Berbert-Born M (eds) Sítios Geológicos e Paleontológicos do Brasil. Brasília-DF, DNPM, pp 249–259
26. Bezerra MAO, Mozeto AA (2008) Deposição de carbono orgânico na planície de inundação do Rio Paraguai durante o Holoceno médio. Oecologia Brasiliensis 12(1):155–171
27. Sallun-Filho W, Karmann I, Boggiani PC, Petri S, Souza Cristalli P, Utida GA (2009) Deposição de Tufas Quaternárias no Estado de Mato Grosso do Sul: Proposta de Definição da Formação Serra da Bodoquena. Revista do Instituto de Geociências USP 9:47–60
28. Whitney BS, Mayle FE, Punyasena SW, Fitzpatrick KA, Burn MJ, Guillen R, Chavez E, Mann D, Pennington RT, Metcalfe SE (2011) A 45 kyr palaeoclimate record from the lowland interior of tropical South America. Palaeogeogr Palaeoclimatol Palaeoecol 307:177–192
29. Whitney BS, Mayle FE (2012) Pediastrum species as potential indicators of lake-level change in tropical South America. J Paleolimnol 47:601–615
30. McGlue MM, Silva A, Zani H, Corradini FA, Parolin M, Abel EJ, Cohen AS, Assine ML, Ellis GS, Trees MA, Kuerten S, Gradella FS, Rasbold GG (2012) Lacustrine records of Holocene flood pulse dynamics in the Upper Paraguay River watershed (Pantanal wetlands, Brazil). Quat Res 78(2):285–294
31. Metcalfe SE, Whitney BS, Fitzpatrick KA, Mayle FE, Loader NJ, Street-Perrott FA, Mann DG (2014) Hydrology and climatology at Laguna La Gaiba, lowland Bolivia: complex responses to climatic forcings over the last 25 000 years. J Quat Sci 29(3):289–300
32. Ledru MP, Bertaux J, Sifeddine A, Suguio K (1998) Absence of last glacial maximum records in lowland tropical forests. Quat Res 49:233–237
33. Ruddiman WF (2001) Earth's Climate: past and future. W. H. Freeman, New York, 465 pp
34. Cohen AS (2003) Paleolimnology: the history and evolution of lake systems. Oxford University Press, Oxford
35. Por FD (1995) The Pantanal of Mato Grosso (Brazil). Kluwer, Dordrecht
36. Costa MF (2007) De Xarayes ao Pantanal: a cartografia de um mito geográfico. Revista do Instituto de Estudos Brasileiros 45:21–36
37. Weyler G (1962) Relatório final dos Poços perfurados no Pantanal Matogrossense. Projeto Pantanal. Distrito de Expl. Sedimentar do Paraná, Petrobrás, Ponta Grossa-PR, 27 pp
38. Catto AJ (1975) Análise geológica e geofísica da Bacia do Pantanal Matogrossense. Rio de Janeiro, Petrobrás (DEPEX/SEDOT n° 5296)
39. Heckman CW (1998) The Pantanal of Poconé. Kluwer, Den Haag

40. Swarts FA (ed) (2000) The Pantanal: understanding and preserving the world's largest wetland. Paragon House, St. Paul
41. Horton BK, DeCelles PG (1997) The modern foreland basin system adjacent to the central Andes. Geology 25:895–898
42. Ussami N, Shiraiwa S, Dominguez JML (1999) Basement reactivation in a sub-Andean foreland flexural bulge: the Pantanal wetland, SW Brazil. Tectonics 18(1):25–39
43. Assine ML (2003) Sedimentação na Bacia do Pantanal Mato-Grossense. Centro-Oeste do Brasil, Rio Claro
44. Assumpção M, Schimmel M, Escalante C, Barbosa JR, Rocha M, Barros LV (2004) Intraplate seismicity in SE Brazil: stress concentration in lithospheric thin spots. Geophys J Int 159:390–399
45. Alvarenga CJS, Boggiani PC, Babinski M, Dardenne MA, Figueiredo MF, Dantas EL, Uhlein A, Santos RV, Sial AN, Trompette R (2011) Glacially influenced sedimentation of the Puga Formation, Cuiabá Group and Jacadigo Group, and associated carbonates of the Araras and Corumbá groups, Paraguay Belt, Brazil. Geological Society, London, Memoirs 36(1):487–497
46. Chase CG, Sussman AJ, Coblentz DD (2009) Curved Andes: Geoid, forebulge, and flexure. Lithosphere 1:358–363
47. Cohen AS, McGlue MM, Ellis GS, Zani H, Swarzenski PW, Assine ML, Silva A (2015) Lake formation, characteristics and evolution in retroarc deposystems: a synthesis of the modern Andean orogen and its associated basins. In: DeCelles PG, Ducea MN, Carrapa B, Kapp P (eds) Geodynamics of a cordilleran orogenic system: the central Andes of Argentina and Northern Chile, Geological Society of America Memoir 212. doi:10.1130/2015.1212(16)
48. Zhou J, Lau KM (1998) Does a monsoon climate exist over South America? J Clim 11:1020–1040
49. Prance GT, Schaller GB (1982) Preliminary study of some vegetation types of the Pantanal, Mato Grosso, Brazil. Brittonia 34:228–251
50. Pinder L, Rosso S (1998) Classification and ordination of plant formations in the Pantanal of Brazil. Plant Ecol 136:151–165
51. Pott A, Silva JSV (2015) Terrestrial and aquatic vegetation diversity of the Pantanal wetland. Hdb Env Chem. doi:10.1007/698_2014_352
52. Hamilton SK, Sippel SJ, Calheiros DF, Melack JM (1997) An anoxic event and other biogeochemical effects of the Pantanal wetland on the Paraguay River. Limnol Oceanogr 42:257–272
53. Junk WJ, Bayley PB, Sparks RE (1989) The flood pulse concept in river-floodplain systems. Can Spec Publ Fish Aquat Sci 106:110–127
54. McGlue MM, Silva A, Corradini FA, Zani H, Trees M, Ellis G, Parolin M, Swarzenski PW, Cohen AS, Assine ML (2011) Limnogeology in Brazil's "Forgotten Wilderness:" a synthesis from the floodplain lakes of the Pantanal. J Paleolimnol 46(2):273–289
55. Costa MP, Telmer KH (2006) Utilizing SAR imagery and aquatic vegetation to map fresh and brackish lakes in the Brazilian Pantanal wetland. Remote Sens Environ 105(3):204–213
56. Costa M, Telmer KH, Evans TL, Almeida TI, Diakun MT (2015) The lakes of the Pantanal: inventory, distribution, geochemistry, and surrounding landscape. Wetl Ecol Manag 2015:1–21
57. Boggiani PC, Coimbra AM (1995) Quaternary limestone of the Pantanal area, Brazil. An Acad Bras Cienc 3(67):343–349
58. Ab'Saber AN (1988) O Pantanal Mato-Grossense ea teoria dos refúgios. Rev Bras Geogr 50 (2):9–57
59. Barbiéro L, Queiroz Neto JP, Ciornei G, Sakamoto AY, Capellari B, Fernandes E, Valles V (2002) Geochemistry of water and ground water in the Nhecolândia, Pantanal of Mato Grosso, Brazil: variability and associated processes. Wetlands 22(3):528–540
60. Furian S, Martins ERC, Parizotto TM, Rezende-Filho AT, Victoria RL, Barbiero L (2013) Chemical diversity and spatial variability in myriad lakes in Nhecolândia in the Pantanal wetlands of Brazil. Limnol Oceanogr 58(6):2249–2261

61. Fávaro DIT, Damatto SR, Silva PSC, Riga AA, Sakamoto AY, Mazzilli BP (2006) Chemical characterization and 210 Pb dating in wetland sediments from the Nhecolândia Pantanal Pond, Brazil. J Radioanal Nucl Chem 269(3):719–726
62. Wetzel RG (2001) Limnology: lake and river ecosystems. Academic, San Diego, 1006 pp
63. Kuerten S, Assine ML (2011) O rio Paraguai no megaleque do Nabileque, sudoeste do Pantanal Mato-Grossense, MS. Rev Bras Geosci 41(4):642–653
64. Volkmer-Ribeiro C, Turcq B (1996) SEM analysis of siliceous spicules of a freshwater sponge indicate paleoenvironmental changes. Acta Microsc 5:186–187
65. Volkmer-Ribeiro C, Motta JFM, Callegaro VLM (1998) Taxonomy and distribution of Brazilian spongillites. Sponge sciences, multidisciplinary perspectives. Springer-Verlag, Tokyo, pp 271–278
66. Parolin M, Volkmer-Ribeiro C, Stevaux JC (2008) Use of spongofacies as a proxy for river-lake paleohydrology in Quaternary deposits of central-western Brazil. Revista Brasileira de Paleontologia 11(3):187–198
67. Latrubesse EM, Stevaux JC, Cremon EH, May J-H, Tatumi SH, Hurtado MA, Bezada M, Argollo JB (2012) Late Quaternary megafans, fans and fluvio-aeolian interactions in the Bolivian Chaco, Tropical South America. Palaeogeogr Palaeoclimatol Palaeoecol 356:75–88
68. Marchant R, Hooghiemstra H (2004) Rapid environmental change in African and South American tropics around 4000 years before present: a review. Earth Sci Rev 66:217–260
69. Parolin M, Volkmer-Ribeiro C, Stevaux JC (2007) Sponge spicules in peaty sediments as paleoenvironmental indicators of the Holocene in the upper Parana River, Brazil. Revista Brasileira de Paleontologia 10:17–26
70. Baker PA, Seltzer GO, Fritz SC, Dunbar RB, Grove MJ, Tapia PM, Cross SL, Rowe HD, Broda JP (2001) The history of South American tropical precipitation for the past 25,000 years. Science 291:640–643
71. Fritz SC, Baker PA, Seltzer GO, Ballantyne A, Tapia P, Cheng H, Edwards RL (2007) Quaternary glaciation and hydrologic variation in the South American tropics as reconstructed from the Lake Titicaca drilling project. Quat Res 68:410–420
72. Talbot MR, Jensen NB, Lærdal T, Filippi ML (2006) Geochemical responses to a major transgression in giant African lakes. J Paleolimnol 35(3):467–489
73. Bonachea J, Bruschi V, Hurtado MA, Forte LM, da Silva M, Etcheverry R, Cavallotto JL, Dantas M, Pejon O, Zuquette LV, Bezerra MA, Remondo J, Rivas V, Gomez-Arozamena J, Fernandez G, Cendrero A (2010) Natural- and human-forcing in recent geomorphic change: case studies in the Rio de la Plata basin. Sci Total Environ 408:2674–2695
74. Silva JSV, Abdon M, Silva SMA, Moraes JA (2011) Evolution of deforestation in the Brazilian Pantanal and surroundings in the timeframe 1976–2008. Geografia 36:35–55
75. Godoy JM, Padovani CR, Guimarães JR, Pereira JC, Vieira LM, Carvalho ZL, Galdino S (2002) Evaluation of the siltation of River Taquari, Pantanal, Brazil, through 210Pb geochronology of floodplain lake sediments. J Braz Chem Soc 13(1):71–77
76. Hylander LD, Meili M, Oliveira LJ, Castro E, Silva J, Guimarães RD, Araujo DM, Neves RP, Stachiw R, Barros AJP, Silva GD (2000) Relationship of mercury with aluminum, iron and manganese oxy-hydroxides in sediments from the Alto Pantanal, Brazil. Sci Total Environ 260:97–107
77. Lacerda LD, Salomons W, Pfeiffer WC, Bastos WR (1991) Mercury distribution in sediment profiles from lakes of the high Pantanal, Mato Grosso State, Brazil. Biogeochemistry 14 (2):91–97
78. Schultze E, Niederreiter R (1990) Palaolimnologische Untersuchungen an einem Bohrkern aus dem Profundal des Mondsees (Oberosterreich). Linzer Biol Beitr 22:231–235
79. Zheng Y, Zhou W, Meyers PA, Xie S (2007) Lipid biomarkers in the Zoigê-Hongyuan peat deposit: Indicators of Holocene climate changes in West China. Org Geochem 38(11):1927–1940
80. Zhou W, Zheng Y, Meyers PA, Jull AJ, Xie S (2010) Postglacial climate-change record in biomarker lipid compositions of the Hani peat sequence, Northeastern China. Earth Planet Sci Lett 294(1):37–46

81. Bergier, I., 2010. River level sensitivity to SOI and NAO in Pantanal and Amazonia. 30. Simpósio de Geotecnologias do Pantanal
82. Soares AP, Soares PC, Assine ML (2003) Areiais e lagoas do Pantanal, Brasil: herança paleoclimática? Braz J Geol 33(2):211–224
83. Gierlowski-Kordesch E, Finkelstein DB, Holland JJT, Kallini KD (2013) Carbonate lake deposits associated with distal siliciclastic perennial-river systems. J Sediment Res 83 (12):1114–1129
84. Soreghan GS, Cohen AS (2013) Scientific drilling and the evolution of the earth system: climate, biota, biogeochemistry and extreme systems. Sci Drill 16:63–72
85. Adrian R, O'Reilly CM, Zagarese H, Baines SB, Hessen DO, Keller W, Livingstone DM, Winder M (2009) Lakes as sentinels of climate change. Limnol Oceanogr 54(6):2283
86. Williamson CE, Saros JE, Vincent WF, Smol JP (2009) Lakes and reservoirs as sentinels, integrators, and regulators of climate change. Limnol Oceanogr 54(6):2273
87. Pacheco EB, Da-Silva CJ (2009) Fish associated with aquatic macrophytes in the Chacororé-Sinhá Mariana lake system and Mutum River, Pantanal of Mato Grosso, Brazil. Braz J Biol 69 (1):101–108

Avulsive Rivers in the Hydrology of the Pantanal Wetland

Mario Luis Assine, Hudson Azevedo Macedo, José Cândido Stevaux, Ivan Bergier, Carlos Roberto Padovani, and Aguinaldo Silva

Abstract This chapter presents and discusses the avulsive nature of the Pantanal rivers and shows how the ever-changing drainage network influences the surface hydrology and ecology. Besides, the systemic portrait here outlined provides new insights concerning the Pantanal hydrodynamics, in its particularities and as a whole system. A simple model of the avulsion process is illustrated, and several realistic examples of the processes leading to river avulsions are shown and discussed. The north-to-south flood-pulse wave due to the presence of bottlenecks is further described in detail. This systemic approach allows identifying that the fluvial "avulsive and bottleneck" dynamics seasonally affects both local and regional ecohydrological processes. Moreover, it shows that avulsive processes are commonplace in Pantanal, and changes in land use, particularly in river headwaters in the highlands, accelerate the avulsions, making the sustainable use of the Pantanal lowland areas difficult.

Keywords Flood dynamics, Fluvial avulsion, Fluvial bottlenecks, Fluvial megafans, Multichannel systems

M.L. Assine (✉), H.A. Macedo, and J.C. Stevaux
Universidade Estadual Paulista – Unesp, Instituto de Geociências e Ciências Exatas, Campus de Rio Claro. Avenida 24A, 1515 Rio Claro 13506-900, Brazil
e-mail: assine@rc.unesp.br

I. Bergier
Laboratory of Biomass Conversion, Embrapa Pantanal, Corumbá, Brazil

C.R. Padovani
Laboratory of Geoprocessing, Embrapa Pantanal, Corumbá, Brazil

A. Silva
Department of Geography, Federal University of Mato Grosso do Sul, Corumbá, Brazil

I. Bergier and M.L. Assine (eds.), *Dynamics of the Pantanal Wetland in South America*, Hdb Env Chem (2016) 37: 83–110, DOI 10.1007/698_2015_351,

Contents

1 Introduction

The Pantanal wetland is located in the middle of South America in the upper portion of the La Plata Basin, where seasonal changes in rainfall largely control the annual flood pulse of river floodplains [1]. Inter-annual and inter-decadal fluctuations in intensity, duration, and magnitude of the flood pulse are modulated by global-scale phenomena as the Intertropical Convergence Zone (ITCZ) and the South Atlantic Convergence Zone (SACZ) [2–5]. The convergence of airflows into the ITCZ overrides the opposite effects of wind patterns known as easterlies [6]. Rainfall quantity and distribution are usually affected by changes in sea surface temperature [7], which in turn influences the South American Monsoon System [8, 9].

The annual movement of the overhead sun causes the ITCZ to migrate northerly and southerly throughout the year, which affects wet climates in tropical latitudes. The Subtropical Atlantic Anticyclone shifts from S30° northward in the summer and produces NE-to-NW winds which push the continental equatorial air mass toward the Upper Paraguay Basin. Because of this phenomenon, the Pantanal region has a typical wet-dry climate whose rainfall regime is the most important climatic variable [10, 11]. Although temperature range can seasonally vary from −1°C to 41°C, the seasonal mean temperature is virtually constant and ranges between 20°C in July and 27°C in December, whereas rainfall is, in general, well marked seasonally [12, 13]. According to Garcia [10], other factors may also influence the regional climate, as the South Amazon humid air mass and the cold front of polar instability that reaches the SE and S portion of the Pantanal.

The Pantanal wetland is an immense lowland of approximately 150,000 km^2 (altitudes <200 m a.s.l.) located in the Upper Paraguay Basin (Fig. 1). The annual precipitation in river headwaters is not homogeneous but varies from 1,200 to 1,350 mm at north-northeast to 710–1,200 at the south-southwestern sector, with the lowest annual precipitation of 700 mm in the center of the Pantanal (Fig. 2). This precipitation/discharge dynamics largely relies on the “monsoon-like effect” produced by the altitudinal gradient between low- and highlands [14]. Also, the majority of the annual rainfall takes place from October to March, whereas July to September is the driest period [12].

This chapter provides insightful information interlinking climate, geology, and hydrology for better portraying and understanding the Pantanal dynamics in its particularities and as a whole system.

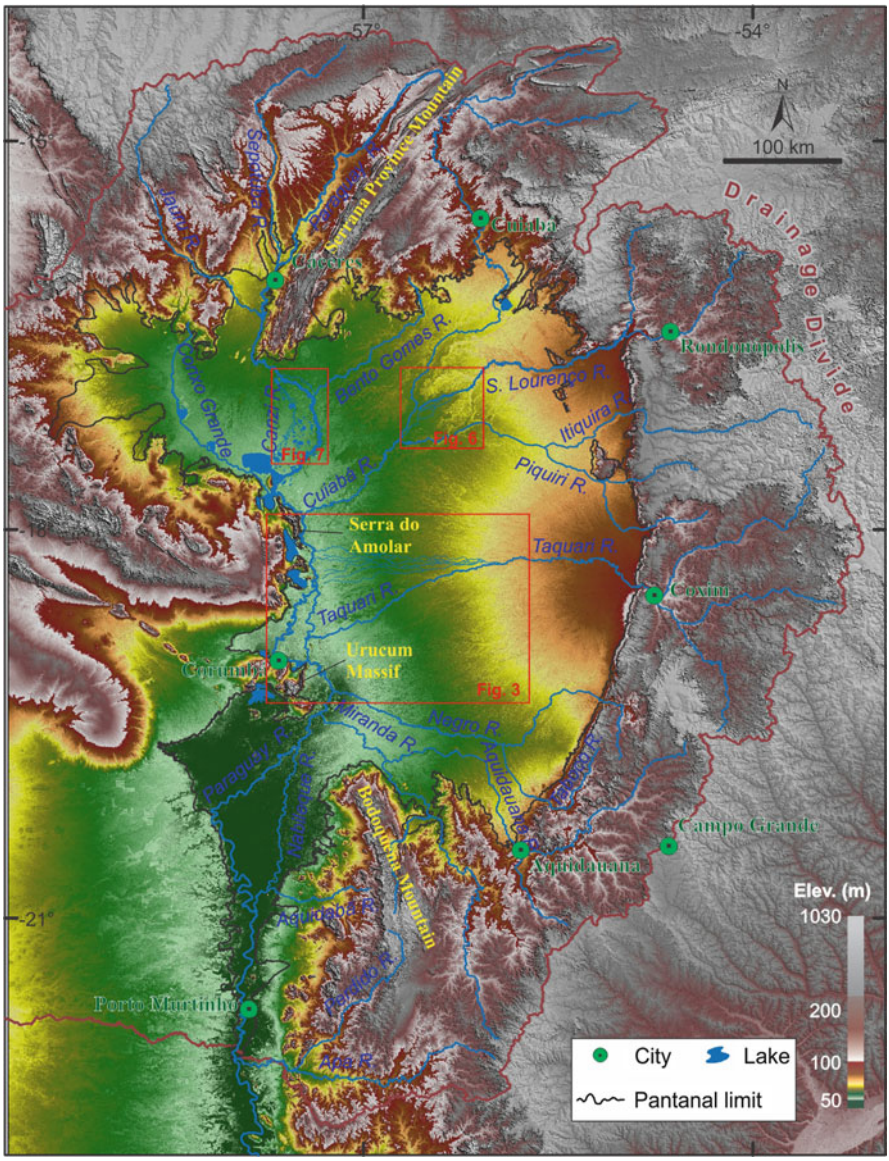

Fig. 1 Hypsometry and the drainage network of Upper Paraguay Basin, with indication of the Pantanal area (digital elevation model from Shuttle Radar Topographic Mission – SRTM)

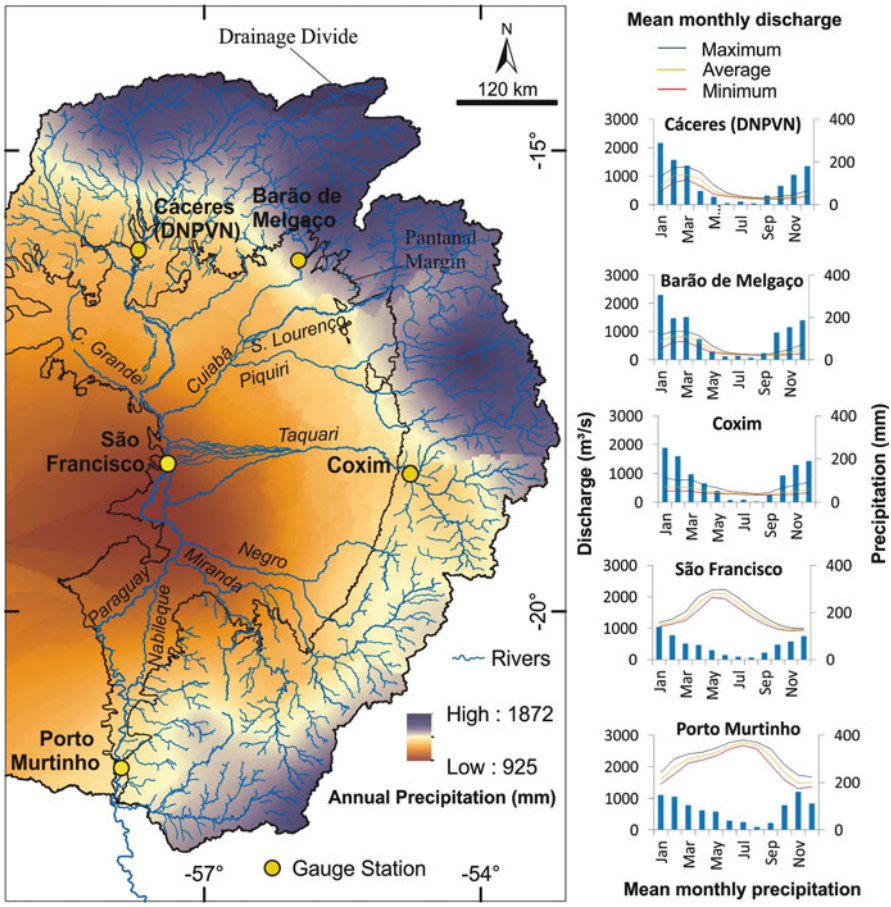

Fig. 2 Hydrographs of some rivers of the Upper Paraguay Basin (monthly mean during the period 2003–2012). The annual precipitation map was obtained by the Kriging interpolation of data in the same period (Data source: ANA – Brazilian Agency of Water)

2 Avulsive Rivers in Distributary and Multichannel Systems

Rivers in the catchment area surrounding the Pantanal wetland are essentially bedrock rivers, which means watercourses formed by erosion of underlying rocks with valley. Many small stream rivers flowing into a large river (main stem) compose the tributary drainage networks, such as the drainage basins of the rivers Miranda, Aquidauana, Taquari, São Lourenço, Paraguay, and Cuiabá (see Fig. 1). Incision processes carve valleys and confine the flow in thalwegs. The sediment generated by erosion is transported downstream, with little and short-lived alluvial deposition along the valley.

The lateral slopes vanish when the confined rivers reach the Pantanal basin and the rivers develop into unconfined systems. Sedimentation takes place and the rivers turn into alluvial with poorly defined valleys with no apparent slopes. Sedimentation occurs due to the combination of valley unconfinement, sudden drop in the river gradient, and flow speed reduction. The unconfinement increases downstream with terrace slopes decreasing favoring overflow, crevassing, and channel splitting. Both channel bifurcation and sedimentation lead to changes in the position of channels, and, eventually, the main channel may fully change position and the river course shifts to another portion of the floodplain, a phenomenon termed *avulsion*.

The Pantanal is a large subsiding sedimentary basin that continuously creates accommodation space for deposition [15]. The rivers deposit sediments carried from the catchment-source area, filling portions of the basin, whereas other areas remain starved. Consequently, the river changes continually its position within the basin to distribute sediments all over the area, which means that the river behavior is avulsion dominated and the system is avulsive [16]. Fluvial avulsion is a step-by-step serial processing that abruptly shifts the river course.

Avulsive channel systems commonly lead to a fluvial distributary drainage pattern, characterized by networks of channels radiating from the apex of the system, with one or more perennial and many intermittent channels that are active only during floods. These systems are termed *fluvial megafans* and are distinguished from debris flow dominated alluvial fans not only because they are dominated by rivers, but also due to their large areas reaching 10^3–10^5 km^2 while alluvial fans are generally $<10^2$ km^2 [17]. The Kosi River system in India is an example of large fans since Gole and Chitale [18] reported records of river shifts of ~100 km from east to west across the fan surface, over a period of 230 years (1731–1963). The Kosi fan typifies braided river-dominated alluvial fans in the threefold classification of fluvial subaerial fans [19]. In this classification, the Okavango fan in Botswana is a suitable model for the second group of stream-dominated fans: the low sinuosity/meandering river-dominated fans.

The importance of fluvial megafans was recently emphasized by Weissmann et al. [20] and Hartley et al. [21], although they chose the term "distributive" (instead of distributary) and have referred them as distributive fluvial systems (DFS). The use of satellite images was crucial to recognize where large distributary systems occur today worldwide, and how they are strongly influenced by climate to establish fluvial drainage patterns [17, 20, 21].

The distributary drainage network and the dimensions of the alluvial systems of the Pantanal Basin [22–24] are typical of fluvial megafans [15]. The Taquari megafan is unquestionably the most studied of them and the largest distributary fluvial system in the basin with ~50,000 km^2 [25–28].

All Pantanal megafans are depositional systems driven by avulsive rivers. Fluvial avulsion is frequently an autogenic phenomenon since it emerges exclusively from intrinsic factors related to the construction and abandonment of depositional fan lobes. Fluvial avulsion is hence discernible from stream piracy, in which a river captures an adjacent river because of regressive erosion processes

or crustal movements in active tectonic areas. Avulsion is very common because the rivers do not drift laterally and gradually in the plain, but shift suddenly to areas far from the active main channel. Shifts of the Taquari River course have been quite frequent in the modern distributary lobe. A remarkable avulsion took place during the 1990s in the lower course at the fringe of the Taquari megafan, in the locality named "Zé da Costa." The channel shifted 30 km northward its confluence in relation to its original mouth at Porto da Manga locality [25]. The avulsion was quick as time lapses only 10 years and the succession of events is very well documented in satellite images (Fig. 3).

An avulsion of greater magnitude has been evolving since the beginning of the 2000s near the apex of the modern fan lobe (Caronal farm), where the meander belt unconfines. Frequent overflow and many in the natural levees on the right margin of the Taquari River with drainage of sediment-laden waters have been diverting the flow to the floodbasin. The distributary channels distribute the sediments over a broad accumulating alluvial area where a new avulsion belt is under construction. The new channels divide into numerous channels with frequent rejoin characterizing an anabranching (multichannel) river system, but channels fade away downstream and the waters flow unconfined in an extensive floodbasin. Most of the river water is already flowing through those newly formed channels (Figs. 3 and 4), and the changing landscape has been documented by satellite images (e.g., [27]). The Taquari River can shift its course and abandon the main channel, changing its mouth a hundred kilometers toward north, as previously envisaged by Assine [25].

Avulsion commonly results from the association of many factors, and the triggering occurs during a discharge event of magnitude at or near the avulsion threshold [29]. Although there is no consensus on the causes that initiate the avulsions in the Taquari megafan, one of the most important causes for avulsion is the channel aggradation [25, 27, 30]. Zani et al. [28] pointed out that avulsions are occurring progressively closer to the apex (intersection point of the megafan) and suggested that the system is being filled in a toe-to-apex direction. Based in these observations, they concluded that the base level is above the longitudinal profile downstream of the intersection point, where accommodation space is available for in-channel sedimentation, which causes avulsion triggering.

Flow deceleration downstream of the intersection point results in the channel aggradation and riverbed shoal formation (Figs. 3 and 4). Progressively the channel belt becomes a few meters higher than the adjacent floodbasins because of the aggradation inside the channel and increasing height of marginal levees, causing the channel to lose capacity to convey flood discharge. Channel overflow and crevassing (*arrombados*) create favorable condition for avulsion, beginning with channel splitting. The process can be very rapid because the slope down to the adjacent floodbasin is higher, diverting the flow and causing the abandonment of the main channel (Fig. 5).

Avulsive river shifting in the modern distributary lobe of the Taquari River is a natural response of the system to accommodate sediment supply coming from the catchment area. In this context, channel aggradation has been likely intensified by land use (livestock and farming) in the basin highlands [31, 32]. Besides, river

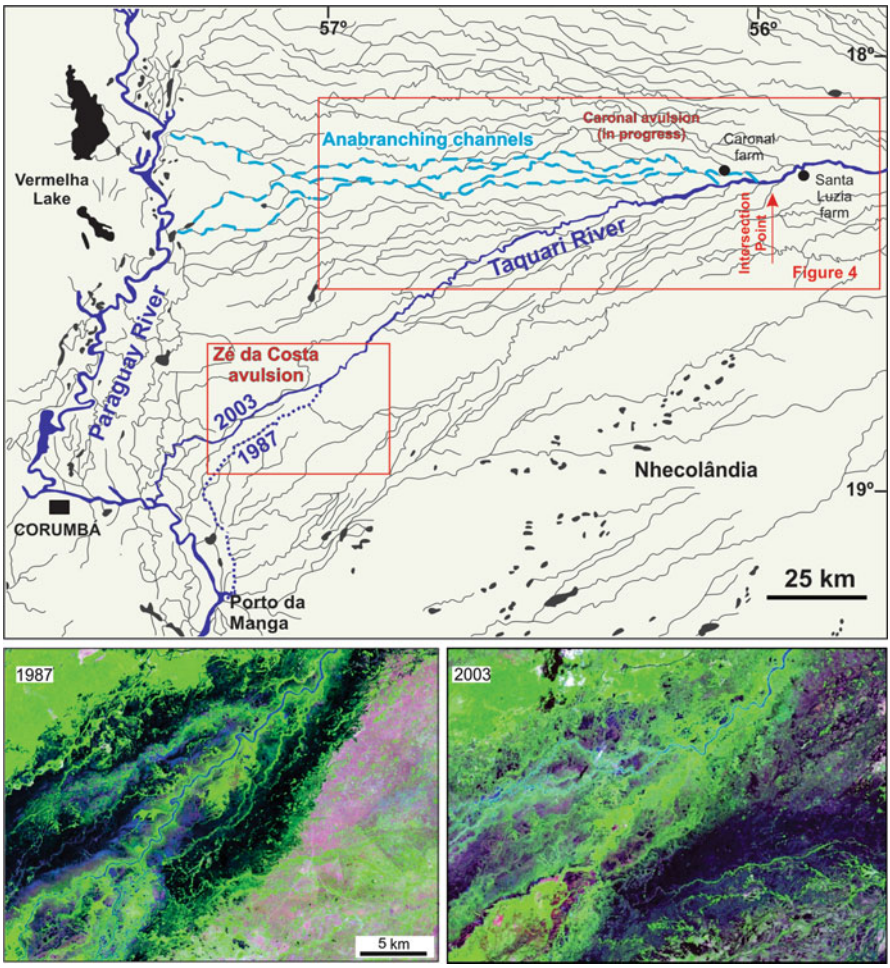

Fig. 3 Avulsions on the modern depositional lobe of the Taquari megafan (IP = intersection point). A large-scale avulsion is in progress at the apex near the intersection point of the megafan at the Caronal farm. The new distributary channels on the right margin of the river envisaged by Assine [23, 25] are now very active draining more the 70% of the river discharge and shifting approximately a hundred kilometers north from its confluence with the Paraguay River. The well-known "Zé da Costa" avulsion has occurred in a time lapse of two decades, as documented by multitemporal Landsat images taken in 1987 and 2003 (false-color composition R7G4B3)

avulsions in lowlands may also result from increased rainfall since 1973, following a very dry decade.

Despite the recently anthropogenic interference, avulsion is a geomorphologic result of a natural depositional mechanism in fluvial megafans. The São Lourenço megafan gives us an important evidence of this natural behavior. The "Boca Brava" avulsion (Fig. 6) caused the abandonment of its former main channel, the "Braço do São Lourenço," and the confluence with Piquiri River and shifted the river to its

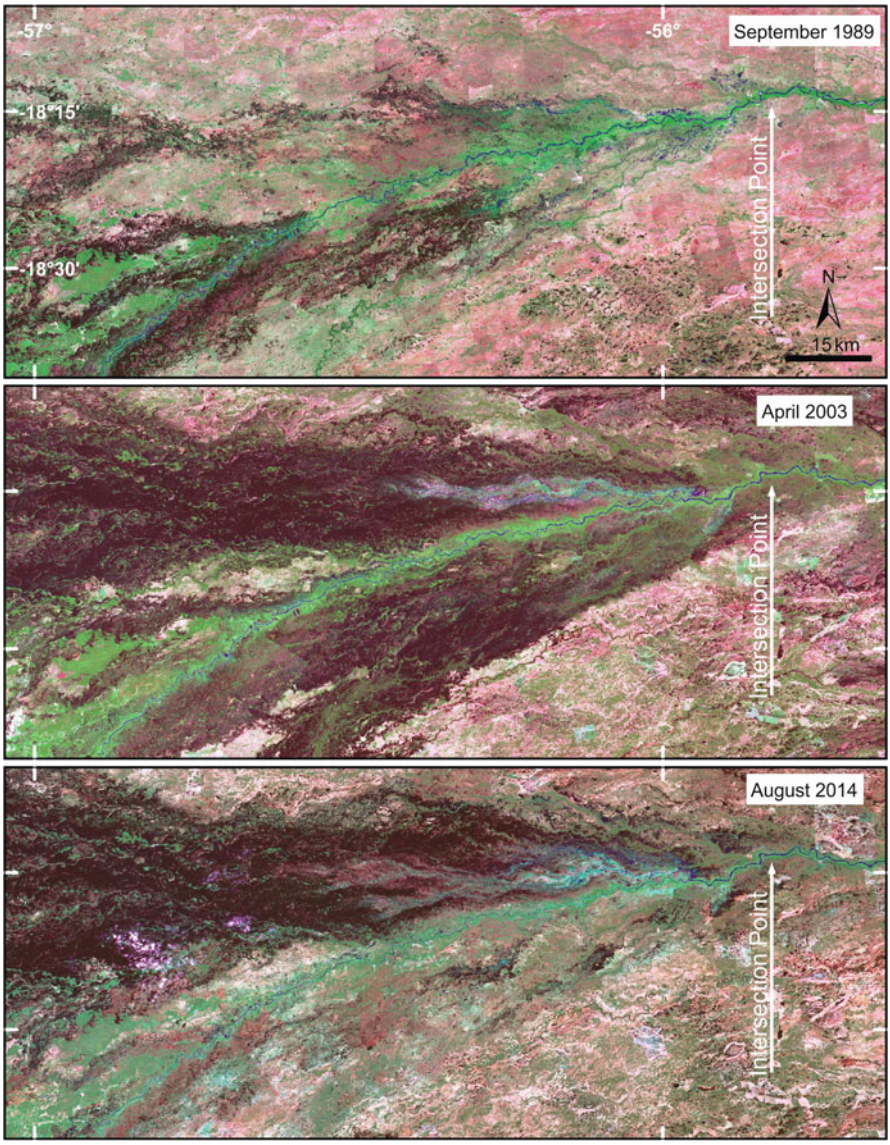

Fig. 4 Channel changes and the deposition of an avulsion belt associated with the Caronal avulsion as seen in multitemporal satellite images taken in 1989, 2003, and 2014. (Satellite images: 1989 TM5 R7G4B3; 2003 ETM+ R7G4B3; 2014 OLI R7G5B3)

present course and actual confluence with the Cuiabá River [33]. The shift took place between 1890 and 1915 [33] and indicates that avulsions in the Pantanal are commonplace, independently of accelerated sedimentation due to anthropogenic activity, which became much more intense with agricultural and ranching practices

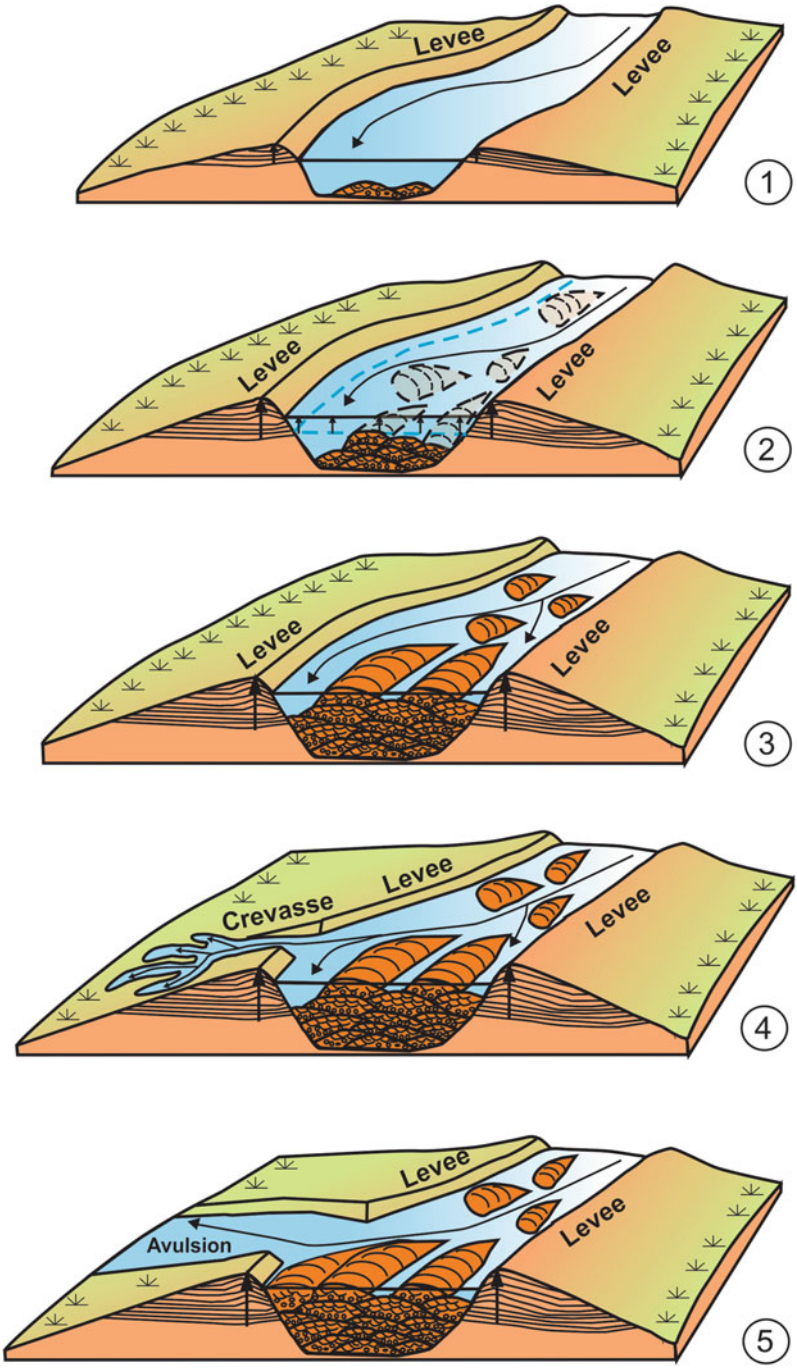

Fig. 5 Schematic evolution of the phenomenon of channel splitting and avulsion of the Taquari River [26]: (*1*) the channel steadily rises in relation to its adjacent areas due to the levees built through subsequent seasonal flood overflows. (*2*) The riverbed rises through sediment aggradation

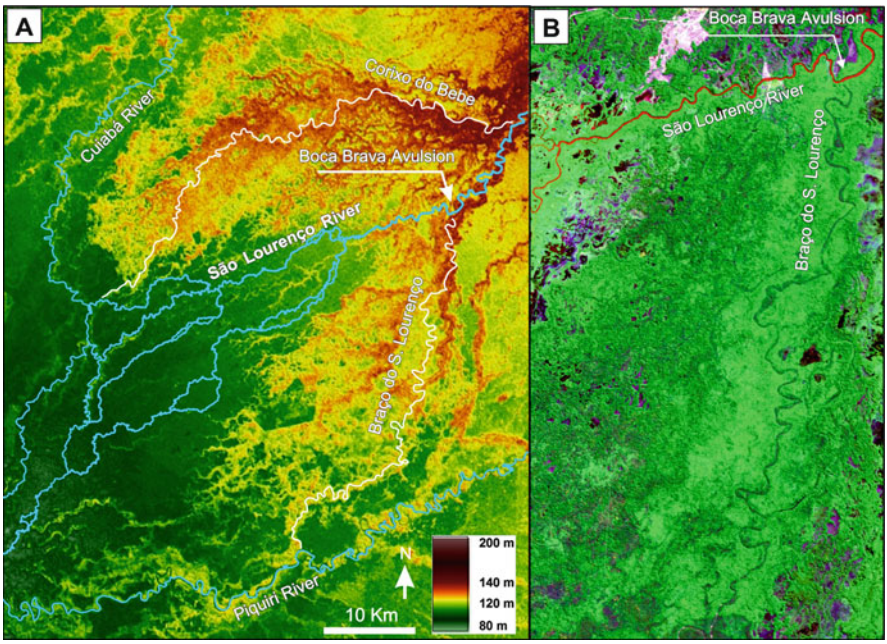

Fig. 6 Avulsion and establishment of distributary channels in the modern depositional lobe of the São Lourenço megafan. *Left-sided* image is SRTM data, and the *right-sided* image is a box section obtained by false-color band composition of Landsat TM data, GeoCover, RGB742, 1990

after the 1970s. The time span (<25 years) is similar to the rate of recent avulsions observed in the Taquari megafan [25]. The abandoned "Braço do São Lourenço" channel now behaves solely as an intermittent stream flowing during wet seasons, but remains a prominent morphologic feature on the landscape. Nowadays, sedimentation on the active depositional lobe of the "São Lourenço" megafan occurs in its most distal position, between the "Corixo do Bebe" and the "Braço do São Lourenço" abandoned lobes, an area with available accommodation space where river splits into two or more distributary channels, each one presenting many divides and rejoin (Fig. 6).

The Paraguay River itself has been building a large megafan at the river entrance into the northwestern border of the Pantanal. The drainage pattern is distributary on the modern depositional lobe, and the Taiamã Island resulted from the split off and rejoin of the main channel [35]. Minor avulsions have commonly occurred in this

Fig. 5 (continued) in the channel and in the marginal levees. (*3*) Following the silting process of the channel, the sand bars emerge even in flood times, causing reduction in channel capacity of water retaining. (*4*) Sooner or later, a seasonal flood induces the crevassing of the marginal levee and the splitting of the channel. (*5*) The water flow is steadily diverted to the new channel and, finally, the river changes its course with the abandonment of the main channel

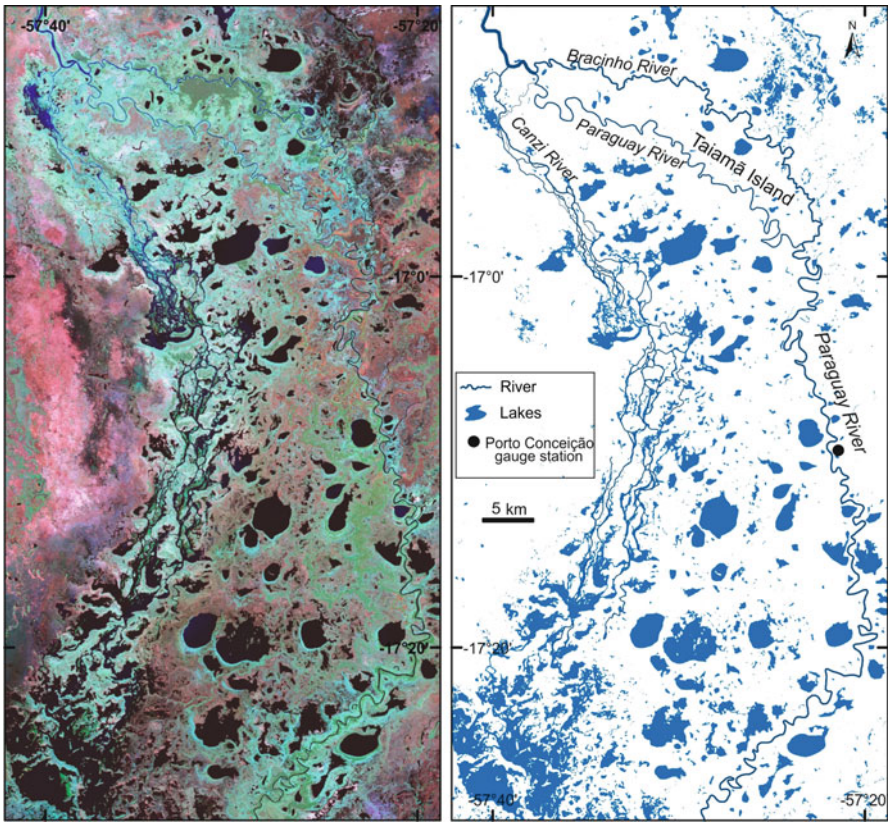

Fig. 7 Avulsion in progress on the right margin of the Paraguay River upstream of the Taiamã Island. Waters from the diverting channels are contributing to form the anabranching channels of the Canzi River

modern distributary lobe, as indicated by many abandoned channels within the floodplain. Emphasis must be addressed to an important avulsion in progress upstream of the Taiamã Island, where water is flowing out from the channel through some crevasses on the right margin of the Paraguay River. This pattern suggests a probable abandonment of the present channels of the Paraguay River and a future attachment of the Taiamã Island to the floodplain (Figs. 7 and 8).

Successive dividing and rejoining results in an anabranching fluvial pattern, which characterizes many reaches of modern depositional lobes of Taquari and São Lourenço River megafans. The Cuiabá River also exhibits anabranching channels in the modern depositional lobe, but differently from the former, it presents important reaches characterized by the existence of multiple small channels in the upper megafan setting [36].

Multiple dividing and rejoining river channels encompass a wide variety of river patterns, referred elsewhere as *braiding*, *anastomosing*, or *anabranching* which can

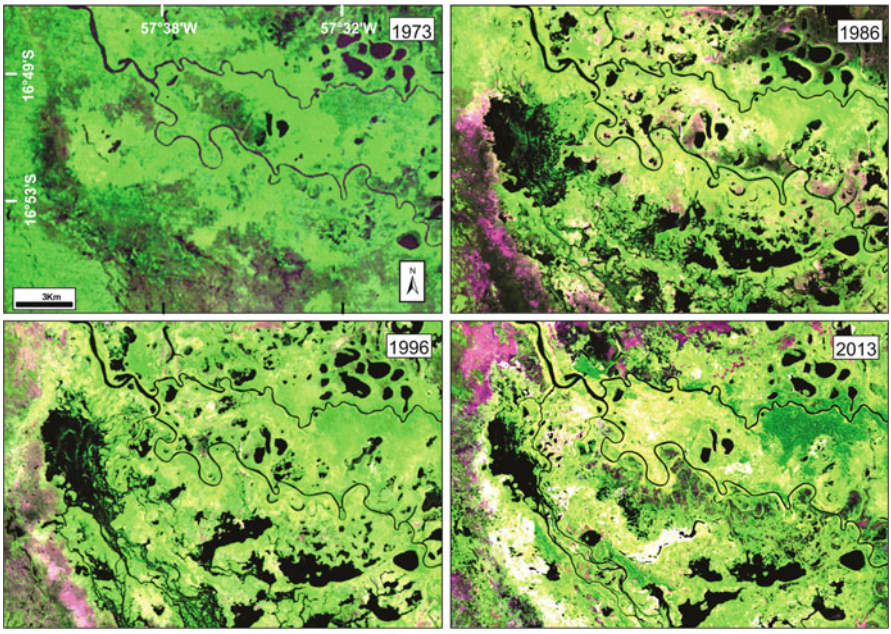

Fig. 8 Crevassing and diverting channels on the right margin of the Paraguay River as seen in multitemporal satellite images (Landsat 1 MSS, RGB475, August 1973; Landsat TM5, RGB547, October 1986; Landsat TM5, RGB547, July 1996; and Landsat 8 OLI, RGB657, June 2013

be referred altogether as *multichannel rivers* [37]. Despite the differences in channel style, multichannel rivers are present in the Pantanal wetland, not only in the fluvial megafans, but also along the Paraguay River main stem. The Paraguay flows from its catchment at north to the exit of the Pantanal wetland, crossing a heterogeneous floodplain and collecting the waters from the whole basin. Multichannels are present in many geomorphic zones of the floodplain, and their importance to the Pantanal hydrology is presented in the following section.

3 Depositional Tract and Surface Hydrology Dynamics

Flowing from southward along the western margin of Pantanal wetland, the Paraguay River is the mainstem river of a depositional tract composed of many fluvial megafans and interfan systems, lakes, and swamp areas (Fig. 9; see [15]). Accordingly, the drainage system is very complex due to the coexistence and interaction of these different systems. Within the Pantanal, the drainage networks display channel bifurcations and avulsions in the megafan distributary systems, and multichannel reaches are frequent in the modern megafan depositional lobes, as well as in the Paraguay River mainstem plains. These peculiarities cause a very complex flood

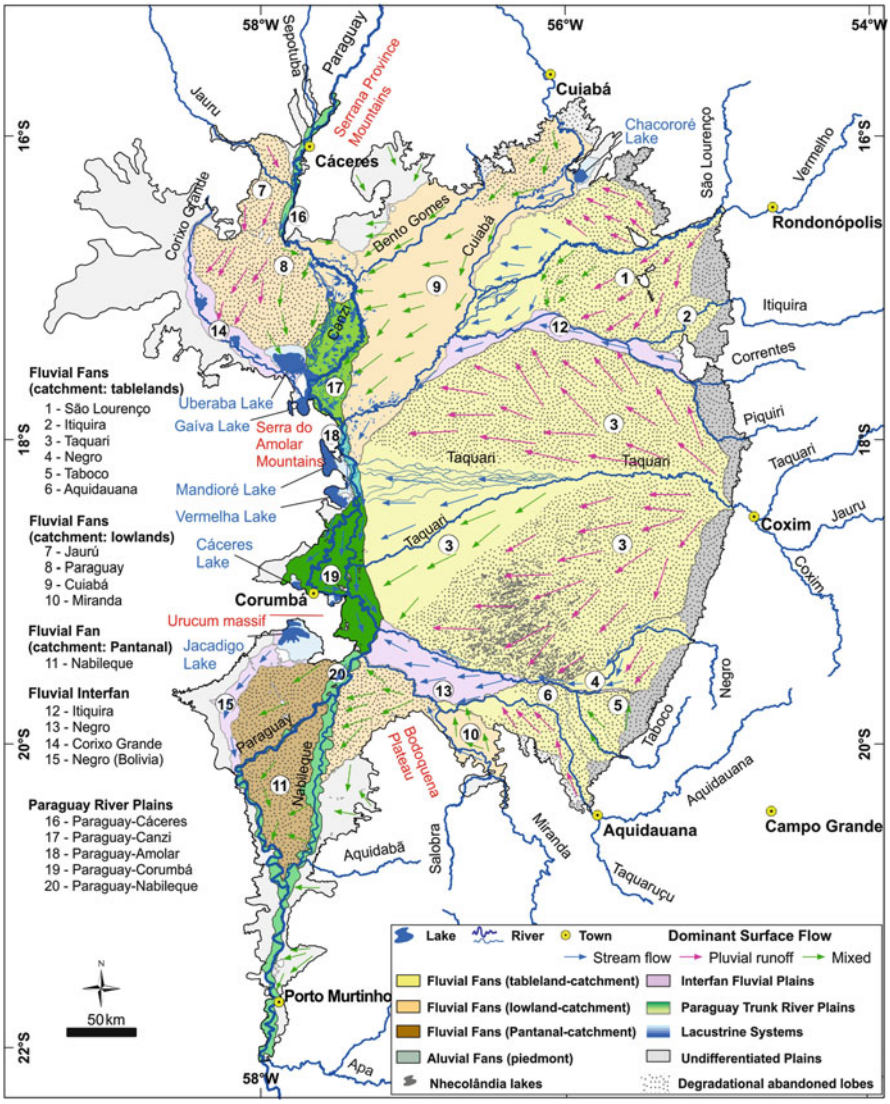

Fig. 9 The Pantanal alluvial depositional system tract with drainage pathways (streamflow, pluvial runnof, and mixed flow) [33]

regime within the Pantanal wetland with ecological and socioeconomic implications.

The hydrology of the Upper Paraguay Basin is very complex [38]. Rivers in the catchment area have comparable regimes with strong direct in-phase correlation between rainfall and discharge (Fig. 2), but in the fluvial megafans, the peak of fluvial discharge occurs one to two months after maximum rainfall. In the fluvial

megafans, meander belts are confined in the upper fan and the river works as a bypass transporting water from the catchment area directly to the modern lobes, and the abandoned lobes do not receive water from the river. In the abandoned lobes, the surface runoff is essentially pluvial during floods and sustained by subsurface return flow (throughflow) after flood peaks. Outflow of the ground in springs is the source of water to many small streams (named "corixos") that drain the surface of abandoned lobes following the wet season. Some of these abandoned lobes, especially those of the megafans situated on the south portion of the Pantanal (Aquidauana, Miranda, and Nabileque), are characterized by mixed surface runoff because there are contributions of pluvial water as well as sheet flow from unconfined fluvial waters (Fig. 9).

In general, the fluvial fans of the Pantanal have a concave-down morphology that favors the water dispersion, preventing water retention. The Taquari and São Lourenço megafans exemplify the morphological control on water transfer (Fig. 10). In the upper portion of the fan, the river is normally incised and runs in a narrow meander belt entrenched on their ancient lobes. The active lobes have a grossly triangular shape with the vertex toward the fan apex. Sedimentation processes are very active in these sites, avulsion being the main fluvial phenomenon of sediment dispersal. Following avulsion, the river becomes unconfined and the waters flow radially by a system of distributary and anabranching channels.

The hydrographs of the Taquari and São Lourenço rivers show that during mid-lower water level, the flow occurs only in the channel, both for the incised and anabranching reaches (Fig. 10). As these rivers do not receive any tributary along the fan, the discharge measured in the upper, mid, and lower gauge stations are practically the same. However, during the flood pulse, the gauge stations in the anabranching reach of both rivers show an impressive loss of water for secondary anabranching channels. Differently from common fluvial basins, the channel belt in the uppermost portions of the fluvial plain is a bypass and works as a "drainage divide" for surface runoff. The Hortonian flow lines drawn over the topographic maps of the Taquari and São Lourenço fluvial fans indicate a dispersive trend of water from the channel belt toward the fan fringes (Fig. 10).

The Paraguay River collects water from multichannel streams present in the modern distributary lobes of fluvial megafans and from streams of interfan fluvial plains, each one with very different hydrological functioning. Hydrographs along the Pantanal mainstem river display an opposite behavior relatively to the rivers in the catchment area (Fig. 2). Whereas the fluvial discharge in the catchment area (Cáceres, Barão de Melgaço, and Coxim stations) varies in phase, in São Francisco and Porto Murtinho stations, respectively, at the center and at the end of the Paraguay River plain, the discharge varies out of phase with local rainfall.

The historical gauge station series of the Pantanal rivers vary in data extension, continuity, and quality. Collischonn et al. [39] identified for the Ladário gauge station – the longest historical series constructed since 1900 – a period of low hydrometrical level from 1962 to 1973 followed by the present period of high hydrometrical level. An expedite hydrological comparison between dry and humid periods measured for eleven gauge stations along the Paraguay River shows a

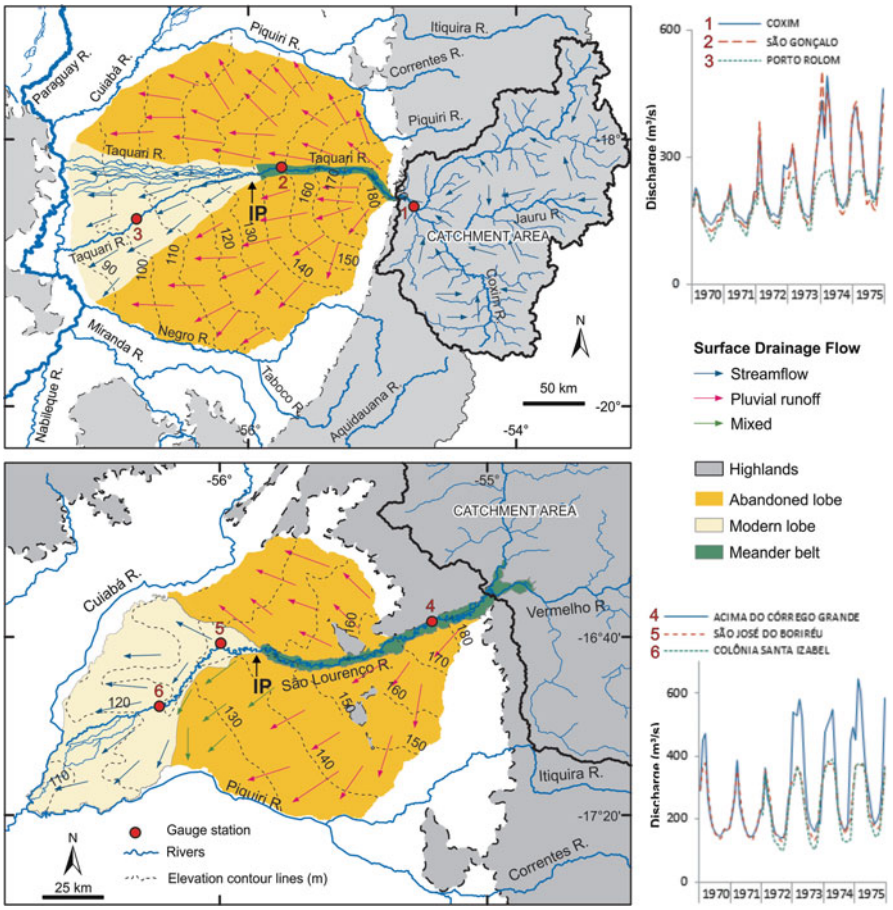

Fig. 10 Surface hydrology of the two large Pantanal megafans: Taquari (*upper*) and São Lourenço (*lower*). Both megafans are characterized by similar morphology and surface hydrology. Water from catchment areas reach the modern depositional lobes through feeder channels confined in meander belts entrenched in the upper fan (IP = intersection point). Abandoned lobes in both systems do not receive water from the catchment nor directly from the feeder channel, and most of the flooding comes from pluvial runoff. The rivers lose water to the floodplain in the modern depositional lobes, especially during rainy years, as occurred in 1974–1978 when the monthly mean discharge was higher than previous years. Hydrographs presented on the right refer to gauge stations: Coxim (*1*), São Gonçalo (*2*), Porto Rolom (*3*), Acima do Córrego Grande (*4*), Colônia Santa Izabel (*5*), and São José do Borireu (*6*)

difference from 81% in the annual average discharge at Porto Murtinho gauge station (Fig. 11). The intense land-use change in the Pantanal highlands during the last four decades also contributes to significant changes in the ecohydrology [40] of the Pantanal. Forest suppression in highlands for crop and livestock [41–45] is responsible for increasing river discharge while reducing evapotranspiration and

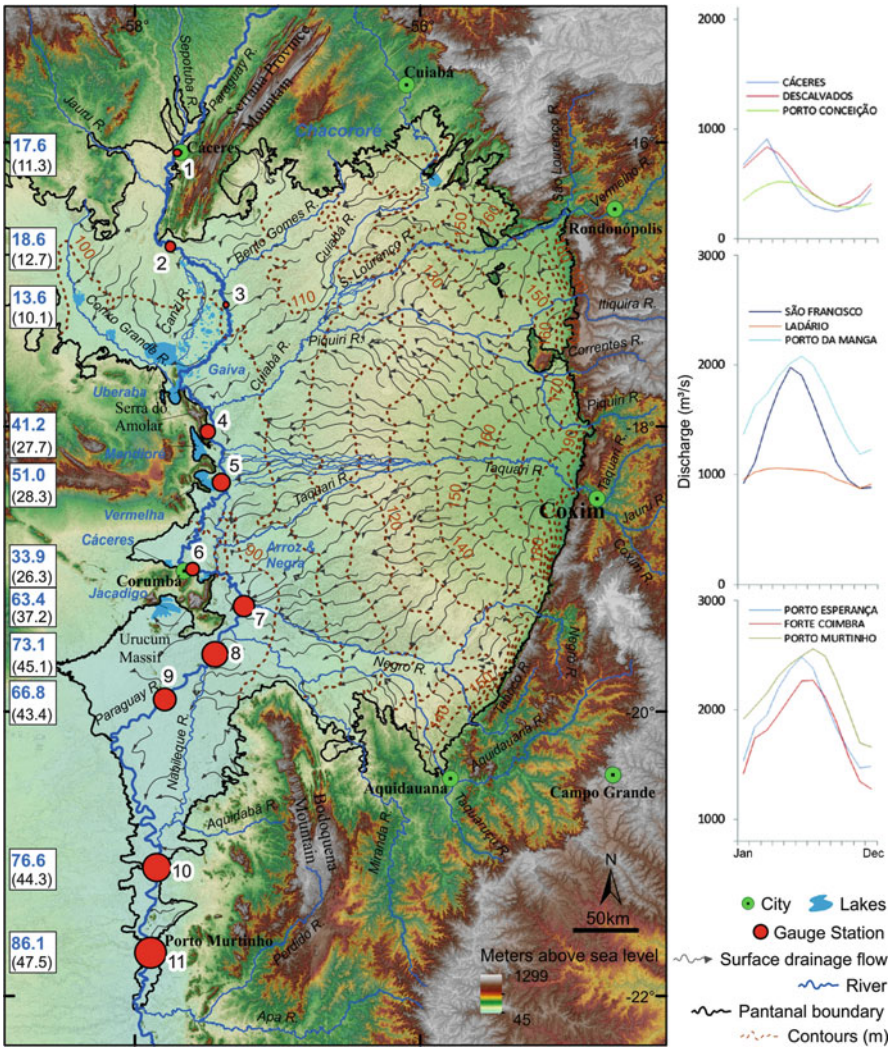

Fig. 11 The Pantanal hydrology of the land surface system. The main rivers are represented as well as runoff pathways (*sinuous arrows*) of surface waters extracted from the SRTM data. Numbers in white boxes are the mean total annual discharge (km^3 $year^{-1}$) at each gauge station during the dry 1970–1974 period (*black*) and during the 1974–1978 humid period (*blue*). Gauge stations in the Paraguay River: (*1*) Cáceres, (*2*) Descalvados, (*3*) Porto Conceição, (*4*) Amolar, (*5*) São Francisco, (*6*) Ladário, (*7*) Porto da Manga, (*8*) Porto Esperança, (*9*) Forte Coimbra, (*10*) Barranco Branco, and (*11*) Porto Murtinho. The flood wave from north to south is evident in hydrographs of nine of these gauge stations, grouped in sets of three according to its geographical position: upstream (Cáceres, Descalvados, and Porto Conceição), middle (São Francisco, Ladário, and Porto da Manga), and downstream (Porto Esperança, Forte Coimbra, and Porto Murtinho)

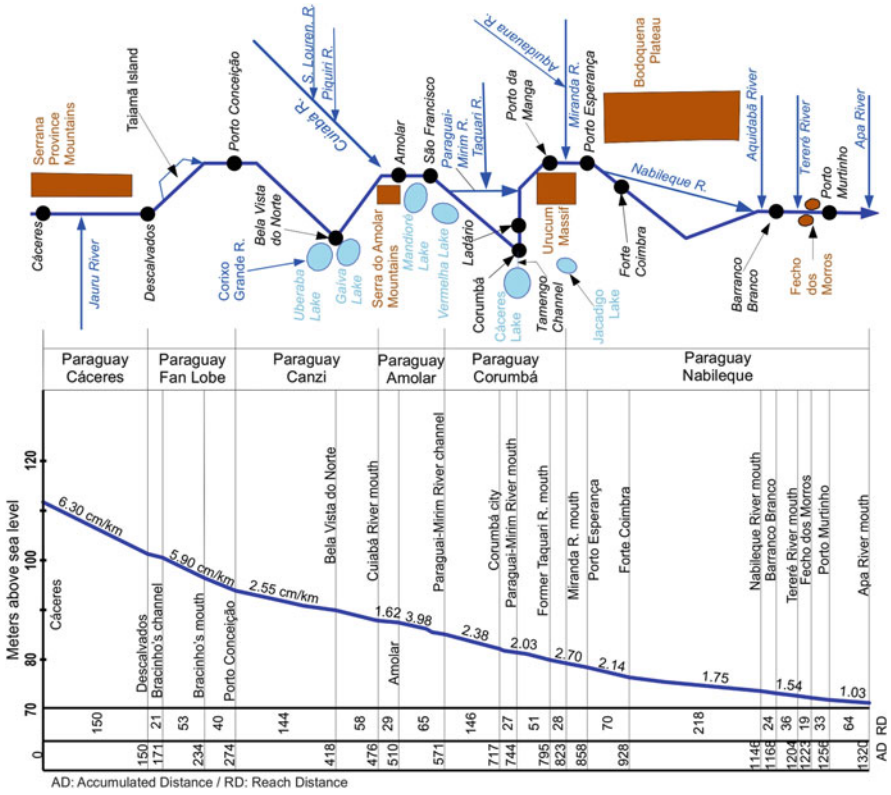

Fig. 12 Hydrographic scheme of the Upper Paraguay River in relation to its gradient profile (not to scale). Longitudinal profile was based on data of Franco and Pinheiro [47]

cloud formation in highlands [32] that could distribute rainfall in lowlands areas without floodplains as the Nhecolândia [46].

The Paraguay River plain has geomorphologic heterogeneity in consequence of its geologic position on the western faulted border of the sedimentary basin [15]. The river-mainstem plain comprises five distinct fluvial floodplain compartments, each one presenting different morphologic characteristics, channel pattern, and hydrologic functioning (Fig. 9). The Paraguay River floodplain is variable in style and width, reflecting tectonic control on the western margin of the Pantanal basin and interaction with the distal portion of fluvial megafans. The longitudinal profile of the Paraguay River shows subtle knickpoints in the limit of these compartments (Fig. 12).

The northmost Paraguay-Cáceres river plain compartment, located at the entrance of the Pantanal (Fig. 9) and ending in the farm of Descalvados (gauge station number 2 on Fig. 11), is a 4–5-km-wide confined floodplain, limited by the Jaurú fluvial fan at the right side and the NE lineaments of Serrana Province Mountains at the left margin. The river channel has irregular meanders with some

small anabranching channels, oxbow lakes, and island along this reach. The flood pulse is coincident with austral summer precipitation, and both Cáceres and Descalvados hydrographs show approximately the same behavior with a small increase in the annual discharge in Descalvados station, which results from the confluence of the Jaurú River in the middle of reach (Fig. 11).

Leaving the confined Paraguay-Cáceres river plain, the river forms the modern lobe of the Paraguay megafan ([35]; Fig. 9), an active depositional lobe characterized by two main anabranching systems. An important bifurcation of the Paraguay River channel (Bracinho River) and the downstream channel rejoining form the 30-km-long Taiamã Island. Recently, crevasses upstream of the Taiamã Island are diverting important water flow into the floodplain on the right margin of the river, turning the Canzi River a multichannel system with many anabranching channels (Fig. 7). A comparison among hydrographs of gauge stations situated upstream (Cáceres and Descalvados) and downstream (Porto Conceição) of these crevasses confirms important loss of water to the Canzi River during the river peak discharge (Fig. 11). When water level is sufficiently high, the Paraguay also loses water southward as sheet flow over the surface of the abandoned lobes. Myriad small lakes in the floodplain accumulates large amount of water diverted from the main channel and contributes to retarding the flood wave.

The Paraguay-Canzi plain is a compartment with reduced river gradient in relation to the upstream reaches (Figs. 9 and 12). The floodplain is a large area of active sedimentation, receiving water and sediment from the Paraguay and Canzi rivers. The plain also receives water and sediments from the Cuiabá River. A large number of lakes form in the floodplain, including the largest Uberaba and the Gaíva lakes. The water accumulation in this lake-floodplain is so forceful that the peak in the Amolar gauge station, at the end of this floodplain, occurs in May–June, about 60 days after it passes by Descalvado gauge on March. The Paraguay-Amolar floodplain produces a bottleneck effect on the water coming from the Paraguay and Cuiabá, incurring the delay of the flood-pulse wave. Such a huge mass of dammed water accumulates in the Paraguay-Canzi floodplain, feeding lakes and swamps and producing a huge continuous water body of more than 10,000 km^2 during June and July (Fig. 13). The importance of this area in the hydraulic regulation of the Upper Paraguay River was highlighted in the report [48].

The Paraguay-Amolar is a narrow floodplain limited by the Serra do Amolar mountains and the Cuiabá and Taquari megafans that conjointly acts as a bottleneck for the flow of the Paraguay River (Figs. 9 and 13). It has about 53 km long, ending with the floodplain extension near the Vermelha Lake. Despite only 6 km wide, the Paraguay-Amolar floodplain has empty spaces constituted by the large Vermelha and Mandioré lakes and a series of irregular water bodies covered by floating macrophytes and cut by channel-levees. The Cuiaba River that flanks the eastern side of the floodplain also supplies the area with large amount of sediment through crevasse splays (Fig. 13). The reach is also influenced by the Cuiabá and the north portion of the Taquari active fans (Fig. 9), which supplies with water the Paraguay through many anabranching distributive channels. Thereby, the hydrograph of the São Francisco gauge station in the middle portion of the reach also shows it flood-

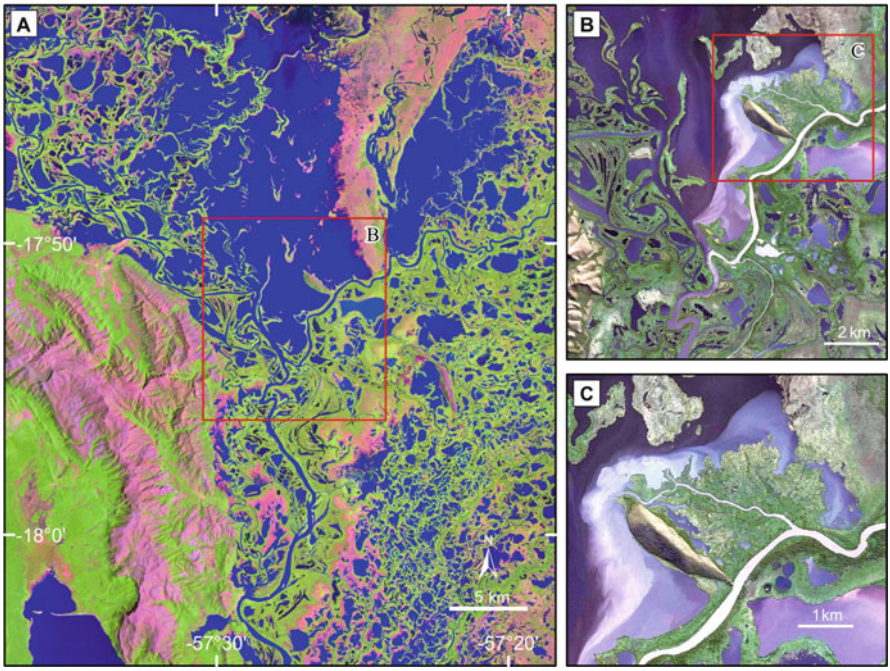

Fig. 13 Narrow river plain in the Serra do Amolar bottleneck causes flow constriction and backwater flooding upstream. (**a**) In consequence, the water level rises in the floodplain of the Paraguay and Cuiabá rivers, as well as in the Uberaba and Gaíva lakes, creating a large area often inundated (Satellite image Landsat 5 TM, R5G4B3, from December 1985). (**b**, **c**) The reduction in sediment load transport makes this area a site of active sedimentation, exemplified by crevasse splays in the lower course of the Cuiabá River

pulse peak on May, about three months later than in those verified for Cáceres and Descalvados stations.

Placed downstream of the Vermelha Lake, the Paraguay-Corumbá compartment is a 27-km-wide plain drained by an anabranching reach formed by the Paraguay and the Paraguai-Mirim rivers. This flat floodplain (slope around 2.3 cm/km) is not homogeneous but covered by paleochannels of anabranching channels of the ancient Paraguay River ([49]; Fig. 14). Inactive during the low-medium water level, these paleochannels receive water during the flood, so that flood-pulse peak takes a month to run from São Francisco to Porto da Manga gauge stations, the last one located near the mouth of the Miranda River at the end of the Paraguay-Corumbá river plain. The hydrographs of São Francisco and Ladário gauge stations show that 10% of the Paraguay discharge is diverted to the Paraguai-Mirim. However, this difference increases twofold during the flood (Fig. 14). The narrowing of the Paraguay floodplain near the mouth of the Miranda River, constrained by the highlands of the Urucum Massif and the fringe of the Miranda fluvial fan, constricts the river flow and functions as a second bottleneck along the Paraguay River course (Urucum Bottleneck).

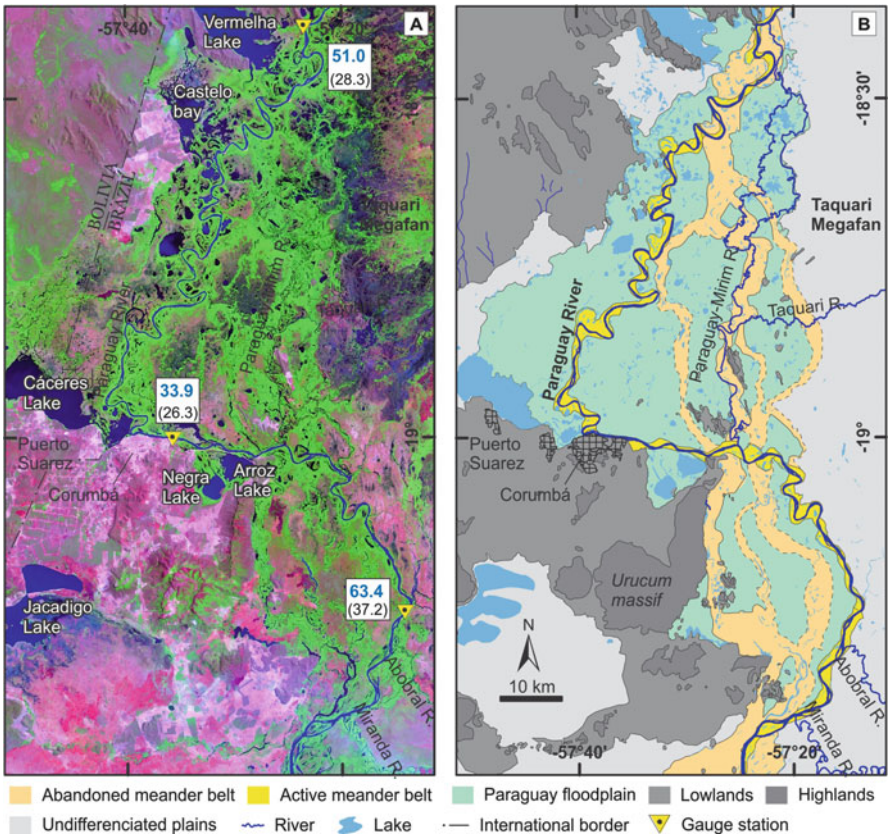

Fig. 14 Hydrology in the large Paraguay-Corumbá plain is strongly controlled by active landforms. This reach of the Paraguay River is marked by abandoned meander belts, where the Paraguay River channels were formerly placed before its avulsion to its actual meander belt. Many lakes are closely influenced by the Paraguay flooding dynamics. (**a**) Landsat 7 ETM+ (R7G4B3) image from September 1999; (**b**) geomorphological map showing distinct zones and paleo landforms (after [49]). Numbers in white boxes are the mean total annual discharge (km^3 $year^{-1}$) at São Francisco (5), Ladário (6) and Porto da Manga (7) gauge stations during the dry 1970–1974 period (*black*) and during the 1974–1978 humid period (*blue*)

Downstream the confluence of the Miranda River, the Paraguay River enters in a less subsiding area at the south portion of the wetland. In this area, the actual meander river belt cut the Pleistocene deposits of the Nabileque megafan [50]. Remarkable is the presence of a large paleomeander belt of the Paraguay River in which today the Nabileque River flows as an underfit stream resulted from an important avulsion occurred around 4,000 years ago ([51]; Fig. 9). Comparing the hydrographs of Porto Esperança, upstream of the avulsion point, with Forte Coimbra, located downstream of the avulsion point, it is possible to verify that the Paraguay River loses about 10% of its water to the Nabileque River during the flood seasons (Fig. 11).

4 Hydraulic Bottlenecks and the Flooding Wave

Inundation dynamics in the Pantanal wetland are greatly dependent of its geomorphology and many attempts to define patterns and forecast river water levels were made [52–56]. The inundation paths result from the intricate pattern of interconnected fluvial fan and interfan systems that link many catchment areas. The complex flooding wave is also constrained by the heterogeneous Paraguay River plains, formed by alternation of extensive floodplains separated by natural bottlenecks.

The structure and function of the flow dynamics of these floodplains are very important for navigation as well as for the sustainable exploitation of the ecosystem services provided by the Pantanal wetland (including tourism; see [57]). The more impressive and important hydrological phenomenon in the Pantanal is the backwater effect produced by the narrow reaches of Paraguay-Amolar and Paraguay-Nabileque over their respective upstream reaches. The flood permanence is always larger than 50% with extremes of 85% (ANA/GEF/PNUMA/OEA 2005).

Backwater is controlled by geological features reflected by knickpoints in the river longitudinal profile (Fig. 12). Furthermore, gauging backwater reaches is very difficult because the relation between water level and discharge during the flood is unclear (Ponce, op. cit.). Through satellite image, however, it is possible to identify the influence of the bottlenecks of Serra do Amolar and Urucum that favors water accumulation in the upstream reaches of Paraguay-Canzi and Paraguay-Corumbá, respectively (Fig. 15).

ANA/GEF/PNUMA/OEA (2005) report presents a simulation for the Paraguay-Canzi river compartment considering a water level elevation of 1.0 m in the Amolar gauge station. The backwater extends by 270 km from Amolar up to the Descalvados gauge station. Under this condition, the average hydraulic slope is reduced from 3.5 to 1.8 cm/km, whereas the discharge remains constant (943 m^3/s). A continuum backwater includes waters from both the Paraguay River and the lower Cuiabá River (Figs. 13 and 15).

A comprehensive view of Pantanal flood dynamics is depicted in Fig. 16. Nine satellite images (MODIS data) in the hydrological year of 2006 compose a temporal window of the wave, flood-pulse advancement, the bottleneck damming effects, water transference, and the strong control of tributary fans over the hydrology in the mainstem river. The Pantanal is fully dry in the beginning of January. The areas of permanent water accumulation are restricted to floodplain lakes and to some portions of the active lobe in the Taquari River megafan. During the dry period, water flows only through river channels. The flood initiates on January, and the Paraguay-Canzi river plain starts to flood due to the bottleneck effect imposed by the Sera do Amolar and the Cuiabá River plains. Up to April, all floodplains upstream of the Paraguay-Amolar bottleneck are completely flooded. Some areas of the active and ancient lobes of the Taquari River megafan are also flooded. On May, the Paraguay-Corumbá river plain is also flooded, and the huge water body includes the active portions of Taquari megafan. On June, the flood spreads over all

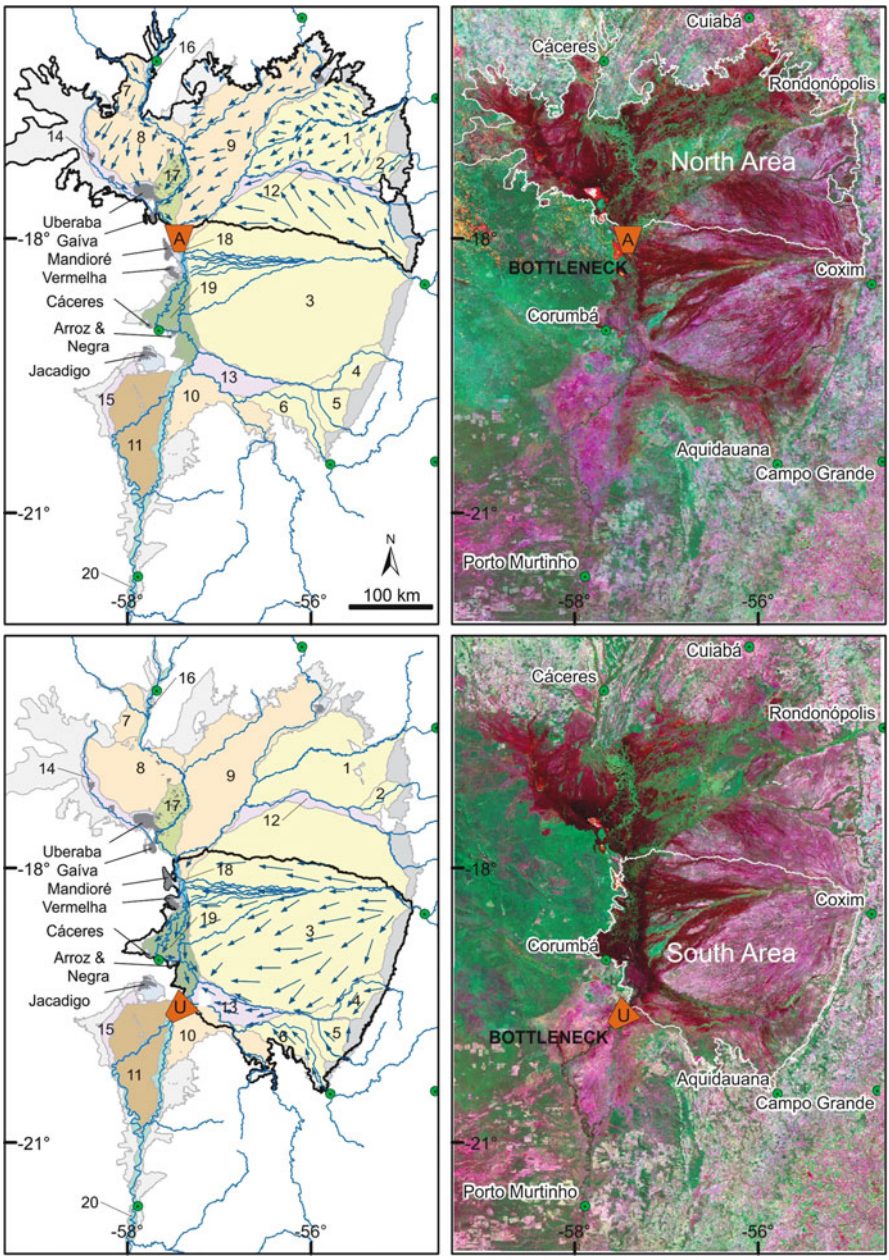

Fig. 15 The two bottlenecks that exert strong control (damming effect) on the flooding extent, magnitude, and duration in the Pantanal wetland. The Serra do Amolar bottleneck (A) delays the northerly flood-pulse wave. The Urucum bottleneck (U) slows down the flood-pulse wave southward and enhances the inundation in the Paraguay-Corumbá plain, in the fringe of the Taquari megafan and in areas draining to the Negro River interfan floodplain (numbers refer to depositional systems as identified in the Fig. 9)

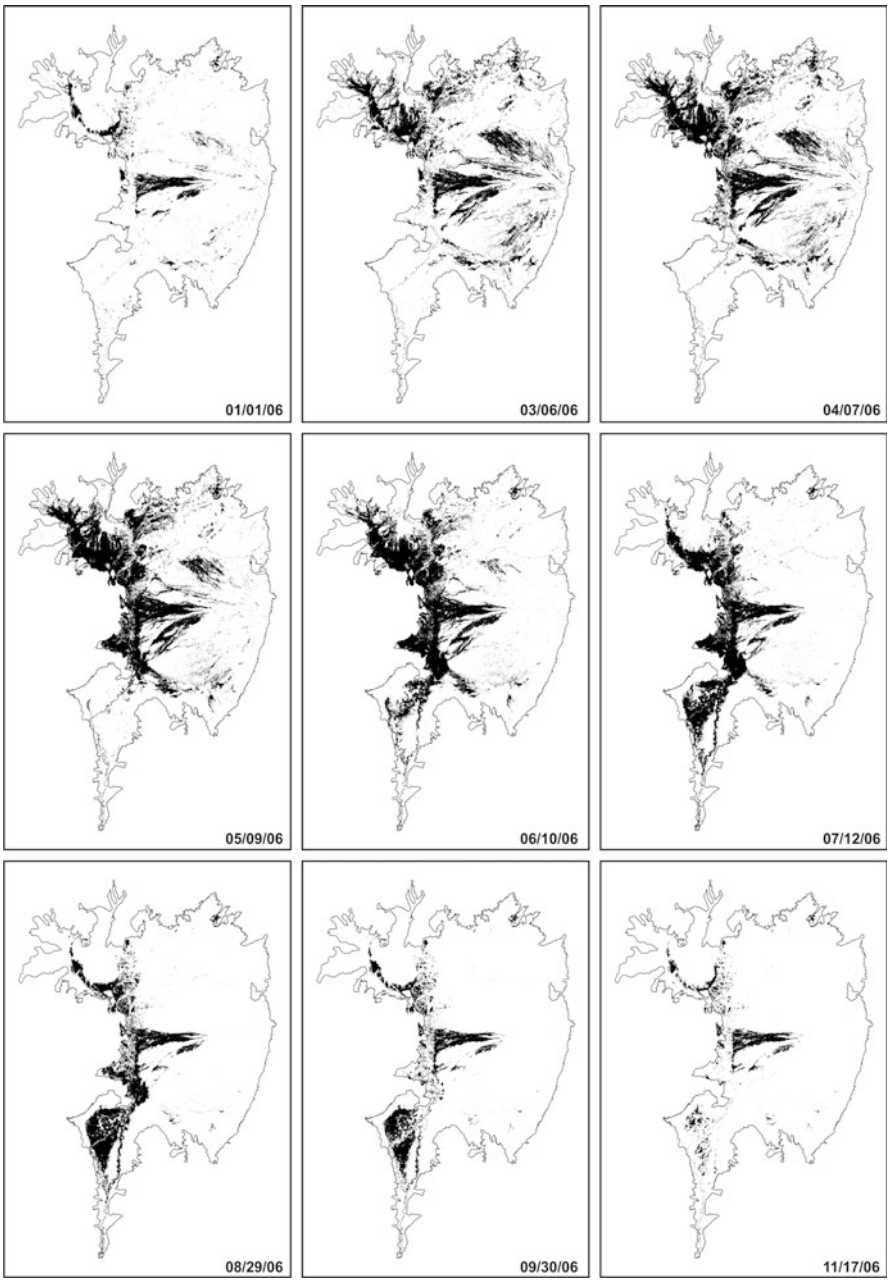

Fig. 16 Synoptic view of the annual spatial and temporal flood-pulse dynamics in 2006 (January to November) based on multitemporal MODIS images [54]. The successive images record the water transfer from borders to center and from north to south and how bottlenecks are effective in damming the water flow and enhancing the upstream floods. The effect of the Urucum bottleneck is clear after comparing images from May 9 to August 29

the Pantanal including the Paraguay-Nabileque river plain that begins to be flooded. On July, the upper plains start draining, and the flood in the Paraguay-Nabileque reaches its maximum. During August and September, all upper river plains are drained and only the Paraguay-Nabileque remains flooded. At the end of the year, the Pantanal is dry again (Fig. 16) and the annual hydrologic cycle resets following the summer rainfall.

The water and sediment flows running over the irregular and rough surface of the floodplain develop erosive and depositional sites forming complex habitats. However, the original concept of *moving littoral* [58] is not applied in all areas of the Pantanal where the water enters the floodplain through different paths mainly through the anabranching channel systems, water body intercommunications, and the rising of the groundwater. Unlike the Amazon floodplain, in Pantanal the flooded areas may or may not exchange water with rivers [54]. Natural levees within floodplains work like dams because water only overpasses these levees at a certain water level threshold. Otherwise, small channel splits, temporarily or permanently connected to the mainstream, transfer the rising water to distant areas of the floodplain, before the rising river waters overpass the levees [53]. The Pantanal flood pulse is therefore distinct from the flood-pulse concept developed by Junk et al. [58] as a model for large Amazon rivers, in which the exchanges occur between the river and its surrounding floodplain. In the Amazon floodplain, the river is active and the floodplain receives and returns the water passively.

In the Pantanal, the river eventually loses water to the floodplain, and the water does not return to the river channel at the same river stretch but kilometers downstream. The relatively long time span of water damming into different floodplains of different provenance can affect water quality of the mainstem river in different moments of the hydrological year with strong influence on the Pantanal ecology and biogeochemistry. One of the well-known but still poorly studied phenomena related to water quality and ecology is regionally named “dequada” or “decoada” [59]. The phenomenon is associated to the return of floodplain water to the channel, which changes in water tranparency, pH, electron conductivity, dissolved oxygen (DO) and carbon dioxide (CO_2) lead to fish mortality [50, 60]. “Decoada” has also great relevance to greenhouse gas exchanges with the atmosphere, in particular methane (CH_4) and carbon dioxide (CO_2) [60]. The flood magnitude and “decoada” intensity show a direct relation measured by an intensity index for the “decoada” in the Paraguay River and its main tributaries [61].

5 Conclusion

Due to its morphology, drainage structure, and dynamics, the fans present very peculiar ways in transferring water and sediment to the mainstem river, with profound implications to flow regime, ecology, biodiversity, and local socioeconomy [63–65].

The narrow relation between the Pantanal ecology and its hydrological regime is well known [49, 61, 66, 67]. Water and sediment loads (dissolved, suspended, and

bed loads) are very important not only for the floodplain morphogenesis and system maintenance, but on recycling nutrients to the biota. In this case, the action of the flood pulse [58], with variables as frequency, recurrence, intensity, tension, and permanence, over sites of different morphology has a relationship (connectivity in the concept of [68]) with the riparian vegetation and other ecological variables [69].

This chapter also highlights that avulsions and bottlenecks largely dictate the hydrodynamics and the ecohydrology of the Pantanal wetland. On the other hand, land-use changes (deforestation) in the highlands [31, 41, 70] necessarily need to be reverted (reforestation and livestock-agroforestry systems; see [32]) to likely decelerate the actual sediment load rate. By reintroducing tree elements in the Pantanal headwater landscape, besides to recover important ecosystem services as evapotranspiration and carbon storage [40], it is likely to reduce the rate of an eventual "anthropogenic accelerated avulsions" into the plains that ultimately can reduce ecosystems' resilience and make it difficult to promote the sustainable development in the lowlands. This issue is particularly important considering the possible climate change scenarios for the region [12].

The fluvial "avulsive and bottleneck" dynamics seasonally affects both local and regional ecohydrological processes, such as flora (and consequently fauna) distribution [42], tree biomass allocation [42], as well as biogeochemistry dynamics in floodplains and lakes [46, 60]. Moreover, it shows that avulsive processes are commonplace in Pantanal, and changes in land use, particularly in river headwaters in the highlands [44, 45], can accelerate the avulsions, making difficult a sustainable use of the Pantanal lowlands.

Acknowledgments The authors thank the São Paulo Research Foundation (FAPESP 2014/06889-2) and FUNDECT/CNPQ (23/200.628/2012) for financial support to our research in the Pantanal Basin, the National Council of Technological and Scientific Development (CNPq) for grants to MLA (308563/2013-1) and to AS (312386/2014-1), Fernanda Quaglio for helpful suggestions to improve the manuscript, and Patrícia Colombo Mescolotti for assistance in the preparation of figures.

References

1. Hamilton SK, Sippel SJ, Melack JM (2002) Comparison of inundation patterns among major South American floodplains. J Geophys Res 107(D20):8038
2. Nobre P, Shukla J (1996) Variations of sea surface temperature, wind stress, and rainfall over the tropical Atlantic and South America. J Clim 9:2464–2479
3. Lenters JD, Cook KH (1999) Summertime precipitation variability over South America: role of the large-scale circulation. Monthly Weather Rev 127:409–431
4. Thompson LG, Mosley-Thompson E, Henderson KA (2000) Ice-core palaeoclimate records in tropical South America since the Last Glacial Maximum. J Quat Sci 15:377–394
5. Marengo JA, Liebmann B, Kousky VE, Filizola NP, Wainer IC (2001) Onset and end of the rainy season in the Brazilian Amazon Basin. J Clim 14:833–852
6. Balek J (1983) Hydrology and water resources in tropical regions. Elsevier, Amsterdam

7. Liebmann B, Camargo SJ, Seth A, Marengo JA, Carvalho LMV, Allured D, Fu R, Vera CS (2007) Onset and end of the rainy season in South America in observations and the ECHAM 4.5 Atmospheric General Circulation Model. J Clim 20:2037–2050
8. Zhou J, Lau K-M (1998) Does a monsoon climate exist over South America? J Clim 11:1020–1040
9. Vera C, Higgins W, Amador J, Ambrizzi T, Garreaud R, Gochis D, Gutzler D, Lettenmaier D, Marengo J, Mechoso C, Nogués-Paegle J, Silva Dias PLC (2006) Zhang toward a unified view of the American Monsoon Systems. J Clim 19:4977–5000
10. Garcia EAC (1984) O clima no Pantanal Mato-grossense, vol Circular técnica 14. EMBRAPA-UEPAE Corumba
11. McGregor GR, Nieuwolt S (1998) Tropical climatology: an introduction to the climates of the low latitudes. 2nd edn. John Wiley and Sons, Chicester, England
12. Marengo J, Sampaio G, Alves LM (2015) Climate change scenarios in the Pantanal. Hdb Env Chem. doi:10.1007/698_2015_357
13. Krepper CM, García NO, Jones PD (2006) Paraguay river basin response to seasonal rainfall. Int J Climatol 26(9):1267–1278
14. Valeriano MM, Salvi LL, Aragão JRL Relações entre a distribuição da precipitação e o relevo da bacia do alto Paraguai. In: 4° Simpósio de Geotecnologias no Pantanal, Bonito, MS, 2012. Anais. Embrapa Informática Agropecuária/INPE, pp 289–298
15. Assine ML, Merino ER, Pupim FN, Warren LV, Guerreiro R, McGlue MM (2015) Geology and geomorphology of the Pantanal basin. Hdb Env Chem. doi:10.1007/698_2015_349
16. Richards K, Chandra S, Friend PF (1993) Avulsive channel systems: characteristics and examples. In: Best JL, Bristow CS (eds) Braided rivers. Special Publication 75. Geological Society, London, pp 195–203
17. Leier AL, DeCelles PG, Pelletier JD (2005) Mountains, monsoons, and megafans. Geology 33 (4):289–292
18. Gole CV, Chitale SV (1966) Inland delta building activity of the Kosi River. J Hidraul Div 92:111–126
19. Stanistreet IG, McCarthy TS (1993) The Okavango Fan and the classification of subaerial fan systems. Sediment Geol 85(1–4):115–133
20. Weissmann GS, Hartley AJ, Nichols GJ, Scuderi LA, Olson M, Buehler H, Banteah R (2010) Fluvial form in modern continental sedimentary basins: distributive fluvial systems. Geology 38(1):39–42
21. Hartley AJ, Weissmann GS, Nichols GJ, Warwick GL (2010) Large distributive fluvial systems: characteristics, distribution, and controls on development. J Sediment Res 80:167–183
22. Braun EWG (1977) Cone aluvial do Taquari, unidade geomórfica marcante da planície quaternária do Pantanal. Revista Brasileira Geografia 39(4):164–180
23. Assine ML (2003) Sedimentação na Bacia do Pantanal Mato-Grossense, Centro-Oeste do Brasil. Tese de Livre-Docência, Universidade Estadual Paulista – Unesp, Rio Claro
24. Assine ML, Soares PC (2004) Quaternary of the Pantanal, west-central Brazil. Quat Int 114 (1):23–34
25. Assine ML (2005) River avulsions on the Taquari megafan, Pantanal wetland, Brazil. Geomorphology 70(3–4):357–371
26. Assine ML, Padovani CR, Zacharias AA, Angulo RJ, Souza MC (2005) Compartimentação geomorfológica, processos de avulsão fluvial e mudanças de curso do Rio Taquari, Pantanal Mato-Grossense. Revista Brasileira Geomorfologia 6(1):97–108
27. Buehler HA, Weissmann GS, Scuderi LA, Hartley AJ (2011) Spatial and temporal evolution of an avulsion on the Taquari river distributive fluvial system from satellite image analysis. J Sediment Res 81:630–640
28. Zani H, Assine ML, McGlue MM (2012) Remote sensing analysis of depositional landforms in alluvial settings: method development and application to the Taquari megafan, Pantanal (Brazil). Geomorphology 161–162:82–92

29. Jones LS, Schumm SA (1999) Causes of avulsion: an overview. In: Smith ND, Rogers J (eds) Fluvial sedimentology VI. Blackwell Science, Oxford, UK, pp 171–178
30. Makaske B, Maathuis BHP, Padovani CR, Stolker C, Mosselman E, Jongman RHG (2012) Upstream and downstream controls of recent avulsions on the Taquari megafan, Pantanal, south-western Brazil. Earth Surf Process Landf 37(12):1313–1326
31. Galdino S, Vieira LM, Pellegrin LA (2006) Impactos ambientais e socioeconômicos na Bacia do Rio Taquari – Pantanal, 1st edn. Embrapa Pantanal, Corumbá
32. Bergier I (2013) Effects of highland land-use over lowlands of the Brazilian Pantanal. Sci Total Environ 463–464:1060–1066
33. Assine ML, Corradini FA, Pupim FN, McGlue MM (2014) Channel arrangements and depositional styles in the São Lourenço fluvial megafan, Brazilian Pantanal wetland. Sediment Geol 301:172–184
34. Correia Filho V (1942) Cuiabá, afluente do Paraguai. Revista Brasileira de Geografia IV(1):3–20
35. Assine ML, Silva A (2009) Contrasting fluvial styles of the Paraguay River in the northwestern border of the Pantanal wetland, Brazil. Geomorphology 113(3–4):189–199
36. Pupim FN, Zaparoli FCM, Assine ML (2012) O megaleque fluvial do rio Cuiabá, Pantanal do Mato Grosso. In: 9° Simpósio Nacional de Geomorfologia, Rio de Janeiro
37. Carling P, Jansen J, Meshkova L (2014) Multichannel rivers: their definition and classification. Earth Surf Process Landf 39(1):26–37
38. Bravo J, Allasia D, Paz AR, Collischonn W, Tucci EM (2012) Coupled hydrologic-hydraulic modeling of the Upper Paraguay River Basin. J Hydrol Eng 17(5):635–646
39. Collischonn W, Tucci CEM, Clarke RT (2001) Further evidence of changes in the hydrological regime of the River Paraguay: part of a wider phenomenon of climate change? J Hydrol 245(1–4):218–238. doi:10.1016/s0022-1694(01)00348-1
40. D'Odorico P, Laio F, Porporato A, Ridolfi L, Rinaldo A, Rodriguez-Iturbe I (2010) Ecohydrology of terrestrial ecosystems. Bioscience 60(11):898–907. doi:10.1525/bio.2010.60.11.6
41. Silva JSV, Abdon MM, Silva SMA, Moraes JA (2011) Evolution of deforestation in the Brazilian Pantanal and surroundings in the timeframe 1976–2008. Geografia (Rio Claro) 36 (Especial):35–55
42. Pott A, Silva JSV (2015) Terrestrial and aquatic vegetation diversity of the Pantanal wetland. Hdb Env Chem. doi:10.1007/698_2015_352
43. Bergier I, Salis SM, Mattos PP (2015) Metabolic scaling applied to native woody savanna species in the Pantanal of Nhecolândia. Hdb Env Chem. doi:10.1007/698_2015_354
44. Dores E (2015) Pesticides in the Pantanal. Hdb Env Chem. doi:10.1007/698_2015_356
45. Buller LS, Silva GB, Zanetti MR, Ortega E, Moraes A, Goulart T, Bergier I (2015) Historical land-use changes in São Gabriel do Oeste at the Upper Taquari River basin. Hdb Env Chem. doi:10.1007/698_2015_355
46. Bergier I, Krusche A, Guérin F (2015) Alkaline lakes dynamics in the Nhecolândia landscape. Hdb Env Chem. doi:10.1007/698_2014_327
47. Franco MSM, Pinheiro R (1982) Geomorfologia. In: Brasil (ed) Ministério das Minas e Energia. Secretaria Geral. Projeto RADAMBRASIL. Folha SE.21 Corumbá e parte da Folha SE.2 (Levantamento de Recursos Naturais, 27). MME/SG/RADAMBRASIL, Rio de Janeiro, pp 161–224
48. ANA/GEF/PNUMA/OEA (2005) Modelo de Simulação Hidrológica do Alto Paraguai. Projeto Implementação de Práticas de Gerenciamento Integrado de Bacia Hidrográfica para o Pantanal e Bacia do Alto Paraguai. Subprojeto 5.4 – Modelo Integrado de Gerenciamento Hidrológico da Bacia do Alto Paraguai. Agência Nacional de Águas, Fundo para o Meio Ambiente Mundial, Programa das Nações Unidas para o Meio Ambiente, Organização dos Estados Americanos, 333 pp
49. Macedo HA, Assine ML, Pupim FN, Merino ER, Stevaux JC, Silva A (2014) Mudanças paleo-hidrológicas na planície do rio Paraguai, Quaternario do Pantanal. Revista Brasileira de Geomorfologia 15:75–85

50. Kuerten S, Assine ML (2011) O rio Paraguai no megaleque do Nabileque, sudoeste do Pantanal Mato-Grossense, MS. Rev Bras Geosci 41(4):642–653
51. Kuerten S, Parolin M, Assine ML, McGlue MM (2013) Sponge spicules indicate Holocene environmental changes on the Nabileque River floodplain, southern Pantanal, Brazil. J Paleolimnol 49(2):171–183
52. Hamilton SK, Sippel SJ, Melack JM (1996) Inundation patterns in the Pantanal wetland of South America determined from passive microwave remote sensing. Arch Hydrobiol 137 (1):1–23
53. Padovani CR, Vettorazzi CA, Shimabukuro YE, Adami M, Freitas RM (2009) Estudo das inundações do Pantanal a partir de imagens MODIS. In: 14° Simposio Brasileiro de Sensoriamento Remoto, Natal, Anais. INPE, pp 1–8
54. Padovani CR (2010) Dinâmica das Inundações do Pantanal. Universidade de São Paulo/ ESALQ, Piracicaba
55. Prass TS, Bravo JM, Clarke RT, Collischonn W, Lopes SRC (2012) Comparison of forecasts of mean monthly water level in the Paraguay River, Brazil, from two fractionally differenced models. Water Resour Res 48(5), W05502
56. Paz AR, Collischonn W, Bravo JM, Bates PD, Baugh C (2014) The influence of vertical water balance on modelling Pantanal (Brazil) spatio-temporal inundation dynamics. Hydrol Process 28(10):3539–3553
57. Cavazzana GH, Lastoria G, Roche KF, Catalini TGT, Paranhos Filho AC (2015) Natural and environmental vulnerability along the touristic "Estradas Parque Pantanal" by GIS algebraic mapping. Hdb Env Chem. doi:10.1007/698_2014_328
58. Junk JW, Bayley PB, Sparks RE (1989) The flood pulse concept in river floodplain systems. Can Spec Publ Fish Aquat Sci 106:110–127
59. Andrade MHS (2011) O fenômeno da "decoada" no Pantanal do rio Paraguay, Corumba, MS: alteração dos parâmetros limnológicos e o efeito sobre os organismos macroinvertebrados bentônicos. Doctoral Thesis, Universidade de São Paulo, São Paulo
60. Bergier I, Silva APS, Monteiro H, Guérin F, Macedo HA, Silva A, Krusche A, Sawakuchi HO, Bastviken D (2015) Methane and carbon dioxide emissions from the Paraguay River floodplain (Pantanal) during episodic anoxia events. Hdb Env Chem. doi:10.1007/698_2015_353
61. Macedo HA, Stevaux JC, Silva A, Merino ER, Pupim FN, Bergier I Distribuição e classificação da intensidade do fenômeno de dequada no Pantanal. In: 5° Simpósio de Geotecnologias do Pantanal, Campo Grande, MS, 2014b. Anais. Embrapa/INPE, pp 720–730
62. Oliveira MD, Calheiros DF, Padovani CR (2013) Mapeamento e Descrição das Áreas de Ocorrência dos Eventos de Decoada no Pantanal. Boletim de Pesquisa e Desenvolvimento / Embrapa Pantanal, Corumbá-MS, 21 pp
63. Alho CJR (2008) Biodiversity of the Pantanal: response to seasonal flooding regime and to environmental degradation. Braz J Biol 68:957–966
64. Mamede S, Alho CJR (2006) Response of wild mammals to seasonal shrinking-and-expansion of habitats due to flooding regime of the Pantanal, Brazil. Braz J Biol 66(4):991–998
65. Schulz C, Ioris AA, Martin-Ortega J, Glenk K (2014) Prospects for payments for ecosystem services in the Brazilian Pantanal: a scenario analysis. J Environ Dev 1070496514548580
66. Mittermeier RA, de Gusmao CI, Pádua MTJ, Blanck J (1990) Conservation in the Pantanal of Brazil. Oryx 24(02):103–112
67. Resende EK (2008) Pulso de inundação: processo ecológico essencial à vida no Pantanal. Documentos 34. Embrapa, Corumbá
68. Stevaux JC, Corradini FA, Aquino S (2013) Connectivity processes and riparian vegetation of the upper Paraná River, Brazil. J S Am Earth Sci 46:113–121
69. Neiff JJ, Poi de Neiff ASG (2003) Connectivity processes as a basis for the management of aquatic plants. In: Thomaz SM, Bini LM (eds) Ecologia e Manejo de Macrófitas Aquáticas. Editora UEM, Maringa, pp 39–58
70. Embrapa Pantanal; WWF – Brasil (2014) Monitoramento das alterações da cobertura vegetal e uso da terra na bacia do alto rio Paraguai: Porção Brasileira: período de analise: 2010 to 2012. Brasília, 73 pp

Terrestrial and Aquatic Vegetation Diversity of the Pantanal Wetland

Arnildo Pott and João Santos Vila da Silva

Abstract This chapter is a comprehensive summary and an illustrated report of our observations over 30 years of research on flora, vegetation, and geoprocessing based on intensive fieldwork throughout the Pantanal plain and highlands, associated to data compiled from the literature. There is a unique phytogeographic diversity in the Pantanal, a region of confluence of various biogeographic provinces, such as Cerrado, Amazon, Atlantic Forest, and Chaco, plus a *wide distribution group* and the exotic plants. The proportions of the flora are approximately 50% wide-ranging species, 30% Cerrado species, and 20% shared among other phytogeographic origins. Considering the 350 woody plants, the Cerrado group is the most numerous (66 species), followed by Cerrado and seasonal forest (47), wide distribution (31), Chaco (29), and seasonal forest (23). There is little endemism, probably due to the recent geological age of the Pantanal. So far, the Pantanal is yet the most conserved biome in Brazil. The vegetation is very resilient, flexible, and adapted to wet-and-dry seasonal and decadal cycles, including fire, and shall remain diverse as long as the hydrological balance is not disrupted by homogenization toward either an entirely dry or a fully wet system.

Keywords Flooded forest, Flooded savanna, Flora, Land-use changes, Phytogeography

A. Pott
Botany Laboratory, Federal University of Mato Grosso do Sul, Campo Grande, MS, Brazil

J.S.V. da Silva (✉)
Embrapa Informatics and Agriculture, Campinas, SP, Brazil
e-mail: joao.vila@embrapa.br

I. Bergier and M.L. Assine (eds.), *Dynamics of the Pantanal Wetland in South America*, Hdb Env Chem (2016) 37: 111–132, DOI 10.1007/698_2015_352,

Contents

1 Introduction

The Pantanal wetland is a seasonally flooded savanna, a complex alluvial tract composed by the Paraguay River main stem and several marginal fluvial fans/megafans [1]. It is one of the world's largest continuous tropical wetlands, with an area of 138,000 km^2 in Brazil, within a basin of 361,700 km^2 [2]. However, the Brazilian vegetation map of biomes shows an estimated area of 153,000 km^2 for the Pantanal [3] (Fig. 1). The Pantanal also crosses the borders of Bolivia (15,000 km^2) and Paraguay (15,000 km^2) [5], and some large riverine lakes (Uberaba, Gaíva, Vermelha, Mandioré, and Cáceres) (Fig. 1) are shared with Bolivia. The Pantanal plain has been recently divided into 20 subregions, according to landscape and inundation characteristics (see Assine et al. [6]), often called "pantanals," what reinforces the heterogeneity of the region. Further, diversity is found within subregions, and there are several categories regarding flood intensity (low, medium, and high Pantanal), rivers (Pantanal of Taquari, Pantanal of Rio Negro, and Pantanal of Taboco), and others.

The geology and the geomorphology of the Pantanal are well described in Assine et al. [7]. The climate is seasonal, rainy in October-April and dry in May-September, with mean annual rainfall of $1{,}100 \pm 300$ mm. The whole upper Paraguay basin (UPB) can be defined as tropical climate of savanna (Aw), according to the classification of Köppen. However, it is possible to verify variations between Aw and Bw, i.e., between humid and semiarid climates. Utilizing the classification of Thornthwaite, the UPB presents nine climatic types, with the type C_1dA'a' (subhumid/dry) dominating the plain. Considering only the distribution and frequency of rainfall, the UPB has five climatic types, prevailing subhumid megathermic in the plain. The mean annual temperature varies from 22 to 26°C, inversely correlated with altitude. The warmest month is October, and the coolest is July. The thermic amplitude is 4 in the North and 7°C in the South, due to higher incidence of cold air masses in the south of the Pantanal. The maximum annual mean temperature varies from 29 to 32°C, with the highest on the plain, and the minimum from 17 to 20°C, the highest minima also observed on the plain, where eventual frost can occur. In winter (June to August), the temperature varies from 8 to 15 °C and in summer (December to February) between 20 and 23°C [8–11].

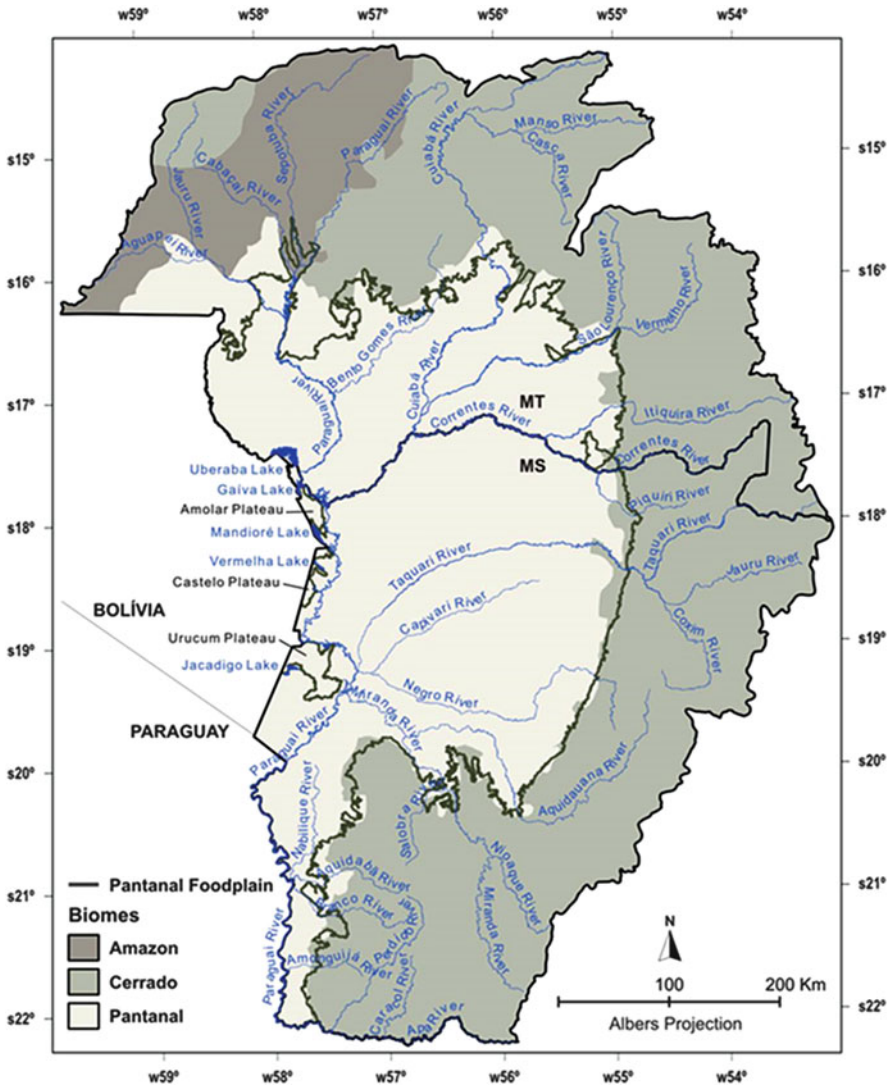

Fig. 1 Delimitation of the Pantanal (plain and biome: in *light gray*) and its upper hydrographic basin (*dark grays*) in Brazilian territory. *Source*: based on [2] and [4]

There is large variation in water regimes over the Pantanal plain. Some areas flood only by local rainfall, while others inundate by rivers or both (see Assine et al. [6]). Evapotranspiration is higher than rainfall, and the seasonal water surplus from the upper watershed largely dictates the water balance on the plain. Occasionally, depending on the intensity of the austral summer rainfall, the annual floods are plentiful or quite absent. The Paraguay River shows a monomodal flood pulse that has been measured since 1900 by the Brazilian Navy Port at the Ladário City

Fig. 2 Riverbed of a paleochannel in the Abrobral subregion during a dry year. Photo credit: Arnildo Pott

[5]. However, at smaller scales, extended areas are inundated by rainfall and months later are further flooded by rivers. In addition, the floodplains of Aquidauana and Miranda rivers, close to the uplands, may receive more than an inundation pulse per year. The Abobral River, indeed a false river or a paleochannel (Fig. 2), may dry out completely in the lack of water overflow from the Aquidauana River. For dryer years, the Negro River disappears in a swamp and stops flowing to the Paraguay River. The flooding of the latter may force Negro River to run backward. Analogously, the groundwater functions as a bank account: it lowers if more spent than deposited, and it may take more than a year to reach the soil surface after a long dry spell.

The soils vary widely in texture and fertility, from very sandy and very poor prevailing on the Taquari alluvial megafan (50,000 km^2) to heavy clays, vertic black soils (swell when wet and crack when dry), very fertile (eutrophic) on the floodplains of the Paraguay and Miranda rivers, and eventually salty soils in the southwestern direction. Over half of the Pantanal soil is pure sand due to the carrying of sediments from the uplands, which enhances the dry seasonal effect. Although the water table may not deepen too much, it barely rises to the top surface due to low soil capillarity. Limited by the wet period, roots of trees in the region are usually horizontal (Fig. 3), even for those species ordinarily deep-rooted found in the *cerrado* latosols (see also Bergier et al. [12]). Generally, fine sediments lay on deep, flooded areas; otherwise, the soil stays longer waterlogged or wet.

Fig. 3 Shallow roots of tree species in the Pantanal (Nhecolândia subregion). Photo credit: Arnildo Pott

2 Vegetation Types

For an untrained eye, cacti growing near aquatic plants would seem odd, though this contrast is commonplace in the Pantanal landscape. For that reason, the vegetation of the Pantanal was coined as "a complex" until the role of flood on the mosaic formation started to be unveiled [13]. On the same ridge may occur various vegetation types, such as deciduous forest in the middle and *cerrado* woodland at the transition with grassland or riparian forest at the edge of a pond.

The vegetation varies mainly according to the flood level, and species composition differs by function of flood and soil. In addition to the flood, soil type has a sharp influence on plant species distribution. Flood is the overriding factor because vegetation may differ on the same soil according to the relief. Hence, the emergent spatial pattern can be noted as a "self-organized chaos" (Fig. 4).

The development of spatial vegetation patterns is also noted, for example, wherever a road embankment is raised. Terrestrial plants start to grow on the bank and aquatics in the borrow pit. As a result, there are three basic vegetation formations in the landscape mosaic: woody on flood-free ground, grasslands on seasonally flooded areas, and aquatic vegetation in water bodies (Fig. 5).

Fig. 4 Self-organized chaos of the vegetation lined up by the flood gradient. The forest islands in varying sizes are barely disturbed by flood events. They constitute of refuges for both wildlife and farm cattle during high floods. Photo credit: Arnildo Pott

Fig. 5 Artificial earth mound (bank) and pond (borrow pit) constructed for a road where we can see the three basic vegetation forms: woody, grassland and aquatic. Photo credit: Arnildo Pott

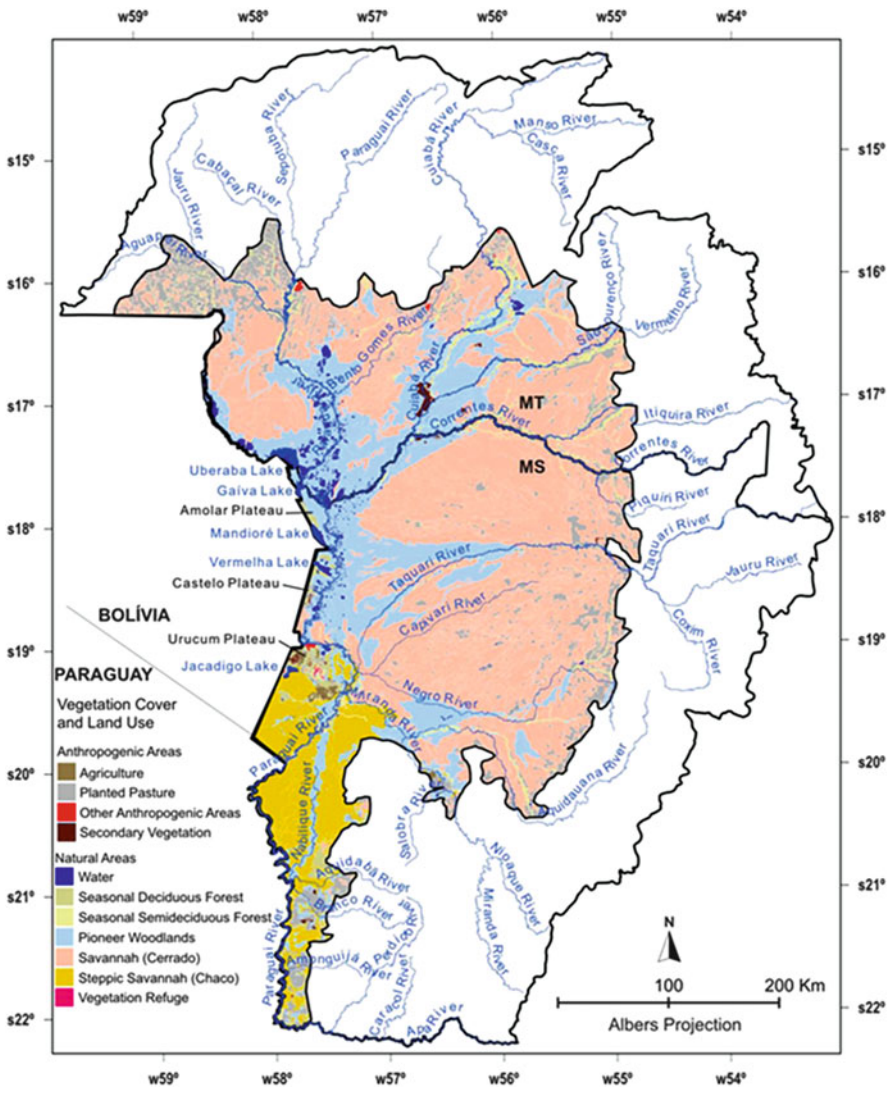

Fig. 6 Vegetation cover and land use map of the Pantanal wetland. In white: upper watershed. Source: based on [11, 12]

2.1 Terrestrial Vegetation

The terrestrial vegetation can be divided into anthropogenic and natural areas (Fig. 6). Natural areas refer to (1) *seasonal deciduous forest* and *seasonal semideciduous forest* (included forest islets and riparian forest), (2) *pioneer woodlands* (including *Vochysia divergens*), (3) *scrub* (thorn scrub, shrub thickets, including *Couepia uiti* and *Licania parviflora*), (4) *herbaceous* (giant sedge, fire

Fig. 7 Refuge of savanna vegetation (grassland and *cerrado* woodland) on iron-rock hills on the Urucum plateau (see Fig. 6). Photo credit: Arnildo Pott

Fig. 8 Example of a natural forest island (locally called "Capão") in the Abobral subregion resulted from the slightly higher altimetry in the terrain. Photo credit: Arnildo Pott

flag, swamp, and floating meadow), (5) *savanna* (*Cerrado*) (including *cerrado* woodland, floodable monodominant savannas, and grasslands), (6) *steppic savanna* (*Chaco*), and, finally, (7) *vegetation refuge*.

The *vegetation refuge* comprises a savanna vegetation on the top of iron-rock hills at the western edge, in Corumbá (Fig. 7) [16].

The forest islands, naturally rounded or elliptic patches of woods in the open plain, usually contain deciduous trees in the center and riparian species on the edge, such as cabbage bark (*Andira inermis*) and Guanandi (*Calophyllum brasiliense*) (Fig. 8); the soil has a concretion horizon of $CaCO_3$ derived from shell deposits [17].

Monodominant savannas and pioneer woodlands are intermingled. The main woody species are yellow trumpet tree (*Tabebuia aurea*), caranday palm

Fig. 9 (**a**) September flowering of *Tabebuia aurea* in the Miranda subregion. (**b**) *Copernicia alba* palm in the Nabileque subregion. (**c**) September flowering of *Vochysia divergens* woodland in the Poconé subregion. (**d**) A scrub of "canjiqueira" *Byrsonima cydoniifolia* in the Nhecolândia subregion. (**e**) *Attalea phalerata* palm tree in the Paraguay subregion. (**f**) *Licania parvifolia* alongside a seasonal stream in the Nhecolândia subregion. Photo credits: (**a**, **b**, **d**, and **f**) Arnildo Pott; (**c**) Fabio Edir Costa; (**e**) Paulo Robson de Souza

(*Copernicia alba*), *Vochysia divergens*, and *Byrsonima cydoniifolia* scrub (see Fig. 9a–d). The pioneer *V. divergens* is considered the worst weed of good natural pastures, as it shades them out (Fig. 9c). The babassu palm (*Attalea speciosa*) forest on old levees would evolve to broad-leaved forest if kept free from fire. *A. phalerata*, a palm locally known as acuri, is shown in Fig. 9e. Alongside the seasonal streams occur stands of *Licania parvifolia*, which evolve to mixed riparian forest on higher banks (Fig. 9f).

The most frequent tree in the Pantanal is the sandpaper tree (*Curatella americana*), often associated with termite mounds ("campo de murundu") (see Fig. 10a, b), dwarfed in wetter areas. However, instead of termite, anthills occur in *T. aurea* savanna (Fig. 10c, d) and Chaco, also adding to plant diversity, since anthills are

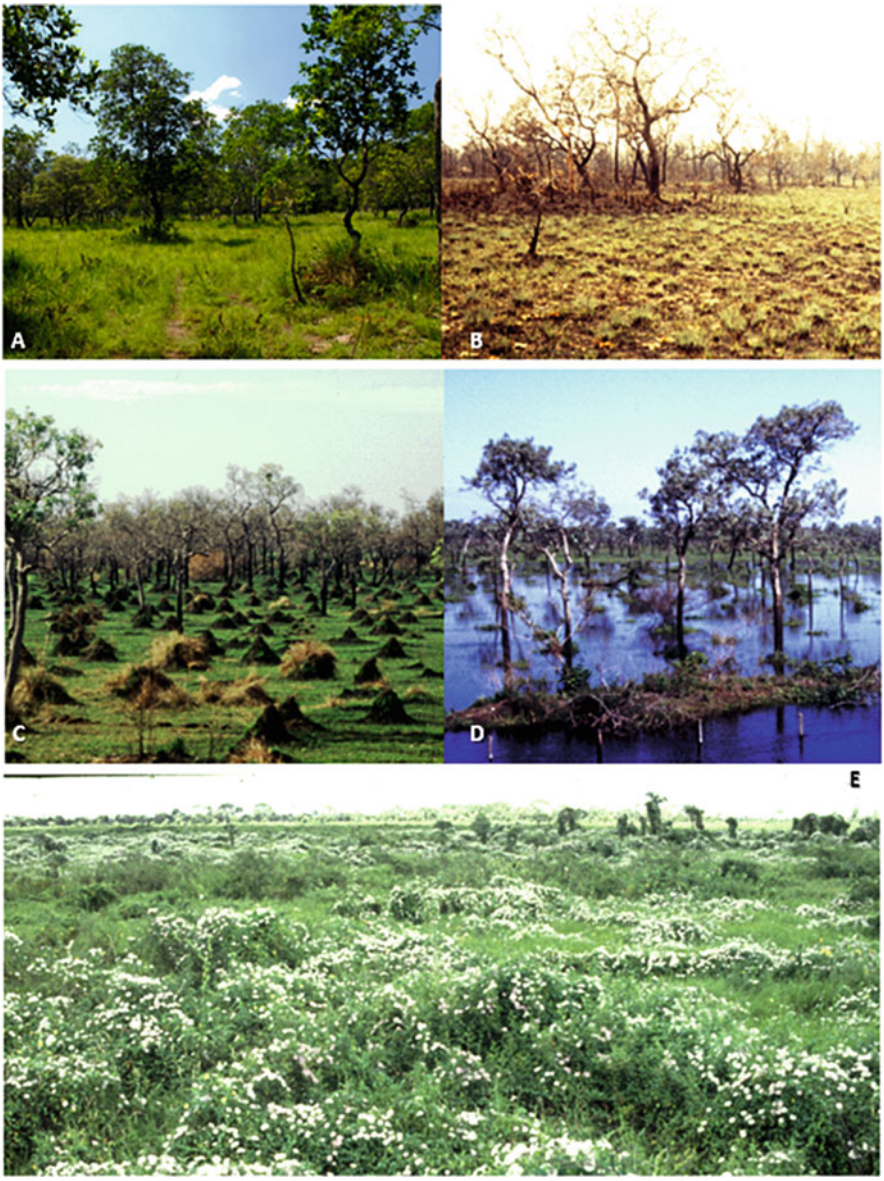

Fig. 10 (**a**) Sandpaper tree (*Curatella americana*) in the Aquidauana subregion, (**b**) often associated with termite mounds ("campo de murundu") in the Paiaguás subregion. (**c**) *T. aurea* savanna and anthills in dry and (**d**) flooded periods in the Miranda subregion. (**e**) Spiny scrub or thorn swamp in the Miranda subregion. Photos credits: (**a**) Paulo Robson de Souza, (**b**–**e**) Arnildo Pott

better drained and hold different species. The thorn swamp seems a paradox, as it occurs on slight depressions, which dry last and is a refuge for fauna; the main species are spiny entangled shrubs of *Bauhinia bauhinioides*, *Byttneria filipes*, *Mimosa* spp., and vines (*Cissus spinosa*) (Fig. 10e).

Grasslands are natural in the Pantanal due to the seasonal flood or waterlogging. The effect of flood holding back on woody vegetation has been observed after some years without flood, when grasslands become shrubby [16]. However, in some parts (e.g., Poconé subregion), grasslands are claimed to have been enlarged or maintained by slashing [18]. There are several types of grasslands according to flood level and soil type, dominated by different grasses such as *Elionurus muticus*, *Axonopus purpusii*, *Paspalum lineare*, *P. carinatum*, etc. [19]. Grasslands have a wet, flooded phase when aquatic plants appear, like the surviving perennials from rhizomes and bulbs such as sword plants (*Echinodorus* spp.), sedges, spike rush (*Eleocharis* spp.), and others from seed (*Bacopa* spp.). Furthermore, there are also the cultivated grasslands (see further in this chapter).

Recent studies have shown that the soil seed bank is very flexible to seasonal fluctuations, composed by aquatic, mesic, and even dryland species (e.g., *Portulaca*) and that after 15 years under exotic creeping signal grass (*Urochloa humidicola*), the seed bank is still active to regenerate native species [20].

2.2 Aquatic Vegetation

The main habitats of the aquatic vegetation are ponds, seasonal ponds, large lakes on the western edge, oxbow lakes, rivers, anabranches, seasonal streams, marshes, and flooded grasslands. All life forms are present, generally configuring a zonation pattern according to water depth. The majority are emergent and amphibious plants [21]. Along the rivers, it grows rooted floating mats of anchored water hyacinth *Eichhornia azurea* (Fig. 11a), while stands of emergent plants develop on the shallow margin, such as smartweeds (*Polygonum* spp.).

Considered true hydrophytes are the submerged, free-floating, and rooted floating plants. Submerged genera (*Cabomba*, *Ceratophyllum*, *Najas*) occur mostly in ponds and streams away from turbid waters in rivers. Free-floating plants are duckweeds (Lemnoideae, the tiniest flowering plants), floating ferns (*Salvinia* spp.), mosquito ferns (*Azolla* spp.), water lettuce (*Pistia stratiotes*), and water hyacinth (*Eichhornia crassipes*). Examples of rooted and floating hydrophytes are Victoria lily (*Victoria amazonica*) (Fig. 11b), the largest aquatic macrophyte that grows in oxbow lakes of the Paraguay River, and water lilies (*Nymphaea* spp.), common in seasonal and permanent ponds.

Emergent plants occur around oxbow lakes and in backswamps and ponds, such as the giant sedge (*Cyperus giganteus*), pickerel weed (*Pontederia parviflora*), and fire flag (*Thalia geniculata*). Amphibious plants are found in floodable grasslands and savannas, many grasses, sedges, and other plants, as bush morning glory (*Ipomoea carnea*), which grow either in flooded or dried ground.

Fig. 11 (**a**) Rooted floating mats of *Eichhornia azurea* and (**b**) Victoria lily (*Victoria amazonica*) found in oxbow lakes of the Paraguay River. Photo credits: Arnildo Pott

Fig. 12 (**a**) Brackish pond at flood with *Copernicia alba*, and (**b**) at drought, surrounded by forested levees in the Nhecolândia subregion. Photo credits: Arnildo Pott

There is a lack of macrophytes inside brackish ponds, with water pH around 8–10, rich in Na^+ and K^+ carbonates (see Bergier et al. [22]). Only a few species grow on the sand shore, such as the palm *Copernicia alba* and halophilous *Paspalum vaginatum* and *Sporobolus pyramidatus*. These ponds, known as "salinas," function as small endorheic systems, which are usually isolated by the surrounding forested levees (Fig 12a, b).

In ponds, oxbow lakes, and other water bodies, there is a succession of aquatic vegetation, forming a floating meadow. After the dry periods, new water bodies are quickly colonized by free-floating plants (*Pistia*, *Salvinia*). On the top of the latter, the Cuban bulrush (*Oxycaryum cubense*) germinates and grows as an epiphyte, until it forms a dense entangled mat (Fig. 13a), later colonized by other plants.

A floating organic soil (histosol) builds up to 1 m deep, when shrubs and treelets such as primrose (*Ludwigia*), pump tree (*Cecropia*), and white trumpet tree (*Tabebuia insignis*) grow on it (Fig. 13b). The floating islet may reach above 100 m in diameter that can clog canals and eventually push aside stakes of wooden bridges at flood (Fig. 13c).

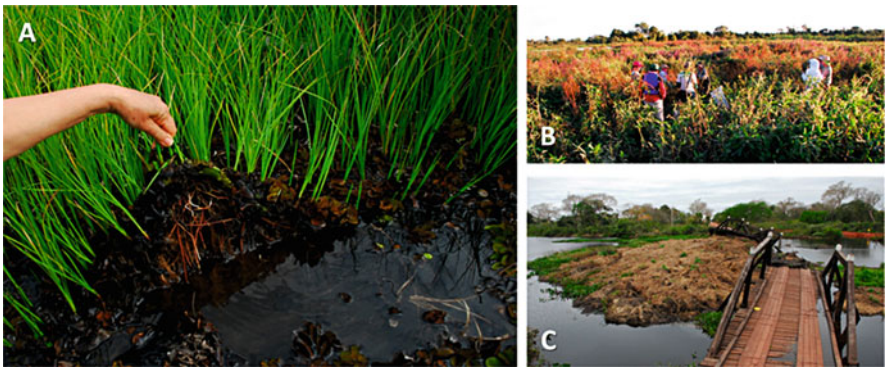

Fig. 13 (**a**) *Oxycaryum cubense* mat growing over free-floating plants, later forming floating meadow islands over histosol that can sustain. (**b**) Walking people, shrubs, and treelets. (**c**) When free-floating due to flood, these enlarged vegetation islands can push aside stakes of wooden bridges. Photo credits: Arnildo Pott

3 Phytogeography

There is a unique phytogeographic diversity in the Pantanal [23], a region of confluence of various biogeographic provinces, such as Cerrado, Amazon, Atlantic Forest, and Chaco [13], plus a *wide distribution group* and the exotic plants [24]. The proportions of the flora are approximately 50% wide-ranging species, 30% *Cerrado* species, and 20% shared among other phytogeographic origins [23]. Considering the 350 woody plants, the Cerrado group is the most numerous (66 species), followed by Cerrado and seasonal forest (47), wide distribution (31), Chaco (29), and seasonal forest (23) [23].

Cerrado (with uppercase "C" when referring to the biogeographic province and lowercase "c" to designate the vegetation form) is the central Brazilian savanna, characterized by thick bark (fire-resistant), tortuous trees. In the Pantanal, the common formation is *cerrado* woodland (Fig 14a) with more or less closed canopy, and some of the ordinary trees are souari nut (*Caryocar brasiliense*), tonka bean (*Dipteryx alata*), stinking toe (*Hymenaea stigonocarpa*), *Astronium fraxinifolium*, *Buchenavia tomentosa*, *Qualea grandiflora*, and *Tachigali aurea* [23], which are also listed among the most frequent species in the Brazilian *cerrados* according to [25].

From the Amazon forest contingent, there are not many species, mainly riparian trees, such as *Licania parvifolia*, *Vitex cymosa*, and *Vochysia divergens* [23]. They benefit from added soil moisture from both rain and lagged flood, since the Paraguay River rises after the rainy season, because of the delayed flow from the northern headwaters (see Assine et al. [6]).

Riparian forests show distinct successional stages according to flood level or bank age: (i) new sediments on riversides are colonized by herbs and shrubs; (ii) then colonized by pioneer multi-stem treelets such as iporuru (*Alchornea*

Fig. 14 (**a**) *Cerrado* woodland in the Nhecolândia subregion. (**b**) Seasonal deciduous forest in the Paiaguás subregion. Photo credits: Arnildo Pott

castaneifolia), *Pterocarpus rohrii*, *Banara arguta*, and *Sapium obovatum*; (iii) later replaced by taller trees such as ice-cream bean (*Inga vera*), coral tree (*Erythrina fusca*), pink trumpet tree (*Handroanthus heptaphyllus*), ant tree (*Triplaris americana*), and *Vitex cymosa*; and, finally, (iv) higher, older riverbanks have dry forest species such as soapberry (*Sapindus saponaria*). Abundant vines cover the edges, and some like *Cissus* spp. form curtains of adventitious roots, which trap sediments and help to raise the bank level.

From the inland Atlantic Forest, or seasonal semideciduous forest, not many species reach the Pantanal, such as tropical cedar (*Cedrela fissilis*), earpod tree (*Enterolobium contortisiliquum*), and stinking toe (*Hymenaea courbaril*) [23].

There are not large areas of forest in the Pantanal, except the seasonal deciduous forest (Fig. 14b) called Mata do Bebe, Cedro, and Fuzil, on higher and broad levees, composed mostly of anemochorous trees such as vilca (*Anadenanthera colubrina*), *Aspidosperma pyrifolium*, *Myracrodruon urundeuva*, *Schinopsis brasiliensis*, and the mentioned *C. fissilis* and a few zoochorous, e.g., yellow mombin (*Spondias mombin*), *E. contortisiliquum*, and *H. courbaril* [17]. Seasonal deciduous forests have large distribution [26].

Chaco or steppic savanna/forest (Fig. 15) is a spinescent, microphyllous, deciduous vegetation, often with green bark such as palo brea tree (*Parkinsonia praecox*).

Common Chaco trees are white quebracho (*Aspidosperma quebracho-blanco*), Argentine *lignum vitae* (*Bulnesia sarmientoi*), *Lonchocarpus nudiflorens*, *Mimosa hexandra*, redflower mesquite (*Prosopis rubriflora*), vinal (*P. ruscifolia*), willow-leaf red quebracho (*Schinopsis balansae*), a single-leaflet trumpet tree (*Tabebuia nodosa*) and the garlic-smelling *Microlobius foetidus*, ground cover of spikemoss (*Selaginella* spp.), and abundant and many species of cacti, from small cephaloid (*Gymnocalycium*), scandent (*Harrisia*) to arborescent ones (*Cereus*, *Stetsonia coryne*), *Bromelia* spp., and epiphytes, e.g., *Tillandsia duratii* with prehensile

Fig. 15 The Chaco vegetation with spiny trees and cacti. Photo credits: Arnildo Pott

curling leaves. The Brazilian Chaco in Porto Murtinho, southernmost portion of the Pantanal, is an extension of the Paraguayan Humid Chaco.

Finally, the *wide distribution group* encloses many grassland species such as *Andropogon bicornis*, *A. hypogynus*, *Cyperus haspan*, and *C. surinamensis*, with broad adaptations to harsh conditions of extremely wet-and-dry habitats. Several aquatic macrophytes are alike to other South American wetlands [27]. Also widespread are ruderal pantropical weeds, which usually grow on disturbed flood-free ground. However, in dry years, many of these exotic species move down to floodable grasslands, e.g., *Dactyloctenium aegyptium* and *Urena lobata*.

3.1 Flora

The number of phanerogams (flowering plants) is estimated as ca. 2,000 species; the richest families are Fabaceae (240 species), Poaceae (212), and Cyperaceae (92); and the richest genera are *Paspalum* (35 species), *Cyperus* (29), *Ipomoea* (24), *Panicum* (22), *Eugenia* (20), *Ludwigia* (19), and *Mimosa* and *Rhynchospora* (18 each) (Pott & Pott 1999, [16]). There is little endemism, probably due to the recent geological age of the Pantanal, e.g., *Euploca pottii* and wild peanuts (*Arachis diogoi*, *A. hoehnei*, *A. vallsii*), but many more are found outside the plain, on surrounding hilly country, such as *Aspilia grazielae*, *Discocactus ferricola*, *Echinopsis calochlora*, *Gomphrena centrota*, and *Vernonia pottii*, and on the uplands [16].

The vegetation is very dynamic under interannual hydrological fluctuations. For instance, from 1963 to 1974, there was a dry period in which woody pioneer species advanced over grasslands, whereas from 1974 to 2014, heavy floods returned and

pushed the woods back to the slightly elevated, less flooded ground. Nevertheless, some riparian trees such as *Vochysia divergens* persistently spread despite the floods.

4 Land Use and Vegetation

The Pantanal has been declared a National Heritage by the Brazilian constitution and a Biosphere Reserve and a Natural Humanity Heritage by UNESCO. Officially protected areas are the National Park of Pantanal, which is also a Ramsar site, and the State Park of Rio Negro. In addition, many private reserves have been created on ranches. However, all the rest of the Pantanal, differently from other regions, is still a wild place.

The natural grasslands of the Pantanal have been utilized for extensive cattle ranching for more than 200 years without evident impacts over the ecosystem functioning. This can be attributed to the near emptiness of herds of large native herbivores. "Therefore, the traditionally managed Pantanal of the early 20th Century can be considered one of the few tropical ecosystems [. . .] sustainably managed" [5]. Despite that the Pantanal is still a rather pristine ecosystem, there are ongoing changes that must be considered.

In the 1980s, flood-free ridges (ancient levees) started to be cleared to plant pastures. The practice is nowadays considered too expensive, and, instead, coarse grasslands have been replaced by *U. humidicola* without relevant (visual) changes of the landscape matrix. The soil seed bank of native species is still rich and abundant under cultivated grassland [20].

For economic reasons, traditional cattle ranches have been steadily sold mainly to outsiders who normally intensify pasture production at the expense of conservation. For example, some new farmers even bring in other types of cowboys, while the local people have a culture of understanding the flooding dynamics and do not hunt for meat but the feral pig (exotic animal). To increase production, about 12.1% of the Pantanal floodplain has already been cleared for cultivated pastures until 2008, while on the plateau, this figure reached 58.9% [4]. A rapid spatial view of clearing in the region shows that the pressure for deforestation in the basin occurs more drastically on the plateau (Fig. 17). When the Pantanal floodplain is considered, the highest rates of clearing took place on the eastern belt, in the northwest, and in the southern part of the Pantanal [4].

Overgrazing occurs either in very dry years or when flood restricts pasture availability. On the other hand, undergrazing generates surplus of grass and consequent accidental or intentional burn. Fire has been said to be a problem, but it surely has already occurred in pre-Columbian times, since savannas are prone to wildfires during dry seasons or periods. Under dry conditions, the flames extend even through swamps. Coarse grasses build up fuel (flammable biomass) and can be managed with controlled burning, depending on official government license. Under cattle exclosure, tall tussock grasses overgrow creeping species (see Fig. 16). In contrast,

Fig. 16 Effect of cattle exclosure on change of short sward (left side of the fence) to tussock grasses (on the right) after a year (1986–1987), Embrapa's Nhumirim Farm. Photo credit: Arnildo Pott

overgrazing causes an increase of Bermuda grass (*Cynodon dactylon*), *Mimosa* spp., sicklepod (*Senna occidentalis*), *Waltheria albicans*, and bare ground.

A few roads cross Pantanal areas beside the tracks to ranches. The Paraguay River is used for local transport and for large barges carrying iron ore and grain. Engineering plans to straighten the river main stem for navigation were unapproved so far. Sugarcane is currently forbidden in the Pantanal watershed in the state of Mato Grosso do Sul, and just two irrigated rice fields are licensed inside the plain, under strict control. There is high potential for crops on black soils, but dikes for flood control are also illegal.

Invasion of alien plants is not a major problem so far. The main exotic weed is tanner grass *Urochloa arrecta* (Fig. 18), which spreads by the water. It excludes native plants, except a few vigorous stoloniferous grasses. Another fearsome aquatic weed, hydrilla (*Hydrilla verticillata*), has still not reached the Pantanal, but it is a matter of time, since it is already spreading in reservoirs of the Paraná River Basin, connected to the Paraguay River. Woody invaders have had little expansion into flooded areas, so far confined to flood-free road embankments, e.g., caster bean (*Ricinus communis*) and guava (*Psidium guajava*), and lately two Caribbean trees, leucaena (*Leucaena leucocephala*) and Jamaican cherry (*Muntingia calabura*). A few others, such as *Bambusa vulgaris*, *Citrus limon*, and *Mangifera indica*, cultivated in home yards, often disseminate a bit along riverbanks and roadsides [23]. Nonetheless, with an eventual reduction in flood height, these and many more species would spread to lower areas.

Most problems and threats originate from outside of the plain, e.g., the river silting due to erosion on deforested areas of the upper watersheds (see Fig. 19a, b), and not well-managed hydroelectric dams on tributaries of the Pantanal, which may cause hydrological changes downstream [28]. Silting of riverbeds is the major problem, causing the kill of trees (Fig. 19c, d) and change in the whole landscape,

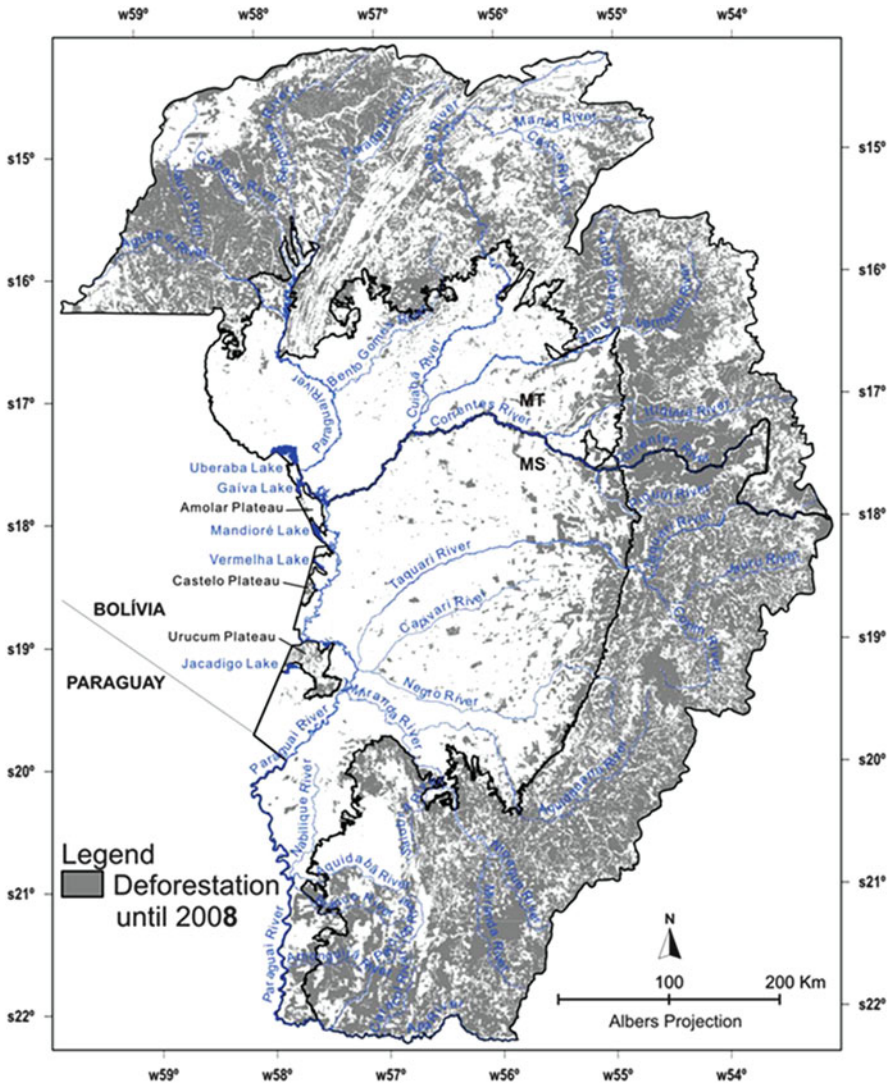

Fig. 17 Map of deforestation of the Brazilian Pantanal plain and upper watershed until 2008. Based on [2, 4]

simplifying a diverse vegetation structure in a permanent monotonous swamp [29]. The worst silting occurred in the Taquari River, where the lower riverbed was lost and the overflow formed enlarged, permanently flooded areas (Fig. 19d) [30, 31].

So far, the Pantanal is yet the most conserved biome in Brazil. The vegetation is very resilient, flexible, and adapted to wet-and-dry seasonal and decadal cycles, including fire, and shall remain diverse as long as the hydrological balance is not disrupted by homogenization toward either an entirely dry or a fully wet system.

Fig. 18 Exotic weed *Urochloa arrecta*. Photo credit: Paulo Robson Souza

Fig. 19 (**a**) Well-conserved limestone spring in the Upper Miranda Basin. (**b**) Gully erosion in the Upper Taquari Basin. (**c**) Silted *vereda* wetland with dead palm *Mauritia flexuosa* in the Upper Taquari Basin. (**d**) Overflowed silted area in the Taquari megafan with dead trees. Photo credits: Arnildo Pott

References

1. Assine ML, Soares PC (2004) Quaternary of the Pantanal, west-central Brazil. Quat Int 114 (1):23–34
2. Silva JSV, Abdon MM (1998) Delimitação do Pantanal brasileiro e suas sub-regiões. Pesq Agrop Brasileira 33:1703–1712
3. IBGE IBDGEE (2004). Mapa de Biomas do Brasil; primeira aproximação. IBGE, Rio de Janeiro
4. Silva JSV, Abdon MM, Silva SMA, Moraes JA (2011) Evolution of deforestation in the Brazilian Pantanal and surroundings in the timeframe 1976-2008. Geografia 36:35–55
5. Junk WJ, Nunes da Cunha C, Silva CJ, Wantzen KM (2011) The Pantanal: a large South American wetland and its position in limnological theory. In: Junk WJ, Silva CJ, Nunes da Cunha C, Wantzen KM (eds) The Pantanal: ecology, biodiversity and sustainable management of a large neotropical seasonal wetland. Pensoft, Sofia-Moscow, pp 23–44
6. Assine ML, Macedo HA, Stevaux JC, Bergier I, Padovani CR, Silva A (2015) Avulsive rivers in the hydrology of the pantanal wetland. Hdb Environ Chem. doi:10.1007/698_2015_351
7. Assine ML, Merino ER, Pupim FN, Warren LV, Guerreiro RL, McGlue MM (2015) Geology and geomorphology of the pantanal basin. Hdb Environ Chem. doi:10.1007/698_2015_349
8. Cadavid-García EA, Rodríguez Castro LH (1986) Análise da freqüência de chuva no Pantanal Mato-grossense. Pesq Agrop Brasileira 21(9):909–925
9. PCBAP PdCdBdAP (1997) Plano de Conservação da bacia do Alto Paraguai. In: MMA/SEMAM/PNMA (ed) Programa Nacional do Meio Ambiente, Brasília
10. Silva JSV, Abdon MM, Pott A, Mauro RA (2003) Fragile ecosystem: the Brazilian Pantanal wetland. In: Sanchez LH (ed) Regional Sustainable Development Review: Brasil. Encyclopedia of Life Support Systems. EOLSS, Oxford, p 39
11. Soriano BMA (1999) Caracterização climática da sub-região da Nhecolândia, Pantanal – MS. In: Pantanal E (ed) Simpósio sobre recursos naturais e sócio-econômicos do Pantanal. Embrapa Pantanal, Corumbá, pp 151–158
12. Bergier I, Salis SM, Mattos PP (2015) Metabolic scaling applied to native woody savanna species in the Pantanal of Nhecolândia. Hdb Environ Chem. doi:10.1007/698_2015_354
13. Adámoli J (1982) O Pantanal e suas relações fitogeográficas com os cerrados; discussão sobre o conceito "Complexo do Pantanal". Congresso Nacional de Botânica. Universidade Federal do Piauí, Teresina, pp 109–119
14. Silva JSV, Abdon MM, Pott A (2007) Cobertura vegetal do bioma Pantanal em 2002. In: XXIII Congresso Brasileiro de Cartografia. Rio de Janeiro, Brasil, 21 a 24 de outubro de 2007, 1030–1038. http://mtc-m17.sid.inpe.br/col/sid.inpe.br/mtc-17@80/2007/11.30.11.31/doc/silva_cobertura.pdf
15. Silva JSV, Abdon MM, Silva AM, Souza L (2007) Banco de dados de vegetação do projeto Probio-Pantanal. In: CBdC CBC (ed) Anais do Congresso Brasileiro de Cartografia. SBC, Rio de Janeiro, pp 1643–1652
16. Pott A, Oliveira AKM, Damasceno-Junior GA, Silva JSV (2011) Plant diversity of the Brazilian Pantanal wetland. Braz J Biol 71:265–273
17. Damasceno GA Jr,, Bezerra MA, Bortolotto IM, Pott A (1999) Aspectos florísticos e fitofisionômicos dos capões do Pantanal de Abobral. In: Embrapa (ed) II Simpósio sobre Recursos Naturais e Sócio-econômicos do Pantanal. Embrapa, Brasília, pp 203–214
18. Nunes da Cunha C, Junk WJ (2011) Landscape units of the Pantanal: structure, function, and human use. In: Junk WJ, Silva CJ, Nunes da Cunha C, Wantzen KM (eds) The Pantanal: ecology, biodiversity and sustainable management of a large neotropical seasonal wetland. Pensoft, Sofia-Moscow, pp 301–326
19. Allem AC, Valls JFM (1986) Recursos forrageiros nativos do Pantanal Mato-grossense. Embrapa, Brasília

20. Bao F, Pott A, Ferreira FA, Arruda R (2014) Soil seed bank of floodable native and cultivated grassland in the Pantanal wetland: effects of flood gradient, season and species invasion. Braz J Bot 34(5)
21. Pott VJ, Pott A, Lima LCP, Moreira SN, Oliveira AKM (2011) Aquatic macrophyte diversity of the Brazilian Pantanal wetland and upper basin. Braz J Biol 71:255–263
22. Bergier I, Krusche A, Guérin F (2015) Alkaline lakes dynamics in the Nhecolândia landscape. Hdb Environ Chem. doi:10.1007/698_2014_327
23. Pott A, Ratter JA (2011) Species diversity of terrestrial plants and human impact on the vegetation of the Pantanal. In: Junk WJ, Silva CJ, Nunes da Cunha C, Wantzen KM (eds) The Pantanal: ecology, biodiversity and sustainable management of a large neotropical seasonal wetland. Pensoft, Sofia-Moscow, pp 281–300
24. Pott A, Pott V (1996) Flora do Pantanal – listagem atual de fanerógamas. In: Embrapa (ed) Simpósio sobre Recursos Naturais e Socioeconômicos do Pantanal, Manejo e Conservação. Embrapa, Corumbá
25. Ratter JA, Bridgewater S, Ribeiro JF (2003) Analysis of the floristic composition of the Brazilian Cerrado vegetation. III: comparison of the woody vegetation of 376 areas. Edinb J Bot 60(1):57–109
26. Prance GT, Schaller GB (1982) Preliminary study of some vegetation types of the Pantanal, Mato Grosso, Brazil. Brittonia 34:288–251
27. Ferreira FA, Mormul RP, Thomaz SM, Pott A, Pott VJ (2011) Macrophytes in the upper Paraná river floodplain: checklist and comparison with other large South American wetland. Rev Biol Trop 59:541–556
28. Bergier I (2013) Effects of highland land-use over lowlands of the Brazilian Pantanal. Sci Total Environ 463–464:1060–1066
29. Pott A, Pott VJ (2005) Alterações florísticas na planície do baixo Taquari. In: Galdino S, Vieira LM, Pellegrin LA (eds) Impactos ambientais e sócio-econômicos na Bacia do Rio Taquari – Pantanal. Embrapa Pantanal, Corumbá, pp 255–289
30. Abdon MM, Silva JSV, Souza MP (2005) Impacto da inundação sobre as fitofisionomias da planície do baixo Taquari. In: Galdino S, Vieira LM, Pellegrin LA (eds) Impactos Ambientais e Socioeconômicos na Bacia do rio Taquari – Pantanal. Embrapa Pantanal, Corumbá, pp 295–302
31. Assine ML (2005) River avulsions on the Taquari megafan, Pantanal wetland, Brazil. Geomorphology 70(3–4):357–371

Metabolic Scaling Applied to Native Woody Savanna Species in the Pantanal of Nhecolândia

I. Bergier, S.M. Salis, and P.P. Mattos

Abstract Scaling invariance in living systems emerges from complex interactions of organisms with the physical world. According to the Metabolic Scaling Theory (MST), the way that energy and materials are distributed generally follows an invariant power law scaling with the body mass, independent on the species and the environment. Such generalization has been defined universal or ubiquitous, which is however not broadly accepted. For native woody savanna species in the Nhecolândia landscape, the scaling between trunk diameter and the whole plant body mass as $d \sim m^{3/8}$ follows MST prediction. Nevertheless, empirical data and model suggest biomass allocation beyond 50% to branches for trunk diameters above 18 cm, whereas root–trunk ratio does not vary significantly with plant size. The elevated water table explains such biomass allocation by limiting vertical root growth while enhancing branch growth to cope with evapotranspiration. Therefore, empirical deviations from MST scaling exponents of biomass partitioning for these plants can be understood as ecohydrological adaptations to conspicuous physical constraints.

Keywords Complexity, Forest allometry, Metabolic ecology, Scale invariance, Universality

I. Bergier
Laboratory of Biomass Conversion, Embrapa Pantanal, Corumbá, Brazil

S.M. Salis (✉)
Laboratory of Plant Ecology, Embrapa Pantanal, Corumbá, Brazil
e-mail: suzana.salis@embrapa.br

P.P. Mattos
Laboratory of Forestry Ecology, Embrapa Florestas, Colombo, Brazil

I. Bergier and M.L. Assine (eds.), *Dynamics of the Pantanal Wetland in South America*, Hdb Env Chem (2016) 37: 133–144, DOI 10.1007/698_2015_354,

Contents

1 Introduction

Allometry or scaling is about measuring proportional relationships [1]. Scaling power laws have the form $y \sim \beta x^{\alpha}$, and they represent the relationship of a variable y on the variable x as a function that involves a normalization constant β and a scaling exponent α. The relative scaling can be rewritten to $\log(y) \sim \alpha \log(x) + \log(\beta)$ to give a linear log–log plot. Scaling laws are mathematical descriptions of myriad patterns in nature though cannot be confused with scientific laws. For instance, vortex patterns in hurricanes or in mollusk shells are not physical laws but complex emergent properties of interacting particles following natural laws.

Empirical power laws describe mathematically the hierarchical, self-affine organization of physical, biological [2, 3], and other natural systems such as river drainage networks [4]. Malamud and Turcotte [5] showed that scaling exponents can be mathematically interchangeable for certain ranges and improved the understanding of stationary and nonstationary time-evolving processes. The "Kolmogorov exponent" $\alpha = -5/3$ [6] is a general emergent behavior of energy dissipation in turbulence phenomena. Kleiber's $\alpha = 3/4$ for the metabolic rate of mammals was further reworked [7, 8] to derive scaling exponents for metabolism, physiology, and anatomy, from organism to ecosystem level, as a function of body mass. For instance, they predicted the scaling between trunk diameter d and total plant mass with $\alpha = 3/8$. Scaling power laws also emerge for lakes with respect to methane emissions as a function of lake area [9]. The application of these lake-emission power laws allowed the derivation of rough methane emissions from worldwide dams [10].

Ecological scaling can be viewed as the unveiling of underlying natural physical laws [3]. Several organism, community, and ecosystem level properties emerge from relatively few allometric and biomechanical rules constrained by resource transport through self-affine vascular networks [7]. These rules ultimately dictate how individuals fill spaces, use resources, and produce and allocate biomass [8]. West et al. [7] have taken this view to show that branching processes in vascular systems can be mathematically described in terms of a hierarchical network to the supply of the entire body of an organism, where the terminations or exchange regions are size-invariant (self-affine), so that the energy required to self-sustain organization is minimized. West et al.'s conjectures are actually recognized as the West–Brown–Enquist model (WBE model), Metabolic Theory of Ecology (MTE),

or Metabolic Scaling Theory (MST). The latter we will refer to throughout this chapter.

1.1 The Metabolic Scaling Theory

MST predicts that a space-filling fractal-like structure [3] is required for the distribution network to supply the entire volume of an organism. A recent example of self-affine, space-filling supply network has been revealed beneath the soil when an artist created aluminum sculptures by void-filling ant colonies.[1] For small and large organisms (we can imagine ants and their colonies as "two distinct organisms at different space scales"), the space-filling hierarchical branching is a natural strategy to keep minimum the energy requirements to sustain life per mass unit, which is expectedly constant at about 300 kcal g^{-1} independent on the body size [11].

MST was recently recognized as a prodigious theory in biology [12]. It provides new approaches to understand life at several time-space scales by examining the organismal level. Nonetheless, MST is still a general theory like any other that represents reality, so empirical measurements eventually deviate from model outputs. In the case of forest stands, Coomes and Allen [13] have shown that measured scaling exponents shall have greater slopes than predicted by MST, particularly for native forests, due to the asymmetric competition for light. Scaling exponents might be greater for forest stands with high aboveground biomass production whereas they might follow MST predictions when aboveground biomass is lower [14]. On the other hand, Enquist et al. [15] argue that environmental constrains are complementary to MST, and Price et al. [16] suggest that critical evaluation of MST requires strong tests of both its theoretical foundations and simplifying assumptions.

This chapter provides indications that MST holds for biomass estimation of a tropical and diversified native savanna physiognomy in the Nhecolândia landscape. It also brings useful information that may support further research for conciliating theory with empirical observations.

2 Power Law Allometry Applied to the Nhecolândia Landscape

Figure 1 shows typical landscape views of the sampled savanna physiognomy at Nhumirim Farm (18°59′S, 56°38′W) and Rio Negro Farm (19°30′S, 56°12′W). The woody species in the Nhecolândia landscape has the characteristics of savanna,

[1] http://instagram.com/anthillart.

Fig. 1 Pictures of the sampled native physiognomy of savanna forested (*left*) and woody savanna (*right*) in the Nhecolândia landscape. Photo credits: Suzana Maria Salis

which is locally known as Cerrado. The Nhecolandia is subjected to annual seasonal climate or eventual flood of slightly low areas in the flat topography [17, 18]. The more elevated savanna physiognomies do not flood, though the water table can rise to ca. 1.5 m below soil level, which constrain root growth [19]. Sampled woody species were roughly segregated in two major elevated savanna physiognomies of Pantanal wetland: woody savanna or the cerrado (vegetation with rather broken canopy and considerable cover of shrubs and ground vegetation, comprising woody species as high as 10 m) and savanna forested or cerradão (dense canopy forest with sparser ground vegetation with tree canopy above 10 m). Main woody species occurring in the region are listed in Table 1. The methodology of sampling and biomass quantification can be checked in [17, 18].

We have derived power law scaling relationships by ordinary least square regressions. The scaling relationships with trunk cross sections (two-dimensional) instead of radius or diameter (one-dimensional) are a suitable alternative to magnify the *x*-axis range of the plot without compromising the residues of statistical regressions that proportionally remain the same [1]. It was considered the diameter at soil level (d_{sl}) because branching for subshrub species like *Annona dioica*, shrub (*Byrsonima cydoniifolia*), or typical savanna tree species (*Mouriri elliptica*, *Curatella americana*) usually occurs below breast level (1.3 m above ground). The power law scaling between d_{bl} and d_{sl} was computed ($r^2 = 0.9366$, $n = 61$), allowing to estimate d_{sl} for all investigated species. The woody part of shrub species, young trees, and small-branched savanna trees were all considered as branches.

Figure 2 illustrates the scaling between trunk cross-section area at soil level and the measured biomass partitioned in root, trunk, branches, and leaves of savanna woody species in the Nhecolândia. The simple power law fittings are reasonably good (r^2 usually above 0.84) over the spanned decades, indicating that, independently on plant size or species, it is possible to derive a common scaling exponent

Table 1 Wood savanna species in the Nhecolândia sampled for biomass estimates

Savanna woody species	*n*	Natural physiognomy wood savanna	Biomass sampled for
Annona dioica A.St.-Hil.	25	Woody savanna	Root, branches,[a] leaves
Mouriri elliptica Mart.	12	Woody savanna	Root, branches,[a] leaves
Byrsonima cydoniifolia Mart.	10	Woody savanna	Root, branches,[a] leaves
Diptychandra aurantiaca Tul.	10	Savanna forested	Trunk, branches, leaves
Licania minutiflora Fritsch	10	Savanna forested	Trunk, branches, leaves
Magonia pubescens A.St.-Hil.	10	Savanna forested	Trunk, branches, leaves
Protium heptaphyllum Marchand	10	Savanna forested	Trunk, branches, leaves
Terminalia argentea Mart.	10	Savanna forested	Trunk, branches, leaves
Curatella americana L.	9	Woody savanna	Root, trunk, branches, leaves
Zanthoxylum rigidum Humb. & Bonpl.	4	Woody savanna	Root, trunk, branches, leaves
Simarouba versicolor A.St.-Hill.	3	Woody savanna, savanna forested	Root, trunk, branches, leaves
Bowdichia virgilioides Kunth	2	Woody savanna	Root, branches,[a] leaves
Sapium haematospermum Müll.Arg.	2	Woody savanna, savanna forested	Root, trunk, branches, leaves
Tabebuia aurea Benth. & Hook.f.	2	Woody savanna	Root, trunk, branches, leaves
Agonandra brasiliensis Benth. & Hook.f.	1	Savanna forested	Trunk, branches, leaves
Andira cujabensis Benth.	1	Woody savanna	Branches,[a] leaves
Astronium fraxinifolium Schott	1	Savanna forested	Trunk, branches, leaves
Caryocar brasiliense Cambess.	1	Woody savanna	Root, branches,[a] leaves
Casearia sylvestris Sw.	1	Woody savanna	Root, branches,[a] leaves
Cecropia pachystachya Trécul	1	Woody savanna	Root, trunk, branches, leaves
Cordiera sessilis Kuntze	1	Savanna forested	Trunk, branches, leaves
Couepia grandiflora Benth.	1	Savanna forested	Trunk, branches, leaves
Diospyros hispida A.DC.	1	Woody savanna	Branches,[a] leaves

(continued)

Table 1 (continued)

Savanna woody species	*n*	Natural physiognomy wood savanna	Biomass sampled for
Dipteryx alata Vogel	1	Woody savanna	Root, trunk, branches, leaves
Hymenaea stigonocarpa Mart. ex Hayne	1	Savanna forested	Trunk, branches, leaves
Pouteria sp.	1	Savanna forested	Trunk, branches, leaves
Rhamnidium elaeocarpum Reissek	1	Savanna forested	Trunk, branches, leaves
Stryphnodendron adstringens (Mart.) Coville	1	Woody savanna	Root, branches,[a] leaves
Swartzia jorori Harms	1	Savanna forested	Trunk, branches, leaves
Tocoyena formosa K. Schum.	1	Woody savanna	Branches,[a] leaves
Vatairea macrocarpa Ducke	1	Savanna forested	Trunk, branches, leaves
Total	136		

[a]Shrub species, sapling, or tree of savanna very branched without easy separation of trunk and branches. The woody part was considered as branches

and a common normalization constant associated to woody plants in the regional landscape. There are evidently some individual deviations (large residues) from the power law models depicted in Fig. 2. Those deviations can be attributed to genetic variability or damages induced by environmental stressors as water, fire, wind, and local fauna and land use, without discarding eventual methodological concerns on sampling or weighting samples.

Annona dioica is a small shrub species (average height 1.17 ± 0.38 m) that produces a delightful fruit. The trunk usually branches first very close to the soil. The easily accessible fruits and the pronounced plant ramification can induce large statistical residues for biomass branches in the lower scaling range (Fig. 2, lower left corner). Nevertheless, in general, considering the number of samples and the spanned decades in the *y*-axes, it is possible to consider that all measured species share singular scaling laws with respect to biomass allocation. What is unique to all plots in Fig. 2 is that the scaling covers a wide size range for the 31 species evaluated in the region, which may allow considering the natural savanna as a single species unit for general modeling purposes. This is particularly useful when dealing, for instance, with biomass or carbon estimations to forest stands.

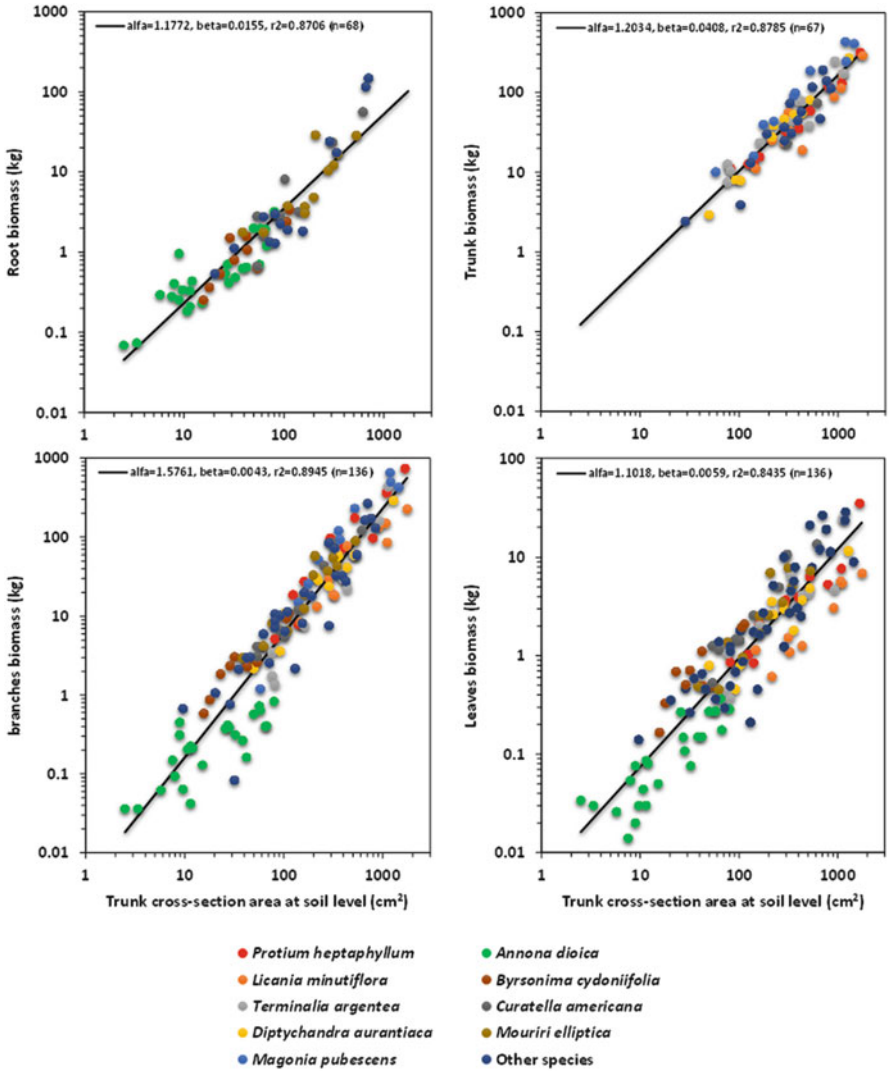

Fig. 2 Scale invariance between trunk cross section at soil level and the biomass of root (*upper left corner*), trunk (*upper right corner*), branches (*lower left corner*), and leaves (*lower right corner*) for savanna woody species in the Nhecolândia landscape

3 Comparing Empirical to Theoretical MST Scaling Exponents

The comparisons of empirical scaling exponents with theoretical exponents from MST are shown in Table 2. Empirical exponent values were calculated by using the obtained power laws shown in Fig. 2. Theoretical MST α values shown in Table 2 were obtained from [7, 8, 20].

Table 2 Theoretical and empirical scaling parameters α and β for trunk diameter at soil level (cm), biomass (kg), and plant height (m) of woody species in the Nhecolândia savanna physiognomy

Scaling model $y \sim \beta x^{\alpha}$	Theoretical MST α	Estimated α	Estimated β
Leaf mass ~ trunk diameter at soil level diameter	2	2 + 0.2036	0.0208
Leaf mass ~ trunk mass	3/4	3/4 + 0.1656	0.1104
Leaf mass ~ root mass	3/4	3/4 + 0.1859	0.2915
Trunk basal area ~ root mass	1	1 + 0.0223	2.8881
Root mass ~ aboveground mass	1	1 – 0.1372	0.2953
Trunk diameter at soil level ~ total plant mass	3/8	3/8 – 0.0013	1.8054
Plant height ~ trunk diameter at soil level	2/3	2/3 + 0.0522	4.4192

Theoretical α value between leaves biomass and trunk diameter d_{sl} is 2, and the empirical value was about 10% greater. The biomass scaling between leaves and trunk is theoretically 3/4, and the empirical value is 22% greater. Leaves and root scale also as 3/4, and the empirical scaling is 25% larger. The deviation from $\alpha = 1$ between trunk and root scaling is only +2.2%, while that between root and aboveground biomass is −14%. Plant height and trunk diameter scale as 2/3 + 8% (empirical data, plot not shown, $n = 75$, $r^2 = 0.7088$). The lowest deviation from theoretical value, −0.4%, was calculated for the scaling between trunk diameter (d_{sl}) and total plant biomass (m = root + trunk + branches + leaves) which is 3/8. From these results, it is clear that MST remarkably holds for the scaling $d_{sl} \sim m$, but deviates for the scaling to other partitioned biomass. Then, it is possible to conjecture that severe environmental constrains are indeed playing a role particularly in relative plant biomass allocation, as suggested by [13, 14].

For the especial case of the Nhecolândia, water cycle and topography can play a significant role. Firstly, the flat landscape is influenced by eventual flood in rainy years. This regional feature, however, may interfere only in the spatial distribution of the savanna woody physiognomies, where tallest stands are restricted to areas less subjected to inundation [21]. Consequently, eventual water flooding may play a role in the spatial distribution of the woody forest in the landscape but not in the biomass partitioning of the trees.

A closer look into tree biomass partition is given in Fig. 3. The theoretical biomass partitioning as a function of trunk diameter was calculated by integrating the power laws provided in Fig. 2. As the diameter increases, the relative proportion between trunk and branches inverts. The complete inversion takes place for $d_{sl} > 18$ cm (Fig. 3). This indicates that larger woody species allocates more biomass in branches, which could be objectively attributed, for instance, to asymmetric competition for light [14]. Nevertheless, as further discussed, the selective force is the water table level. Figure 4 illustrates biomass ratios between below- and aboveground, root and trunk, and root and branches as a function of plant size (d_{sl}).

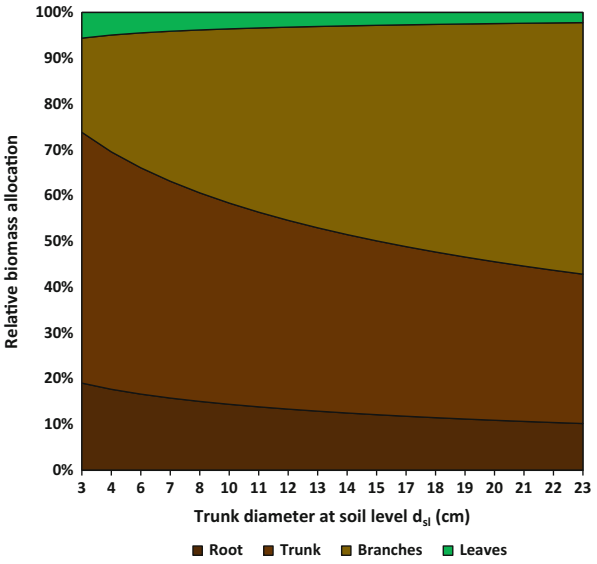

Fig. 3 Theoretical biomass partitioning as a function of trunk diameter for savanna woody species in the Nhecolândia landscape. The figure was generated by integrating the power law models shown in Fig. 2

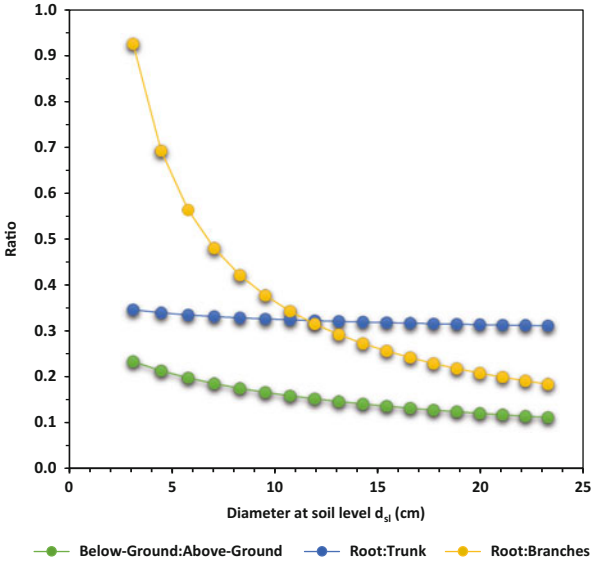

Fig. 4 Biomass allocation ratios as a function of trunk diameter expected (model) for savanna woody species in the Nhecolândia landscape

Note the decay of the root–branch ratio for increasing plant size. Alternatively, root–trunk ratio does not change notably (Fig. 4). For tropical savannas, the below to aboveground biomass ratio may be on average 1.88 ± 1.41 (derived from Table 1 in [22]). This value is about 10 to 20 times of that found in the Nhecolândia landscape, which varies from 0.2 to 0.1 (Fig. 4).

It is very likely that a peculiar environmental factor in the Nhecolândia is playing a big role in changing natural plant behavior (MST predictions), leading woody species to allocate more biomass above ground, particularly in branches. Salis et al. [19] have demonstrated that the peculiar factor is likely the water table, which oscillates between ca. 1 and 2 m below the top soil surface. This unique feature of the Nhecolândia, the elevated water table, limits the vertical growth of root [19]. The predominant sandy soil in the region acts as a limiting factor to the forest stand, restraining biomass productivity. In contrast, the closer water table is a source of water and nutrients in particular to the metabolism of large woody species that present deeper root systems. As noted in Fig. 3, large woody species allocate more biomass in branches, which, alternatively to the light-competing hypothesis [14], might be an ecohydrological [23] adaptation to maximize evapotranspiration due to the closer water table. Coomes and Allen [13] suggest that scaling exponents might follow MST predictions when aboveground biomass is lower and exceed MST predictions for higher aboveground biomass. This is the case of the savanna in the Nhecolândia, in which scaling exponents are slightly greater than MST predictions according to larger aboveground biomass. Nonetheless, the major driving of the process is not sunlight but the closer water table, which conspicuously constrains the growing space to plant roots [19].

It is not a surprise that the scaling $d \sim m^{3/8}$ of the Nhecolândia savanna firmly holds MST prediction. One can postulate that total and relative plant biomass may scale as predicted by MST under "non-severe" conditions [7, 8]. Relative biomass allocation, however, can naturally deviate from MST as an ecological adaptation of the plant community to cope with severe environmental constraints. In this view, both empirical data and MST are indeed complementary [15, 24]. Further advances in research can also focus on likely spectrum of scaling exponents according to key severe environmental factors [25]. A multifractal approach might be surprisingly useful, as the Tsallis' nonextensive thermodynamics was to modeling turbulence intermittence and stock market fluctuations [26].

4 Concluding Remarks

This chapter sheds new lights on the applicability of the Metabolic Scaling Theory to native savanna woody species in the Nhecolândia, Pantanal. Scaling is a general pattern in nature, and self-affine patterns represented by power laws can be very useful to understand and manage nature for humankind sustainability. The model can be further developed, for instance, to measure ecohydrological and carbon sequestration services [23, 27], also considering latitudinal/altitudinal temperature effects [28].

Acknowledgments The authors thank Zachary Brym (Utah State University) for kindly reviewing this chapter.

References

1. Glazier DS (2013) Log-transformation is useful for examining proportional relationships in allometric scaling. J Theor Biol 334:200–203
2. West GB, Enquist BJ, Brown JH (2009) A general quantitative theory of forest structure and dynamics. Proc Natl Acad Sci 106(17):7040–7045
3. Brown JH, Gupta VK, Li B-L, Milne BT, Restrepo C, West GB (2002) The fractal nature of nature: power laws, ecological complexity and biodiversity. Philos Trans R Soc Lond B Biol Sci 357(1421):619–626
4. Turcotte DL (1997) Fractals and chaos in geology and geophysics. Cambridge University Press, New York
5. Malamud BD, Turcotte DL (1999) Self-affine time series: measures of weak and strong persistence. J Stat Plan Inference 80(1–2):173–196
6. Kolmogorov AN (1941) Dissipation of energy in locally isotropic turbulence. Dokl Akad Nauk SSSR 32:16–18
7. West GB, Brown JH, Enquist BJ (1999) The fourth dimension of life: fractal geometry and allometric scaling of organisms. Science 284(5420):1677–1679
8. Enquist BJ, Niklas KJ (2001) Invariant scaling relations across tree-dominated communities. Nature 410(6829):655–660
9. Bastviken D, Cole J, Pace M, Tranvik L (2004) Methane emissions from lakes: dependence of lake characteristics, two regional assessments, and a global estimate. Global Biogeochem Cycles 18(4), GB4009
10. Lima IBT, Ramos FM, Bambace LAW, Rosa RR (2008) Methane emissions from large dams as renewable energy resources: a developing nation perspective. Mitig Adapt Strat Gl 13 (2):193–206
11. West GB (1999) The origin of universal scaling laws in biology. Physica A 263(1–4):104–113
12. Whitfield J (2004) Ecology's big hot idea. PLoS Biol 2:e440
13. Coomes DA, Allen RB (2009) Testing the metabolic scaling theory of tree growth. J Ecol 97 (6):1369–1373
14. Coomes DA, Lines ER, Allen RB (2011) Moving on from metabolic scaling theory: hierarchical models of tree growth and asymmetric competition for light. J Ecol 99(3):748–756
15. Enquist BJ, West GB, Brown JH (2009) Extensions and evaluations of a general quantitative theory of forest structure and dynamics. Proc Natl Acad Sci 10:2009
16. Price CA, Weitz JS, Savage VM, Stegen J, Clarke A, Coomes DA et al (2012) Testing the metabolic theory of ecology. Ecol Lett 15(12):1465–1474
17. Salis SM, Assis MA, Mattos PP, Pião ACS (2006) Estimating the aboveground biomass and wood volume of savanna woodlands in Brazil's Pantanal wetlands based on allometric correlations. For Ecol Manage 228(1–3):61–88
18. Salis SM, Assis MA, Crispim SMA, Casagrande JC (2006) Distribuição e abundância de espécies arbóreas em cerradões no Pantanal, estado do mato grosso do sul Brasil. Braz J Bot 29:339–352
19. Salis SM, Lehn CR, Mattos PP, Bergier I, Crispim SMA (2014) Root behavior of savanna species in Brazil's Pantanal wetland. Glob Ecol Conserv 2:378–384
20. Niklas KJ, Spatz H-C (2004) Growth and hydraulic (not mechanical) constraints govern the scaling of tree height and mass. Proc Natl Acad Sci U S A 101(44):15661–15663
21. Pott A, Silva JSV (2015) Terrestrial and aquatic vegetation diversity of the Pantanal wetland. Hdb Env Chem. doi:10.1007/698_2014_352
22. Grace J, José JS, Meir P, Miranda HS, Montes RA (2006) Productivity and carbon fluxes of tropical savannas. J Biogeogr 33(3):387–400
23. D'Odorico P, Laio F, Porporato A, Ridolfi L, Rinaldo A, Rodriguez-Iturbe I (2010) Ecohydrology of terrestrial ecosystems. BioScience 60(11):898–907
24. Tredennick AT, Bentley LP, Hanan NP (2013) Allometric convergence in savanna trees and implications for the use of plant scaling models in variable ecosystems. PLoS One 8(3):e58241

25. Kempes CP, West GB, Crowell K, Girvan M (2011) Predicting maximum tree heights and other traits from allometric scaling and resource limitations. PLoS One 6(6):e20551
26. Ramos FM, Rosa RR, Neto CR, Bolzan MJA, Abren Sá LD (2001) Nonextensive thermostatistics description of intermittency in turbulence and financial markets. Nonlinear Anal Theory, Methods Appl 47(5):3521–3530
27. Watanabe MDB, Ortega E (2014) Dynamic energy accounting of water and carbon ecosystem services: a model to simulate the impacts of land-use change. Ecol Model 271:113–131
28. Gillooly JF, Brown JH, West GB, Savage VM, Charnov EL (2001) Effects of size and temperature on metabolic rate. Science 293(5538):2248–51

Alkaline Lake Dynamics in the Nhecolândia Landscape

Ivan Bergier, Alex Krusche, and Frédéric Guérin

Abstract Alkaline lakes are diversified ecosystems of the Nhecolândia landscape in the southern Taquari Megafan, Pantanal. By 1985 they covered an approximate area of 1,060 km^2 distributed in nearly 12,761 shallow water bodies. Historical Landsat-5 image analysis from 1985 to 1998 indicates a reduction of 24% in the area and 28% in the number of these shallow lakes. The alkaline lakes in the region can be generally arranged in three major ecological typologies: macrophyte lakes (autotrophic above waterline, lower electron conductivity (EC), and pH), bacterial lakes (heterotrophic, moderate EC, and pH), and saline lakes (autotrophic below waterline, elevated EC, and pH). During 1985–1998, the relative area of macrophyte lakes and bacterial lakes decreased 22 and 40%, respectively, while saline lakes increased 53%. Alkaline lakes may interchange their ecological typologies as a function of short- and long-term water rainfall, surface water flows, and interplay with the aquifer. The decline of lake area and number, and the particular increase in saline lakes, can be associated to highland deforestation and its impact on the regional rainfall distribution. Ancillary data of water chemistry and greenhouse gases allowed sketching a general biogeochemical model of macrophyte and saline typologies and deriving a gross estimation of carbon exchanges with the atmosphere from these alkaline lakes in the Nhecolândia landscape.

Keywords Alkaliphiles, Carbon cycle, Extremophiles, Saline lakes, Wetland

I. Bergier (✉)
Laboratory of Biomass Conversion, Embrapa Pantanal, Corumbá, Brazil
e-mail: ivan.bergier@embrapa.br

A. Krusche
Center for Nuclear Energy in Agriculture, University of São Paulo, Piracicaba, Brazil

F. Guérin
Géosciences Environnement Toulouse (GET), Observatoire Midi Pyrénées, Université de Toulouse, CNRS, IRD, 14 avenue E. Belin, F-31400 Toulouse, France

I. Bergier and M.L. Assine (eds.), *Dynamics of the Pantanal Wetland in South America*, Hdb Env Chem (2016) 37: 145–162, DOI 10.1007/698_2014_327,

Contents

1 Introduction

The Nhecolândia landscape, as defined by Hamilton et al. [1] in the southern Taquari Megafan (Fig. 1), harbors a singular myriad of shallow alkaline lakes, whose water depth usually does not exceed 1 m at deepest sites. The altitude in the Taquari Megafan ranges between 190 and 85 m a.s.l., resulting in a very low average topographic gradient of ~0.36 m km^{-1} [2]. The climate is usually warm (up to ~40°C in daylight) and the year can be split in two marked seasons based on rainfall: (1) a dry season during the austral winter (May to September, rainfall ~180 mm) and (2) a wet season during the austral summer (October to April, rainfall ~855 mm). Nhecolândia is an abandoned lobe of the Taquari Megafan, where sedimentation by rivers is actually inactive (Fig. 1) and the drainage system is slightly connected to major fluvial systems [3].

The landscape of the region is a patchwork of forests; savanna; native and introduced pastures; seasonal waterways; herbaceous vegetation around alkaline lakes, which can be colonized by aquatic macrophytes [4]; and other various lakes with contrasting water electrical conductivity (EC) and pH. Some of these lakes with high values of EC and pH harbor alkaliphile and extremophile microorganisms with peculiar characteristics [5]. These organisms have special and complex enzymatic systems that allow their survival and optimal physiological performance at elevated pH levels [6]. The microorganisms are cyanobacteria, which are able of photosynthesis at high pH [7], and heterotrophic bacteria, such as methanogens [8] and methanotrophs [9]. These singular aquatic ecosystems and their biota play an important role in the global carbon cycle [10] and might be vulnerable by future human-induced land-use and climate changes [11].

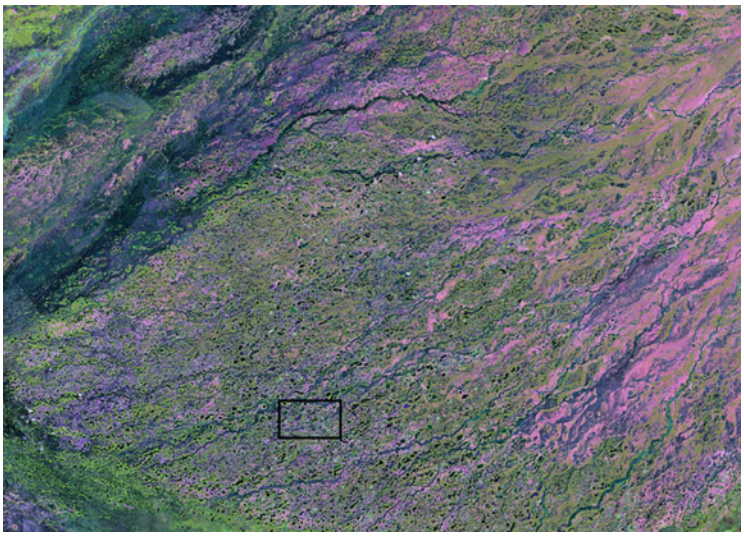

Fig. 1 Thematic Mapper Landsat-5 (orbit 226, dot 073, 5R4G3B band composition) data acquired in 1985 evidencing the lakes of the Nhecolândia subregion in the southern Taquari Megafan. The *box* defines a detailed view of the landscape shown in Fig. 3

1.1 Major Environmental Factor Governing the Spatial Heterogeneity in the Landscape

The alkaline lakes in the Nhecolândia landscape are analogous to aquatic environments known worldwide as soda lakes [12]. The underlying complexity of the formation and evolution of these particular water bodies in Nhecolândia has long been intensively studied, and the environmental factors controlling their biogeochemical functioning at short space scales were identified [13–16]. In general, the coexistence of saline (very alkaline), oligosaline (moderately alkaline), and freshwater (less alkaline) lakes [4, 17] can be attributed to the height distribution of a low-permeable sandy loam soil [18]. Besides short- and long-term summer rainfall trends, as further explored in this chapter, the development of sandy loam layers in the landscape largely governs the spatial heterogeneity of the alkaline lakes in Nhecolândia [14]. This layer originates from the precipitation of amorphous silica in lake sediment pores usually under very high alkaline conditions [15]. The sandy loam layer enhances the isolation of the lake from the aquifer and surface water flows [15, 18]. The development of the saline lakes occurs mainly when summer rainfall decreases (enhanced evaporation and concentration) and when the sandy loam horizon gets close to the top soil surface [16, 17].

1.2 Major Ecological Typologies Based on Functional Biogeochemistry

Key variables that biogeochemically discriminate these shallow lakes are EC and pH, related to the type and quantity of dissolved ions in lake waters, and the lake metabolism (autotrophy or heterotrophy). Figure 2 illustrates how the different types of lakes can be discriminated according to the pH and EC of their water following Almeida et al. [19] and Martins [17] and group discriminations from Timms [20], Martins [17], and Evans and Costa [4].

All together, the key environmental features allow differentiating three major ecological typologies based on functional biogeochemistry (Fig. 2):

- *Macrophyte or* "*freshwater*" *lakes* (M): autotrophic metabolism based on photosynthesis predominantly above the lake waterline with EC < 2,000 μS cm^{-1} and pH < 7.5
- *Bacterial or* "*oligosaline*" *lakes* (B): predominance of heterotrophic metabolism with 500 < EC < 5,000 μS cm^{-1} and 7 < pH < 9.5
- *Saline lakes* (S): autotrophic metabolism based on photosynthesis below the lake waterline, predominantly by cyanobacteria, with 700 < EC < 65,000 μS cm^{-1} and 7.9 < pH < 10.5

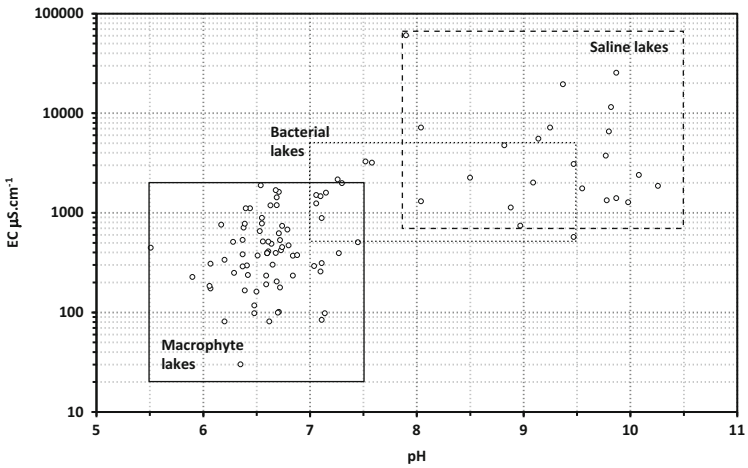

Fig. 2 Electrical conductivity (EC) and pH continuum obtained for 85 alkaline lakes measured by Almeida et al. [19] and Martins [17]. Grouping of ecological typologies in the pH and EC continuum was based on Timms [20], Martins [17], and Evans and Costa [4]

2 Identification of Lake Ecological Typologies in the Nhecolândia Landscape

Landsat-5 images are so far the best available long-term register of the Earth landscape. Despite its limited radiometric and spatial resolutions, Landsat-5 historical images are very useful to identify temporal changes in the landscape. In Fig. 3, a box section of Fig. 1 is depicted. The landscape complexity of Nhecolândia is unveiled by several lakes (intricate colors), waterways in dark green shades, and forest corridors in light green (as a response of band 4 in the near-infrared range of the Thematic Mapper sensor). Lands covered with grasses and shrubs are discernible as magenta (a mixture of signals from band 5 in the mid-infrared and band 4). For the majority of the lakes, it is possible to note the eventual occurrence of macrophytes. The letter M in Fig. 3 indicates 12 lakes partially or totally covered with macrophytes. They are irregularly shaped with some degree of connectivity with waterways.

Mostly rounded and isolated lakes are eventually dark due to greater depth and higher sunlight extinction coefficients, while others are blue due to signal return in band 3, in the visible red, indicating the presence of suspended solids or light-dispersing sediments. Those lakes are likely associated to bacterial alkaline lakes [20] and five of them are identified by the letter B in Fig. 3. Saline lakes are those seen in green moss color (a combined response of bands 3 and 4) associated to abundant colonization of cyanobacteria. The letter S in Fig. 3 identifies four saline lakes. Note the usual circular shape of the saline lakes as a result of its greater isolation from waterways.

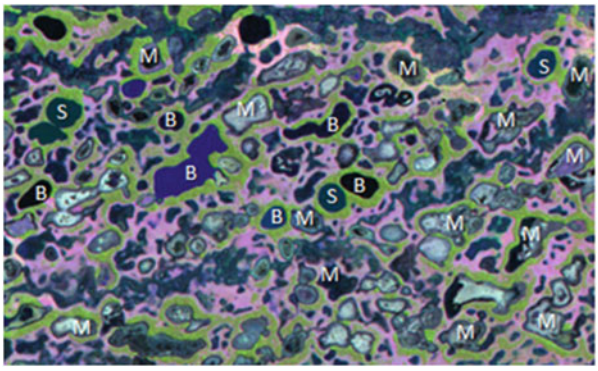

Fig. 3 Landscape features of Nhecolândia derived from the Landsat-5 color composition shown in Fig. 1. The letters M, B, and S indicate, respectively, macrophyte, bacterial, and saline lakes, according to the functional biogeochemical criterion herein discussed

3 Temporal Changes in Number and Area of Alkaline Lakes in the Nhecolândia Landscape

Landsat-5 Thematic Mapper (bands 3, 4, and 5) imagery was used in the SPRING (http://www.dpi.inpe.br/spring/english/index.html) Geographical Information System (GIS) to evaluate the temporal changes in the area and number of the alkaline lakes. Landsat-5 images were obtained between June and August from 1985 to 1998. Landsat-5 images from 1999 and so on were not suited for analysis by this method due to excess drying of the region, reducing signal discrimination of lakes with respect to dry lands and dried waterways. An ordinary image registering process was made to achieve an average accuracy of ± 1 pixel. Principal components analysis (PCA) with band 4 of the 1985–1998 imagery dataset was performed to produce an overlay mask by the first component (PC-1). The classification of PC-1 by *k*-means algorithm successfully separates the overall surface of alkaline lakes in the landscape. The mask PC-1 was then manually edited to eliminate, in particular, connected waterways.

Figure 4 shows the mask obtained for alkaline lakes in Nhecolândia. According to this map, the maximum area eventually occupied by alkaline lakes between 1985 and 1998 was roughly 1,208 km^2, ranging from 9,249 to 13,251 km^2 of alkaline lakes. In contrast, Oliveira et al. [21] estimated a total of 17,539 km^2 of alkaline

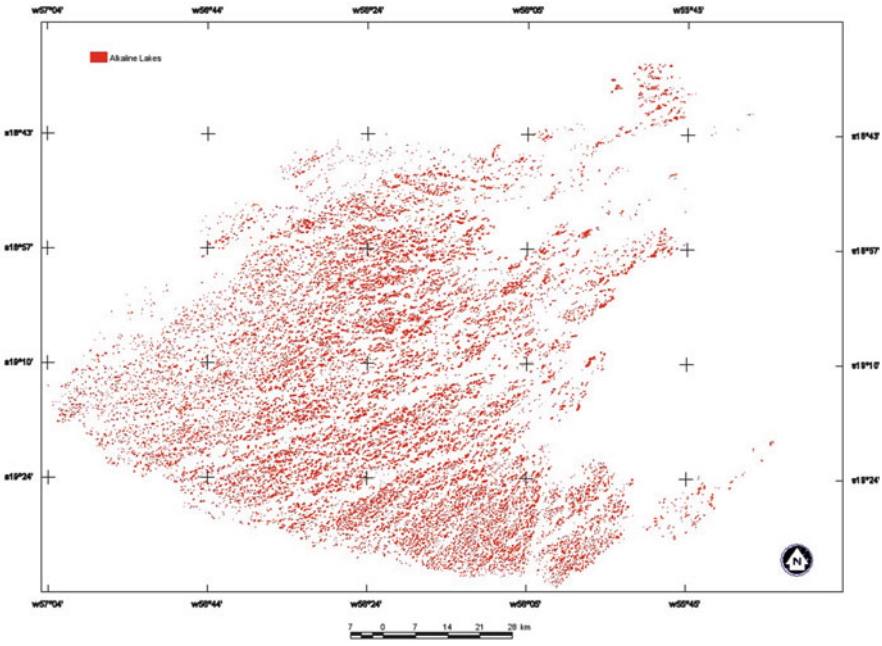

Fig. 4 Recovered mask of alkaline lakes in the Nhecolândia landscape by *k*-means classification of PC-1 derived from band 4 for the entire dataset 1985–1998

lakes, and number divergences with this respect can be attributed to differences in image data and processing.

The mask shown in Fig. 4 was overlaid on bands 3, 4, and 5 of every analyzed year by using spatial algebraic programming language (LEGAL) available in SPRING GIS (http://www.dpi.inpe.br/spring/english/tutorial/legal.html) to create new image layers with digital numbers exclusively from pixels below the mask. Masked layer data for each year were later processed by segmentation (contextual object-oriented classification) followed by supervised classification in SPRING GIS. The supervised classification mapping of M (macrophyte), B (bacterial), and S (saline) ecological typologies for each year was obtained by means of the spectral characteristics assigned in Fig. 3. The area A_y and number of lakes N_y for a given year y were then computed as $A_y = M_{Ay} + B_{Ay} + S_{Ay}$ and $N_y = M_{Ny} + B_{Ny} + S_{Ny}$.

Figure 5 shows a reduction by 24% in the area and by 28% in the number of alkaline lakes from 1985 to 1998. For the evaluated period, the annual loss in total lake area was estimated to be nearly 22.6 km^2 corresponding to the disappearance of 231 alkaline lakes. Declining of lake area and number can be attributed to the gradual decrease in summer rainfall by roughly -7 mm year^{-1} over 30 years (see Fig. 6). Land-use changes in the Pantanal headwater highlands drastically modify the ecohydrology functioning of the whole drainage basin. The reduction in soil infiltration, aquifer recharge, and evapotranspiration in highland areas increase river discharges [22] at the same time that may reduce cloud formation and the ulterior rainfall redistribution throughout lowland areas less influenced by riverine floods, as is the case of the Nhecolândia subregion.

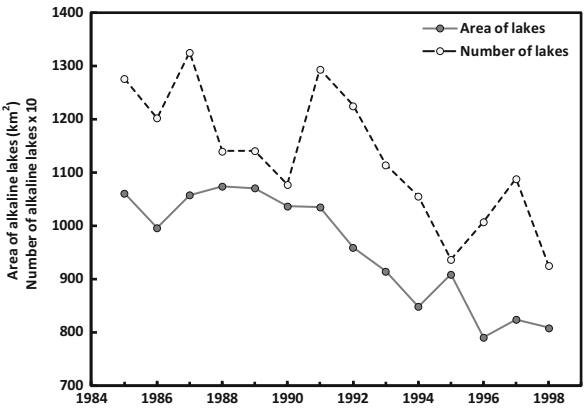

Fig. 5 Changes in the area and number of alkaline lakes from 1985 to 1998 in Nhecolândia as estimated by Landsat-5 image processing

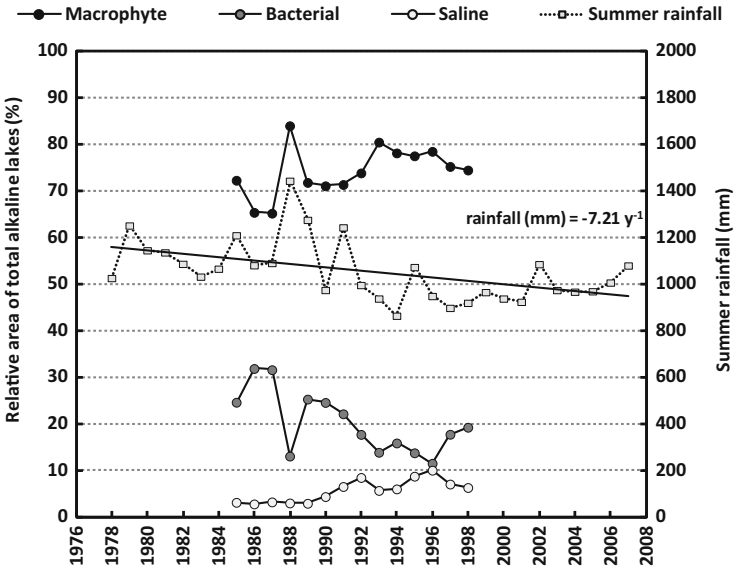

Fig. 6 Changes in the area proportion of ecological typologies of the alkaline lakes in the Nhecolândia landscape from 1985 to 1998 as a function of the austral summer rainfall in the Nhumirim Farm (Embrapa) from 1977 to 2007

3.1 Temporal Changes of Alkaline Lake Ecological Typologies in the Nhecolândia Landscape

Temporal changes in the relative proportions of ecological typologies, namely, macrophyte, bacterial, and saline, are associated to summer rainfall changes (Fig. 6). Whereas the evolution of the relative proportions of macrophyte and bacterial lake typologies does not significantly correlate, the saline lake typology inversely correlates with summer rainfall (-0.53, $p < 0.05$). The proportion of macrophyte lake typology correlates negatively with the proportion of bacterial lake typology (-0.94, $p < 0.001$) evidencing the likelihood of bacterial converted to macrophyte, and vice versa (Fig. 6). The negative correlation between the proportions of bacterial and saline typologies (-0.68, $p < 0.004$) also suggests interchanges between these two lake typologies. The weaker positive correlation was between the proportions of macrophyte and saline lake typologies (0.39, $p < 0.08$), indicating that they do not usually interchange their ecological status, which is naturally expected for extreme ecological typologies. It suggests that they pass through the intermediate bacterial stage in the EC and pH continuum shown in Fig. 2.

Figure 7 illustrates the conceptual model that describes the potential ecological changes in the states of alkaline lakes in the Nhecolândia landscape as a function of the regional hydrology. The Nhecolândia alkaline lake model is based on the EC and pH continuum shown in Fig. 2 and is also an adaptation of a model originally

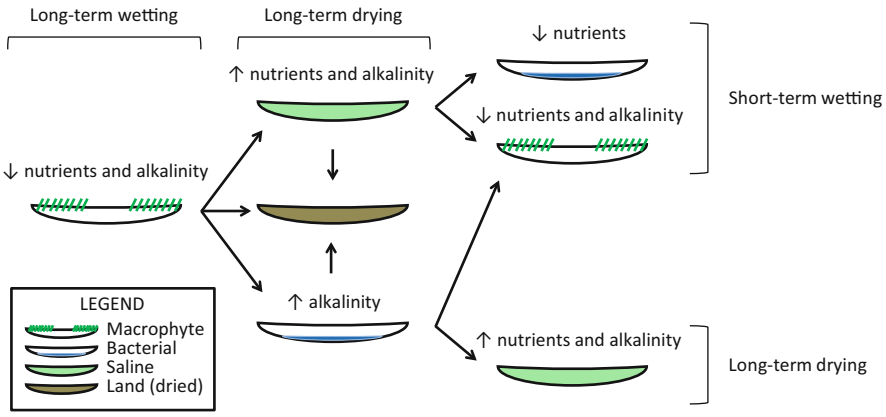

Fig. 7 Potential changes in the ecological states of alkaline lakes in the Nhecolândia landscape as a function of regional hydrology at different timescales. The model was adapted from Timms [20] and is fundamentally based on the EC and pH continuum shown in Fig. 2

conceived for Australian saline lakes [20]. The model relates the level of nutrients and alkalinity with the most likely ecological state of an alkaline lake at a given time under dry or wet conditions. A macrophyte lake can turn into saline lake if nutrient and alkalinity levels rise (also as a function of a change in the height of the less impermeable soil loam) or into bacterial lake if only alkalinity increases. A bacterial lake can turn into saline lake if nutrient and alkalinity levels rise or into macrophyte with opposite conditions. A saline lake can turn into bacterial lake if only nutrient level decreases or into macrophyte lake if both nutrient and alkalinity levels decrease (Fig. 6), albeit the latter change might be rather improbable due to soil loam constraints.

In spite of its simplicity, the Nhecolândia alkaline lake model driven by short- and long-term regional water cycle fairly agrees with observations made through processing Landsat-5 imagery. To further test model agreements, ecological typology changes of the alkaline lakes in Nhecolândia were investigated by Boolean intersection (crossing) of the classified images with the aid of LEGAL in SPRING GIS. Changes were evaluated in the whole period and in a year-to-year basis, in which every single pixel is looked as a state vector changing or not its status over time. The underlying objective is to identify and quantify classified pixels that either changed their "ecological status" or remained unchanged accordingly to model classifications in macrophyte, bacterial, saline, and dried land shown in Fig. 7.

From 1985 to 1998, the majority of the lakes changed its typological status, and only 5.6 (0.5%), 16.5 (1.4%), and 109 (9%) km^2 remained unchanged as saline, bacterial, and macrophyte, respectively. On the other hand, in a year-to-year basis, usually more than 50% of the area remained unchanged for a given ecological status (Fig. 8). For the macrophyte typology (upper plot in Fig. 8), changes were predominantly associated with drying, i.e., changing to land, followed by changes to

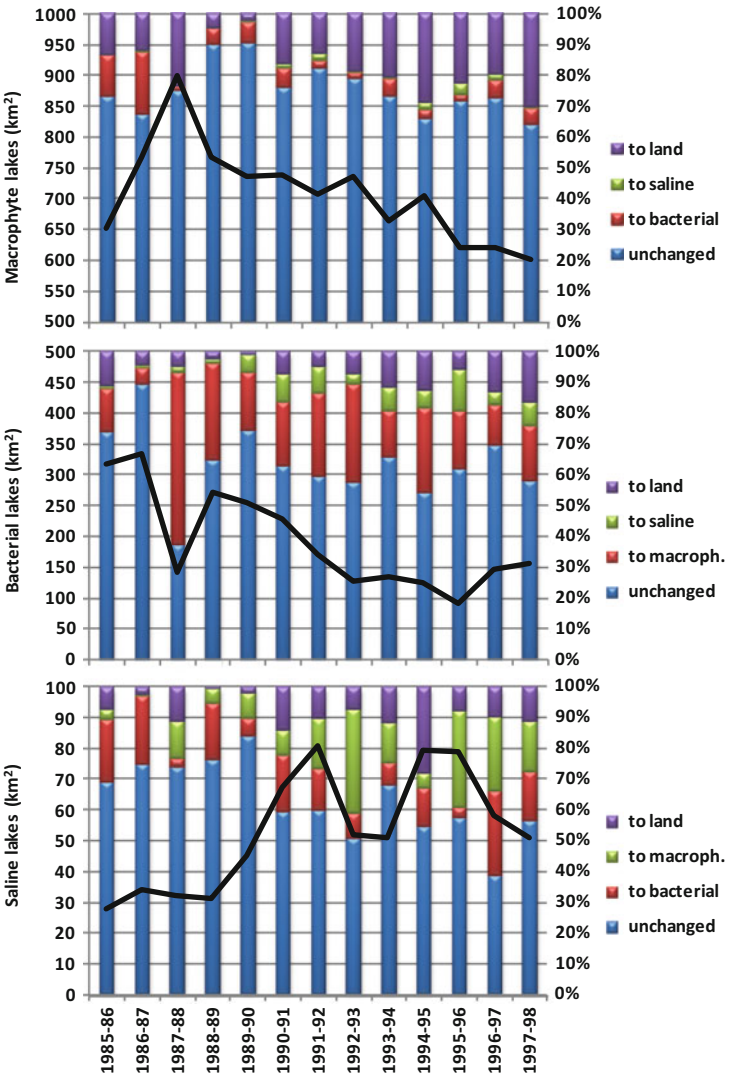

Fig. 8 Proportional year-to-year changes in ecological typologies (macrophyte, bacterial, and saline) of the alkaline lakes in the Nhecolândia landscape from 1985 to 1998. *Black curves* in each plot denote the cover area given in square kilometer of the corresponding ecological typology in the subsequent year, e.g., 1986 for 1985–1986

bacterial typology and, in minor proportion, to saline typology. About 10% of the bacterial lakes (mid plot in Fig. 8) were converted to land yearly. However, most of the interannual changes were the conversion of macrophyte to saline lakes, which is expected when Nhecolândia is subjected to long-term drying. The change of bacterial to macrophyte lakes, however, would be expected for wetter periods (Fig. 7). Hence, it is possible that short-term, instead of long-term, rainfall plays

a significant role in bacterial to macrophyte changes. In this sense, a wetter year can push bacterial lakes to macrophyte lakes, but the long-term drying leads to saline lakes. The model still holds and the time span (short or long) of the hydrology must be carefully taken into account to understand the dynamics of the ecological typologies.

In the case of the saline lake typology (bottom plot in Fig. 8), the doubling in area cover, likely derived from bacterial typology lakes subjected to long-term drying, favoring lake isolation and the development of extremophiles, is noticeable by 1990 [6]. Despite that ~10% of the saline typology changed to land yearly, major interannual changes lead to macrophyte and bacterial typologies. This finding corroborates the hypothesis that long-term drying and short-term wetting play different roles in the ecological state of the alkaline lakes in the Nhecolândia landscape. Indeed, observed interannual changes in ecological typologies (Fig. 8) reflect lake responses to long-term decline in regional summer rainfall (Fig. 6) but also to eventual short-term wetting, in full concordance with the ecological alkaline lake model depicted in Fig. 7 and empirical typology changes shown in Fig. 8 for the Nhecolândia landscape.

4 Biogeochemistry of Saline and Macrophyte Typologies in the Nhecolândia Landscape

Ancillary data on surface and groundwater chemistry (dissolved inorganic carbon and ions) and greenhouse gases (methane and carbon dioxide dissolved in water, sediment bubbles, and chamber fluxes) can illustrate the role of the alkaline lakes in the Nhecolândia landscape in the regional carbon cycle. Data were gathered in 2009 and 2010 at the well-known [5] "Salina do Meio" (saline typology) and "Baía da Sede" (macrophyte typology) alkaline lakes at Nhumirim Experimental Farm, owned by Embrapa Pantanal.

Gas samples were taken with funnels (to collect sediment gas bubbles) and closed chambers (for estimating fluxes at the air-water interface) with the aid of 60 cc plastic syringes. Gas samples in syringes were transferred with needles to rubber-sealed and evacuated glass flasks. Water samples were taken in glass flasks and poisoned for later headspace gas phase extraction [23]. Methane and carbon dioxide were measured at EMBRAPA Pantanal with a SRI/GC8610 gas chromatograph equipped with a flame ionization detector (FID) and a methanizer catalyst. Lake water and groundwater samples from "Salina do Meio" and "Baía da Sede" were collected in clean flasks that were sent to CENA-USP for filtering and chemical characterization using a Foss Tecator Fiastar 5000 flow injection colorimetric system (NO_3^-, NO_2^-, NH_4^+, PO_4^{3-}, and Cl^-) and a Horiba Jobin Yvon Ultima ICP-OES analyzer (Ca^{2+}, Mg^{2+}, K^+, Na^+, Si^{4+}, Fe^{2+}, SO_4^{2-}).

4.1 Anions and Cations in Water and Groundwater

The mean concentrations of anionic and cationic species for lake water and groundwater of saline and macrophyte lake typologies are shown in Figs. 9 and 10, respectively. In general, lake water in Nhecolândia results from simple concentration and dilution of one original source, the chemical composition of which is similar to that of the Taquari River [24]. Due to positive calcite residual alkalinity, lake water develops a sodic alkaline pathway under influence of evaporation, and the concentration is accompanied by mineral precipitations. Biological feedbacks taking place in bacterial and saline lakes may also play a role in this "alkalinization process" [6], where the higher the water Na and K concentrations, the greater are the mineral precipitations, particularly Si, Mg, and Ca [16].

For surface waters, a two-tailed Student *t*-test comparing the mean of the log-transformed data of macrophyte and saline typologies showed that Cl^{-}, NH_4^{+}, PO_4^{3-}, Na^{+}, Mg^{2+}, Fe^{2+}, and SO_4^{2-} are significantly different ($p < 0.05$). Higher concentrations of NH_4^{+}, PO_4^{3-}, and SO_4^{2-} in lake water of the saline typology (Figs. 9 and 10) evidence an aquatic environment naturally eutrophicated, with high net ecosystem production [7], due to both evaporation and the presence of alkaliphile extremophiles that amend their surroundings toward elevated pH [6].

4.2 Carbon Dynamics

Figure 11 presents unique data on water DIC and CO_2 and CH_4 concentrations in the water and sediment gas phases obtained at macrophyte and saline lakes in Nhecolândia. The CH_4 concentration in the sediment gas phase is somewhat higher for the saline typology, but the greater concentration of CO_2 in the sediment gas phase for macrophyte typology indicates that methanogenesis (the biological

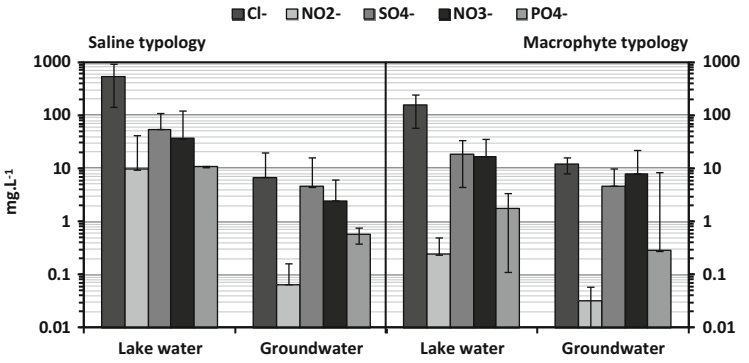

Fig. 9 Anionic concentrations (log-scale of the mean ± 1 SD of monthly water samples from August 2009 to November 2010) in the lake and groundwater of "Salina do Meio" (saline typology) and "Baía da Sede" (macrophyte typology) at the Nhumirim Farm

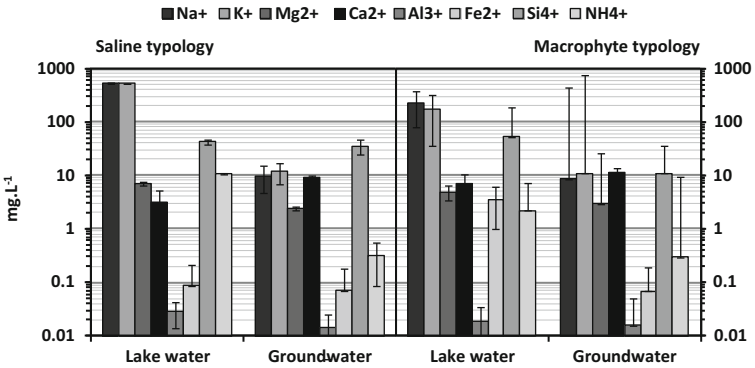

Fig. 10 Cationic concentrations (log-scale of the mean ± 1 SD of monthly water samples from August 2009 to November 2010) in the lake and groundwater of "Salina do Meio" (saline typology) and "Baía da Sede" (macrophyte typology) at the Nhumirim Farm

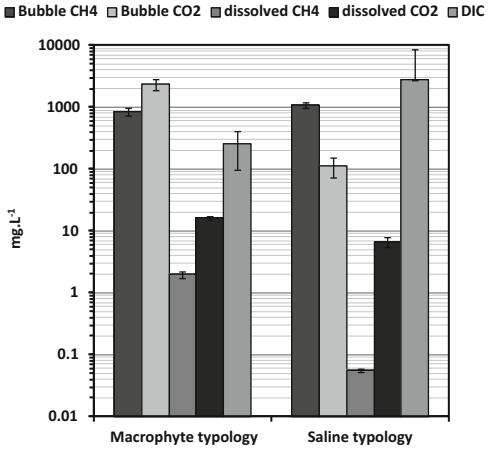

Fig. 11 Methane (CH_4) and carbon dioxide (CO_2) concentrations (log-scale of the mean ± 1 SD) in the sediment (gas phase, known volume of collected bubbles) and in the surface water (dissolved phase) measured in 18 September 2009. DIC data are log-scale of the mean ± 1 SD of monthly water samples from August 2009 to November 2010

conversion of an organic carbon source to methane) routes and the kind of bacteria (e.g., acetoclastic or hydrogenotrophic) involved are absolutely distinct. Furthermore, bacterial methanogenesis might be more efficient for the saline typology, leading to greater methane concentrations in the sediment gas phase, which, in turn, may be responsible for greater bubbling CH_4 emissions (not measured). On the other hand, dissolved methane concentration in the lake water was much lower in the saline lake typology compared to the macrophyte lake typology (Fig. 11).

These observations indicate an intricate enzymatic architecture of alkaliphile extremophiles in the saline lake typology that efficiently produces CH_4 in

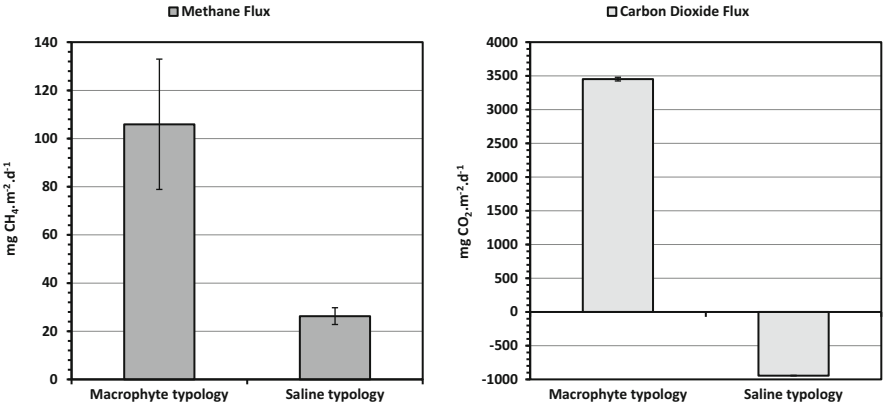

Fig. 12 Methane (CH_4) and carbon dioxide (CO_2) exchanges (mean $\pm$ 1 SD, $n = 3$) at the air-surface interface of macrophyte and saline typologies measured in September 2009. *Positive values* represent net sources

sediments from the decomposition of organic matter and, at the same time, efficiently oxidizes CH_4 to CO_2 in the water column by alkaliphilic methanotrophs.

Another remarkable feature of the naturally eutrophicated saline typology is the dominance of alkaliphilic cyanobacteria in the water column, for which is assumed that the produced CO_2 can be promptly available for underwater photosynthesis. These biogeochemical feedbacks might also be responsible for fast turnover and high net ecosystem production in these environments. The much higher DIC concentrations in saline typology support this hypothesis (Fig. 11).

CH_4 and CO_2 emissions to the atmosphere from the two investigated lakes are shown in Fig. 12. Methane and carbon dioxide emissions are nearly 4- and 3.5-fold superior, respectively, in the macrophyte typology. Note the saline typology as a net sink of CO_2. The high productivity due to high nutrient content and specialized microbial life operating at high pH and EC result in efficient pumping of C from the atmosphere into the lake. Nevertheless, for a better portrait of the C budget for these lakes, it would be also necessary to include bubbling as a mechanism of gaseous emissions.

Based on the previous findings and premises, it is possible to sketch a theoretical carbon dynamic model for saline and macrophyte typologies (Fig. 13). The model discerns two basic pathways that highlight the importance of alkaliphile extremophiles in saline lake carbon dynamics. Saline typology is highly efficient in (1) sequestering atmospheric and/or dissolved CO_2 (by photosynthesis of extremophile cyanobacteria), (2) producing methane in sediments (methanogenic extremophile bacteria), and (3) oxidizing dissolved CH_4 in the water column (methanotrophic extremophile bacteria). Carbon burial in the saline typology sediments might therefore be greater than that in the macrophyte typology (Fig. 13).

By combining Landsat-5 mapping of alkaline lakes with in situ data, it is possible to further derive a rough estimate showing the role of saline and macrophyte lakes in the carbon exchange of the Nhecolândia landscape with the atmosphere. Not accounting for bubbling emissions, it is calculated that the area of saline

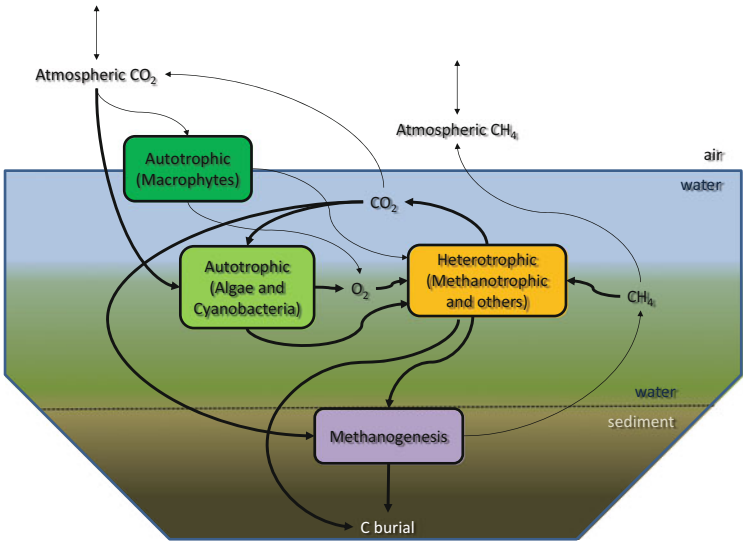

Fig. 13 Theoretical biogeochemical model for saline (emphasized by *thick lines*) and macrophyte typologies of alkaline lakes in the Nhecolândia landscape

lakes may annually sequester about 3.4 ± 1.2 Gg C (1 Gg $= 10^9$ g), while macrophyte lakes are responsible for an annual net emission of 186 ± 21 Gg C year^{-1}. The previous standard deviations represent a measure that reflects lake area changes accordingly to wet or dry years.

The present chapter does not attempt to cover exhaustively all relevant aspects of the ecological and biogeochemical functioning of alkaline lakes in the Nhecolândia landscape. Further investigations are needed to better characterize their particular ecological functioning and biogeochemistry promoted by the very singular biota living in these lakes, which can be largely affected by the ongoing land-use and climate changes.

Acknowledgments The authors thank Cleomar Berselli (Embrapa) and Alexandra Montebelo Mayres (CENA) for handling water sampling and analyses and Luiz Pellegrin and Rafaela Silva for the support with Landsat-5 imagery processing. This work was partially funded by FAPESP, Research Program on Global Climate Change (PFPMCG), Project "The role of rivers on the regional carbon cycle," grant number 2008/58089-9.

References

1. Hamilton SK, Sippel SJ, Melack JM (1996) Inundation patterns in the Pantanal wetland of South America determined from passive microwave remote sensing. Arch Hydrobiol 137:1–23
2. Zani H, Assine ML, McGlue MM (2012) Remote sensing analysis of depositional landforms in alluvial settings: method development and application to the Taquari megafan, Pantanal (Brazil). Geomorphology 161(162):82–92

3. Pott VJ, Pott A (2011) Species diversity, distribution and biomass of aquatic macrophytes of the Pantanal. In: Junk WJ, Silva CJ, Cunha CN, Wantzen KM (eds) The Pantanal: ecology, biodiversity and sustainable management of a large neotropical seasonal wetland. Pensoft Publishers, Sofia-Moscow, pp 257–280
4. Evans TL, Costa M (2013) Landcover classification of the lower Nhecolândia subregion of the Brazilian Pantanal wetlands using ALOS/PALSAR, RADARSAT-2 and ENVISAT/ASAR imagery. Remote Sens Environ 128:118–137
5. Santos KR, Sant'Anna CL (2010) Cianobactérias de diferentes tipos de lagoas ("salina", "salitrada" e "baía") representativas do Pantanal da Nhecolândia, MS, Brasil. Rev Bras Bot 33(1):61–83
6. Horikoshi K (1999) Alkaliphiles. CRC, Boca Raton, p 368
7. Santos KRS, Jacinavicius FR, Sant'anna CL (2011) Effects of the pH on growth and morphology of *Anabaenopsis elenkinii* Miller (Cyanobacteria) isolated from the alkaline shallow lake of the Brazilian Pantanal. Fottea 11(1):119–126
8. McGenity TJ (2010) Methanogens and methanogenesis in hypersaline environments. In: Timmis KN (ed) Handbook of hydrocarbon and lipid microbiology. Springer, Berlin/Heidelberg. doi:10.1007/978-3-540-77587-4_53
9. Khmelenina V, Shchukin V, Reshetnikov A, Mustakhimov I, Suzina N, Eshinimaev B, Trotsenko Y (2010) Structural and functional features of methanotrophs from hypersaline and alkaline lakes. Microbiology 79:472–482
10. Duarte CM, Prairie YT, Montes C, Cole JJ, Striegl R, Melack J, Downing JA (2008) CO_2 emissions from saline lakes: a global estimate of a surprisingly large flux. J Geophys Res 113, G04041. doi:10.1029/2007JG000637
11. Lerman A (2009) Saline lakes' response to global change. Aqua Geochem 15:1–5. doi:10.1007/s10498-008-9058-8
12. Oren A, Naftz DL, Wurtsbaugh WA (2009) Saline Lakes around the world: unique systems with unique values. In: Saline lakes around the world: unique systems with unique values, vol 15. 10th ISSLR conference and 2008 FRIENDS of Great Salt Lake Forum, May 11–16, 2008. University of Utah, Salt Lake City Natural Resources and Environmental Issues. http://digitalcommons.usu.edu/nrei/vol15/iss1/1
13. Costa MPF, Telmer KH (2006) Utilizing SAR imagery and aquatic vegetation to map fresh and brackish lakes in the Brazilian Pantanal wetland. Remote Sens Environ 10:204–213
14. Furquim SAC, Graham RC, Barbiéro L, Queiroz Neto J, Vidal-Torrado P (2010) Soil mineral genesis and distribution in a saline lake landscape of the Pantanal Wetland, Brazil. Geoderma 154:518–528
15. Almeida TIR (2011) Salinas e Baías do Pantanal: enigma biogeoquímico parcialmente resolvido. Ciência Hoje 47:20–25
16. Furian S, Martins ERC, Parizotto TM, Rezende-Filho AT, Victoria RL, Barbiero L (2013) Chemical diversity and spatial variability in myriad lakes in Nhecolândia in the Pantanal wetlands of Brazil. Limnol Oceanogr 58(6):2249–2261
17. Martins ERC (2012) Tipologia de lagoas Salinas no Pantanal da Nhecolândia (MS). Ph.D. thesis, University of São Paulo, Brazil, p 188
18. Barbiero L, Rezende Filho A, Furquim SAC, Furian AY, Sakamoto AY, Valles V, Graham RC, Fort M, Ferreira RPD, Queiroz Neto JP (2008) Soil morphological control on saline and freshwater lake hydrogeochemistry in the Pantanal of Nhecolândia, Brazil. Geoderma 148 (1):91–106
19. Almeida TIR, Sígolo JB, Fernandes E, Queiroz Neto JP, Barbiero L, Sakamoto AY (2003) Proposta de classificação e gênese das lagoas da baixa Nhecolândia-MS com base em sensoriamento remoto e dados de campo. Rev Bras Geociên 33(2):83–90
20. Timms BV (2005) Salt lakes in Australia: present problems and prognosis for the future. Hydrobiologia 552:1–15
21. Oliveira APG, Ribeiro AA, Wassouf ER Jr., Souza GF, Bernadi I, Penatti NC, Almeida T IR, Paranhos Filho AC (2011) Uso de Sensoriamento Remoto na quantificação das lagoas do

Pantanal da Nhecolândia, Mato Grosso do Sul. In: Simpósio Brasileiro de Sensoriamento Remoto (SBSR), Curitiba, vol 15. INPE, Anais. São José dos Campos, pp 3695–3702. DVD, Internet. ISBN 978-85-17-00056-0 (Internet), 978-85-17-00057-7 (DVD). http://urlib.net/3ERPFQRTRW/3A557NL

22. Bergier I (2013) Effects of highland land-use over lowlands of the Brazilian Pantanal. Sci Tot Environ 463(464):1060–1066
23. Guérin F, Abril G, Richard S, Burban B, Reynouard C, Seyler P, Delmas R (2006) Methane and carbon dioxide emissions from tropical reservoirs: significance of downstream rivers. Geophys Res Lett 33, L21407. doi:10.1029/2006GL027929
24. Rezende-Filho AT, Furian S, Victoria RL, Mascré C, Valles V, Barbiero L (2012) Hydrochemical variability at the Upper Paraguay Basin and Pantanal wetland. Hydrol Earth Syst Sci 16:2723–2737

Methane and Carbon Dioxide Dynamics in the Paraguay River Floodplain (Pantanal) in Episodic Anoxia Events

Ivan Bergier, Ana P.S. Silva, Hernandes Monteiro, Frédéric Guérin, Hudson A. Macedo, Aguinaldo Silva, Alex Krusche, Henrique O. Sawakuchi, and David Bastviken

Abstract Worldwide wetlands contribute to the global carbon cycle by emitting about a third of the global methane (CH_4) emissions. However, CH_4 and carbon dioxide (CO_2) dynamics remain poorly understood in the largest tropical wetland on Earth, the Pantanal. In this chapter, we aim to characterize the CH_4 and CO_2 biogeochemistry in the floodplain of the Paraguay River, near Corumbá, during the course of annual anoxia phenomena locally known as *dequada*. The strong anoxia is associated to the flooding of terrestrial habitats that enhances respiration, dissolved oxygen (DO) consumption, and methanogenesis. The extremely low DO also leads to high fish mortality in the region. CH_4 and CO_2 concentration in surface waters and diffusive water–air fluxes were measured in the oxbow Tuiuiú Lake and in the Paraguay River main stem in order to identify temporal and spatial patterns. The whole dataset shows that, for instance, dissolved CH_4 and diffusive CH_4 fluxes increased dramatically during the *dequada*. In the study area, CH_4 emissions can

I. Bergier (✉), A.P.S. Silva, and H. Monteiro
Laboratory of Biomass Conversion, Embrapa Pantanal, Corumbá, Brazil
e-mail: ivan.bergier@embrapa.br

F. Guérin
Géosciences Environnement Toulouse (GET), Observatoire Midi Pyrénées, Université de Toulouse, CNRS, IRD, 14 avenue E. Belin, 31400 Toulouse, France

H.A. Macedo
Department of Geosciences and Environment, Paulista State University, Rio Claro, Brazil

A. Silva
Department of Geography, Federal University of Mato Grosso do Sul, Corumbá, Brazil

A. Krusche and H.O. Sawakuchi
Center for Nuclear Energy in Agriculture, University of São Paulo, Piracicaba, Brazil

D. Bastviken
Department of Thematic Studies – Environmental Change, Linköping University, Linköping, Sweden

I. Bergier and M.L. Assine (eds.), *Dynamics of the Pantanal Wetland in South America*, Hdb Env Chem (2016) 37: 163–178, DOI 10.1007/698_2015_353,

reach 9–85 mg CH_4 m^{-2} h^{-1} during *dequada* climax. Riverine anoxic waters steadily penetrate the oxbow Tuiuiú Lake, indicating water inflow from the river main stem, whereas small reminiscent patches of oxbow waters not mixing with anoxic river waters may function as survival refuges to the aquatic wildlife. Clearly, the DO distribution during several *dequadas* in major rivers of the Pantanal highlights the importance of geomorphology on the biogeochemistry in the riverine floodplains of the Pantanal wetland.

Keywords Carbon cycle, Dequada, Fish mortality, Flood pulse, Wetland

Contents

1 Introduction

Methane (CH_4) emissions from global wetlands correspond to about a third of the annual global CH_4 sources, estimated in between 500 and 600 Tg CH_4 (1 Tg = 10^{12} g) [1]. Despite indications that more than a half of the global wetland CH_4 emissions originate from tropical wetlands [2], CH_4 cycling is still better known in northern wetlands [3]. Amazonia rivers and wetlands [4] and the Pantanal [5] may contribute to annual emissions of roughly 29.3 and 3.3 Tg CH_4, respectively. Together they represent about 5–7% of the global wetland CH_4 emissions. Nonetheless, those numbers might increase if ebullition is properly accounted for in the CH_4 budget [6, 7].

An interesting aspect of the CH_4 cycling in the Pantanal, particularly in the riverine floodplains, is the occurrence of severe anoxic events [8, 9]. Dissolved oxygen (DO) depletion due to organic matter degradation and CH_4 oxidation in the water column and sediments are most marked when river water invades the floodplains. This happens during the rising water of the annual flood pulse [10]. The extreme anoxia enduring over several weeks is responsible for fish mortality [9]. *Dequada* is the Brazilian name given for this phenomenon, and understanding its spatiotemporal variability and intensity is crucial for the careful management of

the Pantanal's floodplains. For instance, it has been argued that ecohydrological changes promoted by the ongoing land use of the Pantanal headwaters in uplands have made *dequada* events more frequent interannually [11]. More recently, research efforts were carried out to map the synoptic spatial and temporal distributions of the *dequada* in Pantanal's rivers and floodplains [12, 13].

The present chapter sheds new light on the spatiotemporal variability of CH_4 and CO_2 emissions, in addition to dissolved CH_4 and CO_2 in surface waters, on the course of two *dequada* events in the Paraguay River floodplain. Moreover, a complementary overview of the DO distribution during several *dequadas* in major rivers of the Pantanal highlights the crucial role of geomorphology on the biogeochemistry in the riverine floodplains of the Pantanal wetland.

2 Methodology

2.1 Study Area

Gaseous concentrations and flux changes during the *dequada* were monitored in the Paraguay River upstream of Corumbá City (red box in Fig. 1). The *dequada* occurs annually between March and May during the rising water phase of the flood pulse (see also [14]). The riverine system comprises the river main stem surrounded by floodplains (shown in dark colors in Fig. 1). The flood intensity depends largely upon rainfall, which usually exceed 1,000 mm during the austral rainy season from October to March [15]. Perennial marginal lakes are evident in the floodplain, whereas the long-term geomorphological changes in river sinuosity produce abandoned meanders or oxbow lakes that can be perennial or intermittent accordingly to their topography and the highly variable hydrology of the Pantanal [14, 16].

2.2 Measurements of Gas Fluxes at the Water–Air Interface and Dissolved Gases in Surface Waters

The fieldworks were carried out on the course of *dequada* events taking place in 2011 and 2014. The Paraguay River level gauge at Ladário City, in the Brazilian Navy Port, marked an annual maximum of 5.62 and 5.40 m in 2011 and 2014, respectively, which correspond to well-developed flood pulses in the historical records since 1900 [15].

2.2.1 Flux Measurements During the Dequada of 2011

In 2011 a set of four floating static chambers was used for estimating CH_4 and CO_2 diffusive fluxes across the water–air interface in the Paraguay River near the spatial

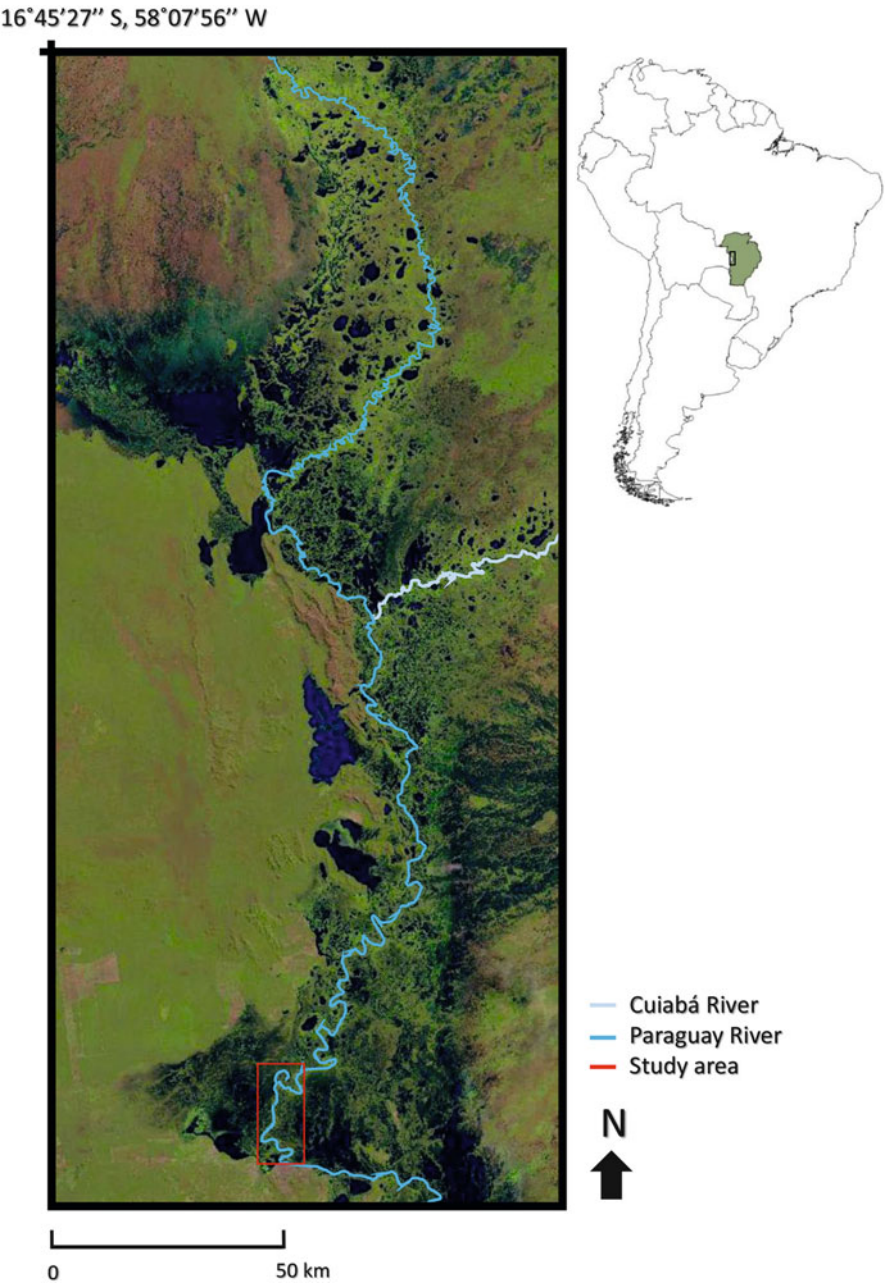

Fig. 1 Location of the study area in South America (Brazil-Bolivia frontier), detailed in the *red box*. R-G-B color composition of bands 5-4-3 of Landsat-8/OLI data obtained on 11 August 2014, orbit 227, dots 72 and 73

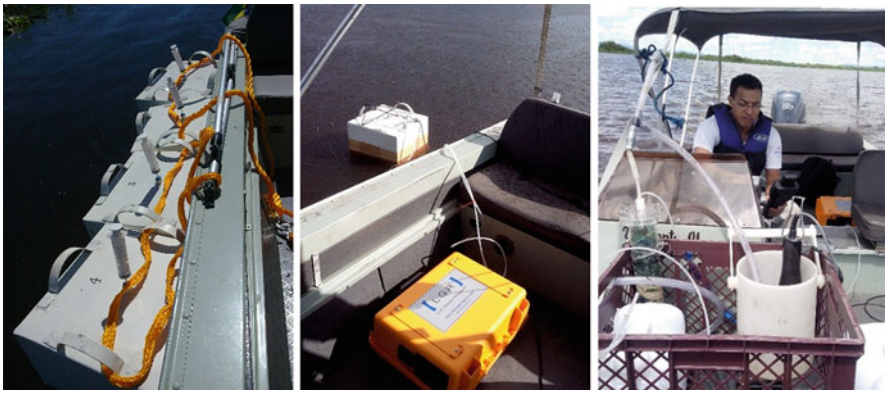

Fig. 2 Sampling technique of chamber gas fluxes with gas sampling for later GC–FID analysis (April–May 2011, picture on the *left*) and in situ measurements of chamber fluxes and gas partial pressure (equilibrator) with the UGGA-LGR (March–April, 2014, pictures in the *middle* and to the *right*)

coordinates 18°59′5.59″S and 57°39′15.28″W. Measurements were undertaken on six occasions between 7 April and 14 May in 2011. For each sampling date, four chambers were deployed twice, yielding eight estimated fluxes per sampling day (see Fig. 2, left picture).

Each chamber was constructed in dual galvanized 1-mm metal sheets. The outer dimensions (length, depth, and height) of the chamber are 40 × 40 × 40 cm, whereas internally its dimensions are 30 × 30 × 25 cm. The inner 5-cm space between the metal sheets was filled with expansible polyurethane for temperature insulation and chamber flotation. The outer chamber was adapted with handles and painted in white color to facilitate transport and minimize surface heating, respectively. The chamber penetrated below the water surface by about 10 cm and the enclosed air volume was 22.5 L. A black butyl rubber stopper with a needle port was adapted in a metal tube fixed in the central portion of the upper surface of the chamber for allowing inner pressure equilibration while sampling.

The chambers freely floated aside the free-moving boat in order to minimize the generation of artificial turbulence [17]. The chambers were sampled with 60-cc plastic syringes adapted with 3-way Luer lock valves for gas storage (Fig. 2). Gas samples were taken every 4 min for 12 min of deployment ($n = 4$). CH_4 and CO_2 concentrations in the syringe gas samples were determined in the same day by gas chromatography (SRI Inc. model 8610C) equipped with a methanizer, a 1-mL sampling loop, and a flame ionization detector. Concentrations were calibrated with external standards. Each gas sample was analyzed twice by splitting the syringe gas volume into two separate GC runs. Linear regressions of the mean measured gas concentrations with time were computed for estimating the slope of the gas flux, considered valid for $r^2 > 0.85$ (81% of the measured fluxes). Therefore, these measurements represent diffusive flux only. CH_4 and CO_2 flux data in mg m^{-2} h^{-1} was calculated accounting for the ideal gas law and chamber dimensions. Numbers reported represent averages and ranges of valid chamber measurements.

2.2.2 Flux and Dissolved Gas Partial Pressure Measurements During the Dequada of 2014

In 2014, the measurements were extended to the oxbow Tuiuiú Lake (18°48′33.01″S, 57°39′19.87″W). CH_4 and CO_2 fluxes at the water–air interface were determined in this lake and in the Paraguay River immediately upstream of Corumbá, whereas the partial pressures of CO_2 (pCO_2) and CH_4 (pCH_4) in surface waters were continuously measured in the Tuiuiú Lake and in the Paraguay River from Tuiuiú Lake to Corumbá (see box delimiting the study area in Fig. 1). Chamber gas fluxes and pCO_2 and pCH_4 in surface waters were determined with an ultra-portable gas analyzer (UGGA, Los Gatos Research Inc.) with a built-in air pump. Gas fluxes were estimated using a single chamber, the same as used in 2011, fitted to a closed-air loop between the chamber and the UGGA, which was programmed to store data at a rate of 5 or 10 s (see Fig. 2, middle picture).

A GPS logger on the boat and an equilibrator made in Plexiglas® filled with glass marbles [18] were used to produce Lagrangian data series of pCO_2 and pCH_4 in the water surface. A 12 V submersible bilge pump (water flow ~1.16 L s^{-1}) was fixed in the right side of the boat stern, away from the motor, with the water intake about 30 cm below the water surface. A tubing system was used to continuously feed the top of the equilibrator with water (see Fig. 2, left picture). A "T" connector tubing diverted excess water from the equilibrator (~0.3 L s^{-1}). A 3 V high performance, mini diaphragm air pump with an airflow rate at ~0.1 L s^{-1} was connected to the air inlet at the bottom side of the equilibrator. A long tiny tube connected to the upper side of the equilibrator (the gas headspace) allowed inner pressure equilibration with the atmosphere. The UGGA with moisture and water traps was connected in-line (open-air circuit) with the air leaving the equilibrator to measuring outgoing headspace concentration. Both air and water flows inside the equilibrator were kept constant while sampling with the boat moving at a maximum speed between 2 and 2.5 m s^{-1}.

The equilibrator was calibrated through a comparison between the results of the equilibrator and the traditional headspace extraction technique [19, 20]. The headspace extraction was made on August 2014 with a 1-L acrylic bottle filled with 500 mL of the surface water. The bottle was sealed with a silicone rubber stopper pierced with two independent tubing with 3-way Luer lock valves. The two tubing were differently sized inside the bottle: a short tube to deliver air to UGGA and a long, submerged tube to receive air from UGGA, bubbling into the water sample. Valves were locked and the bottle was vigorously shaken for about 4 min. After a few seconds, the valves were opened, and the two tubing were quickly connected to the UGGA air-closed system between the bottle headspace of 500 mL and the UGGA system. The CO_2 and CH_4 concentrations were calculated according to [21] and [22], respectively. From the obtained results, the correction factors were 20.5 for pCH_4 and 5.4 for pCO_2. After correction, the georeferenced partial pressure data were processed in the Spring GIS (www.dpi.inpe.br/spring/) for modeling layers of regular grid by the nearest neighborhood algorithm applied to each gas and sampling day.

3 Methane and Carbon Dioxide Emissions in the *Dequadas* of 2011 and 2014

The average and the range of the measured chamber fluxes in 2011 and 2014 are shown in Table 1. Table lines were stratified accordingly to the *dequada* timing: "onset," "climax," and "offset." A second stratification level concerns the site of measurement: river "main stem" or "oxbow" lake. Main stem CH_4 emissions in the *dequada* climax spanned two orders of magnitude compared to the other timing and site (see Table 1). The corrected pCH_4 measured in 2014 are higher during the *dequada* climax in the river main stem (Table 1).

The diffusive emission of CH_4 during the *dequada* climax ranged from 8.9 to 84.8 mg CH_4 m^{-2} h^{-1} (Table 1). Previous estimate of the average diffusive CH_4 flux in the Paraguay River, in Ladário, was 0.4 mg CH_4 m^{-2} h^{-1} (ranging from 0.08 to 0.80 mg CH_4 m^{-2} h^{-1}) [6], which correspond to periods out of *dequada* climax (see Fig. 3). Similar observations can be extended to CO_2 emissions and partial pressures, though the relative changes in flux magnitudes were less prominent (Table 1). CO_2 and CH_4 partial pressures and emissions increase by 1 to 2 orders of magnitude during the dequada. CO_2 and CH_4 are likely contributed from distant and local sediment sources but mainly from local and distant flooded terrestrial areas, which are usually flooded during normal or well developed flood pulses. Further studies are needed to discriminate the relative importance of these contributing sources.

An interesting nonlinear aspect of the CH_4 and CO_2 dynamics is unveiled when plotting chamber flux data in log–log scale (Fig. 3). During the onset and offset of the *dequada*, CH_4 fluxes are usually < 1 mg CH_4 m^{-2} h^{-1} and CO_2 fluxes range from ca. 100 to 1,000 mg CO_2 m^{-2} h^{-1}. Note an inverse relationship in onset/offset phases, suggesting the prevailing of methanotrophs, oxidizing CH_4 into CO_2. When CH_4 fluxes exceed a certain threshold of approximately 10 mg CH_4 m^{-2} h^{-1} already in the *dequada* climax, the relationship between CH_4 and CO_2 fluxes

Table 1 Chamber gas flux in the water–air interface and gas partial pressures in surface waters obtained during *dequadas* in April/May 2011 and March/April 2014

			Chamber flux				pCH_4	pCO_2
			mg CH_4 m^{-2} h^{-1}		mg CO_2 m^{-2} h^{-1}		µatm	µatm
Year	Timing	Site	Mean	Range	Mean	Range	Mean	Mean
2014	Onset	Main stem	0.23	0.1–0.18	493.37	379.04–632.37	422	27,610
2014	Onset	Oxbow	0.23	0.15–0.36	261.62	168.25–388.04	891	22,732
2011	Climax	Main stem	37.27	10.14–84.79	709.62	244.64–1,184.05	–	–
2014	Climax	Main stem	13.94	8.92–18.14	418.58	265.91–560.17	55,277	27,303
2014	Climax	Oxbow	2.02	0.03–10.03	503.55	184.44–1,072.19	6,311	22,519
2011	Offset	Main stem	0.38	0.3–0.47	141.82	70.27–214.91	–	–

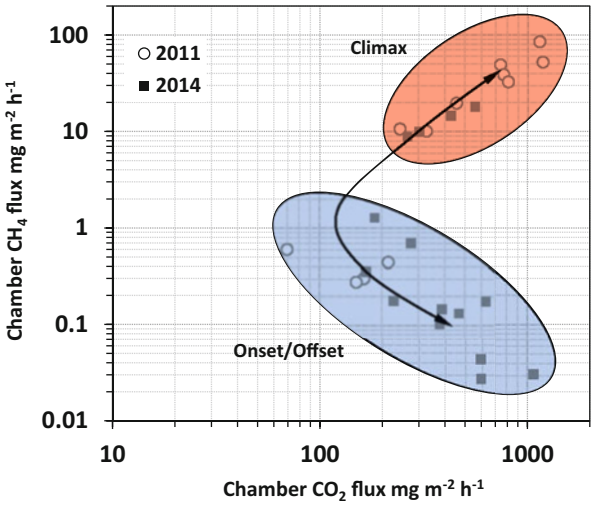

Fig. 3 Log–log plot (phase space) of chamber flux data obtained during the onset, offset, and climax of *dequada* events in 2011 and 2014

becomes positive. The contrasting relationships in Fig. 3 indicate different source–sink balances for CH_4 and CO_2 during the different phases of *dequada*. One possibility is that there is a shift in contributions of end products from oxic to anoxic metabolism during the onset/offset phases. Under normal and more oxic condition, much more CO_2 rather than CH_4 is produced from metabolic processes in water and surface sediments. When DO declines leading to anoxic metabolism, the increased sediment release of CH_4 (and other reduced metabolic products) will then contribute with more CH_4 relative to CO_2, causing a negative relationship between CH_4 and CO_2 emissions. When CH_4 concentrations in the water become large enough to sustain extensive CH_4 oxidation, which can be very efficient also at hypoxic DO levels, large amounts of CO_2 can be formed from methane oxidation possibly generating the observed positive relationship during the *dequada* climax. Other explanations may also be possible and more studies are needed to fully understand the observed pattern.

4 Large-Scale and Local Spatial Patterns of Dissolved Methane and Carbon Dioxide

In the Pantanal wetland, *dequada* distribution and intensity has been recently mapped [12, 13]. Based solely on DO, the Paraguay River usually shows the highest anoxia intensity (Fig. 4). In the Paraguay River, upstream of Cuiabá River confluence, a large floodplain area registers high *dequada* intensity (Fig. 4). During the *dequada*, DO in this area remains steady around 1 mg L^{-1} over three subsequent months, indicating that the measured influence of the *dequada* on CH_4 concentrations and fluxes can be a large-scale phenomenon for long time periods.

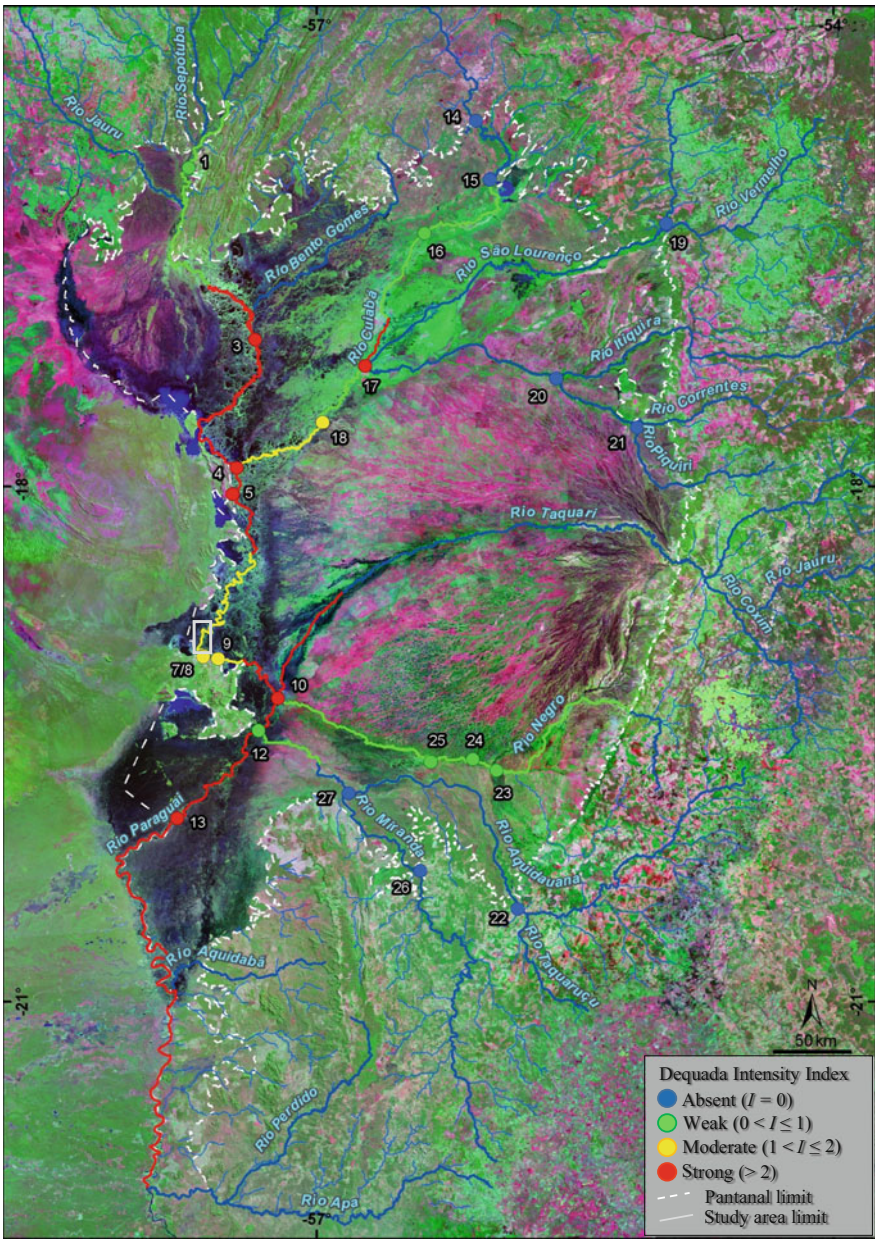

Fig. 4 Spatial distribution of the *dequada* intensity in the Pantanal wetland. The dequada intensity I is defined as $I = D/\overline{DO_d}$, where D is the duration time of the *dequada* in months and $\overline{DO_d}$ is the average of the DO during *dequada* for values lower than 3 mg L^{-1}. Numbers indicate the ANA (Brazilian National Water Agency) stations where DO data was gathered from 2003 to 2012. The study area is delimited by the *gray box*. Adapted from [12]

The anoxic phenomenon is far more intense in larger floodplains, where main stem–floodplain exchanges are maximized. Water exchanges between the main stem and the floodplain are common in the Pantanal. Nonetheless, exchanges eventually occur in main stem-to-floodplain direction only (river main stem exportation), without any evidence of return of the floodplain to main stem in the same site. This is the case for the Paraguay River nearby the study area (see Fig. 4), where the exported riverine water returns to the main stem several kilometers downstream, in the confluence with the Paraguay-Mirim River (indeed an abandoned main stem (paleochannel) of the Paraguay River), downstream of Corumbá [23]. The same is true for the Nabileque River in the southern Pantanal, which is also a paleochannel of the Paraguay River main stem [14, 16]. Recent Acoustic Doppler Current Profiler (ADCP) data gathered in Vermelha Lake suggest that the main stem exports huge amounts of waters to the floodplain, which also corroborate to this assumption; the Paraguay River exports approximately 1,000 $m^3\ L^{-1}$ of water to the floodplain in Vermelha Lake, recovering these waters downstream in the Paraguay-Mirim River confluence (H. Macedo, unpublished results). Moreover, the overflow of the Taquari megafan, particularly in the fringe of the Paiaguás subregion, may also steadily contribute to better-quality waters to the Paraguay River main stem (Fig. 4). Consequently, *dequada* in the study area might be lessened, and it is very likely that the magnitude of CH_4 and CO_2 emissions, despite its strength, can also be lower relative to other floodplain areas of the Paraguay River. These findings highlight the requirement of a larger spatial and temporal coverage of chamber water–air measurements for an accurate upscaling of the Pantanal wetland CH_4 emissions, particularly during the *dequada* events but also during the decrease of the water level to capture the fate of the CH_4 exported from floodplains.

4.1 Spatial and Temporal Changes in the Oxbow and River Main Stem in the Study Area

The spatial distribution of pCH_4 and pCO_2 during the onset and the climax of the *dequada* measured in 2014 is presented in Fig. 5. During the onset on 14 March 2014 the oxbow lake was more supersaturated in CH_4 (800–3,200 μatm) than the river main stem ($\leq$800 μatm). By April 2014, during the *dequada* climax, the incoming river main stem waters had a much higher pCH_4 (20,000 to 80,000 μatm). For pCO_2, temporal changes in the main stem are not evident, and the study area remains always oversaturated with respect to CO_2, which is not surprising as CO_2 concentrations depend on several heterotrophic bacterial processes (organic matter respiration and fermentation) as well as primary production.

It is notable that the main stem "low-quality" (i.e., low-DO) waters invade the floodplain and confine "better-quality" (higher DO and low pCH_4 and pCO_2) waters in the oxbow lake (see Fig. 5). These local waters, less affected by the *dequada*, probably function as fish survival refuges during the extreme anoxia and deserve careful attention for aquatic wildlife management and protection.

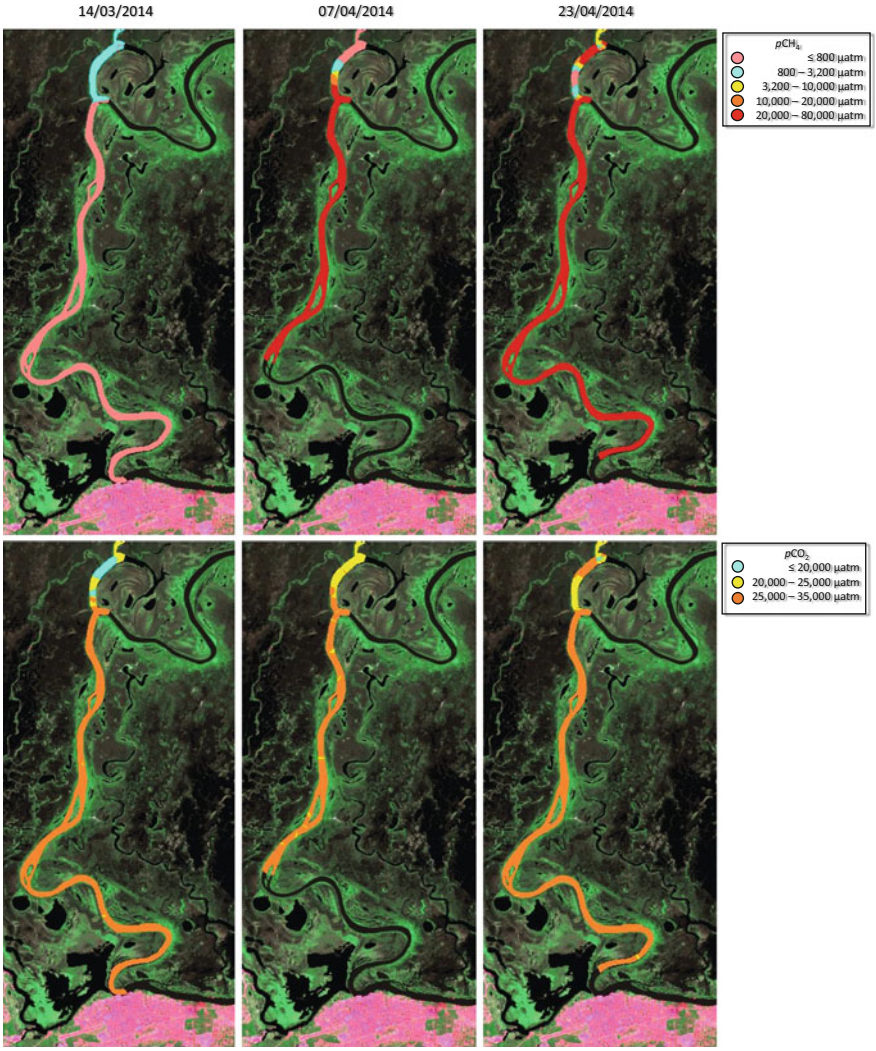

Fig. 5 Spatial and temporal changes of pCH_4 (*upper panels*) and pCO_2 (*lower panels*) during the *dequada* event measured in 2014. Corumbá City is shown below in *magenta*

4.2 Margin-to-Margin Variability in Dissolved Gases in Oxbow and River Main Stem

The gridded GIS data on gas partial pressures allowed a preliminary investigation on the transversal (margin-to-margin) gradient of surface pCH_4 and pCO_2 in the oxbow and the main stem of the Paraguay River. Figure 6 presents the five random transects in the oxbow lakes. On 14 March 2014, surface pCH_4 was usually around 1,000 µatm with no clear indication of transect gradient. In April 2014 some transversal gradient is developed; however, they do not display any clear pattern

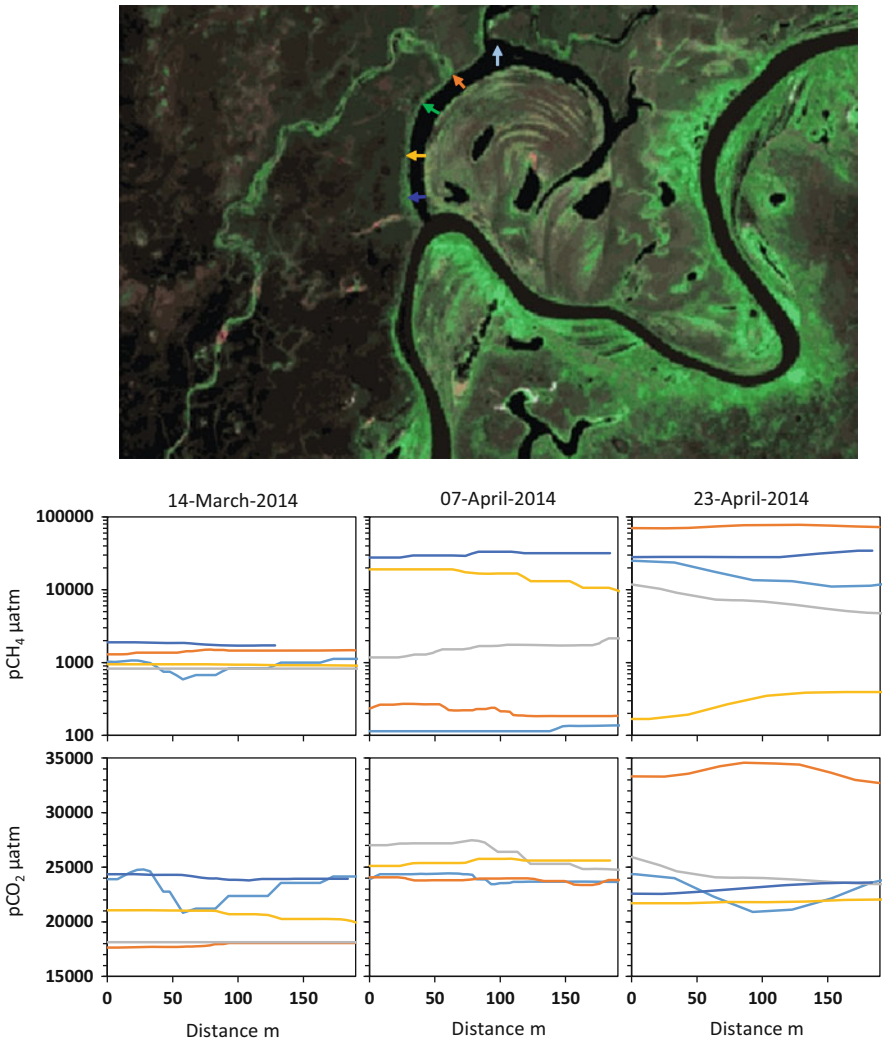

Fig. 6 Transversal profiles of methane and carbon dioxide partial pressures in the surface waters of the oxbow Tuiuiú Lake measured during the *dequada* event in 2014

that could suggest gases locally produced (e.g., hotspot areas). The same is valid for surface pCO_2 in the oxbow (Fig. 6). Instead, the transects corroborate the hypothesis that main stem dequada waters are gradually replacing "better-quality" oxbow waters in some regions of the oxbow.

Figure 7 shows the same approach as Fig. 6 for the main stem surface waters, downstream of the oxbow Tuiuiú Lake. Surface pCH_4 transects lack any evident gradient and similarly confirm the abrupt change of three orders of magnitude in the dissolved methane due to the *dequada* event. For surface pCO_2, the transects did not

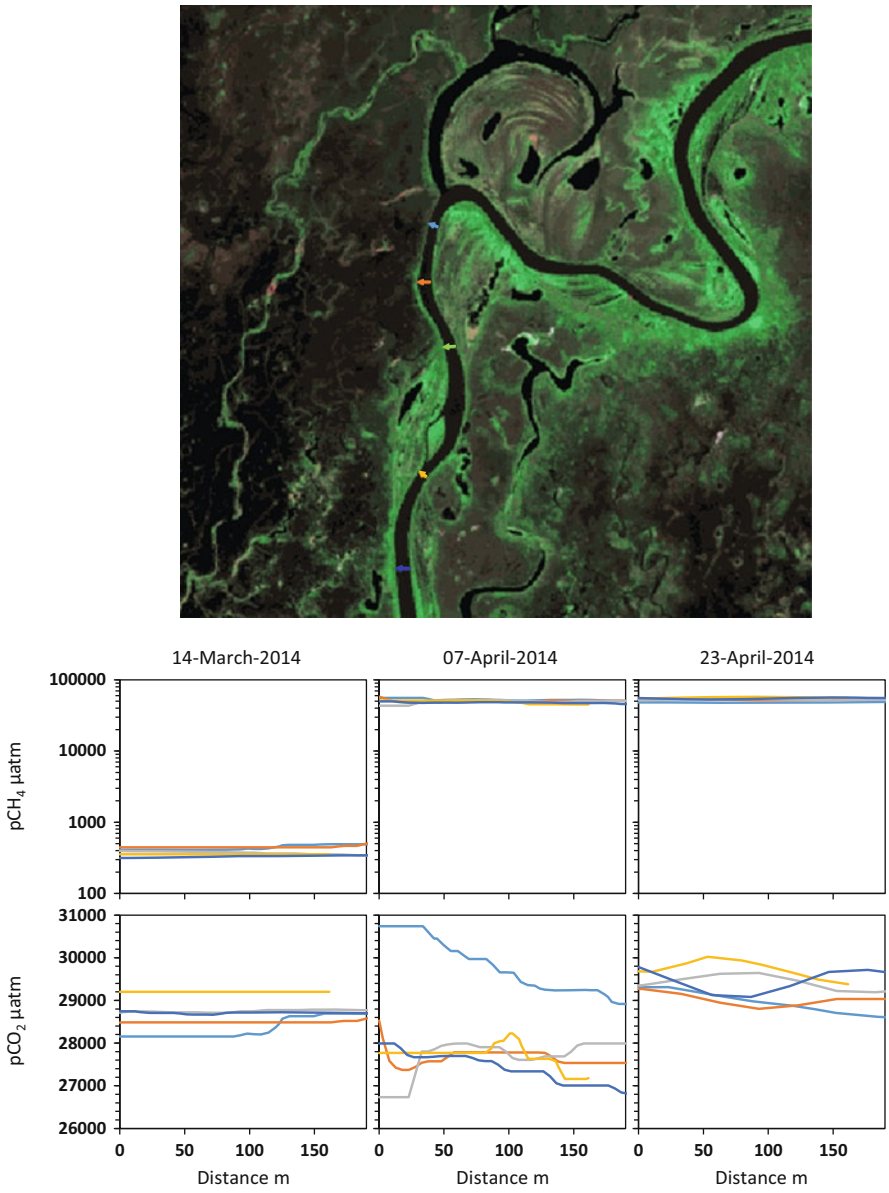

Fig. 7 Transversal profiles of methane (log scale) and carbon dioxide partial pressures in surface waters of the upper portion of the Paraguay River, downstream of the oxbow Tuiuiú Lake, measured during the *dequada* event in 2014

change much during the evolution of the *dequada*, remaining in between ca. 27,000 and 31,000 µatm. Some differences between the surface pCO_2 transects may be a response of local geomorphology, associated, for instance, to water current velocity and interplay with the surrounding abandoned meanders and plains.

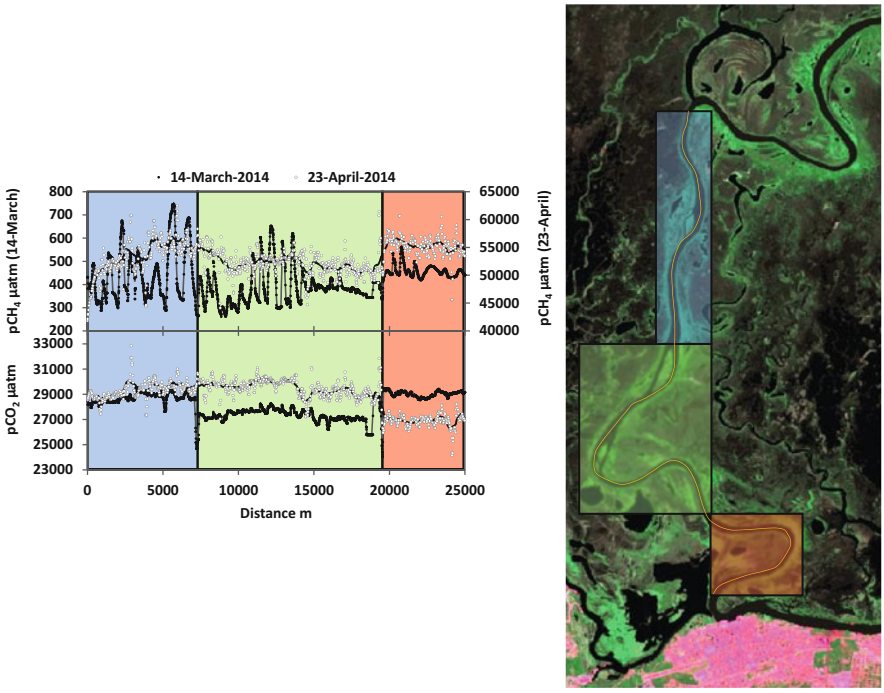

Fig. 8 Profiles of methane and carbon dioxide partial pressures in the surface waters of the Paraguay River (*orange line* in the Landsat-8 image). Trendlines for each time series were obtained by a moving average kernel with a window size of ca. 120 m

4.3 Longitudinal Riverine Variability in Dissolved Gases

To check the interplay between the main stem and the floodplain, a longitudinal river transect of the gridded pCH_4 and pCO_2 was produced and modeled in GIS (Fig. 8). From the oxbow Tuiuiú Lake to nearby Corumbá, it is possible to recognize at least three distinct patterns of main stem and floodplain exchanges. The results illustrate complex local patterns together with long reaches where the main stream river seems well mixed likely associated to exchanges with recently flooded areas nearby. This is important for understanding mid- to large-scale impacts of the *dequada* [12, 13] and will need further investigations to be clarified, including CH_4 and CO_2 measurements in the surroundings of the Paraguay River.

5 Concluding Remarks

The Pantanal is markedly dynamical with respect to the carbon turnover between the terrestrial and aquatic phases of the flood pulse. This chapter is an attempt to unveil some features of the intriguing flood-pulse event named *dequada*, in which

water quality deteriorates and spreads throughout the Paraguay River floodplain. The complex geomorphology of the area coins the prevailing biogeochemistry functioning that is usually heterotrophic but hyperheterotrophic during the climax of the *dequada*, resulting in massive methane emissions to the atmosphere. A broadened examination on the spatial and temporal variability in dissolved gases (e.g., CH_4, CO_2, O_2) during the *dequada* climax is vital for portraying a better picture on the Pantanal contributions to the global methane budget and to identify and define survival refuges for the aquatic wildlife which could be suitable areas for priority conservation.

Acknowledgments This work was partially funded by FAPESP grant numbers 2008/58089-9 and 2014/06889-2, FUNDECT grant number 23/200.628/2012, and CNPq grant numbers 562441/2010-7, 447402/2014-5 and 312386/2014-1.

References

1. Dlugokencky EJ, Nisbet EG, Fisher R, Lowry D (2011) Global atmospheric methane: budget, changes and dangers. Philos Trans A Math Phys Eng Sci 369:2058–2072
2. Melton JR, Wania R, Hodson EL, Poulter B, Ringeval B, Spahni R, Bohn T, Avis CA, Beerling DJ, Chen G, Eliseev AV, Denisov SN, Hopcroft PO, Lettenmaier DP, Riley WJ, Singarayer JS, Subin ZM, Tian H, Zürcher S, Brovkin V, van Bodegom PM, Kleinen T, Yu ZC, Kaplan JO (2013) Present state of global wetland extent and wetland methane modelling: conclusions from a model inter-comparison project (WETCHIMP). Biogeosciences 10:753–788
3. Bridgham SD, Cadillo-Quiroz H, Keller JK, Zhuang Q (2013) Methane emissions from wetlands: biogeochemical, microbial, and modeling perspectives from local to global scales. Glob Chang Biol 19:1325–1346
4. Melack J, Hess L, Gastil M, Forsberg B, Hamilton S, Lima I, Novo E (2004) Regionalization of methane emissions in the Amazon Basin with microwave remote sensing. Glob Chang Biol 10:530–544
5. Marani L, Alvalá PC (2007) Methane emissions from lakes and floodplains in Pantanal. Brazil Atmos Environ 41:1627–1633
6. Bastviken D, Santoro AL, Marotta H, Pinho LQ, Calheiros DF, Crill P, Enrich-Prast A (2010) Methane emissions from Pantanal, South America, during the low water season: toward more comprehensive sampling. Environ Sci Technol 44:5450–5455
7. Sawakuchi HO, Bastviken D, Sawakuchi AO, Krusche AV, Ballester MVR, Richey JE (2014) Methane emissions from Amazonian rivers and their contribution to the global methane budget. Glob Chang Biol 20:2829–2840
8. Hamilton SK, Sippel SJ, Melack JM (1995) Oxygen depletion and carbon dioxide and methane production in waters of the Pantanal wetland of Brazil. Biogeochemistry 30:115–141
9. Hamilton SK, Sippel SJ, Calheiros DF, Melack JM (1997) An anoxic event and other biogeochemical effects of the Pantanal wetland on the Paraguay river. Limnol Oceanogr 42:257–272
10. Junk JW, Bayley PB, Sparks RE (1989) The flood pulse concept in river floodplain systems. Can Spec Publ Fish Aquat Sci 106:110–127
11. Bergier I (2013) Effects of highland land-use over lowlands of the Brazilian Pantanal. Sci Total Environ 463–464:1060–1066
12. Macedo HA, Stevaux JC, Silva A, Merino ER, Pupim FN, Bergier I (2014) Distribuição e classificação da intensidade do fenômeno de dequada no Pantanal. In: Silva JV (ed) Geopantanal 2014. INPE/Embrapa, Campo Grande

13. Oliveira MD, Calheiros DF, Padovani CR (2013) Mapeamento e Descrição das Áreas de Ocorrência dos Eventos de Decoada no Pantanal. In: Pantanal E (ed). Embrapa, Corumbá, p 21
14. Assine ML, Macedo HA, Stevaux JC, Bergier I, Padovani C, Silva A (2015) Avulsive rivers in the hydrology of the Pantanal wetland. Hdb Env Chem. doi:10.1007/698_2015_351
15. Bergier I, Resende EK (2010) Dinâmica de cheias no Pantanal do rio Paraguai de 1900 a 2009. In: Silva JVd (ed) Geopantanal. INPE/Embrapa, Cáceres, MT, Brazil, pp 35–43
16. Assine ML, Merino ER, Pupim FN, Warren LV, Guerreiro R, McGlue MM (2015) Geology and geomorphology of the Pantanal basin. Hdb Env Chem. doi:10.1007/698_2015_349
17. Guérin F, Abril G, Serça D, Delon C, Richard S, Delmas R, Tremblay A, Varfalvy L (2007) Gas transfer velocities of CO_2 and CH_4 in a tropical reservoir and its river downstream. J Mar Syst 66:161–172
18. Frankignoulle M, Borges A, Biondo R (2001) A new design of equilibrator to monitor carbon dioxide in highly dynamic and turbid environments. Water Res 35:1344–1347
19. Bastviken D, Cole JJ, Pace ML, Van de Bogert MC (2008) Fates of methane from different lake habitats: connecting whole-lake budgets and CH_4 emissions. J Geophys Res Biogeosci 113, G02024
20. Guérin F, Abril G (2007) Significance of pelagic aerobic methane oxidation in the methane and carbon budget of a tropical reservoir. J Geophys Res Biogeosci 112, G03006
21. Weiss RF (1974) Carbon dioxide in water and seawater: the solubility of a non-ideal gas. Mar Chem 2:203–215
22. Yamamoto S, Alcauskas JB, Crozier TE (1976) Solubility of methane in distilled water and seawater. J Chem Eng Data 21:78–80
23. Macedo HA, Assine ML, Silva A, Pupim FN, Merino ER, Stevaux JC (2014) Mudanças paleo-hidrológicas na planície do rio Paraguai, Quaternário do Pantanal. Revista Brasileira de Geomorfologia 15:75–85

Pesticides in the Pantanal

Eliana Freire Gaspar de Carvalho Dores

Abstract This chapter presents a brief discussion on the potential for contamination of the Pantanal by pesticides and reviews the studies, which evaluated these substances in different matrices in the Pantanal and its surroundings. Agricultural activities occur mainly in the highlands around the floodplain and represent the main source of pesticides to the Pantanal. It is evident that they can be transported to the lowlands, but the pesticides were detected in low frequency and concentrations so far. There is no monitoring program, and a few studies regarding this contamination are limited in sampling frequency and spatial distribution as well as in analyzed substances that considered the large spectrum of pesticides used. Moreover, only water and sediment have been subject to analysis, and no biological indicators have been studied. Also, to the moment, no risk analysis has been carried out indicating the need for more studies in the region in order to prevent future damages to this important ecosystem.

Keywords Agriculture, Herbicides, Insecticides and fungicides, Land use

Contents

E.F.G. de Carvalho Dores (✉)
Federal University of Mato Grosso, Cuiabá, MT, Brazil
e-mail: elidores@uol.com.br

I. Bergier and M.L. Assine (eds.), *Dynamics of the Pantanal Wetland in South America*, Hdb Env Chem (2016) 37: 179–190, DOI 10.1007/698_2015_356,

1 Agriculture and Cattle Breeding in the Pantanal and Its Surroundings

The Pantanal is a unique area influenced by activities developed in the high areas surrounding it, particularly those carried out in areas drained by many rivers that feed this ecosystem. It comprises, in Brazil, two states – Mato Grosso and Mato Grosso do Sul – whose economic base is agriculture and cattle breeding.

Presently, Mato Grosso shows a large expansion in the area under cultivation for soya bean, cotton, maize, bean, and sugarcane in the highlands surrounding the Pantanal, mainly in the drainage basins of Casca, Manso, Sepotuba, Paraguay, Vermelho, and São Lourenço rivers. In Mato Grosso do Sul, this growth is also observed in the highlands surrounding the Pantanal, mainly in the drainage area of Alto Taquari, Miranda, Aquidauana, and Negro rivers, except for cotton that is not grown in this region and for sugarcane, whose increase forecast is more significant than in Mato Grosso [1]. A land use map in the Upper Paraguay basin is shown in [2] of this book. The decree n. 6,961 from the Brazilian Presidency published in 17 September 2009 approved the agroecological zoning for sugarcane in Brazil, and this activity was forbidden in the Pantanal and the High Paraguay river basin [3].

Productivity in these cultures has increased greatly due to the use of modern technologies. In general, these cultures are grown in extensive areas (monoculture systems) demanding mechanization and intensive inputs of agrochemicals, particularly, pesticides and fertilizers.

According to the Brazilian National Sanitary Vigilance Agency (ANVISA) [4], between 2000 and 2010, the pesticides Brazilian market increased 190%, a growth rhythm much higher than the registered in the world market (93%). In the crop period 2010/2011, pesticides consumption in Brazil reached the mark of 936,000 tons.

Pesticides (herbicides, insecticides, and fungicides) constitute a large spectrum of chemical compounds with different chemical structures which present variable behavior in the environment and consist on one of the main technologies used to control insects, fungus, plant diseases, and invasive weeds in the plantations and grasslands aiming to guarantee high productivity. Due to the extremely variable chemical properties of these molecules, the estimation of their dynamics in the environment is difficult, and no generalization is possible.

After application in the plantations, the major destination of pesticides is the soil, where it can undergo several processes which can lead to off-site transportation reaching nontarget areas particularly the water courses.

The mobilization of large amounts of sediment as a consequence of deforestation, soil tilling, and animal trampling to lower lands can make available to the aquatic environment elements or substances present in the sediment such as the pesticides.

The headwaters of the rivers in the Upper Paraguay basin are localized in the highlands, where monocultures of agriculture or pasture are developed in large

scale. Transported sediments can eventually be contaminated by pesticides and settle down in the Pantanal lowlands, where water velocity is reduced due to the low declivity of the terrain [5]. Frequently, good agricultural practices are not observed, increasing soil erosion and sediment transportation to rivers.

In the lowlands, the main economic activity in large scale is extensive cattle breeding. The hydrological regime and low natural soil fertility were responsible for the establishment of the low-impacting extensive cattle breeding in the Pantanal floodplain. In 2010, among the municipalities in the Pantanal lowlands, cattle breeding was developed in 84% of the farms; only 10% were used for agriculture and 6% for both [6]. However, changes in the last years with implantation of soya plantation in the Pantanal borders (see also [7]) have increased the concern of potential impacts of pesticide contamination. Although incipient, the soya production has shown good profitability that has stimulated the farmers in the region to invest in this culture [8].

2 Transportation of Pesticides to the Pantanal

After having contact with the soil, several physical, chemical, and biological processes determine the behavior of pesticides. According to Spadotto et al. [9], pesticide dynamics in soil is driven by process of retention, transformation, transport, and by the interaction of these processes.

These processes depend largely upon the physical-chemical properties of the molecules, physical characteristics of the environment (relief, soil type, and climate) as well as the management practices of the cultures.

The transport of pesticides can occur in several ways, including migration in water (suspended or dissolved), in soil particles (sorbed), or in vapor state [10]. Among the transportation processes between the environmental compartments, the movement from soil to water via runoff and/or leaching is the most important.

Runoff is the movement of pesticides along the soil surface by rain or irrigation water to river, lakes, or areas of lower elevation. Runoff constitutes the main route of surface water contamination either associated to suspended particles or dissolved in water [11].

Runoff is highly dependent on pesticide use system, pesticide chemical properties, climate, and topography associated to soil physical and chemical properties. Dabrowski et al. [12], studying the application of modeling to estimate runoff, emphasize that the most important catchment variables determining runoff seem to be buffer strip width, presence of erosion rills, and slope.

One of the properties that greatly influence pesticide runoff is the retention in soil, which is generally denominated sorption, and depends mainly on the organic matter content and texture of surface soil, as well as on the molecular structure of the pesticide. The greater the sorption, the higher the potential for runoff associated to suspended material [13].

The adoption of conservation practices in soil preparation such as no-tilling and direct sowing can be good alternatives for the central region of Brazil that in addition to the positive impacts on soil fertility can reduce runoff. Among the facts that contribute to the sustainability of these practices is the maintenance of vegetable residues on the soil associated to little utilization of agriculture machinery implicating in high efficiency in hydric erosion reduction and, consequently, less soil, nutrient, and pesticide loss by runoff [14, 15].

The knowledge about pesticides transport processes in the environment is essential to orientate the elaboration of management plans. The variety of pesticides used from many different chemical classes makes the interaction forms of these compounds with different environmental components also extremely variable.

Leaching through the soil tends to result in groundwater contamination, and in this case, the chemical substances are transported in solution together with percolating water. Contaminated groundwater in the Pantanal may represent a risk to surface water since water table is very shallow in the lowlands.

In a literature review, Carter [16] reported that for herbicides, losses of up to 0.25% of applied quantity by runoff and 5% by leaching have been reported. In Center-Western Brazil, Dores et al. [17] determined herbicide loss of 3% and 1% by runoff adsorbed to soil particles and dissolve in water, respectively. On the other hand, Matallo et al. [18], based on experimental data, reported that 52% of applied amount of a herbicide used in sugarcane in Southern Brazil leached through the first 50 cm of a sandy soil during a year-end. Using a mathematical model, these authors estimate that 96% can leach below 12 cm (depth where there is a desired weed control) in 67 days.

A pesticide property that is very important to the potential impacts in the environment is the persistence. Laabs et al. [19] concluded that a medium-term accumulation in the sediment of tropical ecosystems can be expected for chlorpyrifos and endosulfan isomers (11–35% of applied amount still extractable at 50 days after application).

The evaluation of pesticide dissipation in two different Brazilian soils (Ustox and Psamments) demonstrated that persistence was mostly greater in the clayey than in the sandy soils. In comparison with temperate regions, dissipation of pesticides was 5 to 10 times faster, except for alachlor, deltamethrin, and λ-cyhalothrin, which exhibited a less reduced persistence than under temperate conditions [20].

Another route of off-site pesticides transportation that may be more important in tropical regions is the movement in the atmosphere. Volatilization of pesticides may be enhanced due to the high temperatures, and studies that analyzed pesticides in rainwater in Mato Grosso detected significant pesticide concentrations near the agricultural areas [21].

In rainwater samples collected in the highlands around the Pantanal, substantial insecticide (endosulfan, profenofos, monocrotophos) and herbicide (metolachlor, alachlor, trifluralin) concentrations were found by Laabs et al. [22], showing a high deposition rate in this region. In the lowlands, at about 75 km distance from the next application areas, maximum pesticide concentrations in rainwater were about

fivefold, and deposition was about tenfold lower than in the highlands surrounding them. Despite the lower deposition in the lowlands, this study showed that transportation by the atmosphere may be an important route of pollution of areas distant from application sites.

3 Organochlorine Pesticides in the Pantanal

Organochlorine pesticides, forbidden in Europe and United Sates in the seventieth decade and in agriculture in Brazil since 1985, due to their high environmental persistence and bioaccumulation potential, can still be found in several environmental compartments in Brazil [23–29].

These pesticides belong to the dirty dozen substances (to which endosulfan has been recently added) included in the Stockholm Convention, ratified by 178 countries and the European Union, where a joint effort to elimination/reduction of the use of these substances is proposed [30].

The Latin America Regional Report on POPs monitoring reported that scarce information regarding POPs in the environment in this region is available [31]. Although there is no continuous monitoring program of these pesticides in Brazil, particularly in the Pantanal, punctual studies have detected organochlorine in water and sediments in the floodplain and in rivers whose riverheads are located in highlands and that go downward to the plains.

Although the use of organochlorine pesticides in agriculture was forbidden in Brazil since 1985, DDT was used in health campaigns for vector control up to 1997 [32]. Only endosulfan had its use allowed in agriculture up to July 2013 since its persistence was much lower than the other organochlorines. In 2011, the National Sanitary Vigilance Agency, following the inclusion of endosulfan in the Stockholm convention, determined its total ban in agriculture up to July 2013.

In a study carried out by Laabs et al. [22], five organochlorine pesticides and two metabolites were analyzed in water and sediment samples collected in tributaries of the São Lourenço River (e.g., the Tenente Amaral) and the São Lourenço River itself in the highlands and in the Cuiabá River, the mouth of the Mutum River at the Sia Mariana lake, and the Sia Mariana lake itself in the floodplain. The sampling period began on 10 November 1999 and ended on 2 March 2000. The authors did not find detectable concentrations of formerly used organochlorine pesticides (lindane, p,p′-DDT, quintozene) in water samples but detected p,p′-DDT and p,p′-DDE at low concentrations in sediments either in the sampling points in the highlands and in the lowlands with concentrations slightly higher in the lowlands showing potential for accumulation. Regarding endosulfan, its isomers were detected in stream water and in river waters in the highlands near application areas in less than 14% of analyzed samples while the metabolite endosulfan sulfate was detected in 50% of river water samples in the highlands and in 10.5% in the lowlands. In sediments, β-endosulfan and endosulfan sulfate were detected only in the highlands.

Troli [33] analyzed 16 organochlorine (ten pesticides and six metabolites) in 66 water and 64 riverbed sediment samples collected in 2002/2003 in points divided in what the author called of three routes. Route 1 comprised points in the rivers Aquidauana, Miranda, and Negro collected in the dry season (September 2002); route 2 comprised points in Cuiabá, São Lourenço, Piquirí, Paraguay-Mirim, Branco, Abobral, Miranda, Negro, and Apa rivers, all of which are affluents of Paraguay river, in the beginning of the rainy season (December 2002); and route 3 whose sampling points were localized in Taquari River Basin (São Lourenço, Vermelho, Taquari, Coxim, Itiquira, Piquirí, Correntes rivers, and Gaucho creek) in the rainy season (January 2003). In water samples, the author detected only heptachlor epoxide (a metabolite of heptachlor) in five samples in concentrations ranging from 0.15 to 0.62 μg L^{-1} and the DDE isomers (o,p′- and p,p′-DDE) in concentrations varying from 0.78 to 14.65 μg L^{-1}. No pesticides were detected in the points in route 1 that comprises sites located in the Pantanal, far away from agricultural areas. The DDE isomers were detected in the points situated along route 2 and heptachlor hepoxide in route 3. Both DDE and heptachlor epoxide are metabolites which present high persistency in the environment. In sediments, the only detected pesticide was lindane ranging from 20.00 to 71.11 μg kg^{-1} in three points located along routes 2 and 3. Sediments were collected using core samplers and were subsampled at three depths. In two of the sampling points, lindane was detected in the three subsamples while in one sampling point was detected in only one subsample. The detected concentrations may represent risks to the biota according to Brazilian legislation; however, as the detection was eventual and the study was carried out in a short time period, more studies are necessary to analyze the real risk to the Pantanal ecosystem.

Miranda et al. [34] detected p,p′-DDT (3.6 μg kg^{-1}) in only one riverbed sediment sample collected in the Miranda river, in a study where sampling was performed in 17 rivers from the highlands/lowlands transition area from November to March 2004. The authors determined aldrin, dieldrin, endrin, endosulfan isomers, endosulfan sulfate, methoxychlor, p,p′-DDE, and p,p′-DDT.

Calheiros and Dores [35] analyzed riverbed sediment samples collected in the main tributaries of Miranda and Aquidauana rivers in 21 sampling points throughout the watershed distributed in the highlands and in the floodplain. Dieldrin which is a pesticide and also a metabolite of aldrin was detected in all sediment samples collected in May 2005 in concentrations ranging from 9.5 to 10.8 mg kg^{-1} and in 88% of the samples collected in December 2005 from 9.3 to 15.4 mg kg^{-1}. The insecticide p,p′-DDT was detected in only one sample in the Miranda river and one sample in an irrigation channel in May 2005 which is a period shortly after the rainy season when water level is reducing. This insecticide was detected near irrigated cultures of rice, sorghum, and bean at 1.0 mg kg^{-1} and in the irrigation channel at 20.3 mg kg^{-1}. On the other hand, its main metabolite p,p′-DDE was detected in all sediment samples from 1.2 to 14.4 mg kg^{-1}. Since the use of DDT is no longer authorized in Brazil since 1997, the concentration ratio DDE/DDT is an indicator of the contamination period, where a high ratio indicates past contamination, while when the contamination is recent, this ratio is low. Since in most samples where

DDE was detected DDT was not, this contamination is likely related to past use except for the point located in the irrigation channel whose DDT concentration was particularly high. Coincidently, the irrigated crops are developed in the medium Miranda river where there are high densities of fish eggs and larvae [36], which are particularly sensitive to contaminants [37].

The most recent study reporting organochlorine in this region analyzed water samples collected in three rivers from the Alto Paraguay river basin, Cuiabá, Perigara/São Lourenço, and Piquirí rivers. A total of 188 samples were collected in the dry season in June and July 2012. Samples were collected while traveling downstream on the rivers. A total of 24 sampling points were located along Cuiabá river, 18 along Perigara/São Lourenço rivers, and 21 along Piquirí river. Each river was sampled three times from 17 to 20 June 2012, 11 to 13 July 2012, and 17 to 18 July 2012. There were only ten contaminated samples all of which were from the second sample set and from the downstream portion of the Rio Cuiaba. Endosulfan sulfate – the most important metabolite of endosulfan which is the only organochlorine pesticide whose use was authorized in agriculture in Brazil until July 2013 – was detected in only one sample, while the p,p′-DDT metabolites (p,p′-DDD and m,p′-DDD) were detected in nine samples in concentrations ranging from 0.7 to 3 μg L^{-1} [38]. The author [38] attributed the overall low incidence of pesticide pollution to the period of sample collection (dry season with consequent low runoff) and the prohibition of organochlorine pesticides usage in agriculture since 1985 (except for endosulfan at the time of this study). Endosulfan sulfate and DDD are very stable compounds, so it is unknown whether their occurrence in the water samples from the second collection was due to recent application or runoff processes. Endosulfan sulfate has been shown to bioconcentrate and possess high toxicity [39]. As nonpoint source pollution, pesticide contamination is difficult to trace. This author also emphasizes the urge that Brazilian policymakers look to sad examples such as the problems with Everglades in Florida, USA, where farmland expansion and increased development of the wetland caused severe impacts among them contamination by pesticides.

4 Currently Used Pesticides (CUP) in the Pantanal

In contrast to organochlorine pesticides, currently used pesticides (CUP) are much less persistent in the environment, but due to their intensive use in the surrounding areas of the Pantanal, they may also pose a risk to this environment. As endosulfan is an organochlorine pesticide that was currently and intensively used up to July 2013, it was also included in this discussion.

As well as the organochlorine, CUP has not been monitored frequently, and a few studies [22, 33–35, 38, 40] have analyzed these pesticides in the Pantanal, most of them carried out by researchers at the Brazilian universities. Those studies indicate that there is a potential for pesticide transport from the highlands to the lowlands mostly associated to suspended matter in waters.

Laabs et al. [22] showed in a pilot monitoring study evidence of occurrence of several pesticides of different chemical classes (29 pesticides and 3 metabolites) in the northeastern Pantanal basin. From the investigated substances, 22 were detected at least once, leading to an overall pesticide detection frequency of 68% in surface water samples ($n = 139$), 87% in rainwater samples ($n = 91$), and 62% in sediment samples ($n = 26$). Pesticides were detected in stream and river waters in concentrations below 0.1 μg L^{-1} and in sediments below 10 μg kg^{-1}.

Pesticides with higher detection frequency and/or persistence in that study region were triazines (atrazine, simazine, ametryn), acetanilides (alachlor, metolachlor), trifluralin, and endosulfan compounds (especially β-endosulfan and endosulfan sulfate). Some organophosphorus pesticides (e.g., monocrotophos, profenofos, triazophos) showed higher peak concentrations in environmental samples but were rarely detected outside the application regions, presumably due to their low persistence. In the lowlands, the pesticides alachlor, endosulfan sulfate, malathion, metolachlor, simazine, and trifluralin were detected in more than 10% of the water samples. In sediments collected in the Pantanal area, only the formerly used organochlorine pesticides p,p′-DDT and p,p′-DDE were detected in 25% of the samples. Higher percentage of detection was found in the rivers in the highlands near the agricultural areas.

However, those authors detected in highlands rain water substantial insecticide (endosulfan, profenofos, monocrotophos) and herbicide (metolachlor, alachlor, trifluralin) concentrations, leading to a high deposition rate in this region. Conversely, in the lowlands, at about 75 km distance from the next application areas, maximum pesticide concentrations in rainwater were about fivefold, and deposition was about tenfold lower than in the highlands surrounding them.

Miranda et al. [34] analyzed riverbed sediments of 17 rivers that drain to the Pantanal, in the beginning of the floodplain, in November 2004. They identified three currently used active ingredients (pyrethroids) at the following concentrations: λ-cyhalothrin (1.0–5.0 μg kg^{-1}), deltamethrin (20.0 μg kg^{-1}), and permethrin (1.0–7.0 μg kg^{-1}).

Another study carried out in the Cuiabá watershed analyzed pesticides in sediments collected monthly in 15 sampling points located along the Cuiabá and São Lourenço rivers from the highland areas to the Pantanal floodplain, from August 2010 to July 2011. From a total of 216 samples, only ten presented detectable concentrations of at least one pesticide. The pesticides chlorpyrifos, endosulfan (α- and sulfate), λ-cyhalothrin, malathion, metolachlor, and permethrin were detected at concentrations ranging from 5.7 to 79.3 μg kg^{-1}. Although detected at low frequency, samples collected in the Pantanal floodplain presented residues of metolachlor, λ-cyhalothrin, endosulfan sulfate, and malathion indicating that there is a potential for transportation of pesticides used in agriculture carried out in the high areas reaching the lowlands [40].

Pyrethroid insecticides have been detected in riverbed sediments in several countries [41–44] with emphasis to cypermethrin, deltamethrin, bifenthrin, λ-cyhalothrin, and permethrin. The last two pyrethroids were detected in the abovementioned studies carried out in the Pantanal [34, 35]. This is probably due

to the intensive use of insecticides of this chemical class in several crops associated to their high soil sorption coefficient (Koc from 100,000 to 1,000,000 mL g^{-1}) that contribute to their transport associated to particulate carried in runoff.

Other pesticides frequently detected in sediment by several authors in different regions around the world are endosulfan (alpha and beta isomers and their main metabolite endosulfan sulfate) and chlorpyrifos [26, 43, 45, 46]. As the pyrethroids, these pesticides present high soil sorption coefficients, low water solubility, and moderate persistency.

A dissipation study developed by Laabs et al. [19] in the Pantanal using mesocosms pointed out that β-endosulfan followed by metolachlor, atrazine, simazine, and chlorpyrifos were the most persistent ones among the nine studied pesticides and tended to accumulate in the sediment. This observation explains the detection of some of these pesticides in the studies described above.

5 Potential Risks to the Pantanal from Pesticides Pollution

Most studies regarding pesticide transport to the Pantanal have been carried out using periodic sampling plans, usually monthly or less frequently. This sampling strategy is not the most appropriate for risk evaluation since the entry of pesticides in the aquatic environment is not continuous but episodic, mainly associated to intensive precipitation events that cause runoff. In this way, peak concentrations of pesticides are missed due to rapid dissipation dynamics of pesticides in the aquatic environment, either as a consequence of dilution, degradation, absorption by living organisms, or sorption to particulate. Also, no studies determined pesticide concentration in aquatic organisms.

Moreover, there is no study regarding acute impact of peak concentrations to aquatic organisms in water in this ecosystem, making it very difficult to evaluate the actual risks to the Pantanal environment.

Nevertheless, the studies published so far indicate that pesticides can be transported to the Pantanal, and so, mitigating measures should be stimulated in order to prevent significant impacts to occur.

Examples of possible mitigating measures are the use of less persistent and toxic pesticides, reduction of chemical pesticide usage in the highlands, use of soil conservation measures with particular attention to erosion reduction measures as well as maintenance and recovery of the riparian vegetation which function as a buffer to runoff, complying with the current Brazilian legislation [47].

As a result, although detected with low frequency and relatively low concentrations, pesticides may interfere in the Pantanal ecosystem, and little is known about the potential effects indicating that more research is needed in this regard.

References

1. Vieira LM, Galdino S (2004) A problemática socioeconômica e ambiental da bacia do rio Taquari e perspectivas. http://ainfo.cnptia.embrapa.br/digital/bitstream/CPAP/56369/1/ADM049.pdf. Accessed 09 May 2014
2. Pott A, Silva JSV (2015) Terrestrial and aquatic vegetation diversity of the pantanal wetland. Hdb Environ Chem. doi:10.1007/698_2015_352
3. Brazil Decree n. 6961, Aprova o Zoneamento Agroecológico da Cana-de-Açúcar no Brazil, 17 September 2009. http://www.planalto.gov.br/ccivil_03/_Ato2007–2010/2009/Decreto/D6961.htm. Accessed 11 November 2014.
4. ANVISA (2012) Mercado e regulação dos agrotóxicos. http://portal.anvisa.gov.br/wps/wcm/connect/b064b7804c1890a395ccd5dc39d59d3e/Semin%C3%A1rio + ANVISA + Mercado + e + Regula%C3%A7%C3%A3o + de + Agrot%C3%B3xicos + 2012 + %5BSomente + leitura %5D.pdf?MOD = AJPERES. Accessed 27 May 2014
5. Figueiredo DM, Dores EFGC, Paz AR, Souza CF (2012) Availability, uses and management of water in the Brazilian Pantanal. In: Ioris AAR (ed) Tropical wetland management. Ashgate, Surrey, pp 59–98
6. Rossetto OC, Girardi EP (2012) Dinâmica agrária e sustentabilidade socioambiental no Pantanal brasileiro. Revista Nera 21:135–161
7. Buller LS, Silva GB, Zanetti MR, Ortega E, Moraes A, Goulart T, Bergier I (2015) Historical land-use changes in São Gabriel do Oeste at the Upper Taquari River Basin. Hdb Environ Chem. doi:10.1007/698_2015_355
8. APROSOJA (2014) Produtores da região do Pantanal apostam na integração de culturas. http://www.aprosoja.com.br/noticia/produtores-da-regiao-do-pantanal-apostam-na-integracao-de-culturas/. Accessed 27 May 2014
9. Spadotto AA, Scorza Junior RP, Dores EFGC, Gebler L, Moraes DAC (2010) Fundamentos e aplicações da modelagem ambiental de agrotóxicos. Embrapa Monitoramento por Satélite, Campinas
10. Schnoor JL (1992) Chemical fate and transport in the environment. In: Schnoor JL (ed) Fate of pesticides & chemicals in the environment. Wiley-Interscience, New York, pp 1–23
11. Wauchope RD (1978) Pesticide content of surface-water draining from agricultural fields – review. J Environ Qual 7:459–472
12. Dabrowski JM, Peall SKC, Reinecke AJ, Liess M, Schulz R (2002) Runoff-related pesticide input into the Lourens River, South Africa: basic data for exposure assessment and risk mitigation at the catchment scale. Water Air Soil Pollut 135:265–283
13. Arora K, Mickelson SK, Helmers MJ, Baker JL (2010) Review of pesticide retention processes occurring in buffer strips receiving agricultural Runoff1. J Am Water Resour Assoc 46:618–647
14. Pinho AP, Morris LA, Jackson CR, White WJ, Bush PB, Matos AT (2008) Contaminant retention potential of forested filter strips established as SMZs in the piedmont of Georgia. J Am Water Resour Assoc 44:1564–1577
15. Locke MA, Zablotowicz RM, Reddy KN, Steinriede RW (2008) Tillage management to mitigate herbicide loss in runoff under simulated rainfall conditions. Chemosphere 70:1422–1428
16. Carter AD (2000) Herbicide movement in soils: principles, pathways and processes. Weed Res 40:113–122
17. Dores EFGC, Spadotto CA, Weber OLS, Carbo L, Vecchiato AB, Pinto AA (2009) Environmental behaviour of metolachlor and diuron in a tropical soil in the central region of Brazil. Water Air Soil Pollut 197:175–183
18. Matallo MB, Spadotto CA, Luchini LC, Gomes MAF (2005) Sorption, degradation, and leaching of tebuthiuron and diuron in soil columns. J Environ Sci Health B 40:39–43
19. Laabs V, Wehrhan A, Pinto A, Dores E, Amelung W (2007) Pesticide fate in tropical wetlands of Brazil: an aquatic microcosm study under semi-field conditions. Chemosphere 67:975–989

20. Laabs V, Amelung W, Pinto A, Zech W (2002) Fate of pesticides in tropical soils of Brazil under field conditions. J Environ Qual 31:256–268
21. Nogueira EN, Dores EFGC, Pinto AA, Amorim RSS, Ribeiro ML, Lourencetti C (2012) Currently used pesticides in water matrices in Central-Western Brazil. J Braz Chem Soc 23:1476–1487
22. Laabs V, Amelung W, Pinto AA, Wantzen M, da Silva CJ, Zech W (2002) Pesticides in surface water, sediment, and rainfall of the northeastern Pantanal basin, Brazil. J Environ Qual 31:1636–1648
23. Corbi JJ, Strixino ST, do Santos A, Del Grande M (2006) Environmental diagnostic of metals and organochlorinated compounds in streams near sugar cane plantations activity (Sao Paulo state, Brazil). Quim Nova 29:61–65
24. Torres JPM, Malm O, Vieira EDR, Japenga J, Koopmans GF (2002) Organic micropollutants on river sediments from Rio de Janeiro state, Southeast Brazil. Cad Saúde Pública 18:477–488
25. del Grande M, Rezende MOO, Rocha O (2003) Distribution of organochlorine compounds in water and sediments from Piracicaba River Basin/SP – Brazil. Quim Nova 26:678–686
26. Silva DML, Camargo PB, Martinelli LA, Lanças FM, Pinto JSS, Avelar WEP (2008) Organochlorine pesticides in Piracicaba River Basin (São Paulo/Brazil): a survey of sediment, bivalve and fish. Quim Nova 31:214–219
27. Dias PS, Cipro CVZ, Taniguchi S, Montone RC (2013) Persistent organic pollutants in marine biota of Sao Pedro and Sao Paulo Archipelago, Brazil. Mar Pollut Bull 74:435–440
28. de Souza AS, Torres JPM, Meire RO, Neves RC, Couri MS, Serejo CS (2008) Organochlorine pesticides (M) and polychlorinated biphenyls (PCBs) in sediments and crabs (Chasmagnathus granulata, Dana, 1851) from mangroves of Guanabara Bay, Rio de Janeiro state, Brazil. Chemosphere 73:S186–S192
29. Lailson-Brito J, Dorneles PR, Azevedo-Silva CE, Azevedo AD, Vidal LG, Mango J, Bertozzi C, Zanelatto RC, Bisi TL, Malm O, Torres JPM (2011) Organochlorine concentrations in franciscana dolphins, Pontoporia blainvillei, from Brazilian waters. Chemosphere 84:882–887
30. UNEP The new POPs under the Stockholm Convention. http://chm.pops.int/TheConvention/ThePOPs/TheNewPOPs/tabid/2511/Default.aspx. Accessed 26 May 2014
31. Countries UN-GoLAaC (2009) Global monitoring plan for persistent organic pollutants. First regional monitoring report Latin America and the Caribbean Region
32. Dores EFGC, Carbo L, Abreu ABG (2003) Serum DDT in malaria vector control sprayers in Mato Grosso state, Brazil. Cad Saúde Pública 19:429–437
33. Troli AC (2004) Praguicidas em rios da Bacia Hidrográfica do Alto Paraguai. Dissertation, Universidade Federal de Mato Grosso do Sul
34. Miranda K, Cunha MLF, Dores EFGC, Calheiros DF (2008) Pesticide residues in river sediments from the Pantanal wetland, Brazil. J Environ Sci Health B 43:717–722
35. Calheiros DF, Dores EFGC (2008) Contaminação por agrotóxicos na bacia do rio Miranda, Pantanal (MS). Rev Bras Agroecol 3:202–205
36. Nascimento FL, Nakatani K (2005) Variação temporal e espacial de ovos e larvas das espécies de interesse para a pesca na sub-bacia do rio Miranda, Pantanal-MS, Brasil. Acta Sci Biol Sci 25:251–258
37. McKim JM (1977) Evaluation of tests with early life stages of fish for predicting long-term toxicity. J Fish Res Board Can 34:1148–1154
38. de Sena A (2013) Organochlorine Pesticides in the Pantanal: A Qualitative and Semi-Quantitative Water Analysis. Dissertation, College of William and Mary
39. Carriger JF, Hoang TC, Rand GM, Gardinali PR, Castro J (2011) Acute toxicity and effects analysis of endosulfan sulfate to freshwater fish species. Arch Environ Contam Toxicol 60:281–289
40. Possavatz J, Zeilhofer P, Pinto AA, Tives AL, Dores EFGC (2014) Resíduos de pesticidas em sedimento de fundo de rio na Bacia Hidrográfica do Rio Cuiabá, Mato Grosso, Brasil. Ambiente Água 9:83–96

41. Delgado-Moreno L, Lin K, Veiga-Nascimento R, Gan J (2011) Occurrence and toxicity of three classes of insecticides in water and sediment in two Southern California coastal watersheds. J Agric Food Chem 59:9448–9456
42. Ensminger M, Bergin R, Spurlock F, Goh KS (2011) Pesticide concentrations in water and sediment and associated invertebrate toxicity in Del Puerto and Orestimba Creeks, California, 2007–2008. Environ Monit Assess 175:573–587
43. Li HZ, Sun BQ, Lydy MJ, You J (2013) Sediment-associated pesticides in an urban stream in Guangzhou, China: implication of a shift in pesticide use patterns. Environ Toxicol Chem 32:1040–1047
44. Toan PV, Sebesvari Z, Blasing M, Rosendahl I, Renaud FG (2013) Pesticide management and their residues in sediments and surface and drinking water in the Mekong delta, Vietnam. Sci Total Environ 452:28–39
45. Miglioranza KSB, Gonzalez M, Ondarza PM, Shimabukuro VM, Isla FI, Fillmann G, Aizpun JE, Moreno VJ (2013) Assessment of Argentinean Patagonia pollution: PBDEs, OCPs and PCBs in different matrices from the Rio Negro basin. Sci Total Environ 452:275–285
46. Masia A, Campo J, Vazquez-Roig P, Blasco C, Pico Y (2013) Screening of currently used pesticides in water, sediments and biota of the Guadalquivir River basin (Spain). J Hazard Mater 263:95–104
47. Brazil LEI N° 12.651, Dispõe sobre a proteção da vegetação nativa, 25 May 2012. http://www.planalto.gov.br/ccivil_03/_ato2011–2014/2012/lei/l12651.htm. Accessed 26 May 2014

Historical Land-Use Changes in São Gabriel do Oeste at the Upper Taquari River Basin

Luz Selene Buller, Gustavo Bayma-Silva, Marilia Ribeiro Zanetti, Enrique Ortega, Anibal de Moraes, Thiago Goulart, and Ivan Bergier

Abstract Agricultural expansion in uplands of the Pantanal in recent decades suppressed a large fraction of native vegetation. In the case of the municipality of São Gabriel do Oeste (SGO), located in the Upper Paraguay River Basin, the processing of historical Landsat imagery indicates from 1984 to 2013 a relative land cover increase in soybean/corn cropland from 25% to 30% and pasture from 17% to 41%, whereas a decrease in native forest from 57% to 28%. These land-use changes produced several outstanding economic indexes as the *per capita* gross domestic product (GDP), 48% higher than that of Brazil. The total GDP increased by 259% from 1999 to 2011. Besides, SGO Human Development Index (HDI) of 0.729 in 2010 was about 2% higher than the Brazil's HDI average. On the other hand, the agricultural development reflected in alterations of major ecohydrological regulations (carbon and water) at the watershed, notwithstanding the economic concentration. Croplands mostly develop in areas of low vulnerability (55%), while

L.S. Buller (✉) and E. Ortega
Ecological Engineering Laboratory, Food Engineering School, State University of Campinas, R. Dr. Josué de Castro 40, Cidade Universitária, Campinas 13083-862, SP, Brazil
e-mail: selene@fea.unicamp.br

G. Bayma-Silva and M.R. Zanetti
Embrapa Satellite Monitoring, Brazilian Agricultural Research Corporation, Campinas, SP, Brazil

A. de Moraes
Department of Agricultural Sciences, Federal University of Paraná, Curitiba, PR, Brazil

T. Goulart
Agricultural Department, Agricultural Cooperative of São Gabriel do Oeste (COOASGO), São Gabriel do Oeste, MS, Brazil

I. Bergier
Biomass Conversion Laboratory, Embrapa Pantanal, Brazilian Agricultural Research Corporation, Corumbá, MS, Brazil

I. Bergier and M.L. Assine (eds.), *Dynamics of the Pantanal Wetland in South America*, Hdb Env Chem (2016) 37: 191–208, DOI 10.1007/698_2015_355,

almost all of the pasture areas are preferably in vulnerable areas (42%). Due to climate changes, the promotion of state social inclusive and low-carbon agriculture is necessary to mitigate greenhouse gas (GHG) emissions and to recover important ecohydrological processes at the drainage basin level. In this chapter, we explore a new sustainable design of agroecosystems (integrated crop-livestock and forestry) in the Upper Taquari River Basin, which can maximize and optimize both the sharing of rural productivity and carbon/water regulations at the watershed.

Keywords Agriculture, Deforestation, Integrated agroecosystems, Land use, Livestock, Sustainability

Contents

1 Introduction

The main agricultural and industrial development during the first half of the nineteenth century occurred in the east coast of Brazil. The west and north regions were demographically and economically empty for decades. As a strategic policy to populate and promote the economic growth of these regions, several Brazilian government development programs included the expansion of the agricultural frontier in the Middle West region over the Cerrado biome [1, 2]

The Pantanal is located in the Upper Paraguay River Basin lowlands, and its plateau, the highlands in Cerrado biome, keeps the headsprings of the basin main rivers. Until the 1960s, the major land use in the plateau was pasture for cattle ranching. Along the 1970s, the agricultural expansion became an important land use in the Cerrado. During the 1980s, a more intense occupation initiated, whereas from the 1990s, the large-scale farming of commodity crops greatly expanded at the expense of native vegetation [3].

Human intervention in the Pantanal's highlands for the agriculture expansion in the last three decades has suppressed large areas of native vegetation, including riparian and gallery forests. The diagnosis of changes in land cover and land use for the Upper Paraguay River Basin from 2002 to 2008 indicated that 87% of the natural vegetation remain in the floodplain, while in the plateau, only 42% of the natural vegetation is still preserved. Livestock (cattle) has occupied 43% and

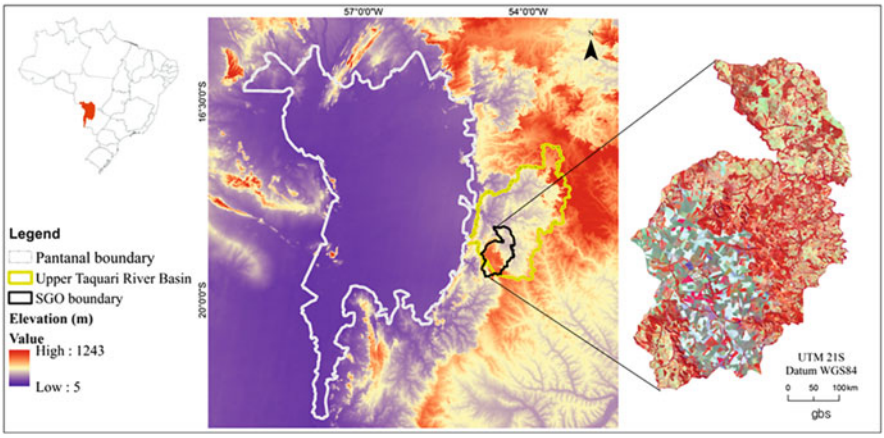

Fig. 1 ASTER digital elevation model and a detail of the study area in false color composite 5(R), 6 (G), 4 (B) OLI/Landsat-8, acquired in July 2013

agriculture 10% of the plateau, such that traditional models of fisheries and livestock were replaced by intensive production [4].

The Upper Paraguay River Basin altitude varies from 1,243 m in the edge of the plateau to 5 m in the Pantanal floodplain (Fig. 1). The topographic condition associated to the crop and livestock occupation, lacking adequate soil management for many years, turned the plateau into an uncontrolled source of sediments carried to riverbeds, accompanied by residual chemicals from fertilizers and pesticides [5], which flow into the floodplains. The abnormal sediment deposition causes widespread siltation such as the one observed in the Taquari River [6]. Due to its geomorphology (see also [7]), the lower Taquari River is subjected to river avulsion (a process that leads to changing its course) that usually occurs as a natural phenomenon, but it has been accelerated in the last four decades as a combination of drastic land-use changes and above normal rainfall from 1974 to 1995 [8].

Deforestation for crops and pasture simplifies the ecohydrological functioning of the ecosystems by affecting ecosystem services as carbon sequestration (in soils and vegetation), green water regulation (minimizing evapotranspiration and infiltration in the soil while enhancing runoff and discharge), and biodiversity (macro and micro life-forms) [9]. Unnatural changes in the decadal regime of the annual flood pulse of the Paraguay River are likely associated to the upland forest suppression, resulting, for instance, in a higher interannual frequency of the natural anoxic fish-killing phenomena [10]. At a global level, climate change has been attributed to the anthropogenic interference in the ecosystems, and agriculture plays a prominent role in greenhouse gas (GHG) emissions. Overall, agriculture, land-use, and forestry sectors contribute for almost a third of the total GHG emissions mainly due to enteric fermentation followed by manure left on pasture [11].

In addition to the imminent need to decrease the deforestation rate, a low-carbon agriculture is mandatory in order to mitigate GHG emissions and to recover carbon

and water regulations in the drainage basin. The Brazilian government has established the Low-Carbon Agriculture Plan (ABC) in 2010 aiming to lead the promotion of sustainable technologies for the agricultural development over the next 20 years. GHG mitigation and farmers income increasing are the primary targets of ABC Plan.

The Production Program for Integrated Farming Systems in Watersheds (PISA) coordinated by the Ministry of Agriculture, Livestock and Supply (MAPA), linked to ABC Plan, disseminates technologies and provides continued training for producers. Overall, PISA was established through an institutional arrangement consisting of technical coordination by the Federal University of Paraná and Rio Grande do Sul (UFPR/UFRGS), Brazilian Agricultural Research Company (EMBRAPA), and local partners (municipalities, associations, the industry, etc.). PISA aims to promote sustainable development within the watershed, the basic unit of planning by the diffusion of (ecological, socioeconomic) sustainable technologies to generate employment, income and improved quality of life, getting safe food production, quality, and competitiveness.

In optimized, sustainable integrated systems, crops rotate with pasture and vice versa, whereas tree plants also compose the landscape. In general, the use of pastures in integrated systems restructures the soil. It is commonly used in annual or biennial rotation with crops in order to increase straw for tillage. The benefits related to integrated systems are increased soil organic matter; reduction and control of pests, diseases, and weeds; water reclamation and conservation; soil carbon and nitrogen fixation; high carbon sequestration; soil loss reduction; GHG emissions reduction; nutrient cycling; soil bioremediation; increased biodiversity; and increased productivity [12].

Agricultural integration is a strategy that recognizes the environmental benefits in regulating ecohydrological processes (carbon and water) by the agroecosystem. Furthermore, integrated livestock-crop and forestry systems represent a sustainable intensification strategy that reduces environmental vulnerability and increases yields and financial gains when compared to monocultures or nonintegrated livestock farming systems [12]. In this chapter, we explore new sustainable design of integrated agroecosystems in the Upper Taquari River Basin, particularly in São Gabriel do Oeste (SGO), which can optimize both the sharing of rural productivity and carbon/water regulation at the watershed level.

2 Location and History of São Gabriel do Oeste (SGO)

SGO is located in the state of Mato Grosso do Sul (MS) in the east border of the Upper Paraguay River Basin (Fig. 1). The municipality is almost entirely comprised in the Upper Taquari River Basin with intensive land use (Fig. 1).

The SGO agricultural occupation started in the 1950s, when southern Brazilian farmers migrated to the area. During the 1960s, the economy was based on extensive cattle and subsistence crops, later succeeded by coffee crops. The latter

did not adapt to local characteristics, being replaced by soybean and corn during the Brazilian Cerrado agro-expansion wave. In the 1990s, a large-scale monocrop agriculture had been established, which is the milestone of the era of intensive swine breeding. The municipality experienced rapid and outstanding development and has been the target of agricultural research, development, and innovation initiatives [13] ever since. The first intense study in the location was performed by EMBRAPA that produced an Agroecological Zoning Study and Recommendations [14]. The document has provided technical guidelines for planning, management, and monitoring and has made available a complete database for municipal, state, and federal decision makers.

3 SGO Landscape Characterization

The potential vegetation map (Fig. 2) of the studied area indicates the vegetation types present in the pristine landscape derived from biophysical aspects such as soil, geology, geomorphology, and topography without anthropogenic intervention [14].

The phytophysiognomy of the wooded Cerrado initially occupied 271,088 hectares (ha), about 70% of the county area, followed by areas of Cerrado woodland with 41,206 ha (11%) and transition enclave areas with 33,690 ha (9%). The

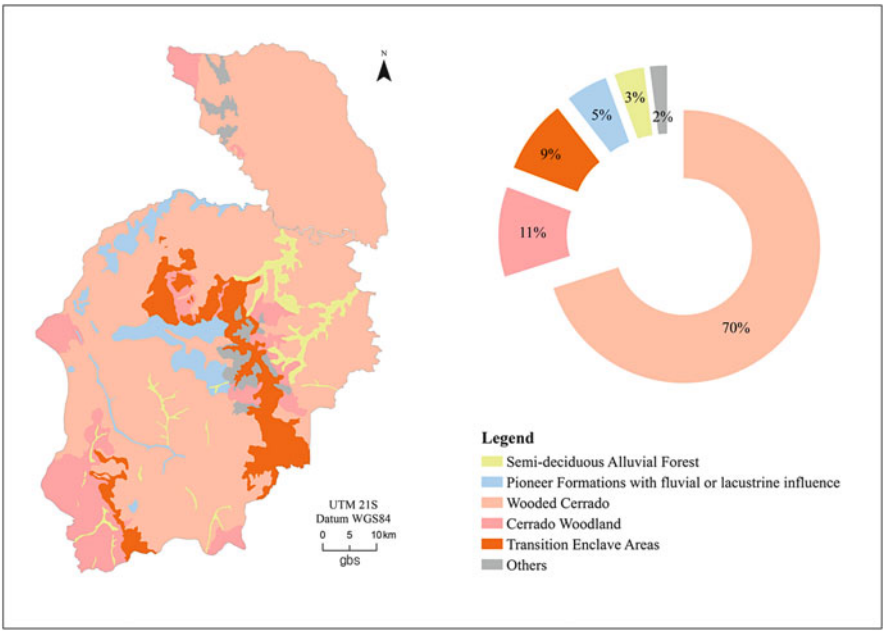

Fig. 2 SGO potential pristine vegetation map and distribution of physiognomies

wooded Cerrado region is characterized as campestral physiognomy formed by low vegetation species distributed sparsely over the ground and covered by a continuous grass layer. This vegetation structure has a floristic composition similar to the Cerrado woodland but with lower (±5 m) and open trees structure. The region of Cerrado woodland occurs on steep slopes, contributing to its preservation, or areas where the soil is more fertile. Cerrado woodland floristic composition also presents species that occur in areas of seasonal forest (canopy of 15 m in height).

Transition enclave areas are characterized by areas of disjoint vegetation that contact but have similar physiognomic structures that hamper their separation by simple photointerpretation. The floristic survey of each transition enclave area phytoecological region is necessary. The forest physiognomy is associated to drainage areas like the pioneer formations with fluvial or lacustrine influence where the buriti palms (*Mauritia flexuosa*) occur and seasonal semi-deciduous alluvial forest. Respectively, the two last phytophysiognomies accounted for 19,230 ha (5%) and 13,723 ha (3.5%) of SGO area.

In relation to the soil (Fig. 3), about 212,753 ha (that corresponds to 55% of the SGO area) is occupied by oxisol soils which are stable, highly watered, and tropical mineral soils with highly oxidized subsurface horizons. Once oxisol low fertility is corrected, they present high potential for farming. In SGO, its incidence lies mostly in the south-central plateau, locally known as "*chapadão*," which is precisely where the land use is cropland. Entisols (Quartzipsamment) occupy 123,609 ha (32%) of the total SGO area. Entisols (Quartzipsamment) are sandy, well-drained deep soils that, when destituted of vegetation cover, are more susceptible to erosion and usually develop deep erosion (ravines) (see also [16]). Entisols (Lithic Orthent) are shallow soils usually covered by grasslands and are found in the lowest elevation regions of SGO corresponding to 34,309 ha (9%). The remaining soils of the municipality are Entisols (Aquent) that occupy 16,105 ha (4%). This soil originates from alluvial sediments and is located in lowland areas, where high water table and flood risk are frequent. It presents agricultural limitations due to its poor drainage. Artificial drainage is essential to fit this soil to agricultural use for larger crops and there are also limitations to the use of agricultural machinery [17, 18].

Regarding the vulnerability to soil surface erosion (Fig. 4) that is related to local soil, relief (Fig. 5), and climate features, SGO presents more than half of its area under some risk of natural erosion, namely:

1. Twenty-one percentage (82,526 ha) corresponding to areas of extremely high vulnerability that present very strong surface erosion, concentrated runoff, incidence of ravines, and eventual sheet erosion; fast or slow shifts in land mass; and possible fall of large portions of soil
2. Thirty-two percentage (122,337 ha) corresponding to areas of very high vulnerability, which have strong to moderate surface erosion, relief slopes from 19% to 27%, fast diffuse runoff, sheet erosion, ridges and ravines presence, and slow movements of land mass

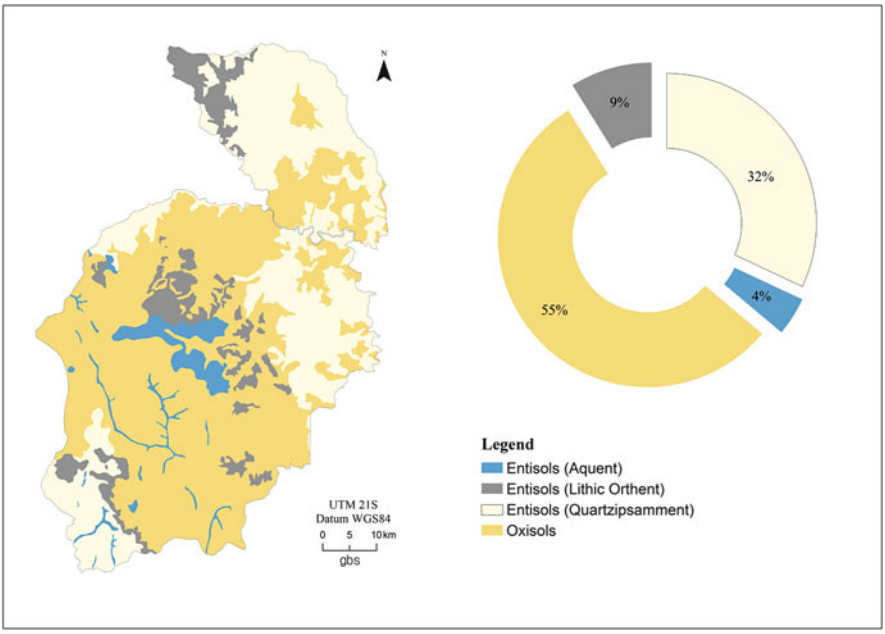

Fig. 3 SGO soil map distribution. Classification according to [15]

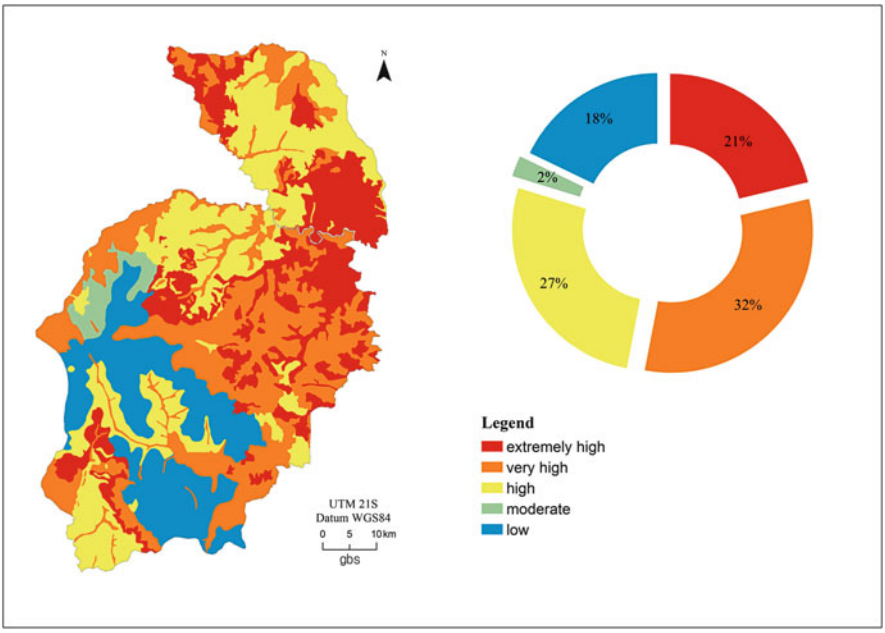

Fig. 4 SGO vulnerability map to surface soil erosion

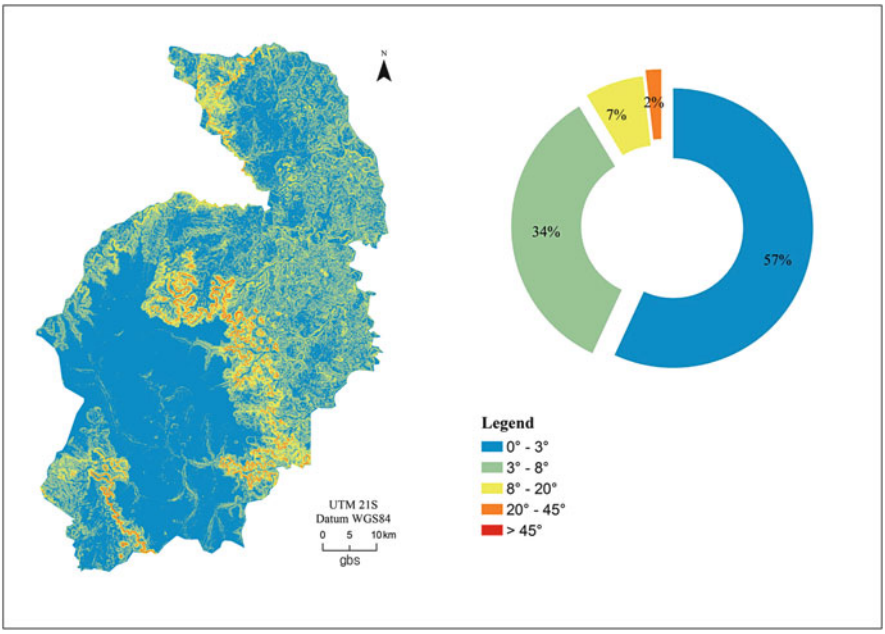

Fig. 5 SGO relief map from the TOPODATA dataset. Source: [19]

3. Twenty-seven percentage (103,436 ha) corresponding to areas of high vulnerability, which are characterized by moderate to strong surface erosion and soils with moderate erodibility

4 SGO Land-Use and Land Cover Evolution

Land-use and land cover (LULC) maps (Fig. 6) were prepared to identify SGO anthropogenic areas. Primitive (pristine) vegetation maps were recovered from the Agroecological Zoning Study and Recommendations [14]. The overlap of land-use information of the years 1984 and 2013 in the areas of primitive natural vegetation cover allowed the identification of the remaining natural vegetation cover in both years. This methodology was proposed by Silva et al. [20], and it was applied before in land cover and land use for the state of Maranhão, Brazil, in order to prepare its macro ecological and economic zoning [21].

The anthropogenic classes mapping consisted firstly in obtaining TM/Landsat images, available in the "Earth Explorer" catalog from the US Geological Survey (http://earthexplorer.usgs.gov/). In the aforementioned catalog, images with geometric correction "level 1–L1T" were selected. This product uses reference data field (ground control points) and digital elevation data of the terrain to obtain the best possible accuracy of the land surface. To cover the entire study area, the

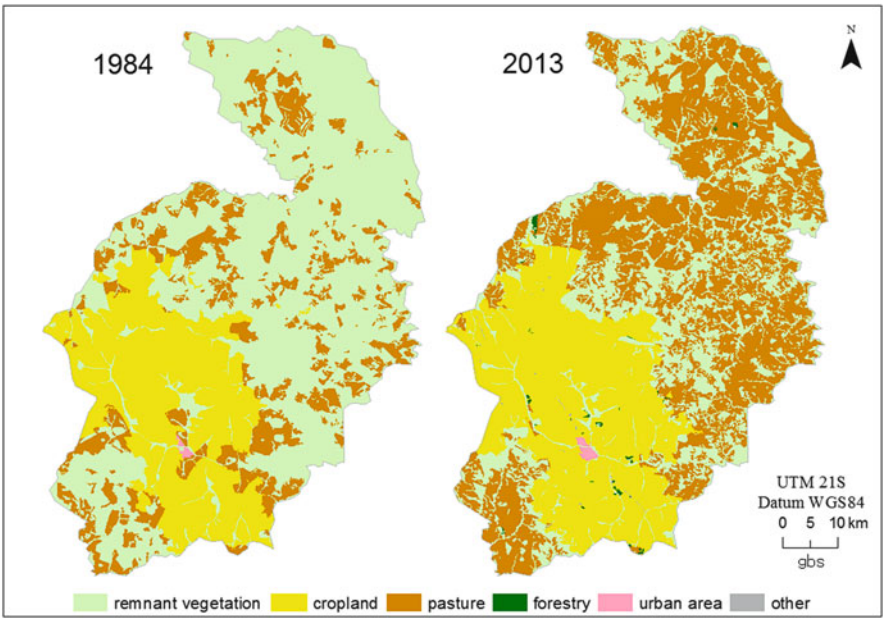

Fig. 6 Land-use map of SGO from 1984 to 2013. Both maps are available on a Web-based platform for geospatial information http://geoinfo.cnpm.embrapa.br/maps/1083/view and http://geoinfo.cnpm.embrapa.br/maps/724/view

images 225-73 of April 20, 1984, and of July 24, 2013, were obtained. Images of the rainy season were also used to highlight the contrast between areas of grassland and agriculture, because in the dry period, the straw from crops presents similar spectral response as dry grassland, as indicated in [22].

The Geographic Information System software SPRING [23] was used to create a geographical database and to segment the selected images. The polygon segmentation process was chosen to automatize the process in order to obtain time and precision leverages [24, 25]. The segments created in SPRING were exported as shapefiles and manually classified by using the software Quantum GIS. An interpretation key with auxiliary information for the visual classification of the interest classes, cropland, forestry, pasture, urban area, and others was established using the method proposed by Gomes et al. [26] and Espírito-Santo [27].

Additional information like temporal series of enhanced vegetation index (EVI-2) [28] provided by the Brazilian National Institute for Space Research (INPE) [29] was also used for the interpretation key. LULC detailed analysis is further discussed.

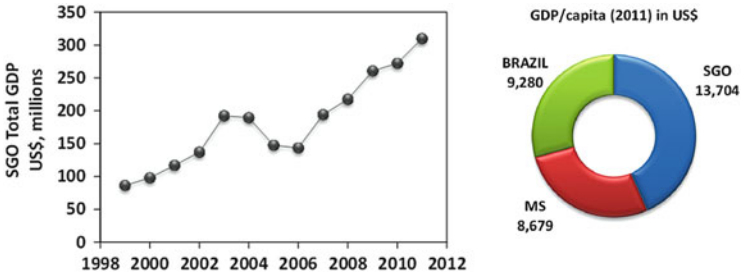

Fig. 7 Historical SGO total GDP and *per capita* GDP in 2011. Source: Brazilian Institute of Geography and Statistics – IBGE, http://www.ibge.gov.br

5 SGO Economy

SGO is a unique location with several outstanding economic indexes like *per capita* GDP that is 58% higher than that of MS state and 48% higher than that of Brazil. SGO total GDP increased by 202% from 1999 to 2009 and 259% from 1999 to 2011 (Fig. 7).

Regarding the social aspects, SGO also showed very good results. In 2010, SGO Human Development Index (HDI) of 0.729 is 2% above Brazilian HDI.

6 SGO Production and LULC Evolution Analysis

Concerning the livestock production, SGO cattle population increased slightly from 2006 to 2012, while the swine population increased in 55% for the same period (Table 1) and presented a remarkable increase of 175% from 1995 to 2012. Grain crops (Table 2) showed a huge increase of 507% in corn and 704% in soybean. Both quantities and production economic value of corn and soybean increased substantially.

The estimated expansion of anthropogenic areas in SGO (Table 3) indicates a significant increase of pasture areas, 132%, or 89,521 ha in 19 years (~4,700 ha. yr^{-1}). In 2013, this activity accounted for 41% of total anthropogenic areas, while in 1984, it represented only 17.5%.

Agricultural areas distribute mainly throughout the plateau and occupied 118,440 ha in 2013, in comparison to 96,703 ha in 1984, figuring 21,737 ha of new agricultural areas. From 1984 to 2013, the native remnant vegetation retracted in 51%, more precisely 112,924 ha. Crop expansion corresponds to 22% and the urban area increased 88% for the same period.

Crops and pasture areas suppressed, respectively, 17,874 and 65,801 ha (Table 4) of natural wooded Cerrado vegetation. Furthermore, both land uses suppressed approximately 1,700 and 5,000 ha of seasonal semi-deciduous alluvial forest and pioneer formations with fluvial or lacustrine influence, which are the vegetation that

Table 1 SGO livestock production

Livestock		1995	2006	2012
Cattle	Heads	178,430	199,104	205,109
Swine	Heads	67,782	120,544	186,510

Source: IBGE, http://www.sidra.ibge.gov.br/bda/acervo/

Table 2 SGO grain production

Grain			2006	2012	Relative change (%)
Soybean	Quantity	Tons	208,746	349,800	+68
	Value	1,000 US$	41,272	106,925	+159
Corn	Quantity	Tons	78,191	474,800	+507
	Value	1,000 US$	9,513	76,479	+704

Source: IBGE, http://www.sidra.ibge.gov.br/bda/acervo/

Table 3 SGO LULC comparison of the years 1984 and 2013

	Area in 1984		Area in 2013		Relative change	
LULC	ha	%	ha	%	ha	%
Crop	96,703	25	118,440	30	21,737	22
Pasture	67,568	17	157,089	41	89,521	132
Remnant vegetation	221,582	57	108,659	28	−112,923	−51
Water bodies	475	0	474	0	−1	0
Forestry	0	0	985	0	985	-
Urban area	448	0	841	0	393	88
Others	0	0	288	0	288	-
Total	386,776	100	386,776	100	-	-

provide protection environmental services against erosion or siltation of margins and springs. Pastures have suppressed about 12,000 ha of Savannah Park, or Parkland, whose floristic characteristic is spaced herbaceous trees of medium or low height over continuous grassland that facilitates the cattle grazing and ultimately facilitates the conversion of these areas to anthropogenic use without deforestation.

Crops occupied precisely the region dominated by oxisols (Table 5), which are more appropriate to croplands after soil preparation (locally referred to as "calagem," the "Cerrado miracle"), and presented 102,591 ha, or 87% of total agricultural land. In 1984, 53% of oxisol areas were occupied by pasture. In 2013, the same proportion corresponded to areas of Entisols (Quartzipsamment) or 55,211 hectares (Table 5). Silva et al. [22] and Trabaquini et al. [30] observed that both soil classes were the most used for these anthropogenic activities from 1990 to 2001 and, in general, in the Cerrado of Mato Grosso.

A spatiotemporal analysis of 1984 relative to 2013 on the soil, relief, and LULC maps (Figs. 3, 5, and 6) indicates that pasture areas are found in portions of lower altitude. Moreover, in the most recent occupation, pasture advanced mainly in Entisol soils prone to erosion enhanced by cattle trampling. Nonetheless, the

Table 4 Areas of primitive vegetation converted to crop and pasture

Remnant vegetation	Area in 1984 (ha)	Area in 2013 (ha)	Relative change (%)
Cropland			
Wooded cerrado	80,812	98,686	22
Pioneer formations	988,906	11,640	18
Cerrado woodland	4,968	5,784	16
Seasonal semi-deciduous alluvial forest	736	970	32
Transition enclave areas	196	856	337
Others	102	504	394
Total croplands	96,703	118,440	22
Pasture			
Wooded cerrado	47,765	113,566	138
Cerrado woodland	11,316	11,629	3
Transition enclave areas	3,745	10,282	175
Pioneer formations	1,992	3,714	86
Seasonal semi-deciduous alluvial	2,288	5,406	136
Others	463	12,492	2,599
Total pasture	67,568	157,089	132

Table 5 Crop and pasture areas distributed per soil classes

	Crop			Pasture		
Soil class	Area in 1984 (ha)	Area in 2013 (ha)	Relative change (%)	Area in 1984 (ha)	Area in 2013 (ha)	Relative change (%)
Entisol (Quartzipsamment)	233	1,335	472	27,796	83,007	199
Entisol (Aquent)	10,465	13,315	27	1,600	1,034	−35
Oxisol	85,572	102,591	20	35,595	63,578	79
Entisol (Lithic Orthent)	432	1,200	178	2,577	9,471	268
Total	96,703	118,440	22	67,568	157,089	132

2006 Brazilian agricultural census indicated that 87% of the total areas occupied by pastures were of cultivated pasture in good conditions, 5% were degraded, and 8% were natural pasture.

Another issue is the environmental vulnerability of the study area (Table 6). The concept of [31] was used for the purpose of the study of the expansion of anthropogenic areas, especially crop and pasture. Croplands occur mostly in areas of low vulnerability (55%), and this fact can be explained by its distribution on the plateau. On the other hand, almost all of the pasture areas established in regions of a certain level of vulnerability are 42% in areas of high vulnerability, 35% in areas of very high vulnerability, and 23% in areas of extremely high vulnerability. It is

Table 6 Crop and pasture distribution according to vulnerability classes

Vulnerability	Area in 1984		Area in 2013		Relative change %	
	ha	%	ha	%	ha	%
Crop						
Extremely high	479	0.5	2,328	2	1,849	386
Very high	20,972	22	28,803	24	7,831	37
High	11,940	12	14,175	12	2,236	19
Moderate	5,374	6	8,544	7	3,170	59
Low	57,939	60	64,590	55	6,652	11
Total	96,703	100	118,440	100	21,737	22
Pasture						
Extremely high	9,587	14	35,611	23	26,024	271
Very high	24,086	36	54,787	35	30,701	127
High	26,066	39	65,472	42	39,406	151
Moderate	1,713	3	380	0	−1,333	−78
Low	6,117	9	840	1	−5,278	−86
Total	67,568	100	157,089	100	89,521	132

Table 7 Land-use changes (ha) for a 30-year period

	1994	Crop	Pasture	Remnant vegetation	Urban area	
1984	Crop	94,163	276	1,878	22	
	Pasture	18,843	41,866	6,517	103	
	Remnant vegetation	12,219	76,053	133,467	101	
	Urban area	44	3	12	389	
	2004	Crop	Pasture	Remnant vegetation	Urban area	
1994	Crop	123,205	840	330	0	
	Pasture	2,447	112,323	3,577	12	
	Remnant vegetation	2,088	33,569	106,951	0	
	Urban area	0	0	0	616	
	2013	Crop	Pasture	Remnant vegetation	Urban area	Forestry
2004	Crop	116,250	6,677	5,069	241	579
	Pasture	148	123,645	22,358	0	321
	Remnant vegetation	2,271	26,568	81,105	23	75
	Urban area	27	0	11	589	0

noteworthy that from 1984 to 2013, pasture areas more than doubled in all "critical" vulnerability classes.

At last, a cross-year evaluation of land-use change (Table 7) is especially useful to understand which land use has, in fact, expanded from time to time and which class had its area suppressed.

Table 8 Land-use evolution (ha) for a 30-year period

Land-use class	1984	1994	2004	2013
Crop	96,340	125,270	128,300	118,616
Pasture	67,329	118,199	146,532	156,725
Remnant vegetation	221,841	141,874	110,498	108,783
Urban area	448	616	627	854
Forestry	0	0	0	979

It is clear that pasture is the main cause for remnant vegetation suppression; 136,191 ha of remnant vegetation were converted to pasture in 30 years, as it was previously concluded in the land-use comparison (Table 3). The conversion of remnant vegetation to cropland represents 16,578 ha. In the course of those 30 years, pasture (cultivated and natural are both accounted here) advanced over 21,437 ha of croplands.

From 1984 to 1994, about 12,219 and 76,053 ha (Table 8), respectively, of remnant vegetation have been cleared and converted to croplands and pasture. These values were lower from 1994 to 2004 (2,088 and 33,569 ha) and from 2004 to 2013 (2,271 and 26,568 ha). This could be an evidence that livestock preferably occupy new anthropogenic areas.

From the total pasture area in 1994 (118,199 ha), only 35% (41,866 ha) were pasture in 1984. In this period, the remnant vegetation gave way to 76,053 ha of pasture area, i.e., 64% of the pasture areas in 1994 were remnant vegetation in 1984. The direct conversion of remnant vegetation for pasture has decreased from 1994 to 2004, 33,369 ha, and from 2004 to 2013, 26,798 ha. In spite of the observed decrease, the conversion of croplands to pasture (6,261 ha) from 2004 to 2013 also has contributed to increase pasture area over the last 30 years.

The area of cropland remained relatively stable when compared to pasture and remnant vegetation. The lowest area occurred in 1984 (96,340 ha) and increased in 2004 to 128,300 ha. From 1984 to 1994, 18,843 and 12,219 ha of pasture and remnant vegetation were converted to croplands. However, from 2004 to 2013, the cropland area was reduced to 118,616 ha, which can be explained by the conversion of 6,261 ha to pasture and 5,069 ha to remnant vegetation (may be abandoned areas exposed to the regeneration of natural vegetation). It is noteworthy that forestry (reforestation) is present only in 2013, and of the total area of 979 ha, 579 ha (59%) are due to cropland conversion.

An important outlook here is that the conversion from pasture to remnant vegetation, 32,452 ha, is larger than the conversion from croplands to remnant vegetation, 7,276 ha. The total area probably abandoned and naturally recovered from anthropic to regenerated natural vegetation is 39,729 ha (Fig. 8).

However, the Brazilian Forestry Code (Brazil, Law 12.651 of May 25, 2012) establishes that rural properties located in regions outside the Legal Amazon, as is the case of SGO, must keep 20% of their native vegetation area. Once SGO keeps only 28% of its native vegetation, the deforestation has become a real bottleneck for further agricultural expansions. Moreover, soil management in vulnerable areas is

Fig. 8 Possible abandoned areas with native vegetation regeneration in São Gabriel do Oeste. Photos taken on Oct 10, 2014 (19°02′35″S and 52°32′37″W, 19°02′56″S and 54°32′09″W, respectively). Photos credit: Luz Selene Buller

crucially necessary in order to keep soil fertility and to avoid mid- and long-term erosion.

7 Sustainable Perspectives by Integrated Agroecosystems

In 2010, a new Brazilian governmental project, named *Intensive and Integrated Farm Systems for Smallholders* (granted by the Brazilian Ministry of Science, Technology and Innovation (MCTI) and the Brazilian National Research Networks in Agrobiodiversity and Agricultural Sustainability program, CNPq/REPENSA), became effective in SGO and was responsible to disseminate integrated agroecosystems. A pilot farm was established in a rural settlement to monitor and evaluated different integrated system designs in terms of socioeconomic and environmental aspects. The pilot farm project followed PISA design as a successful strategy. Apart from crops and pasture rotation, swine is included in a new scheme called integrated swine-crop-pasture-eucalyptus system [32]. The pilot farm has swine manure treatment (anaerobic biodigester), biogas conversion to electric power (40% efficiency), and organic fertilizer (digester effluent) in liquid and solid states. Electric power and organic fertilizer are destined to self-consumption, and there is the possibility to export the surplus (solid state). In addition to the nutrient recycling and consequent lower dependence on external resources, there are new products to incorporate the farm product portfolio and revenue. Nutrient recycling and swine manure management create interesting opportunities to reduce pollution and obtain gains in ecosystem services, GHG emission mitigation, and socioeconomic benefits, particularly if it is considered the eventual evolution of the landscape from large monocrop patches to small integrated livestock-crop-wood-fertilizer with more environmental and social services [13, 32, 33].

Carbon and water ecosystem services related to land-use change in the Taquarizinho River nearby São Gabriel do Oeste were evaluated in [34]. Their

overall results showed that, in comparison with the native vegetation, the economic losses in terms of ecosystem services for tillage agricultural systems are 70%, for no-tillage systems 36%, for systems under soil improvement 27%, and for integrated livestock-crop and forestry systems only 8%. The aforementioned technologies that consider ecohydrological principles of landscape management [9] improve ecosystem services and can also reflect positively in the lowland areas of the Pantanal. This may contribute for the restoration of the water regulation and sediment discharges to reestablish the natural variability of the interannual flood pulse [10].

The transition to new agricultural models in the Pantanal plateau, and in the Cerrado in general, requires land-use intensification, which can be a preoccupying alternative when intensification is based solely on economic inputs (chemicals, synthetic fertilizers, and machinery, for instance) which places the farm in an extremely nonrenewable resources dependence and provides no nutrient cycling and no GHG emission abatement. Nutrient recycling and renewable energy are key factors to the future agriculture, as well as agroecosystem integration and soil management to achieve better sustainable performance [33].

Low-carbon agriculture (Brazilian ABC Plan) associated to an energy self-sufficient system (that exports nutrients through liquid and solid organic fertilizers and its electric power surplus) is the ultimate technological solution in a worldwide context. Deforestation can be reduced if the intensification is truly achieved, and arboreal element can be restored to the agroecosystems, as an essential factor for human welfare considering mitigation and adaption to future climate changes [32]. This might be a response to the food security challenge for the next decades and may place rural areas, including smaller farmers, in a new competitive position in the energy and food market [33]. Livestock-crop-wood-fertilizer integration represents, therefore, a suitable agricultural model to the entire Pantanal plateau. It is important to notice that the foreseen agricultural development is expected to occur under certain specific guidelines related to manure treatment, electric power self-sufficiency, soil management and no-tillage system, synthetic fertilizer substitution for organic fertilizer and agroecosystem, and farm product diversification (grain, beef, pork, wood, electric power, and organic fertilizer surplus).

Acknowledgments This work was partially funded by MCTI/CNPq/REPENSA, Grant number 562441/2010-7, and Embrapa/Macroprograma 2, Grant number 02.11.05.002. Special thanks to Eduardo Soriano (MCTI), Rui Ulsenheimer, Ancionei Antônio Thebaldi, Carlos Shimata, Fausto Mariano, Jair Borgmann, Luiz Rieger, Rubia Rech, Matheus Tschaen, André Bortolini, and Léo Grison and to the support given by COOASGO (Agricultural Cooperative of São Gabriel do Oeste) and by the City Hall of São Gabriel do Oeste. The first author gratefully acknowledges the scholarship from the Coordination for the Improvement of Higher Level Education Personnel (CAPES, Brazil).

References

1. Silva LL (2001) O papel do estado no processo de ocupação das áreas de Cerrado entre as décadas de 60 e 80. Caminhos da Geografia. Uberlândia, MG: Instituto de Geografia, Universidade Federal de Uberlândia, pp 24–36
2. Goedert WJ (1989) Região dos Cerrados: Potencial Agrícola e Política Para Seu Desenvolvimento. Pesquisa Agropecuária Brasileira. Embrapa Informação Tecnológica, Brasília, pp 1–17.
3. Lapola DM, Martinelli LA, Peres CA, Ometto JPHB, Ferreira ME, Nobre CA et al (2014) Pervasive transition of the Brazilian land-use system. Nat Clim Chang 4(1):27–35
4. Silva JSV, Abdon MM, Silva SMA, Moraes JA (2011) Evolution of deforestation in the Brazilian Pantanal and surroundings in the timeframe 1976–2008. Geografia 36:35–55
5. Dores E (2015) Pesticides in the Pantanal. Hdb Env Chem. doi:10.1007/698_2015_356
6. Galdino S, Vieira LM, Pellegrin LA (2006) Impactos ambientais e socioecoômicos na Bacia do Rio Taquari – Pantanal 1 ed. Embrapa Pantanal, Corumbá
7. Assine ML, Merino ER, Pupim FN, Warren LV, Guerreiro R, McGlue MM (2015) Geology and geomorphology of the Pantanal Basin. Hdb Env Chem. doi:10.1007/698_2015_349
8. Assine ML (2005) River avulsions on the Taquari megafan, Pantanal wetland, Brazil. Geomorphology 70(3–4):357–371
9. D'Odorico P, Laio F, Porporato A, Ridolfi L, Rinaldo A, Rodriguez-Iturbe I (2010) Ecohydrology of terrestrial ecosystems. BioScience 60(11):898–907
10. Bergier I (2013) Effects of highland land-use over lowlands of the Brazilian Pantanal. Sci Total Environ 463:1060–1066
11. Tubiello FN, Salvatore M, Golec RDC, A. Ferrara SR, Biancalani R, S. Federici HJ et al (2014) Agriculture, forestry and other land use emissions by sources and removals by sinks. FAO
12. Moraes A, Carvalho PCF, Anghinoni I, Lustosa SBC, Costa SEVGA, Kunrath TR (2014) Integrated crop–livestock systems in the Brazilian subtropics. Eur J Agron 57(0):4–9
13. Bergier I, Soriano E, Wiedman G, Kososki A (2013) Intensive and integrated farm systems using fermentation of swine effluent in BraziL. In: Ruane J, Dargie JD, Mba C, Boettcher P, Makkar HPS, Bartley DM, et al. (eds) Biotechnologies at work for smallholders: case studies from developing countries in crops, livestock and fish. Food and Agriculture Organization of the United Nations, pp 109–16
14. Assis DS, Costa JRS, Gomes JBV, Tôsto SG (2003) Zoneamento agroecológico do Município de São Gabriel do Oeste, MS: referencial para o planejamento, gestão e monitoramento ambiental. Embrapa Solos – Outras publicações científicas. Embrapa Solos: IBGE, Rio de Janeiro
15. EUA-USPA (1975) Soil taxonomy. A basic system of soil classification for making and interpreting soil survey. Agriculture handbook 436.Soil Survey Staff, Washington
16. Pott A, Silva JSV (2015) Terrestrial and aquatic vegetation diversity of the Pantanal wetland. Hdb Env Chem. doi:10.1007/698_2015_352
17. Reatto A, Correia JRC, Spera ST, Martins ES (2008) Solos do bioma Cerrado: aspectos pedológicos. In: Sano SM, Almeida SP, Ribeiro JF (eds) Cerrado: ecologia e flora. Embrapa Cerrados, Brasília
18. Guerra AJT, Botelho RGM (2001) Erosão dos Solos. In: Cunha SB, Guerra AJT (eds) Geomorfologia do Brasil. Bertrand Brasil, Rio de Janeiro
19. Valeriano MM, Rossetti DF (2012) Topodata: Brazilian full coverage refinement of SRTM data. Appl Geogr (Sevenoaks, England) 32:300–309
20. Silva GB, Gomes D, Victoria DC, Vicente LE (2013) Proposta metodológica de mapeamento do uso e cobertura da terra de extensas áreas por meio de multissensores. Documentos. Embrapa Monitoramento por Satélite, Campinas
21. Batistella M, Bolfe EL, Vicente LE, Victoria DDC, Araujo LS (2013) Relatório do diagnóstico do macrozoneamento ecológico-econômico do Estado do Maranhão. Relatório Técnico: Campinas, SP, Embrapa Monitoramento por Satélite. Embrapa Cocais, São Luis

22. Silva GBS, Formaggio AR, Shimabukuro YE (2010) Áreas alteradas em função de atividades antrópicas no bioma Cerrado localizado no estado do Mato Grosso (MT), até o ano de 2001: uma abordagem espaço-temporal. Revista Brasileira de Cartografia
23. Câmara G, Valeriano DM, Vianei J(2006) Metodologia para o Cálculo da Taxa Anual de Desmatamento na Amazônia Legal. São Jose dos Campos
24. Sano EE, Lima CA, Bezerra HS (2008) Mapeamento semi-automatizado de fitofisionomias do Cerrado com imagens Landsat: vantagens e limitações. IX Simpósio Nacional sobre o Cerrado, Brasília
25. Nascimento PSR, Almeida-Filho R (1996) Utilização da técnica de segmentação em imagens TM/Landsat visando otimizar a técnica de interpretação visual. VIII Simpósio Brasileiro de Sensoriamento Remoto, Salvador
26. Gomes D, Macorano RP, Silva GBS, Vicente LE, Victoria DC (2012) Interpretação de alvos a partir de imagens de satélite de média resolução espacial. Circular Técnica. Embrapa Monitoramento por Satélite, Campinas
27. Espírito-Santo FDB (2003) Caracterização e mapeamento da vegetação da região da floresta nacional de Tapajós através de dados óticos, de radar e inventários florestais. Instituto Nacional de Pesquisas Espaciais, São José dos Campos
28. Jiang ZY, Huete AR, Didan K, Miura T (2008) Development of a two-band enhanced vegetation index without a blue band. Remote Sens Environ 112(10):3833–3845
29. Rd F, Arai E, Adami M, Ferreira AS, Sato FY, Shimabukuro YE et al (2011) Virtual laboratory of remote sensing time series: visualization of MODIS EVI2 data set over South America. J Comput Interdiscip Sci 2(1):57–68
30. Trabaquini K, Silva GBS, Formaggio AR, Shimabukuro YE, Galvao LS (2013) Dynamics and distribution of anthropic occupation in the cerrado of Mato Grosso in the period from 1990 to 2008. Geografia 38(2):209–224
31. Tricart J (1977) Ecodinâmica. IBGE – SUPREN, Rio de Janeiro
32. Bergier I, Goulart T, Monteiro H, Franco E, Rech R, Silva D, et al (2012) Fertirrigação e agricultura de baixa emissão de carbono: resultados do projeto CNPq/REPENSA em São Gabriel do Oeste. Boletim de Pesquisa e Desenvolvimento Embrapa Pantanal. Embrapa Pantanal, Corumbá
33. Buller LS, Bergier I, Ortega E, Moraes A, Bayma-Silva G, Zanetti MR (2015) Soil improvement and mitigation of greenhouse gas emissions for integrated crop–livestock systems: case study assessment in the Pantanal savanna highland, Brazil. Agric Syst 137:206–219
34. Watanabe MDB, Ortega E (2014) Dynamic energy accounting of water and carbon ecosystem services: a model to simulate the impacts of land-use change. Ecol Model 271:113–131

Natural and Environmental Vulnerability Along the Touristic "Estradas Parque Pantanal" by GIS Algebraic Mapping

Guilherme H. Cavazzana, Giancarlo Lastoria, Kennedy F. Roche, Taís G.T. Catalani, and Antonio C. Paranhos-Filho

Abstract The state roads MS-184 and MS-228 constitute the *Estradas Parque Pantanal*. Located in the northwestern portion of Mato Grosso do Sul (Brazil), in the hydrographic basin of the Paraguai River, and in the subbasins of the Negro, Miranda, and Taquari rivers, the roads cross an important area of the Pantanal in the State of Mato Grosso do Sul, in the subregions of Paraguai, Paiaguás, Nhecolândia, Abobral, Nabileque, and Miranda. Besides the strategic transportation aspect, there is ecological, cultural, scenic, and recreational potentials leading to tourism. It is an area with special interests, and the lack of data regarding environmental features motivated the study by GIS algebra mapping to consider jointly geology, geomorphology, soil and vegetation maps, information on climate, flooding areas, and land use and occupation. The obtained results are synthesized in natural and environmental vulnerability maps that indicate moderately stable/vulnerable areas tending to moderately vulnerable. The *Estradas Parque Pantanal* is undergoing ecological pressure, which means that further changes applied to the landscape can alter its "status" to vulnerable, increasing the risk of soil losses by erosion.

Keywords Algebraic mapping, Environmental vulnerability, Fauna and flora observation, GIS, Nature tourism

Contents

G.H. Cavazzana (✉), G. Lastoria, K.F. Roche, T.G.T. Catalani, and A.C. Paranhos-Filho
Faculty of Engineering, Architecture, Urbanism and Geography, Federal University of Mato Grosso do Sul, Campo Grande, MS, Brazil
e-mail: cavazzana.ea@gmail.com.br

I. Bergier and M.L. Assine (eds.), *Dynamics of the Pantanal Wetland in South America*, Hdb Env Chem (2016) 37: 209–226, DOI 10.1007/698_2014_328,

1 Introduction

The necessity to conserve natural environments is unquestionable, once their modification can compromise not only natural habitats but also the availability and quality of water resources. For this reason, the National System of Conservation Units – SNUC (*Sistema Nacional de Unidades de Conservação*, SNUC [1]) – was founded, consisting of a policy instrument for the conservation of natural environments in Brazil. In turn, the UC – *Unidade de Conservação* (Conservation Unit) – is a fundamental mechanism to warrant the survival of living creatures in terrestrial and aquatic ecosystems.

The basic objective of the Brazilian UCs of integral protection – Park category – is the preservation of natural ecosystems with large ecologic relevance and scenic beauty, permitting exclusively the indirect use of natural resources, that is, scientific research, development of activities and environmental interpretation, recreation in contact with nature, and ecologic tourism [1]. The understanding of the UC geographic space is indispensable for planning, when it is to be inserted in one of the SNUC categories. Critical areas that need intervention must be thoroughly studied in order to provide the elements for more effective actions to the area protection and control [2].

Remote sensing techniques and GIS (Geographic Information System) were used in this study, where aspects were surveyed for the characterization of a Conservation Unit in Mato Grosso do Sul named EPP – *Estradas Parque Pantanal* (Pantanal Park Roads). The data obtained in this process aided to generate natural and environmental vulnerability charts of the EPP influence areas with an associated GIS database, which is an important tool for the Management Council in scoring the roads in one of the possible classes of the SNUC system.

2 Characterization of the Study Area

The EPP is constituted by the MS-184 State Roads, from the intersection with BR-262, popularly known as *Buraco das Piranhas*, passing by *Passo do Lontra* to *Curva do Leque*, and MS-228 from *Fazenda Alegria*, passing by *Base do Morro Grande* to the intersection with BR-262, named *Lampião Aceso*, close to Corumbá City [3].

EPP stretches out for approximately 132 km; it has 91 wooden bridges, a 300-m wide lane on each side, a little more than 79 km^2 and an influence area of 5 km on each side, totalizing 1,374 km^2. It is localized in the northwestern portion of the State of Mato Grosso do Sul and crosses six subregions of Pantanal: Paraguai, Paiaguás, Nhecolândia, Abobral, Nabileque, and Miranda. It is part of the Pantanal, which is influenced by the Amazonian, *Cerrado* (savanna), Chaco, and Atlantic Forests, where fauna and flora are of rare beauty, abundance, and exuberance. The special biodiversity have acknowledged the Pantanal in 2000 by UNESCO as a "Biosphere Reserve" and "World Natural Heritage Site" [4].

EPP is inserted in the hydrographic basin of the Paraguai River in the subbasins of the Miranda, Negro, and Taquari rivers. The region is covered by four Landsat scenes, 227/073, 227/074, 226/073, and 226/074 [5–8], and three CBERS-2 scenes, 167/121, 166/121, and 166/122 [9–11], which leads to some difficulties and particularities for image processing (Fig. 1).

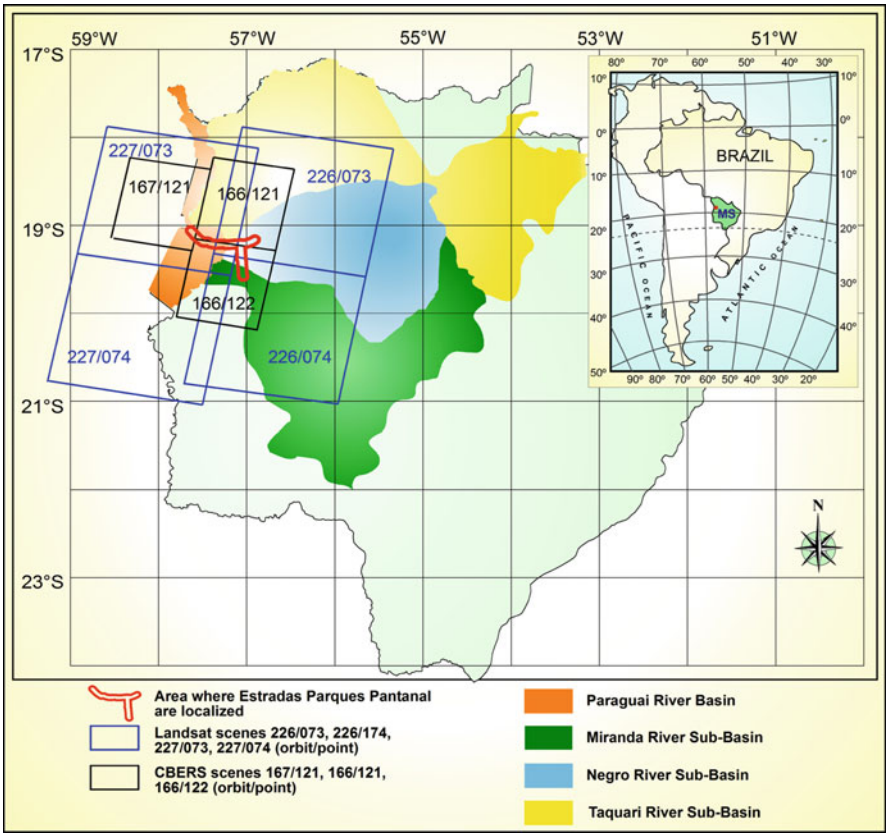

Fig. 1 Landsat and CBERS images and basins and subbasins covering the *Estradas Parque Pantanal*. Delimitation of river basins are based on SEMAC [12]

Historically, these roads, which were drawn by Marshal Cândido Rondon in the nineteenth century, are regionally important because they were the only access by land to Corumbá and Ladário up to 1986, when the MS-262 road was finally built. They are also known as *Estrada da Manga*, *Estrada da Integração*, or *Boiadeira*, the latter due to the strategic importance of the cattle production, the traditional economic activity in the region during dry and wet seasons.

EPP was ranked by the State Decree 7122, published in 17 March 1993, as the first Conservation Unit in the Pantanal in the class of "Special Area of Touristic Interest." The main reasons are the great cultural, ecologic, scenic, and recreational potentials that, in turn, provide landscape; fauna and flora beauties (Fig. 2); high touristic flow, afforded by the good infrastructure; and sport fishing.

The main objectives of this decree were (1) "to promote the touristic development, ensure the preservation and valorization of the cultural and natural heritage, (2) to fix norms for soil use and occupation, and (3) to guide allocation of resources and incentives necessary to meet the goals, regulations and guidelines of the decree." A Technical Commission composed of government and nongovernment members was installed to promote the integrated EPP management [3].

Despite its relevant importance, the region of the roads lacks studies and scientific data on its environmental structure and function, and it is hardly identified on the 1:100,000 cartographic map of the State of Mato Grosso do Sul. This study

Fig. 2 Scenic flora and fauna beauties observed in the *Estradas Parque Pantanal*. Photo credits: Guilherme Henrique Cavazzana

aims to fill the gap of information by surveying elements that characterize the natural and environmental vulnerability of the EPP area. The information is gathered by geoprocessing techniques, such as map algebra, which consists of crossing several natural and anthropic characteristics in a GIS environment with an associated database.

The results presented here can assist the EPP Technical Commission to elaborate a model for ordering and managing the area, once EPP are not under the protection of the Brazilian legislation, that is, they are not committed in any SNUC class categories [1]. This study also aims to provide a GIS tool for the handling and planning on strategic area conservation and contribute to the development of the research project that deals with the "Development of quality indicators for the Tietê/Jacaré (SP) and Miranda River (MS) hydrographic basins, for ranking and maintenance of the quality of water bodies."

3 GIS Algebra Mapping for Valuing Natural and Environmental Vulnerability

The GIS environment is a well-known and suitable method to integrate georeferenced data, information, and charts of different natures and scales so that climatic data and topographic and soil charts can be analyzed and studied as a whole. All the information obtained for a specific study is transferred to a common cartographic basis, enabling the overlay mapping and use of all relevant regional characteristics [13–15]. When GIS is associated with remote sensing images and techniques, it improves the analysis because it guarantees efficiency, speed in data acquisition, and reliability of the obtained results [2, 16]. GIS products obtained by overlay mapping techniques help to direct the studies according to vulnerability concepts or to the potentialities of environmental resources [17].

In this study, the natural vulnerability based on the stability concept was obtained by crossing layers with attributes of the geomorphologic and geologic units, soil, and vegetation. To achieve the environmental vulnerability, which reflects the human dimension on the territorial unit, the natural vulnerability map was crossed with the land-use and occupation chart. The stability concept of the territorial units that reflects the vulnerability scale to soil losses is based on Tricart's [18] Ecodynamics principles, in which values are attributed in a relative and empirical manner accordingly to the morphodynamic evolutionary stage or the morphogenesis processes (weathering) and/or pedogenesis (soil-forming processes), as shown in Table 1.

This concept is also defined as Landscape Ecology or Ecodynamics, which is contrary to an analysis of a preservationist character. It is not grounded on the assessment of the susceptibility of the landscape unit to the degradation and modification of its characteristics. As an example of this difference, a forest (dense vegetation) is vulnerable under the preservationist point of view, because

Table 1 Assessment of the stability of morphodynamic categories [19]

Morphodynamic category	Pedogenesis/morphogenesis relationship	Value
Stable	Pedogenesis prevails	1
Intermediate	Pedogenesis/morphogenesis equilibrium	2
Unstable	Morphogenesis prevails	3

it can undergo anthropic degradation, such as deforestation; regarding stability, this same unit is stable, because it contributes to the protection of the soil against erosion, rainfall, and runoff. The necessary thematic elements to analysis and interpretation are gathered, reflecting the author's personal view, which is based on his insight of the targeted ecosystem, on the available and collected information, as well as on the focus under which these data will be analyzed and interpreted, which can be either the landscape unit stability or the preservationist aspect [20].

The methodology applied to characterize natural and environmental vulnerability followed some procedures adapted from Grigio [16].

Initially it was selected subjectively the best map algebra methodologies to the EPP characteristics and the available cartographic materials. Among the map algebra methodologies [2, 14, 16], the one that fit the proposals of this study is described in Crepani et al. [19]. It considers the stability of the landscape unit in face of soil losses due to erosion and land use [21] including geomorphology, geology, pedology, and vegetation, as well as climatic characteristics, in particular the rainfall intensity. A flooding thematic chart was also added to the database, which reflects the areas susceptible to annual inundation. To obtain the environmental vulnerability chart [16], which also focuses on stability in face of erosion, the natural vulnerability chart was crossed with the theme land use and occupation.

3.1 Preliminary Survey, Acquisition, and Digital Processing of the Cartographic Material

The preliminary survey on the cartographic material was based on Cavazzana et al. [22], consisting in gathering information on location, true road axes, influence area (buffer), and soil cover. Part of the cartographic material was available in RADAMBRASIL [21], such as geology, geomorphology, and soil and vegetation charts, which were digitalized in the GIS.

Landsat-7 2002 scenes 227/073, 227/074, 226/073, and 226/074 were used to georeference the High-Resolution Imaging Camera (HRC) CBERS-2 (China–Brazil Earth Resources Satellite) 2004 and 2006 scenes 167/121, 166/121, and 166/122. Three mosaics were compiled from these scenes: (1) from the Landsat panchromatic band, (2) from CBERS-2 2004 HRC scenes, and (3) from CBERS-2 2006 scenes in false-color band combinations (RGB 4, 3, 2).

For the geometric correction and georeferencing of all charts and scenes, the UTM projection (*Universal Transverse Mercator*), *datum* SAD-69, time zone

21, was used in the Erdas Imagine software [23, 24] together with the mosaic of georeferenced Landsat scenes. The Landsat images were further georeferenced as they showed 20-m displacements in *x* and *y* directions, detected with field-validated 160 GPCs (ground points of control).

3.2 Upgrade of the Chart Vectors and Preparation of Thematic Maps

The software FreeHand [25] and plug-in Avenza MaPublisher [26] were used for geoprocessing. The procedures to feed data into the GIS environment consisted in vectorizing RADAMBRASIL [21] charts, identifying polygons topology, and preparing thematic charts. As these charts are available in the 1:1,000,000 scale, it was necessary to upgrade the vectors to obtain a better precision. Moreover, the thickness of the line polygons is ca. 0.5 mm, which corresponds to 500 m in the field. By redefining the scale, these representations became narrower and the polygon more realistic. In this procedure, the photointerpretation of the vectors representing the geology, geomorphology, and soil was carried out using the Landsat mosaic. Scale enlargement was constrained to 1:250,000 despite the database could provide a better scale.

The classification of the soil chart was upgraded according to the Brazilian System of Soil Classification [27] to the second category level. The upgrade of the vegetation chart was performed by photointerpreting the relatively most recent CBERS-2 2004 mosaic in the dry period, for which the spectral responses are very distinctive from a type of soil cover to another, making simple the upgrade of the vegetation vectors. Sixteen classes of spectral responses were used for Mato Grosso do Sul, as proposed by Paranhos Filho [28]. For the whole EPP influence area, the climate characteristics are rather similar, which resulted in the identification of a single polygon with mean rainfall intensity around 120.4 mm/month. The photointerpretation of the CBERS-2 2006 mosaic in June (flood peak) was used to the identification of areas susceptible to flooding or the flooding cone. The chart for the land use and occupation, which reflects the anthropic dimension in the EPP, was produced by adapting the soil cover chart by Cavazzana et al. [22] with the photointerpretation of the CBERS-2 2004 mosaic.

3.3 Criteria to Determine the Values in the Vulnerability Scale

Because this study relies on the principle of stability of the landscape or Ecodynamics, the criteria used for the attribution of vulnerability grades to soil losses for each theme emphasize the characteristics and parameters that are indicators of

LANDSCAPE UNIT	AVERAGE		VULNERABILITY GRADE	SATURATION GRADE RED	GREEN	BLUE	COLORS
U1	3.0		VULNERABLE	255	0	0	
U2	2.9			255	51	0	
U3	2.8			255	102	0	
U4	2.7			255	153	0	
U5	2.6		MODERATELY VULNERABLE	255	204	0	
U6	2.5			255	255	0	
U7	2.4			204	255	0	
U8	2.3			153	255	0	
U9	2.2		AVARAGELY STABLE / VULNERABLE	102	255	0	
U10	2.1			51	255	0	
U11	2.0			0	255	0	
U12	1.9			0	255	51	
U13	1.8			0	255	102	
U14	1.7		MODERATELY STABLE	0	255	153	
U15	1.6			0	255	204	
U16	1.5			0	255	255	
U17	1.4			0	204	255	
U18	1.3		STABLE	0	153	255	
U19	1.2			0	102	255	
U20	1.1			0	51	255	
U21	1.0			0	0	255	

VULNERABILITY ↑ / STABILITY ↓

Fig. 3 Vulnerability scale of the basic territorial units. Adapted from Crepani et al. [19]

morphodynamic processes and those that potentialize them; Crepani et al. [19] established 21 classes and colors depicted in Fig. 3.

The morphodynamic or denudation processes consist of a group of actions that cause the lowering of the surface by the weathering/erosion interaction. The (physical, chemical, biologic, and anthropic) operating processes, the (rock and mineral) materials involved, the weathered soil in the landscape, and the evolving time must be considered in the analysis [19].

The criteria and relevant aspects considered in a homogeneous distribution of vulnerability and stability grades are [19]:

- *Geology*: the degree of cohesion of the rocks is a preponderant factor in Ecodynamics, once for high cohesion, pedogenesis (soil formation) prevails, and for low cohesion, morphogenesis (change of relief) prevails.
- *Geomorphology*: its influence in morphodynamic processes is related to morphometric parameters (relief amplitude, declivity, and degree of dissection) because kinetic energy is transferred to runoff. For high morphometric values, morphogenetic processes prevail, while for low morphometric values, pedogenetic processes prevail.
- *Pedology*: it is characterized in Ecodynamics by means of maturity, indicating whether morphogenesis prevails, once young and poorly developed soils are generated, or pedogenesis prevails, once mature, developed, and leached soils are generated. The susceptibility to erosion (erodibility) depends on the soil structure, type and quantity of clay, permeability, depth, presence of impermeable layers, as well as the time elapsed to the soil formation.

- *Vegetation*: it protects the landscape unit against erosion by inhibiting the direct impact of raindrops on the terrain, preventing particle disaggregation (erosivity); prevents soil compaction, which would lower its capability of absorption; and increases infiltration of water in the soil, reducing runoff. The higher the density of the vegetation cover, the more pedogenesis prevails, allowing soil development and maturation; the lower the density, the more intensified are the morphogenetic processes.
- *Climate*: contrarily to vegetation, it acts against soil protection, the rainfall intensity being responsible for the definition of the risk to which the landscape unit is exposed. For high rainfall intensity, morphogenesis prevails; for low rainfall, pedogenesis prevails. Crepani et al. [19] gives the annual mean rainfall values (PMA), duration of the rainy season (DPC), and rainfall intensity (IP) for Brazil, divided in 1:250,000 charts, being EPP inserted in three with the same IP of 120.4 mm/month.
- *Flooding cone*: the weathering processes are classified as physical; it consists of the breaking of rocky material by mechanic processes, such as exfoliation and expansion, and chemical changes in the crystalline structure, in which water is the main agent and carrier of reactive products, attacks grains, and removes substances so new rock layers are exposed and weathered. Thus, the areas susceptible to flooding are vulnerable, whereas other unflooded areas are rather stable.
- *Soil land use and occupation*: it represents human interference on the landscape unit and is responsible for potentializing the natural erosion process, for representing the introduction of a new force that the unit may not be able to absorb, causing its destruction. It is represented by anthropic intervention polygons, where the more impacting activities correspond to vulnerability.

Tables 2 and 3 show the values used in the crossings representing vulnerability, based on Crepani et al. [19] methods.

Table 2 Values for the landscape vulnerability to soil land-use and occupation chart, according to methods described in Crepani et al. [19]

Land use and occupation		
Landscape unit	Symbol	Vulnerability degree
Forest	Mat	1.0
Savanna (*Cerrado*)	Cer	1.5
Pasture	Pas	2.6
Humid area	Um	2.4
Lagoons	Lag	2.0
Reflective	Ref	2.8
Roads and gas pipeline	ReG	2.8
Mining site	Min	3.0
Agricultural settlement	Ass	2.6

Table 3 Values for the landscape vulnerability defined to thematic charts according to the interpretations and adaptations after Crepani [19]

Landscape unit	Symbol	Vulnerability
Geology		
Tamengo Formation	pEta	2.8
Bocaina Formation	pEbo	2.9
Santa Cruz Formation	pEsc	2.6
Urucum Formation	pEu	2.5
Rio Apa Complex	pEra	1.2
Present alluvia	Ha	3.0
Pantanal Formation	Qp	3.0
Xaraiés Formation	Qc	2.8
Detríticos Formation	Qd	2.8
Detríticos Formation with iron fragments (mf)	Mf	3.0
Geomorphology		
Tabular structural surface, plained surface, limited by escarpments, structural above 100 m	St	2.5
Acute forms, order of magnitude from 250 to 750 m, and weak drainage deepening	Urucum a22	2.0
Convex forms, order of magnitude from 150 to 750 m, and weak drainage deepening	Urucum c21	1.8
Tabular forms, very weak order of magnitude, and drainage deepening between 250 and 750 m	Urucum t21	1.8
Tabular forms, very weak order of magnitude and drainage deepening between 250 and 750 m, fault escarpment above 100 m on the left-hand side	Urucum t21 Escarpment	1.8
Tabular forms, order of magnitude from 250 to 750 m and very weak drainage deepening, asymmetric crest above 100 m on the left-hand side	Urucum t21 Crest	1.8
Tabular forms, weak order of magnitude and drainage deepening between 250 and 750 m	Urucum t22	2.0
Pediplained surface	Ep	1.0
Inundated pediplain	Epi	1.5
Potential flooded area, humid, average floods	Aai2	1.0
Potential flooded area, very humid, intense floods	Aai3	1.0
Fluvial–lacustrine plain	Apfl	1.5
Pedology		
Ferriluvic spodosols	ES	2.0
Argiluvic chernosols	MT	2.0
Haplic planosols	SX	2.0
Haplic gleysols	GX	3.0
Litholic neosols	RL	3.0
Quartzemic neosols	RQ	3.0
Ebanic vertisols	VE	3.0

(continued)

Table 3 (continued)

Landscape unit			Symbol	Vulnerability
Vegetation				
Seasonal semideciduous florest, alluvial, emergent canopy			Fae	1.6
Seasonal deciduous florest, low lands			Cb	2.2
Seasonal deciduous florest, submontane			Cs	2.2
Dense arboreal savanna			Sd	1.7
Savanna park with no gallery forest			Sps	2.5
Grassy–woody savanna with no gallery forest			Sgs	2.7
Grassy–woody steppic savanna with gallery forest			Tgf	2.7
Flooding cone				
Areas susceptible to flooding			Inund	3.0
Areas not susceptible to flooding			N_Inund	1.0
Climate				
Reference index map	PMA (mm)	DPC (month)	IP (mm/month)	Vulnerability
430	1,000.0	8.7	115.9	1.3
443	1,176.8	9.0	115.7	1.3
444	1,226.8	9.5	129.6	1.3

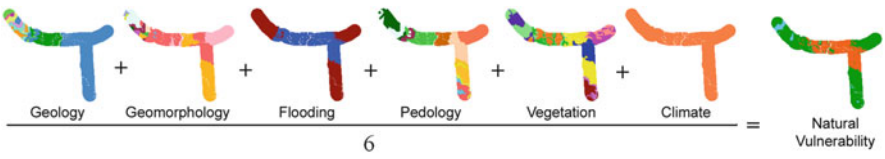

Fig. 4 Map algebra performed to obtain natural vulnerability values

3.4 *Crossing of Thematic Maps*

After defining stability values for the territorial units, theme crossings were performed using PCI Geomatica software [29]. The first crossing was performed to prepare the natural vulnerability chart by adding the vulnerability values of the territorial units of the geology, geomorphology, pedology, vegetation, climate, and flooding cone thematic charts and then dividing the sum by 6, which corresponds to an arithmetic mean, as represented in Fig. 4.

The second crossing involved the natural vulnerability chart and the soil land-use and occupation chart; the former weighed 0.60 and the latter 0.40 (Fig. 5), resulting in the environmental vulnerability chart. The reason for this is that in EPP there is no predominance of anthropic influence, thus evidencing the natural characteristics of the landscape units. Besides, this weighing resulted in a coherent representation of the reality verified in the field.

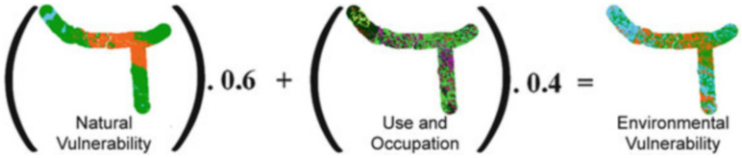

Fig. 5 Map algebra performed to obtain the environmental vulnerability

4 GIS Algebraic Mapping Results

The obtained results were upgraded charts 1:250,000 of the geology, geomorphology, pedology, and vegetation themes, as well as the flooding cone and soil land-use and occupation charts. Moreover, natural and environmental vulnerability charts were also produced, which configure the main results of this study.

Considering the geology vulnerability (Fig. 6a), the EPP area is 92.2% vulnerable, 3.8% moderately vulnerable, and 3.0% stable. The rivers occupy 1% of all thematic charts. The rocks that occur in most parts of the EPP show low cohesion, such as limestones, shales, sandstones, siltites, conglomerates, and unconsolidated sediments. Therefore, the regional geology has a significant influence on the morphogenetic processes that change the relief.

The geomorphologic chart (Fig. 6b) evidenced that the area is 65.9% stable, 27.1% moderately stable, 5.6% averagely stable/vulnerable, and only 0.4% moderately vulnerable. Geomorphology plays an important role in soil formation processes, once the majority of the morphometric indices of the road area of influence indicate low dissection intensities, altimetric amplitude, and declivity, which prevent runoff.

Figure 6c presents a chart with the new soil classification by Embrapa [27]. There is a higher tendency for morphogenetic processes as 54% of the area is vulnerable and 45% is averagely stable/vulnerable. Hence, the majority of the soils covering the EPP area have high erodibility because they are critically developed and the soil profile has not fully evolved. Source materials have been recently deposited under the influence of floods.

The vegetation chart (Fig. 6d) evidences the favoring of processes that modifies the relief because 41.5% of the area is vulnerable. The low-density covers expose the soil and neither prevent raindrops from directly affecting the soil nor reduce the runoff kinetic energy. On the other hand, 18.3% of the area is moderately vulnerable, 20.6% averagely stable/vulnerable, and 18.6% moderately stable.

The climatic conditions found in the three 1:250,000 charts are characterized by low rainfall intensity, averaging 120.4 mm/month. This confers stability to the EPP because rainfall erosivity is low. Regarding the flooding cone (Fig. 7a), 44.5% of the flooded area undergoes chemical weathering for ca. 4 months, from June to September; morphogenetic processes are potentialized, once water acts as a reagent in the rock minerals. On the other hand, 54.5% of the area is not flooded and is consequently stable to inundation and chemical weathering.

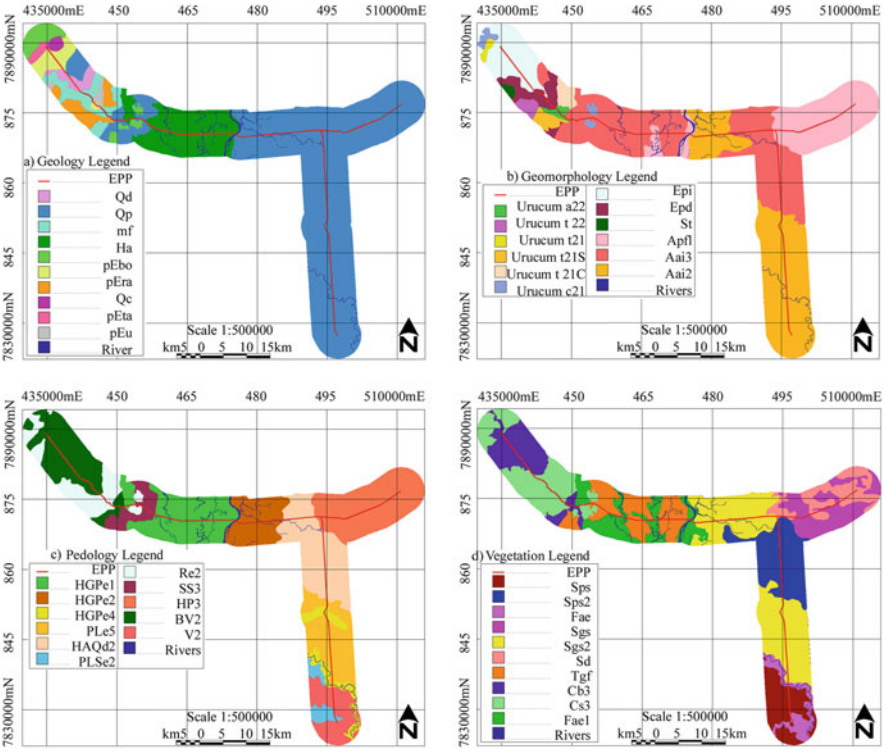

Fig. 6 Geologic (**a**), geomorphologic (**b**), pedologic (**c**), with scale and classification upgraded according to Embrapa [27], and vegetation (**d**) charts from the RADAMBRASIL Project [21] with upgraded scale

The GIS algebraic crossing of the themes depicted in Figs. 6a–d to 7a using the arithmetic mean produced the natural vulnerability chart in Fig. 7b that represents the risk of soil losses by erosion. 62.6% of the region is averagely stable/vulnerable, 32.5% moderately vulnerable, and only 3.8% moderately stable. These result from the fact that three themes have more influence on morphogenesis, whereas other three are influenced by pedogenesis. Nonetheless, the processes that modify the relief predominate due to the prevailing of low-cohesive rocks, the young nature of the soils, and the scary vegetation cover. It is noteworthy that there are no vulnerable or stable areas in the region and that the majority of the moderately vulnerable areas occur in areas susceptible to flooding.

The anthropic influence in the EPP area is low, but it highly affects the landscape. Further to mining, cattle raising, asphalted roads, gas pipeline, and agricultural settlements, there are areas that were so degraded that presently are devoid of natural vegetation cover, herein referred to as reflective areas.

Mining is the most impacting activity in the western EPP, an elevated region locally known as "Morraria" (Fig. 8). Four mining companies exploit iron ore: MMX, EBX, Pirâmide, and Vale – Urucum. The latter also exploits manganese ore.

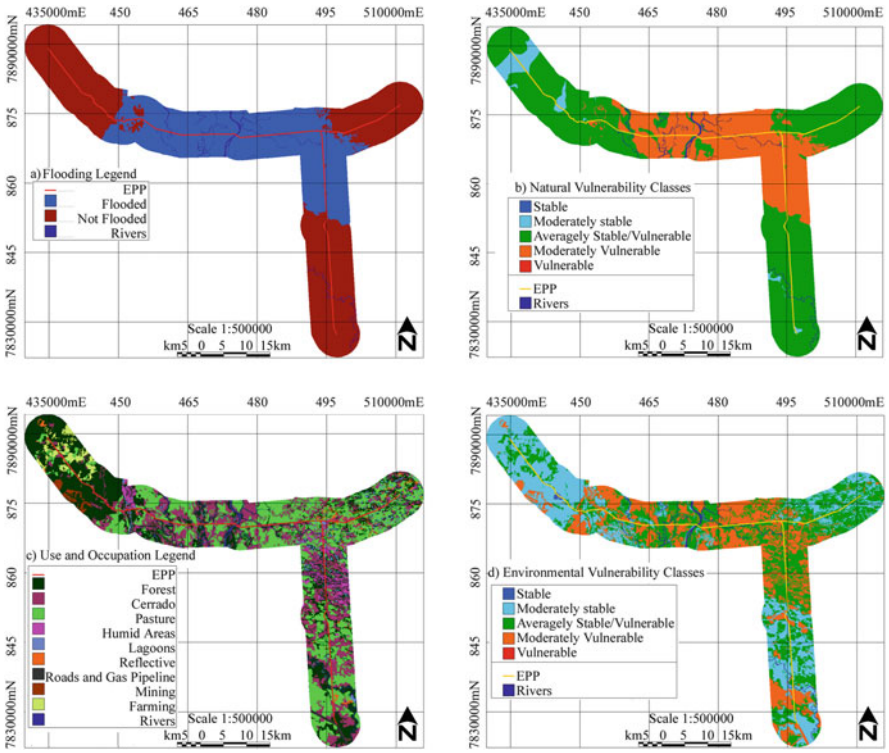

Fig. 7 Chart of the flooding cone for the areas susceptible or not to flooding (**a**). Natural vulnerability chart for the *Estradas Parque Pantanal* (**b**). Soil land-use and occupation chart adapted from Cavazzana et al. [22] (**c**). Environmental vulnerability chart for the *Estradas Parque Pantanal* (**d**)

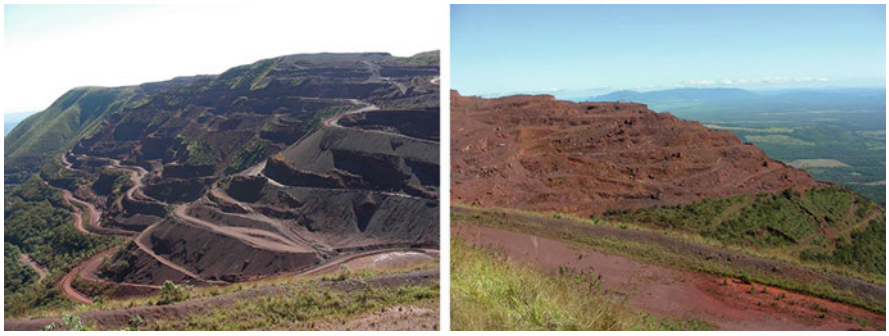

Fig. 8 Mining activities in the EPP influence area in 2008. Photo credit: Giancarlo Lastoria [30]

The environmental aggression it inflicts is evident, despite that mining companies operate to minimize the impacts of its own activities. They have to compromise with the government to recover the natural landscape as similar as possible to pristine conditions when activities are dismissed in the long term.

Natural pastures (Fig. 9) occupy a great portion of EPP, associated with cattle raising, causes degradation, soil compaction and creation of routes and grooves favorable to water discharge. The introduction of exotic pastures unadapted to flooding and soil exposed for a certain period increases the vulnerability of EPP.

Other types of human interference occupy smaller areas, but the relevance is the same. Roads and gas pipelines can be impacting factors due to quarries and the risk to the UC in the case of automotive accidents or gas leakage. The agricultural settlements occupy the western portion of EPP, where seasonal cultures are cultivated, and the soil is eventually exposed throughout the year. Areas uncovered and reflective (Fig. 10) also occur close to *Curva do Leque* and *Lampião Aceso*.

The soil land-use and occupation chart is presented in Fig. 7c, evidencing that 2.7% of the area is vulnerable, 39.1% moderately vulnerable, 2.3% averagely stable/vulnerable, and 54.9% moderately stable and stable. This explains the weight of 60% for natural vulnerability and 40% for soil land use and occupation, once only 4.9% of the area is effectively occupied by people (mining, road, gas pipelines, and agricultural settlement) and the area for pasture is not fully addressed to raising cattle.

Fig. 9 Examples of pasture in the EPP influence area. Photo credits: Guilherme Henrique Cavazzana

Fig. 10 Uncovered reflective areas in the EPP surrounding region. Photo credits: Guilherme Henrique Cavazzana

It is important to highlight that under the preservationist point of view, the forest and savanna units, which were not the focus of this study, can be vulnerable because of the pressure of the coal industry that supplies the iron industry in Corumbá – MS. The aforementioned companies have constitutional right of using vegetal coal for 10 years. Another fact is the increasing needs of minerals in the internal and external markets due to globalization. There is also the discussion on the production of sugarcane for ethanol fuel and sugar in Pantanal.

Crossing the natural vulnerability with the soil land use and occupation led to the environmental vulnerability chart (Fig. 7d), which is the second main result of this study. This chart reflects the anthropization degree in the surrounding areas of EPP and its potential in soil losses by erosion. The region presents 40.9% of averagely stable/vulnerable area, 31.9% of moderately stable area, 26.1% of moderately vulnerable area, and only 1.2% of stable area. This result suggests that under the environmental view, EPP are more stable naturally, that reflects the preferential location in relatively stable areas while soil occupation, such as forest, savanna, and lagoons. There are no vulnerable areas in the region, the majority of the moderately vulnerable areas occur in areas susceptible to flooding and pastures, and people minimally occupy the stable and moderately stable areas.

5 Concluding Remarks and Recommendations

The surrounding area of EPP is constituted naturally and environmentally by averagely stable/vulnerable areas, tending to moderately vulnerable. It can be concluded that they are in ecologic tension, that is, any alteration of the landscape unit can change its "status" to vulnerable, increasing the risk of soil loss by erosion. Besides, as human occupation density increases, the weights used to cross the themes' natural vulnerability and soil use and occupation (40 and 60%, respectively) should be revised.

For new interventions in the EPP area, it is recommended to check the natural vulnerability chart rather than the environmental vulnerability chart. This is because the natural condition of the landscape unit must be checked and crossed again with new available data of soil land use and occupation.

To achieve the sustainable development, it is necessary to study the natural landscape, the interference degree, and the potentialization of the erosion processes that the anthropic intervention causes to these units. This allows to:

- Plan the activities to be engaged in EPP.
- Protect the natural landscape unit from aggressions above its carrying capacity.
- Promote remedial actions on areas where soil land use and occupation are inadequate or leading to land instabilities.

It is desirable that cattle owners take preventive actions as the use of preservationist practices respecting native vegetation. Furthermore, public agencies should intensify the control of coal mining and deforestation.

The GIS database and products of this study are a useful tool to managing and zoning for the conservation and control of EPP. It can also be an instrument to assist several studies in the region, such as the identification of main environmental problems, as those cited by Adámoli [31].

Acknowledgments To CAPES for GHC Masters scholarship and to CNPq for ACPF Research scholarship (process 305300/2012-1).

References

1. BRASIL (2000) Lei Federal n° 9.985, de 18 de julho de 2000. Regulamenta o art. 225, § 1°, incisos I, II, III e VII da Constituição Federal, institui o Sistema Nacional de Unidades de Conservação da Natureza – SNUC e dá outras providências. Publicada no Diário Oficial da União de 19 de julho de
2. Carrijo MGG (2005) Vulnerabilidade ambiental: o caso do Parque Estadual das Nascentes do Rio Taquari – MS. Dissertação de Mestrado, UFMS, Campo Grande
3. Mato Grosso do Sul (1993) Decreto Estadual n° 7.122 de, 17 de março de 1993
4. RBMA (2000) Conselho Nacional Reserva da Biosfera da Mata Atlântica. Pantanal torna-se patrimônio da humanidade. **Notícias RBMA nº 13**. São Paulo, novembro 2000. http://www.rbma.org.br/rbma/noticias_boletim_rbma.asp
5. LANDSAT (2002) ETM+ 7. Canais: 1, 2, 3, 4, 5, 7 e pan. São José dos Campos: Instituto Nacional de Pesquisas Espaciais. Imagens de satélite. Órbita 227 ponto 073. CD-ROM. 19 de setembro de 2002
6. LANDSAT (2002) ETM+ 7. Canais: 1, 2, 3, 4, 5, 7 e pan. Curitiba: Engesat. Imagem de Satélite. Órbita 227 ponto 074. CD-ROM. 28 de Abril de 2002
7. LANDSAT (2002) ETM+ 7. Canais: 1, 2, 3, 4, 5, 7 e pan. Curitiba: Engesat. Imagem de Satélite. Órbita 226 ponto 073. CD-ROM. 8 de June de 2002
8. LANDSAT (2002) ETM+ 7. Canais: 1, 2, 3, 4, 5, 7 e pan. São José dos Campos: Instituto Nacional de Pesquisas Espaciais. Imagens de satélite. Órbita 226 ponto 074. CD-ROM. 24 de June 2002
9. Instituto Nacional de Pesquisas Espaciais (INPE) (2004) Imagem CBERS 2. Sensor CCD. Canais 1, 2, 3, 4 e pan. São José dos Campos: Instituto Nacional de Pesquisas Espaciais. Imagem de Satélite. Órbita 167 ponto 121. De 4 de setembro de 2004. http://www.cbers.inpe.br/pt/index_pt.htm
10. Instituto Nacional de Pesquisas Espaciais (INPE) (2004) Imagem CBERS 2. Sensor CCD. Canais 1, 2, 3, 4 e pan. São José dos Campos: Instituto Nacional de Pesquisas Espaciais. Imagem de Satélite. Órbita 166 ponto 121. De 28 de outubro de 2004. http://www.cbers.inpe.br/pt/index_pt.htm
11. Instituto Nacional de Pesquisas Espaciais (INPE) (2004) Imagem CBERS 2. Sensor CCD. Canais 1, 2, 3, 4 e pan. São José dos Campos: Instituto Nacional de Pesquisas Espaciais. Imagem de Satélite. Órbita 166 ponto 122. De 28 de outubro de 2004. http://www.cbers.inpe.br/pt/index_pt.htm
12. SECRETARIA DE ESTADO DE MEIO AMBIENTE, DO PLANEJAMENTO, DA CIÊNCIA E TECNOLOGIA E INSTITUTO DE MEIO AMBIENTE DE MATO GROSSO DO SUL (SEMAC) (2010) **Plano estadual de recursos hídricos de Mato Grosso do Sul**. UEMS, Campo Grande, MS, p 194
13. Tomlin CD (1983) A map algebra. In: Proceedings of the 1983 Harvard Computer Graphics Conference, Cambridge, MS

14. Barbosa CC, Camara G, de Medeiros JS, Crepani E, Novo E, Cordeiro JPC (1998) Operadores zonais em álgebra de mapas e sua aplicação a zoneamento ecológico-econômico. In: IX Simpósio Brasileiro de Sensoriamento Remoto. Anais do IX Simpósio Brasileiro de Sensoriamento Remoto, Santos, Brasil, 11–18 setembro 1998, INPE, pp 487–500. http://marte.dpi.inpe.br/col/sid.inpe.br/deise/1999/02.08.11.17/doc/7_166o.pdf
15. Paranhos Filho AC, Fiori AP, Disperati L, Lucchesi C, Ciali A (2003) e Lastoria, G. Avaliação multitemporal das perdas dos solos na Bacia do Rio Taquarizinho através de SIG. Boletim Paranaense de Geociências, UFPR, Curitiba, PR, n 52, pp 49–59
16. Grigio AM (2003) Aplicação de sensoriamento remoto e sistema de informação geográfica na determinação da vulnerabilidade natural e ambiental do município de Guamaré (RN): simulação de risco às atividades da indústria petrolífera. Natal – RN. Master Dissertation, Universidade Federal do Rio Grande do Norte, Natal
17. Cunha SB, Guerra AJT (2000) Avaliação e perícia ambiental. Rio de Janeiro, Bertrand Brasil, p 294
18. Tricart J (1977) Ecodinâmica. IBGE, Diretoria Técnica, Superintendência de Recursos Naturais e Meio Ambiente (SUPREN), Rio de Janeiro, p 91
19. Crepani EM, de Medeiros JS, Filho HP, Florenzano TG, Duarte V, Barbosa CCF (2001) Sensoriamento remoto e geoprocessamento aplicados ao zoneamento ecológico-econômico e ao ordenamento territorial. São José dos Campos – INPE (INPE-8454-RPQ/72), p 124
20. Tagliani CRA (2002) Técnica para avaliação da vulnerabilidade ambiental de ambientes costeiros utilizando um Sistema Geográfico de Informação. Galeria de artigos acadêmicos. http://www.fatorgis.com.br
21. RADAMBRASIL (1982) Ministério das Minas e Energia. Secretaria Geral. Folha SE. 21: Corumbá: geologia, geomorfologia e pedologia. Levantamento de Recursos Naturais, 27. Rio de Janeiro, 1982, p 452, il 4 maps
22. Cavazzana GH, Lastoria G, Paranhos Filho AC, Torres TG, da Ferreira TS, Oliveira JMZPS (2005) Identificação da cobertura de solo das Estradas Parque Pantanal. In: IV Simpósio Brasileiro de Engenharia Ambiental. Ribeirão Preto - SP. Abstracts IV SBEA. Ribeirão Preto
23. Erdas Inc. (1997) Erdas imagine version 8.3.1. Erdas Inc., Atlanta, Georgia. 1 CD ROM
24. Erdas Inc. (1997) Erdas field guide, 4th edn. Erdas Inc., Atlanta, Georgia, p 656
25. Macromedia (2000) In. FreeHand version 9. Macromedia Inc. San Francisco – California. February 2000. 1 CD-ROM
26. Avenza Systems Inc. (2001) MaPublisher version 4.0, for Macromedia FreeHand User, for Windows and Macintosh Avenza Systems Inc. 2000–2001. Colorado USAhb
27. Embrapa S (2006) Sistema brasileiro de classificação de solos. Embrapa-SPI; Rio de Janeiro: Embrapa Solos, Brasília, DF, p 412
28. Paranhos Filho AC (2000) Análise geo-ambiental multitemporal: o estudo de caso da região de Coxim e Bacia do Taquarizinho. PhD Thesis, UFPR, Curitiba, p 213
29. PCI GEOMATICS (2003) In: PCI Geomatica version 9.1. PCI Geomatics, Richmond Hill, Ontario, Canada, 1 CD-ROM
30. Lastoria G (2008) Fotos obtidas em visita dos alunos do Programa de Pós-Graduação em Tecnologias Ambientai da Universidade Federal de Mato Grosso do Sul às mineradoras Urucum – Vale e Rio Tinto, Corumbá, MS
31. Adámoli J (1995) Diagnóstico do Pantanal: características ecológicas e problemas ambientais. Programa Nacional do Meio Ambiente, Brasília, p 50

Climate Change Scenarios in the Pantanal

Jose A. Marengo, Gilvan S. Oliveira, and Lincoln M. Alves

Abstract The South America Pantanal is a large floodplain wetland in the center of the Upper Paraguay River Basin, which has a total area of around 360,000 km^2. Large sectors of the Pantanal floodplain are submerged from 4 to 8 months each year by water depths from a few centimeters to more than 2 m. Changes in rainfall and temperature and also on land use can affect significantly the flood season with severe consequences for downstream inhabitants. However, impact of climate change on wetlands is small so far compared to the damage caused by the lack of management at the local level due to land-use change. In this chapter we assess climate and hydrology variability for the present and projections of climate change using the global climate models from the Fifth Assessment Report (AR5) from the Intergovernmental Panel on Climate Change (IPCC). Projections show that by the end of the century, temperatures can increase up to 7°C and rainfall can decrease in both summer and particularly winter. The possibility of longer dry spells and increased evaporation may affect the water balance in the region. However, uncertainties on climate projections are still high, particular for rainfall.

Keywords Climate change, Drought, Flood, Uncertainty, Wetland

J.A. Marengo (✉)
CEMADEN, Rodovia Presidente Dutra, km 39, Cachoeira Paulista, São Paulo 12630-000, Brazil
e-mail: jose.marengo@cemaden.gov.br

G.S. Oliveira and L.M. Alves
CCST INPE, Rodovia Presidente Dutra, km 39, Cachoeira Paulista, São Paulo 12630-000, Brazil

I. Bergier and M.L. Assine (eds.), *Dynamics of the Pantanal Wetland in South America,* Hdb Env Chem (2016) 37: 227–238, DOI 10.1007/698_2015_357,

Contents

1 Introduction

The South America Pantanal is a large floodplain wetland in the center of the Upper Paraguay River Basin, which has a total area of around 360,000 km^2. The Pantanal spreads for about 140,000 km^2 and is shared among Brazil (80%), Bolivia (19%), and Paraguay (1%). During the summer rainy season (November–March), the rivers overflow their banks and flood the adjacent lowlands, forming shallow lakes and innumerable swamps and marshes and leaving island-like areas of higher ground that inundates as much as 70% of the floodplain until July. Large sectors of the Pantanal floodplain are submerged from 4 to 8 months each year by water depths from a few centimeters to more than 2 m. During the drier winter season (April–September), the rivers withdraw into their banks, but the lowlands are only partially drained. The water leaves via the Paraguay River and eventually into the Paraná River, leaving behind grasslands that support grazing animals.

The Pantanal functions as a large reservoir that stores water from the surrounding plateaus during the rainy season and then delivers it slowly to the lower sections of the Paraguay River, delaying for almost 6 months the maximum flows to the Paraná River, thereby minimizing downstream flooding. As a result, any significant change in the rainfall pattern is likely to have major impacts on the local ecology and socioeconomic relations. The peak flood season for the lower Paraná River basin is 2–3 months earlier than the flood season for the Upper Paraguay River. Without the Pantanal, the two flood seasons would be simultaneous, with severe consequences for downstream inhabitants. Conversely, during dry seasons, the Pantanal continuously releases water, meaning that there is more water available downstream when it is needed most.

Climate change is expected to have serious impacts on the Pantanal, and a range of institutional responses has been developed to mitigate and adapt to climate change [1]. While anthropogenic climate change is expected to have serious socioecological consequences around the globe, in particular for wetland areas, land-use changes also can affect climate and hydrology in the region [2]. The impact of climate change on wetlands is small so far compared to the damage caused by the lack of management at the local level. Lessening the stress on wetlands caused by pollution and other human assaults will improve their resiliency and represents an important climate change adaptation strategy.

2 Climate and Hydrology in Pantanal

The Pantanal is located in a tropical and damp climate zone. The average air temperature is 24°C. The Pantanal is a semiarid region. The annual amount of rain is 1,000–1,250 mm, which corresponds to 67–83% of the rain in the neighboring areas in the states of Mato Grosso and Mato Grosso do Sul. Rainfall shows interannual variability with higher or lower rainwater amounts that have caused either severe floods or drastic dry seasons, influencing the flooding. Large-scale climate phenomena such as El Niño, La Niña, or the variability associated to the Atlantic Ocean as well as regional-scale water balance and soil wetness and soil moisture storage influence the seasonality of floods and droughts in the Pantanal [3].

Although the annual temperature value is relatively constant, the temperature sometimes drops down as far as to −1°C or rises as far as to 41°C. The reason for these thermal contrasts is a north-to-south shift in the air currents between the Andes in the west and the Central Brazilian Plateau in the east. In winter (June, July, and August), this corridor channels the cold winds streaming from cold fronts moving northward and thus causes a distinct temperature drop (called "friagem" in the Pantanal). Sometimes this phenomenon can be experienced up to five times a year, while in some years it does not occur at all. This cooling reaches as far as the Amazon valley. One such instance was in July 1975, when the Brazilian west experienced the "chill of the century": cold, dry winds blew across the Pantanal at a speed of 40 km/h and the temperature dropped to 0°C in one night [4].

Interannual rainfall variability with higher or lower rainfalls has caused either severe floods or drastic dry seasons. Marcuzzo et al. [5] and Cardoso and Marcuzzo [6] analyzed the monthly trends in precipitation from 1977 to 2006 from 12 rain gauge stations in Brazilian Pantanal. They noticed a moderate decrease in precipitation and a high interannual variability in this region. They showed a gradual decrease for precipitation from decade 1977 to 1986 to decade 1997 to 2006. Garcia and Pedraza [7] analyzed the temporal variation in the total number of days a year with rainfall and the number of days a year with rainfall above the 100 mm threshold at the rain-gauging stations in northeastern Argentina. The results show an increase in both the frequency of daily rainfall, especially during the winter season, and the frequency of days with heavy rainfall starting in the early 1970s.

According to Alho and Silva [8], El Niño and La Niña influence the seasonality of floods and droughts in the Pantanal. Furthermore, the role of land surface processes on the hydrology of Pantanal is highlighted by Clarke et al. [9]. In this regard, Collischonn et al. [10] assessed the flow records from the rivers Paraguay, Paraná, Negro, and Uruguay in the La Plata Basin and rainfall records from other parts of South America. They found strong evidence of changes in the runoff regime of the La Plata Basin during the last 40 years, not all of which can be attributed to land-use change. This increase in annual precipitation in the last 40 years has been more than 10% over most of the region, but in some places it has reached 30% or more [11, 12].

Analysis of the 105-year record of annual flood peaks at Ladário, downstream of the Pantanal wetland, shows strong evidence of serial correlation between flood peaks in successive years, and the sequence of annual flood peaks is well represented by a lag-one autoregression [9]. He found that no direct relation could be established between Ladário flood peaks and the limited records of Pantanal rainfall, nor did there appear to be any relation between Ladário flood peaks and El Nino/La Nina events. The large volume of natural storage within a drainage basin has a marked effect on its regime of hydrologic extremes. This is somewhat responsible for the lower climate predictability on the region, since soil moisture and natural water storage are still not well represented on climate models.

Alho and Silva [8] show that during the period from 1962/1963 to 1972/1973 in the Pantanal, it was unusually dry (see also Assine et al. [13]). This was then followed by a long wet period, which has lasted until the present day. During the 11-year dry period, there were no records of flooding, except for 1965–1966, when 16 cm of water was observed above the zero mark (82.4 m in relation to sea level), and the majority of the flooding peaks were observed between 1 and 2 m. Since 1973/1974, the Pantanal has been experiencing a period of inundations, with the flood gauge reaching its peak at Ladário in 1988, with a 6.64 m reading. This was considered the Pantanal's greatest-ever inundation. This flood period, which has already lasted for 38 years, is the longest recorded for the region and is different from the previous periods in that the phreatic water (the upper surface of the soil that forms the water table) has risen throughout the entire year, which results in lower intra-annual and interannual variation in droughts and floods. Furthermore, the position of the average river watermark has remained between 3 and 4 m and the minimum mark between 1 and 2 m for the greater part of the year.

According to Goncalves et al. [14], the year with the most memorable floods due to high Paraguay River levels was 1988. During the record flow in 1988, about 95% of the Pantanal plain was flooded. The Ladário station registered, during the outflow of 2007, one of the lowest minimum levels of the last 34 years, that is, 88 cm on 3 November 2007. A dry period between 2010 and 1012 showed 85 cm water level; however, the lowest record was in 1964–1973 with 75 cm. In accordance with the classification by Galdino et al. [15], the flood in the hydrologic period 2007–2008, as well as the floods of the two previous years, may be considered "normal," that is, when the maximum water level in Paraguay River ranges between 5.00 and 5.99 m in Ladário. According to Fantin-Cruz et al. [16], the highest flood was that of 1995 when the floodplain was flooded to a mean depth of 2.56 m. The median flood event (return period 2 years) produced a mean flood depth 1.80 m and lasted 119 days.

Knowledge of severe floods and droughts, which characterize natural disasters in the region, is fundamental for wildlife management and nature conservation of the Pantanal. Plants and wild animals, for example, are affected by tree mortality in riparian forest after extreme flooding, with consequent habitat modification for wild animals. In addition, human activities are also affected since cattle ranching and ecotourism are economically important in the region, and when seasons with unusual floods or droughts occur, areas with human settlements are impacted.

3 Assessment of Climate Change Projections for Pantanal from Global Models

Various studies analyze climate projections data from IPCC Fourth Assessment Report (AR4) and from downscaling experiments using various regional models forced with some of the IPCC AR4 models. The CMIP3 (Coupled Model Intercomparison Program Version 3) represents an archive from all IPCC AR4 models. Some downscaling experiments have been run for various SRES (Special Report Emission Scenarios), among them A2-high emission and B2-low emission, that represent high and low emissions. The projections for the A2 scenario suggest an increase in temperature of the order of 3.5–4.5°C by the end of the twenty-first century, with decreases in the number of cold nights during winter months and decrease in precipitation between 35% and 45%, with an increase in the frequency of consecutive dry days for the entire region [17–20].

For the Pantanal climate change scenarios, we assess the projections from IPCC models used on the Fifth Assessment Report (AR5), stored at the CMIP5 archive. For the IPCC AR5 model runs, the scenario used is the RCPs *Representative Concentration Pathways* [21] that have replaced the SRES. The RCPs represent radiative forcing, where the RCP2.6 represents a scenario with low emissions and low radiative forcing (similar to SRES B1 or B2). The RCP8.5 represents a larger radiative forcing and is similar to a high emission scenario (SRES A1 or A2).

A comparison between the warming projected by 2100 derived from the SRES scenarios used in IPCC AR4 and the RCPs used in the IPCC AR5 is shown in Fig. 1.

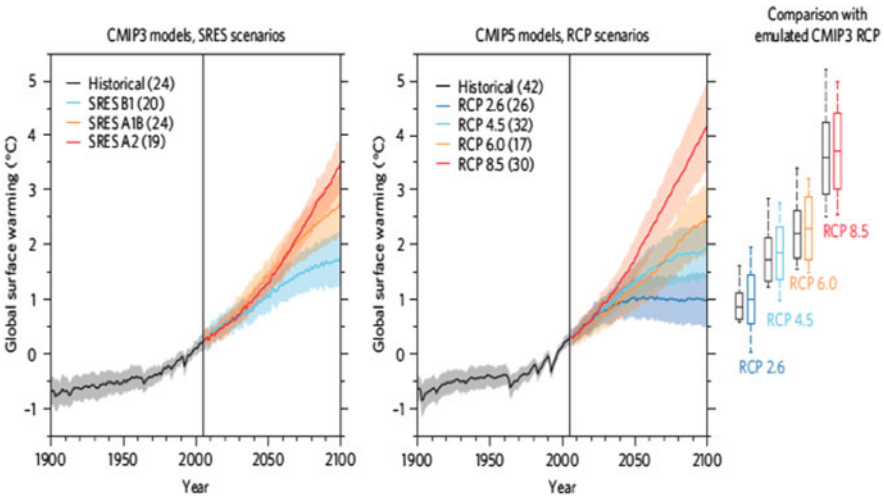

Fig. 1 Changes in mean temperature (*color lines*) and uncertainties (*shades*) relative to 1986–2005 for the SRES IPCC AR4 (*left*) and RCPs of IPCC AR5 (*right*). The number of models is indicated in parenthesis. The *boxes on the right side* of the panel show the mean and the *whiskers* show the standard deviation on the projected warming by 2100 for each scenario [22]

Table 1 List of CMIP5 global models used on this report, showing horizontal resolution (latitude/longitude). The models are organized according to their horizontal resolution [23]

Model	Resolution (latitude/longitude)
CanESM2	2.8° × 2.8°
MIROC-ESM	2.8° × 2.8°
GFDL-ESM2M	2.0° × 2.5°
IPSL-CM5A-LR	1.9° × 3.8°
NorESM1-M	1.9° × 2.5°
CSIRO-Mk3-6-0	1.9° × 1.9°
MPI-ESM-LR	1.9° × 1.9°
CNRM-CM5	1.4° × 1.4°
MIROC5	1.4° × 1.4°
HadGEM2-ES	1.3° × 1.9°
MRI-CGCM3	1.1° × 1.1°
CCSM4	0.9° × 1.3°

The similarities between SRES and RCPs scenarios can be noted, and by 2100 the RCPs seem to show the highest warming.

The CMIP3 and CMIP5 model output is available from the data archives of the Program for Climate Model Diagnosis and Intercomparison (PCMDI, http://www-pcmdi.llnl.gov) and the Earth System Grid data distribution portal (ESG, http://www.earthsystemgrid.org).

Climate changes simulated in the CMIP3 and CMIP5 ensembles are not directly comparable because of the differences in prescribed forcing agents (e.g., CO_2 and aerosols) between the SRES and RCPs scenarios. Furthermore, the models may respond differently to a specific radiative forcing due to different model-specific climate sensitivities. However, based on the underlying radiative forcing (or CO_2 concentrations), one can compare projected changes in the temperature and precipitation indices and provide an estimate of uncertainty related to the different emission scenarios.

In the following the assessed projections of changes in summer and wintertime temperatures and rainfall from the IPCC AR5 models are shown in Table 1 and consider the RCP8.5 only. Figure 2 shows warming between 4°C and 7°C for the Pantanal region for both summer and winter, and while all months agree in the warming for the 2071–2100, some models have shown warming of up to 10°C and other shows warming between 3°C and 4°C.

For rainfall changes, Fig. 3 shows that in December–February (DJF) summer season, the model ensemble show changes between −10 and +10%, and while some models show increase of about +25%, others reduction between 20% and 30%, suggesting large uncertainties in the rainfall projections. During the austral winter June–August (JJA), the model ensemble suggest rainfall reductions between 30% and 40%, but there is still low consensus, since some models show reductions of the order of 60% and others show increase of about 70%. Therefore, from both regional and global model projections, changes in rainfall during the summer peak and

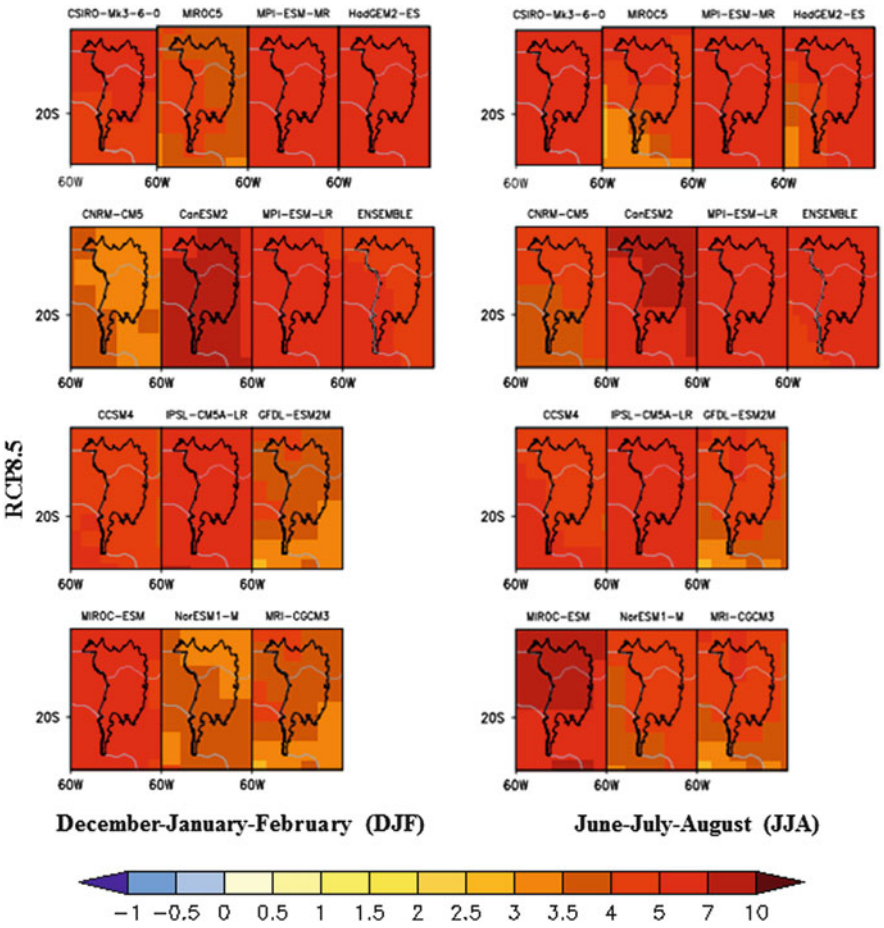

Fig. 2 Changes in air temperature (°C) in Pantanal region for summer (*DJF*) and winter (*JJA*) 2071–2100 relative to 1961–1990 derived from CMIP5/IPCC AR5 global models (listed on Table 1) for the scenario RCP8.5

during the winter dry season are uncertain, as shown by the large intermodel divergence.

The time series depicted in Fig. 4 (a and b, respectively) show that the increases in air temperature are more noticeable in both DJF (summer) and JJA (wintertime) seasons, reaching up to 6°C in 2100 and varying between 3.5°C and 9°C among models. On the near term, up to 2040, the warming could reach 2–3°C, and by 2070, it may reach 4–5°C. Rainfall changes are uncertain (Fig. 4c and d), but there is a slight tendency for reduction in JJA. The tendency is strong on the second half of the twenty-first century (Fig. 4d), but the scatter among model members is extremely large, suggesting high uncertainty on rainfall projections, particularly for the dry season.

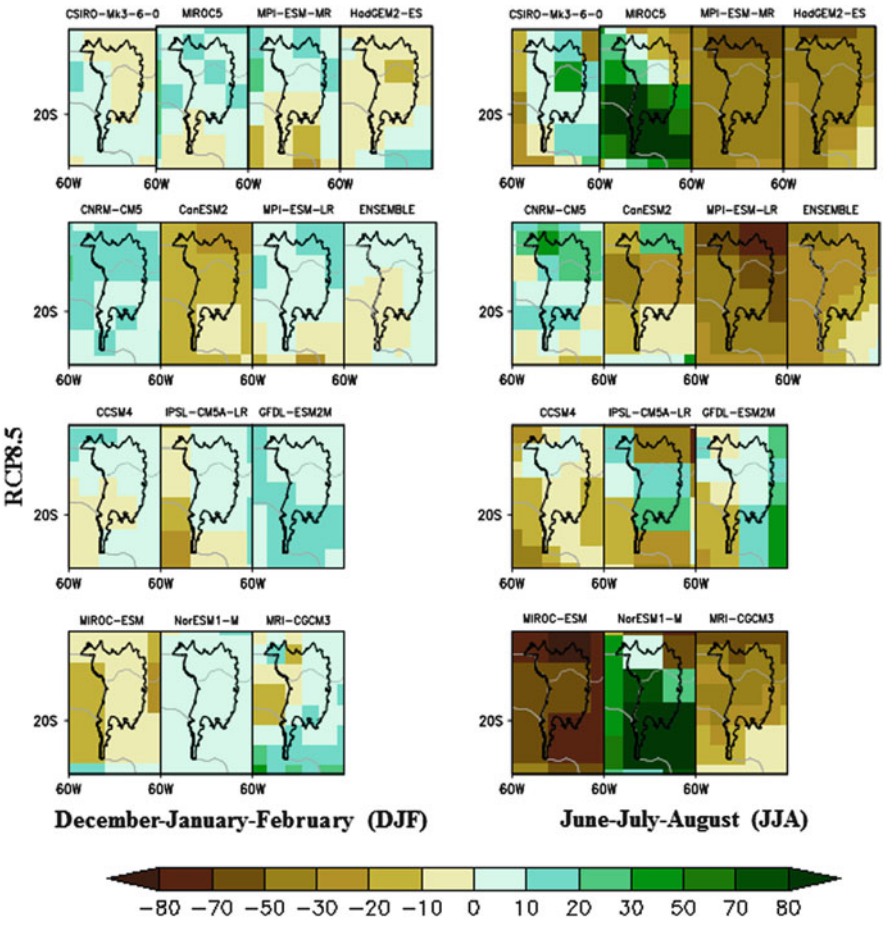

Fig. 3 Same as Fig. 2 but for rainfall (in %)

As for the water balance in the region, with higher temperatures and rainfall reductions by the end of the twenty-first century, Kirtman et al. [24] indicate changes in the components of the water balance derived from the CMIP5 models for the RCP8.5 scenario: annual mean runoff on the region is projected to decrease by about 0.1–0.2 mm/day, and with the reduction in relative humidity by about 4–8%, there is a tendency for evaporation increase by about 0.2–0.4 mm/day and consequently a reduction in near surface soil moisture by about 1–2 mm/day.

On changes in extremes, maximum and minimum temperatures are expected to increase by about 5°C by 2071–2100 relative to 1986–2005, together with an increase in the number of days with warmer nights (by about 70–90 days), with an increase in the number of consecutive dry days by about 20 days, and also an increase in intense precipitation by 10–20%. These scenarios suggest longer dry spells with higher temperatures and water deficiency in the soil, separated by short

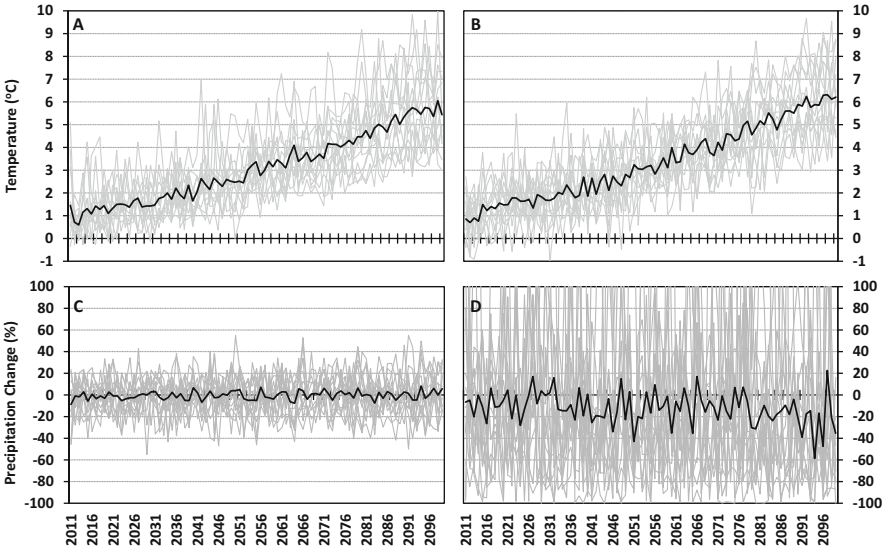

Fig. 4 Time series of air temperature anomalies (**a**, **b**) and rainfall anomalies (**c**, **d**) with respect to 1961–1990 for the Pantanal region for 2011–2100 (*gray lines*) and multi-model ensemble (*black thick line*) under RCP8.5 for austral summer DJF (**a**, **c**) and winter JJA (**b**, **d**)

intense rainfall episodes for the future. While total rainfall is expected to decrease both in summer and winter and the possibility of increase in soil water deficiency, it is hard to conclude on projected changes on the flood pulse in the Pantanal region for the future.

4 Options for Adaptation and Sustainable Development Under Climate Change Risk

Climate change, conversion of habitat into agricultural use, and upstream uses of water are the greatest threats to the Pantanal. Knowledge of severe floods and droughts, which characterize natural disasters, is fundamental for wildlife management and nature conservation of the Pantanal. In addition, human activities are also affected since cattle ranching and ecotourism are economically important in the region, and when seasons with unusual floods or droughts occur, areas with human settlements are impacted.

Throughout the past two centuries, the Paraguay River watershed and, in particular, the Pantanal have sustained productive activities. This has been especially the case with beef production, since large extensions of natural pasturelands have been used while adapting cattle ranching to the typical flood pulse of the Pantanal. On the other hand, the possible future changes in climate and aquatic ecosystems in Brazil are highly uncertain [25].

In spite of the general information regarding the effect of climate change in wetlands, including the effect in the Pantanal and its watershed, this information is disperse and insufficient in describing the magnitude of the impacts of climate change in this ecoregion. World Wide Fund for Nature (WWF) started in 1998 a program to assess impacts of climate and hydrology change through conservation programs in both Bolivia and Brazil. Their focus was (a) the identification of impacts and risks associated with climate change, developing and implementing adaptation strategies, and (b) the recognition of sustainable cattle ranching as a conservation and development strategy for the Pantanal. Their final objective is on systematizing existing information and making it available to key stakeholders working on climate change. Having this information organized will also allow identifying where research still needs to advance, as well as designing strategies that reduce the vulnerability of the watershed in face of climate change. Sustainable cattle ranching activities in the Pantanal consistently link environmental protection with economic development in the region. In addition, it reinforces productive practices and traditional cultural values that, in turn, reinforce the Pantanal's identity and become a real opportunity to make the economic interests of cattle ranching compatible with conservation [26].

It is extremely important to develop and propose options for the Pantanal including an integral vision in relation to changes in climate and land use (see also Pott and Silva [27] and Buller et al. [28]) and their synergic impacts on the Pantanal ecohydrological pulses. Assine [29] has shown that natural changes in the Taquari megafan hydrology were accentuated by the land use in the Upper Taquari Basin. On the other hand, Bergier [2] has shown that the runoff/discharge of the rainfall in the uplands has increased due to upland deforestation over the last four decades. As a result, even for less rainy years, the maximum annual flood pulse in Ladário keeps always elevated, usually above 3 m. The upland soil management by agroforestry (see Buller et al. [28]) is therefore very relevant for restoring the natural interannual flood pulse dynamics and to improve the resilience of the wetland ecosystems in the lowlands with regard to future climate change risk.

Acknowledgments The research leading to results shown on this publication has received funding from Rede CLIMA, the National Institute of Science and Technology (INCT) for Climate Change funded by CNPq Grant Number 573797/2008-0 and FAPESP Grant Number 57719-9, FAPESP-Assessment of Impacts and Vulnerability to Climate Change in Brazil and strategies for Adaptation Options Project, and the CNPq-IRD Project Mudanças, variabilidade e tendências do clima no passado, **PR**esente e futuro e desastres naturais nas Regiões Tropicais e Subtropicais do Bras**I**l: observações e **MO**delagem (PRIMO), Ref: 590172/2011-5.

References

1. Ioris AAR, Irigaray CT, Girard P (2014) Institutional responses to climate change: opportunities and barriers for adaptation in the Pantanal and the Upper Paraguay River Basin. Clim Change. doi:10.1007/s10584-014-1134-z

2. Bergier I (2013) Effects of highlands land-use over lowlands of the Brazilian Pantanal. Sci Total Environ 463–464:1060–1066
3. Bergier I (2010) River level sensitivity to SOI and NAO in Pantanal and Amazonia. In III Simpósio de Geotecnologias no Pantanal, Cáceres-MT, October 2010. Embrapa Informática Agropecuária/INPE, 25–34
4. Marengo JA, Cornejo A, Satyamurty P, Nobre C, Sea W (1997) Cold surges in tropical and extratropical South America: the strong event in June 1994. Mon Weather Rev 125 (11):2759–2781
5. Marcuzzo FFN, Faria TG, Cardoso MRD, Melo DCR (2010) Chuvas no Pantanal brasileiro: análise histórica e tendência futura. Anais do 3o Simpósio de Geotecnologias no Pantanal. Cacéres, MT, p 170–180
6. Cardoso MRD, Marcuzzo FFN (2010) Mapeamento de três decênios da precipitação pluviométrica total e sazonal do bioma Pantanal. Anais do 3° Simpósio de Geotecnologias no Pantanal. Cáceres, MT. 84–94
7. Garcia N, Pedraza RA (2008) Daily rainfall variability over northeastern Argentina in the La Plata River basin. Ann N Y Acad Sci. doi:10.1196/annals. 1446.011
8. Alho Cleber JR, Silva JSV (2012) Effects of severe floods and droughts on wildlife of the Pantanal wetland (Brazil) – a review. Animals 2:591–610, available in: http://www.mdpi.com/2076-2615/2/4/591
9. Clarke RT (2005) The relation between interannual storage and frequency of droughts, with particular reference to the Pantanal wetland of South America. Geophys Res Lett 32, L05402. doi:10.1029/2004GL021742
10. Collischonn W, Tucci CEM, Clarke RT (2001) Further evidence of changes in the hydrological regime of the river Paraguay: part of a wider phenomenon of climate change? J Hydrol 245 (1–4):218–238
11. Castañeda E, Barros V (1994) Las tendencias de la precipitación en el cono Sur de américa al este de los andes. Meteorol 19:23–32
12. Minetti J, Vargas W (1998) Trends and jumps in the annual precipitation in South America, south of the 15 S. Atmósfera 11:205–2221
13. Assine ML, Macedo HA, Stevaux JC, Bergier I, Padovani CR, Silva A (2015) Avulsive rivers in the hydrology of the Pantanal wetland. Hdb Environ Chem. doi:10.1007/698_2015_351
14. Gonçalves HC, Mercante MA, Santos ET (2011) Hydrological cycle. Braz J Biol 71 (1 Suppl):241–253
15. Galdino S, Vieira LM, Oliveira H, Cardoso EL (2002) Impactos da agropecuária nos planaltos sobre o regime hidrológico do Pantanal. Corumbá: EMBRAPA-CPAP. 6 p.
16. Fantin-Cruz I, Pedrollo O, Castro NMR, Girard P, Zeilhofer P, Hamilton SK (2011) Historical reconstruction of floodplain inundation in the Pantanal (Brazil) using neural networks. J Hydrol 399(3–4):376–384
17. Marengo JA, Jones R, Alves LM, Valverde MC (2009) Future change of temperature and precipitation extremes in South America as derived from the PRECIS regional climate modeling system. Int J Climatol 29(15):2241–2255
18. Marengo JA, Ambrizzi T, da Rocha RP, Alves LM, Cuadra SV, Valverde MC, Torres RR, Santos DC, Ferraz SET (2010) Future change of climate in South America in the late twenty-first century: intercomparison of scenarios from three regional climate models. Climate Dynam 35(6):1089–1113
19. Marengo JA, Chou SC, Kay G, Alves LM, Pesquero JF, Soares WR, Santos DC, Lyra AA, Sueiro G, Betts R, Chagas DJ, Gomes JL, Bustamante JF, Tavares P (2012) Development of regional future climate change scenarios in South America using the Eta CPTEC/HadCM3 climate change projections: climatology and regional analyses for the Amazon, São Francisco and the Paraná River basins. Climate Dynam 38(9–10):1829–1848
20. PBMC (2013) Contribuição do Grupo de Trabalho 1 ao Primeiro Relatório de Avaliação Nacional do Painel Brasileiro de Mudanças Climáticas. Sumário Executivo GT1. PBMC, Rio de Janeiro, Brasil, 24 p

21. Van Vuuren DP, Bayer LB, Chuwah C, Ganzeveld L, Hazeleger W, van den Hurk B, van Noije T, O'Neill B, Strengers BJ (2012) A comprehensive view on climate change: coupling of earth system and integrated assessment models. Environ Res Lett 7:024012. doi:10.1088/1748 9326/7/2/024012 (10 pp)
22. Knutti R, Seclacek JK (2013) Robustness and uncertainties in the new CMIP5 climate model projections. Nat Clim Chang 3:369–373
23. Torres RR, Marengo JA (2013) Uncertainty assessments of climate change projections over South America. Theor Appl Climatol 112:253–272
24. Kirtman B, Power SB, Adedoyin JA, Boer GJ, Bojariu R, Camilloni I, Doblas-Reyes FJ, Fiore AM, Kimoto M, Meehl GA, Prather M, Sarr A, Schär C, Sutton R, van Oldenborgh GJ, Vecchi G, Wang HJ (2013) Near-term climate change: projections and predictability. In: Stocker TF, Qin D, Plattner G-K, Tignor M, Allen SK, Boschung J, Nauels A (eds) Climate change 2013: the physical science basis. Contribution of working group I to the fifth assessment report of the intergovernmental panel on climate change. Cambridge University Press, Cambridge, 1535p. doi:10.1017/CBO9781107415324
25. Roland F, Huszar VLM, Farjalla VF, Enrich-Prast A, Amado AM, Ometto JPHB (2012) Climate change in Brazil: perspective on the biogeochemistry of inland waters. Braz J Biol 72(3 Suppl):709–722
26. Santos SA, Abreu UGP, Comastri Filho JA, Crispim SMA, Pellegrin AO, Tomich TR (2008) Desafios e soluções tecnológicas para a produção sustentável de gado de corte no Pantanal [<http://www.cpap.embrapa.br/publicacoes/online/DOC99.pdf] / Sandra Aparecida Santos... [et al]. – Corumbá, Embrapa Pantanal, 2008. 32 p (Documentos / Embrapa Pantanal, ISSN 1981-7223:99)
27. Pott A, Silva JSV (2015) Terrestrial and aquatic vegetation diversity of the Pantanal wetland. Hdb Environ Chem. doi:10.1007/698_2015_352
28. Buller LS, Bayma-Silva G, Zanej MR, Ortega E, Moraes A, Goulart T, Bergier I (2015) Historical land-use changes in São Gabriel do Oeste at the upper Taquari river basin. Hdb Environ Chem. doi:10.1007/698_2015_355
29. Assine ML (2005) River avulsions on the Taquari megafan, Pantanal wetland, Brazil. Geomorphology 70(3–4):357–371

Index

I. Bergier and M.L. Assine (eds.), *Dynamics of the Pantanal Wetland in South America,* Hdb Env Chem (2016) 37: 239–244, DOI 10.1007/978-3-319-18735-8,